Finite Lattice Methods
in
Statistical Mechanics

Murray T. Batchelor

A thesis submitted for the degree of
Doctor of Philosophy of the
Australian National University

June, 1987

Unless otherwise explicitly indicated in the text, all of the work presented in this thesis is my own.

Murray Batchelor

ABSTRACT

This thesis is concerned with the finite lattice study of spin models. The underlying theme in Parts I and II is the exploitation of Bethe ansatz equations to provide finite lattice data well beyond the range normally available.

In Part I the Bethe ansatz equations for eigenvalues of the eight-vertex model are solved numerically to yield mass gap data on infinitely long strips of up to 512 sites in width. The finite-size corrections, at criticality, to the free energy per site and polarization gap are found to agree with recent studies of the XXZ spin chain. The leading corrections to the finite-size scaling estimates of the critical line and thermal exponent are also found, providing an explanation of the poor convergence seen in earlier studies. Away from criticality, the linear scaling fields are derived exactly in the full parameter space of the spin system, allowing a thorough test of a recently proposed method of extracting linear scaling fields and related exponents from finite lattice data.

In Part II, the numerical solutions of the Bethe ansatz equations for the eigen-energies of the XXZ Hamiltonian on very large chains are used to identify, via conformal invariance, the scaling dimensions of various two-dimensional models. With periodic boundary conditions, eight-vertex and Gaussian model operators are found. The scaling dimensions of the Ashkin-Teller and Potts models are obtained by the exact relating of eigenstates of their quantum Hamiltonians to those of the XXZ chain with modified boundary conditions. Eigenstates of the Ashkin-Teller and Potts models with free boundaries are also obtained, allowing an examination of their critical surface properties.

In Part III the critical behaviour of an Ising model with competing first- and third- nearest neighbour interactions on the square lattice is investigated using the finite lattice method. In the ferromagnetic region, the phase boundary is located with an accuracy at least equal to that of alternative methods. In the antiphase region, distinctive structure in the finite lattice estimators is found over an extended temperature range. However, the nature of the transition remains unclear.

ACKNOWLEDGEMENTS

I wish to record my gratitude and sincere thanks to my supervisor, Professor M. N. Barber, from whom I have learnt a great deal over the years; Michael's vitality and enthusiasm alone can inspire those around him. I am also grateful to Francisco Alcaraz, Rodney Baxter, Chris Hamer, Jaan Oitmaa, Paul Pearce and Reinhout Quispel. I have been fortunate to know and work with all of these people. I also thank Brian Davies for friendly advice.

The members of the Mathematics Department have offered cheery support, especially Tina and Clare. Chris Lenard and Yousong Luo have been my fellow students. Thanks are also due to the members of the Colloid and Surface Science group, who have always made me welcome in their department and at their social gatherings. My contemporaries in that group, Phil Attard and Stan Miklavic, continue to be my good friends.

Neville Smythe and Geoff Huston have proven to be extremely helpful system gurus on, respectively, the Macintosh and the Vaxcluster. Anna Zalucki has helpfully typed parts of this thesis as MSR reports.

Throughout the research embodied in this thesis I have been supported by a Commonwealth Postgraduate Research Award, and, while at the University of NSW, a Gordon Godfrey Scholarship.

Lastly, though not least, I thank my wife Wendy for supporting me as a student; she has been both loving and loved.

PUBLICATIONS

1. *Bethe ansatz calculations for the eight-vertex model on a finite strip*
   M. T. Batchelor, M. N. Barber and P. A. Pearce,
   Submitted to *J. Stat. Phys.*

2. *Conformal invariance and the spectrum of the XXZ chain*
   F. C. Alcaraz, M. N. Barber and M. T. Batchelor,
   Phys. Rev. Lett. **58**, 771-774 (1987).

3. *Conformal invariance, the XXZ chain and the operator content of two-dimensional critical systems*
   F. C. Alcaraz, M. N. Barber and M. T. Batchelor,
   In preparation.

4. *The surface exponents of the quantum XXZ, Ashkin-Teller and Potts models*
   F. C. Alcaraz, M. N. Barber, M. T. Batchelor,
   R. J. Baxter and G. R. W. Quispel,
   Report # 7, Mathematical Sciences Research Centre, ANU (1987).
   Submitted to *J. Phys.* A

5. *Conformal anomaly and surface energy for Potts and Ashkin-Teller quantum chains*
   C. J. Hamer, G. R. W. Quispel and M. T. Batchelor,
   Report # 9, Mathematical Sciences Research Centre, ANU (1987).
   Submitted to *J. Phys.* A

6. *Critical behaviour of the BNNNI model in two dimensions*
   J. Oitmaa, M. J. Velgakis, M. T. Batchelor and M. N. Barber,
   J. Magn. Magn. Mater. **54-57**, 665-666 (1986).

7. *A finite lattice study of the critical behaviour of the two-dimensional biaxial next-nearest-neighbour Ising model*
   J. Oitmaa, M. T. Batchelor and M. N. Barber,
   J. Phys. A. **20**, 1507-1519 (1987).

8. *Sparse matrix factorizations of transfer matrices*
   M. T. Batchelor,
   J. Austral. Math. Soc. (*Ser.* B) **28**, 462-475 (1987).

TABLE OF CONTENTS

Chapter 1 *Introduction*

1.1 The finite lattice method 1

1.2 Structure of the transfer matrix 4

PART I

Chapter 2 *Bethe ansatz calculations for the eight-vertex model on a finite strip*

2.1 Introduction 10

2.2 The Bethe ansatz equations for the eight-vertex model 12

2.3 Finite-size scaling 26

2.4 Linear scaling fields 39

2.5 Summary and conclusion 43

Appendices 46

PART II

Chapter 3 *Conformal invariance, the XXZ chain and the operator content of two-dimensional critical systems*

3.1 Introduction 55

3.2 The Bethe ansatz and the spectrum of the XXZ chain 58

3.3 Operator content of the periodic XXZ chain 76

3.4 The XXZ chain and the critical behaviour of the Ashkin-Teller model 89

3.5 The XXZ chain and the critical behaviour of the Potts models 102

Appendix 113

Chapter 4 *Surface exponents and surface energy of Potts and Ashkin-Teller quantum chains*

4.1 Introduction 117

4.2 Bethe ansatz 119

4.3 Conformal anomaly and surface energy 125

4.4 Surface exponents 127

4.5 Exact surface free energy 130

PART III

Chapter 5 *A finite lattice study of the critical behaviour of the two-dimensional biaxial next-nearest-neighbour Ising model*

5.1 Introduction 131

5.2 Block diagonalization of the transfer matrix 134

5.3 Sparse factorization of the transfer matrix 135

5.4 Nature of the leading eigenvalues 144

5.5 The finite lattice method 145

5.6 The ferromagnetic region 147

5.7 The anti-phase region 150

5.8 Conclusion 152

Appendices 153

References 155

1

INTRODUCTION

The idea of a transfer matrix, first introduced by Kramers and Wannier (1941), has greatly facilitated the growth in knowledge of statistical systems. Indeed, with hindsight, we can appreciate that Onsager's original and masterly contribution to the exact solution of the two-dimensional Ising model (Onsager 1944), by explicitly diagonalizing the transfer matrix, heralded in a whole new era in the study of phase transitions and critical phenomena. In subsequent years, a number of models have appeared bearing the title "exactly solved". Perhaps the most famous of these is the eight-vertex model solved by Baxter (1972). This model, in magnetic spin language, contains Onsager's model as a special case when the novel four-spin interactions are absent.

However, many models of physical interest are sufficiently complicated so as to give the impression that they will *never* be solved exactly. For such models, arguably the most powerful numerical method in two dimensions is the application of phenomenological renormalization to *finite* lattices.

1.1 THE FINITE LATTICE METHOD

Phenomenological renormalization, introduced by Nightingale (1976, 1979), is a consequence of finite-size scaling (Fisher 1971; Fisher and Barber 1972). Recent reviews of this technique have been given by Barber (1983a) and Nightingale (1982). To illustrate the ideas, we consider here a simple one parameter system* defined on an

---

* Phenomenological renormalization in multi-parameter systems has been discussed by Barber (1983b, 1985) (see also Section 2.3).

infinitely long strip of width L in two-dimensions. Let $\psi(t)$ be some quantity which in the infinite system diverges at the critical temperature t_c:

$$\psi(t) \sim A\,|\Delta t|^{-\omega} \qquad \text{as} \quad \Delta t = t - t_c \to 0\,. \tag{1.1.1}$$

Here, this critical singularity is "rounded off" due to the system's quasi-one-dimensional nature (see Barber 1983a). Finite-size scaling asserts that in the finite system, the behaviour of $\psi(t\,;L)$ is described by

$$\psi(t\,;L) \sim L^{\omega/\nu}\, Q_\psi\big[L/\xi(t)\big]\,, \tag{1.1.2}$$

where $\xi(t)$ is the correlation length of the infinite system, diverging as

$$\xi(t) \sim \xi_0\,|\Delta t|^{-\nu}\,, \qquad \Delta t \to 0\,. \tag{1.1.3}$$

In (1.1.2), to recover the behaviour (1.1.1) in the limit $L \to \infty$ at fixed (small) Δt we require the scaling function, $Q_\psi(z)$, to satisfy

$$Q_\psi(z) \sim A\,\xi_0^{-\omega/\nu}\, z^{-\omega/\nu} \qquad \text{as} \quad z \to \infty\,. \tag{1.1.4}$$

In particular, if we choose the quantity $\psi(t)$ to be the correlation length itself, then its behaviour in a finite system can be described by the *ansatz*

$$\xi(t\,;L) \sim L\,Q_\xi\big[L^{1/\nu}\Delta t\big]\,, \quad L \to \infty\,, \quad \Delta t \to 0\,, \tag{1.1.5}$$

which follows from (1.1.2) (here, for convenience, we have modified the argument of the scaling function). From this result, t_c can be estimated from the sequences of values of t for which successive ratios of $\xi(t\,;L)$ and $\xi(t\,;L')$ exactly scale, *i.e.* the values of t for which

$$\xi(t\,;L)/L = \xi(t\,;L')/L'\,. \tag{1.1.6}$$

On the other hand, by differentiating (1.1.5), we observe that

$$\left[\frac{\partial\xi(t\,;L)}{\partial t}\right]_{t=t_c} \sim L^{1+1/\nu}\, Q_\xi'(0)\,, \tag{1.1.7}$$

from which the critical exponent ν can be estimated. Specifically, for two strips L and L', we have

$$1+\frac{1}{\nu} \sim \frac{\ell n \left\{ \left[\frac{\partial \xi(t\,;\,L)}{\partial t} \right]_{t=t_c} \Big/ \left[\frac{\partial \xi(t\,;\,L')}{\partial t} \right]_{t=t_c} \right\}}{\ell n\,(L/L')} \,. \qquad (1.1.8)$$

The result (1.1.6) is equivalent to Nightingale's phenomenological renormalization criterion (see Barber 1983a). By regarding this equation as a renormalization in the *temperature* variable the result in (1.1.8) can be obtained in the usual renormalization group manner (see, *e.g.* Barber 1977, 1983a). In practice, the correlation lengths $\xi(t\,;\,L)$ appearing in these results are related to the ratio of eigenvalues of the system's transfer matrix. For a simple Ising model this matrix is of size $2^L \times 2^L$. From a computational point of view, the largest matrix that can be handled for many models is that for a strip of width $L = 16$. Nevertheless, the finite lattice method has proven to be extremely powerful (particularly here in two dimensions) and has provided valuable information on the phase diagrams and critical exponents of many models of physical interest. Of course, the underlying spirit of the method is to use strips of the greatest possible width from which one can more confidently infer the phase boundaries and critical exponents of the system under consideration.

The models appearing under the "exactly solved" banner naturally provide excellent testing grounds for *any* numerical technique. One of the early achievements of the finite lattice method was Nightingale's success in reproducing the critical behaviour of the eight-vertex model in its spin formulation (Nightingale 1977, 1979). There the eigenvalue data was restricted to strips of up to $L = 16$ and despite this success, poor convergence of the conventional finite-size estimates was seen when the four-spin coupling became large in magnitude. This was also apparent in a subsequent study made by Barber (1985). From a historical point of view, the major goal of this thesis was to extend the available finite lattice data for the eight-vertex model, with the prime motivation being to explore the convergence, with increasing system size, of various aspects of the finite lattice method.

The eight-vertex model was originally solved by two closely related techniques

(Baxter 1972, 1973a). The first approach consisted of finding a parametrization of the vertex weights admitting the construction of commuting transfer matrices. On an equal, though more elaborate, footing is Baxter's generalization of the Bethe ansatz (Bethe 1931). Each technique resulted in a set of functional equations implicitly defining all eigenvalues of the transfer matrix from which the passage to the thermodynamic limit could be made. However, no use has been made of the resulting "generalized" Bethe ansatz equations on a finite lattice; an added motivation for this work was thus the solution of the equations themselves.

The results of this study are presented in Part I of the thesis. Apart from early consultation with Paul Pearce, who helped me to understand and develop a feeling for elliptic functions (and in particular, the conjugate modulus form of the vertex weights and functional equations), the bulk of the work in that part is my own. In particular, I have independently developed the methods and programs to solve the Bethe ansatz equations. Similarly, the finite-size solutions of the "ordinary" Bethe ansatz equations (namely those associated with a six-vertex model or XXZ spin chain) presented in Part II, are my own. These results have played a fundamental role in the formulation of our results. However, before proceeding to these results, we briefly review some of the profound developments that have recently taken place in the theory of critical phenomena. (Reviews of these developments have been given by Fisher 1985, 1986, Friedan *et al.* 1986 and Cardy 1986c, 1987.)

1.2 STRUCTURE OF THE TRANSFER MATRIX

At criticality, a remarkable structure in the eigenvalue spectrum of a transfer matrix on a strip of large but finite width has been discovered by Cardy (1984a,b, 1986a). We first give the relevant results; they are discussed further below. In general, we consider the two-point function of a critical operator O_α, such as the spin or energy density, in the (x,y)-plane where the correlations decay with a circular symmetry. Writing $z = x + iy$ and $\bar{z} = x - iy$, the result in the infinite plane may be written

$$\langle O_\alpha(z_1, \bar{z}_1) O_\alpha(z_2, \bar{z}_2)\rangle = (z_1 - z_2)^{-2h_\alpha} (\bar{z}_1 - \bar{z}_2)^{-2\bar{h}_\alpha}, \qquad (1.2.1)$$

where $(h_\alpha, \bar{h}_\alpha)$ are (real) anomalous dimensions associated with the operator O_α. Under the conformal mapping $w = f(z)$, the correlation functions for a conformally invariant system transform as

$$\langle O_\alpha(z_1, \bar{z}_1) O_\alpha(z_2, \bar{z}_2)\rangle = \left[\frac{dw_1}{dz_1}\frac{dw_2}{dz_2}\right]^{h_\alpha}\left[\frac{d\bar{w}_1}{d\bar{z}_1}\frac{d\bar{w}_2}{d\bar{z}_2}\right]^{\bar{h}_\alpha} \langle O_\alpha(w_1, \bar{w}_1) O_\alpha(w_2, \bar{w}_2)\rangle . \qquad (1.2.2)$$

In particular, Cardy (1984a) has chosen

$$f(z) = \frac{L}{2\pi} \ln z , \qquad (1.2.3)$$

which maps the full z-plane onto periodically repeated strips of width L. With this choice, the correlation function in the strip, through (1.2.1) and (1.2.2), is

$$\langle O_\alpha(w_1, \bar{w}_1) O_\alpha(w_2, \bar{w}_2)\rangle = \frac{\left(\frac{2\pi}{L}\right)^{2(h_\alpha + \bar{h}_\alpha)}}{\left[2\sinh\frac{\pi}{L}(w_1 - w_2)\right]^{2h_\alpha}\left[2\sinh\frac{\pi}{L}(\bar{w}_1 - \bar{w}_2)\right]^{2\bar{h}_\alpha}} . \qquad (1.2.4)$$

Setting $w_1 = u_1 + iv_1$ and $w_2 = u_2 + iv_2$, this has the expansion, for $u_1 > u_2$,

$$\left(\frac{2\pi}{L}\right)^{2x} \sum_{j,j'=0}^{\infty} a_j a_{j'} \exp\left[-\frac{2\pi}{L}(x+j+j')(u_1-u_2)\right] \exp\left[\frac{2\pi i}{L}(s+j-j')(v_1-v_2)\right] , \qquad (1.2.5)$$

where

$$a_j = \frac{\Gamma(x+j)}{\Gamma(x)\, j!} . \qquad (1.2.6)$$

Here $x_\alpha = h_\alpha + \bar{h}_\alpha$ is the scaling dimension of O_α, related to its renormalization group eigenvalue by $y_\alpha = 2 - x_\alpha$, and $s_\alpha = h_\alpha - \bar{h}_\alpha$ is an associated "spin".

The correlation length in the strip can alternatively be evaluated using the transfer matrix. Writing the transfer matrix operator as $\hat{T} = \exp(-a\hat{H})$, where a is the lattice spacing, we have (again for $u_1 > u_2$),

$$\langle O_\alpha(u_1, v_1) O_\alpha(u_2, v_2)\rangle =$$

$$\sum_n \langle 0|\hat{O}_\alpha(v_1)|n,k\rangle\, e^{-(E_n - E_0)(u_1 - u_2)} \langle n,k|\hat{O}_\alpha(v_2)|0\rangle \ , \qquad (1.2.7)$$

where $|n, k\rangle$ is a complete set of eigenstates of $\hat{H}$ with energy E_n and momentum k (quantized in units of $2\pi/L$). Comparing this result with (1.2.5), we see that for each primary operator O_α of dimension x_α and spin s_α there exists an infinite *tower* of eigenstates of $\hat{H}$, labelled by j and j', with energy $E_0 + 2\pi(x_\alpha + j + j')/L$ and momentum $2\pi(s_\alpha + j - j')/L$.

We see that the location and ordering of the levels in the finite lattice eigen-spectrum is thus determined by the anomalous dimensions of the operator algebra describing the critical behaviour of the *infinite* system. The same structure is found in the eigen-spectrum of critical quantum Hamiltonians (von Gehlen *et al.* 1986). At the heart of this discovery is Cardy's exploitation of *conformal invariance*. That conformal invariance should be exhibited by correlation functions at a critical point was first suggested by Polyakov (1970). Basically, for conformal invariance to hold, the system is assumed to possess scale invariance (in the renormalization group sense) and both translational and rotational invariance as well as short range interactions. Cardy's results explained the previously observed connection between finite-size scaling amplitudes in strips and critical exponents and have since been verified in a number of models (see, *e.g.* the review by Cardy 1987 and Section 3.1, following).

Besides Cardy's work, other seminal papers exploring the consequences of conformal invariance have appeared in the last few years. Belavin, Polyakov and Zamolodchikov (1984a,b) have *classified* all possible massless field theories (in one space plus one time dimension) which are conformally invariant. Specifically, they proposed that each *minimal* theory describes some *critical* two-dimensional system, each

characterized by a particular number, the so-called "central charge" or "conformal anomaly". Friedan, Qiu and Shenker (1984) showed that for *unitary* models with conformal anomaly number, c, less than unity, c must be quantized according to

$$c = 1 - \frac{6}{m(m+1)} \qquad \text{for } m = 3, 4, \ldots, \tag{1.2.8}$$

and that the allowed values of the scaling dimensions of the *primary* operators (*i.e.* those forming the "starting points" of Cardy's towers) are $(h_{pq}, h_{\bar{p}\bar{q}})$ where

$$h_{pq} = \frac{\left[p(m+1) - qm\right]^2 - 1}{4m(m+1)}, \tag{1.2.9}$$

with $1 \le q \le p \le m-1$. This is the Kac formula (Kac 1979). (This result has helped to explain why so many critical exponents in two dimensions are rational numbers.) For given m (and thus c), various models, in different universality classes, have been identified in this scheme (see, *e.g.* Cardy 1987). Blöte, Nightingale and Cardy (1986) and Affleck (1986) have shown that c is directly related to the leading finite-size correction to the free energy per site of the infinitely long strip. This result gives a way of "measuring" c for a given model (though, as we shall see in Section 3.3.4, care has to be taken in some cases).

In analyzing the eight-vertex model Bethe ansatz equations, I naturally looked at the numerical solution of the simpler equations of the XXZ chain. The motivation for this was associated with the question of *completeness*. In principle, the Bethe ansatz equations give *all* of the eigenvalues, but how many could we compute by actually *solving* the equations? It turns out that several distributions of zeros are particularly simple and the corresponding eigenvalues can be computed on relatively large chains. However, in the course of this work, we became aware of Cardy's results and had some *very nice slices of luck.* I would like to record some of these developments here as a prologue to Part II of the thesis.

Initially, I showed Francisco Alcaraz (as I recall, for no particular reason) the exact finite-size expression for the ground-state of the XXZ chain at the particular

coupling $\Delta = 0$. To our surprise, it agreed, apart from a normalization factor and a doubling of lattice size, with Francisco's ground-state formula at the decoupling point of the critical Ashkin-Teller Hamiltonian (Kohmoto *et al.* 1981). Was this just coincidence? Numerically, we tried some other couplings. To our elation, the two ground-states were exactly related on finite chains for all values of the couplings. We looked at other energies in the eigen-spectra and found common levels in the two models. This was a real breakthrough; since the early calculations of Alcaraz and Drugowich de Felício (1984), eigenvalues of the Ashkin-Teller model have only been calculated on chains of up to length $L = 10$. By numerically solving the Bethe ansatz equations for the corresponding levels in the XXZ Hamiltonian we could then obtain levels in the Ashkin-Teller model for chains of length up to $L = 256$ with relative ease.

Here we began to draw on Michael Barber's experience. Besides conformal invariance, there is a further idea unifying the theory of critical phenomena in two dimensions. This is the notion that there exist general models to which specific models of physical interest can be related by appropriate transformations (see, *e.g.* Nienhuis 1984 and references cited therein, Kadanoff and Brown 1979, Knops 1980, den Nijs 1981). Examples of such "central theories" are the Coulomb (lattice) gas (Nienhuis 1984) and the generalized Gaussian model (Kadanoff and Brown 1979). Analysis of these models can yield detailed information on the critical behaviour of the related physical models. We shall see in Chapter 3 that the anomalous dimensions appearing in the XXZ model are directly related to those found in the Gaussian model.

A natural question that arose was: "Can we also locate energy levels of the critical Potts models in the eigen-spectrum of the XXZ Hamiltonian?" Indeed, it turns out that we can, though the XXZ Hamiltonian needs a special "twisted" boundary condition for which I have derived Bethe ansatz equations and have again solved numerically. Like the Ashkin-Teller model, eigenvalues of the Potts Hamiltonian (Solyom and Pfeuty 1981) had only previously been calculated on small chains.

The equivalences between the XXZ model on the one hand and the critical Ashkin-Teller and Potts models on the other, can all be established exactly. This work

was largely carried out by Francisco Alcaraz and Michael Barber.

Cardy's argument is also applicable to systems with *free* boundary conditions along the edges of the strip (Cardy 1984a). *Antiperiodic* (or "twisted") boundary conditions can also be encompassed (Cardy 1984b, 1986b). Thus we have also examined the predictions of conformal invariance for the Ashkin-Teller and Potts models with free boundaries. This work is presented in Chapter 4. In this case the Bethe ansatz solution of the XXZ Hamiltonian with free edges had been previously derived by Gaudin (1971, 1983). However, the Hamiltonian corresponding to the free edge Potts model was "unsolved" and the equations were largely derived for us by Rodney Baxter. Again it turns out that the Bethe ansatz equations can be solved numerically for levels in the "equivalent" XXZ Hamiltonians to provide eigenvalues in the spectra of the critical Potts and Ashkin-Teller Hamiltonians on relatively large chains, here of length up to $L = 256$.

Finally, in Part III we present a "conventional" finite-size study of a two dimensional Ising model with competing interactions between first- and third-nearest-neighbour spins. Such models are capable of exhibiting rich and complex critical behaviour, particularly when the competition is between antiferromagnetic and ferromagnetic interactions. For this model, the nature of the transition when the antiferromagnetic third-nearest-neighbour interactions were sufficiently strong was unclear; we hoped to settle the issue by using the finite lattice method. This work complements the series analysis of Oitmaa and Vegakis (1987) and was suggested by Jaan Oitmaa.

Independently, I have developed a "graphical" method to help write down the sparse factors of a given transfer matrix. Such factorizations highlight the internal *structure* of the matrix. This can be exploited in the numerical computation of the leading eigenvalues. However, as we have seen above and shall see in the following, there is *further* structure to be found in the levels of the eigen-spectrum at criticality, with the levels containing information about the system's critical exponents.

2

BETHE ANSATZ CALCULATIONS FOR THE EIGHT-VERTEX MODEL ON A FINITE STRIP

2.1 INTRODUCTION

The exact solution of many integrable models in statistical mechanics and field theory, in one form or another, involves the Bethe ansatz and its generalizations (see, *e.g.* Lieb and Wu 1972, Thacker 1981, Fowler 1982, Baxter 1982, Gaudin 1983 and Tsvelick and Weigmann 1983). Generally, the Bethe ansatz equations constitute a set of transcendental equations whose solutions characterize a given eigenvalue and corresponding eigenvector of the transfer matrix or quantum Hamiltonian of the model. In the thermodynamic limit, the number of equations and solutions become infinite, but the equations can be transformed (see, *e.g.* Lieb and Wu 1972 and Baxter 1982) to linear integral equations, which, at least for the dominant eigenvalues that are required for thermodynamic functions such as the free energy or surface tension, can be solved by the use of Fourier transform techniques.

Despite these successes of the Bethe ansatz in the thermodynamic limit, little use has been made, until recently, of the Bethe ansatz to evaluate quantities on *finite* lattices. This is somewhat surprising since solution of the Bethe ansatz equations for a finite system could provide considerable information on the behaviour of not only the finite system itself but also of the bulk system. In particular, the critical behaviour of the bulk system could be explored by finite-size scaling techniques (see, *e.g.* Barber 1983a).

De Vega and Woynarovich (1985) have recently developed a systematic procedure, based on the integral equation approach, for calculating the leading-order finite-size corrections for any model admitting a Bethe ansatz type solution. De Vega

and Woynarovich (1985) originally applied this method to the non-critical region of the XXZ Heisenberg chain. Hamer (1985, 1986a) and Woynarovich and Eckle (1987) have, however, shown how to extend the method to calculate finite-size corrections *at* criticality, and hence to infer critical exponents of the bulk XXZ system; see also Hamer, Quispel and Batchelor (1987). Similar work has been reported for the XYZ chain (Martin and de Vega 1985) and the eight-vertex model (Hamer 1986b).

The method of de Vega and Woynarovich represents the solution of the Bethe ansatz equations for a large finite system as a perturbation (by a sum of delta functions) of the density function that describes the solutions for the infinite lattice. An alternative approach to exploit the Bethe ansatz for a finite lattice is to directly solve the (finite) set of equations for the (finite) number of solutions characterizing the eigenvalues of the finite lattice theory. This is the approach we adopt here for the eight-vertex model; critical parameters being obtained by finite-size scaling techniques.

Several attempts at direct solution of the Bethe ansatz equations for a finite lattice have been reported for the isotropic Heisenberg chain. In particular, Grieger (1984) and Borysowicz *et al.* (1985) have computed ground-state correlation functions. Avdeev and Dörfel (1986) have obtained the leading correction to the ground-state energy and explored the way in which the density of solutions approaches the bulk limit solution of the integral equation. Woynarovich and Eckle (1987) have computed the lowest state in the two largest sectors of the critical XXZ chain, complementing their analytic analysis of the dominant finite-size corrections appearing in the model.

Recently Alcaraz, Barber and Batchelor (1987a,b) and Alcaraz *et al.* (1987) have numerically solved the Bethe ansatz equations of the critical XXZ chain subject to periodic, 'twisted' and free boundary conditions for several states as a means of calculating mass gap amplitudes in the *critical* q-state Potts and Ashkin-Teller chains. This considerably extended the previous numerical estimates of bulk and surface exponents and allowed an examination of the dominant finite-size corrections appearing in the models. This work is presented in Chapters 3 and 4 of this thesis.

In this chapter, we directly solve the Bethe ansatz equations for the eight-vertex model. Our motivation, beyond the solution itself of the equations, is to explore the convergence of finite-size scaling and related techniques for this model. Early finite-size calculations (Nightingale 1977, 1979, Barber 1985) for the eight-vertex model were based on finite lattice data obtained by direct diagonalization of the transfer matrix in the spin formulation. As a result, eigenvalue data was restricted to strips of width up to 16 sites. While the estimates of bulk critical exponents were quite consistent with the exact results, several aspects warrant further investigation with data from larger lattices. Conventional phenomenological renormalization estimates converge well for small values of the four-spin coupling. However, the convergence deteriorates significantly as the magnitude of the four-spin coupling increases and, indeed, appears to become non-monotonic. Data from large strips would clearly allow a non-trivial test of finite-size scaling and related techniques for a system with non-universal behaviour.

The arrangement and content of this chapter is as follows. In Section 2.2, we reformulate and examine the Bethe ansatz equations of the eight-vertex model. We then proceed to numerically solve these equations for the two simplest distributions of zeros. In Section 2.3 we define a mass gap from the corresponding eigenvalues and discuss the convergence rates of finite-size estimates of the critical line and thermal exponent. Finally in Section 2.4 we derive exact expressions for the linear scaling fields in the full parameter space of the eight-vertex model. In this section we implement and fully test a recently proposed method (Barber 1983b, 1985) of extracting linear scaling fields from finite lattice data. The chapter closes with a summary of our results.

2.2 THE EIGHT-VERTEX MODEL BETHE ANSATZ EQUATIONS

2.2.1 Parametrization and functional equations

We begin by summarizing the results derived by Baxter (1972, 1973a) along with some caveats on the original notation. It is convenient numerically to work with

the elliptic function

$$f(z,q) = \prod_{m=1}^{\infty} (1 - q^{m-1}z)(1 - q^{m}z^{-1})(1 - q^{m}) \qquad (2.2.1a)$$

$$= \sum_{m=0}^{\infty} (-)^{m+1} q^{m(m+1)/2} (z^{m+1} - z^{-m}) \qquad (2.2.1b)$$

where nome $q = e^{-\varepsilon}$, $\varepsilon = \pi I'/I$ with I and I' the complete elliptic integrals of the first kind. The usual elliptic theta functions $\Theta(z,q)$, $H(z,q)$ and $h(z,q) = \Theta(z,q)H(z,q)$ which appear in Baxter's formulation are related to this function by

$$\Theta(z,q) = f(qz,q^2), \quad H(z,q) = iq^{1/4}z^{-1/2} f(z,q^2) , \qquad (2.2.2a)$$

$$h(z,q) = iq^{1/4}z^{-1/2} \frac{f^2(q^2,q^6)}{f(q,q^3)} f(z,q) . \qquad (2.2.2b)$$

Some useful properties of the elliptic function (2.2.1) are listed in Appendix 2A.

The connection between the spin and arrow formulations of the model was discovered originally by Wu (1971) and Kadanoff and Wegner (1971); see also Baxter (1982). The allowed arrow configurations, along with one of the two equivalent sets of spin configurations are shown in Figure 2.1. Defining a set of spin couplings $\mathbf{K} = (K_1, K_1', K_2)$ as in Figure 2.2, the vertex weights are

$$a = R\exp(K_1 + K_1' + K_2) , \qquad b = R\exp(-K_1 - K_1' + K_2),$$
$$c = R\exp(K_1 - K_1' - K_2) , \qquad d = R\exp(-K_1 + K_1' - K_2), \qquad (2.2.3)$$

where R is a normalization factor. In terms of the elliptic function defined in (2.2.1) these weights can be written

$$a = \frac{f(qx^{-1}z,q^2)\, f(qxz,q^2)}{f(q,q^2)\, f(qx^2,q^2)} , \quad b = -\frac{q^{1/2}\, f(x^{-1}z,q^2)\, f(xz,q^2)}{z\, f(q,q^2)\, f(qx^2,q^2)} , \qquad (2.2.4a)$$

$$c = \frac{x^{1/2}\, f(qx^{-1}z,q^2)\, f(xz,q^2)}{z^{1/2}\, f(q,q^2)\, f(x^2,q^2)}, \quad d = -\frac{x^{3/2}\, f(x^{-1}z,q^2)\, f(qxz,q^2)}{z^{1/2}\, f(q,q^2)\, f(x^2,q^2)}, \qquad (2.2.4b)$$

where

$$z = \exp(i\pi v/I) , \quad x = \exp(i\pi\eta/I) . \qquad (2.2.5)$$

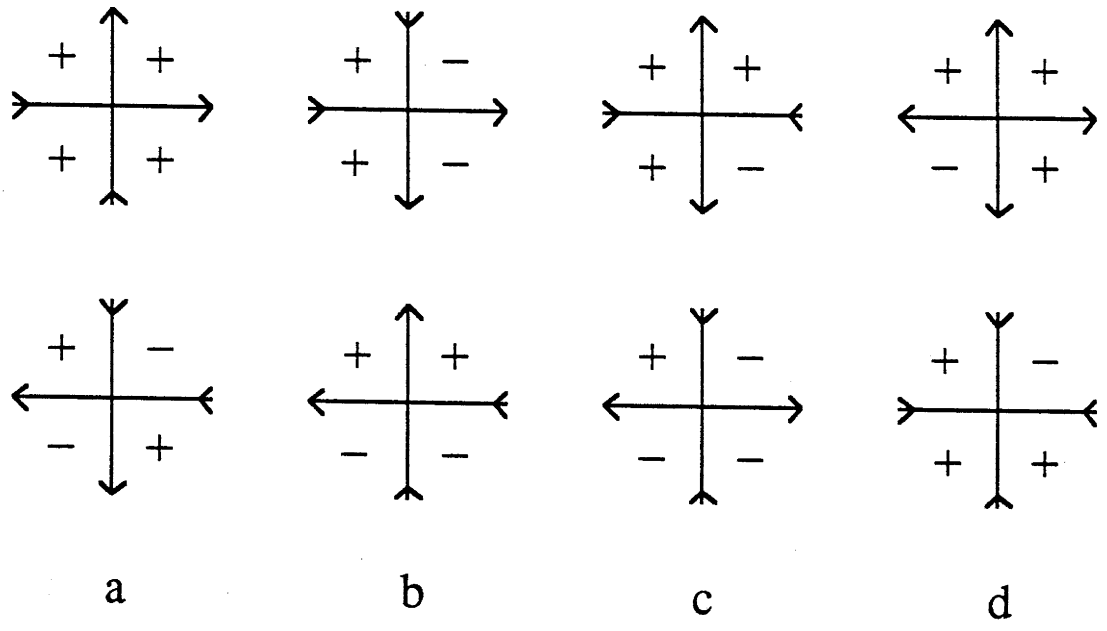

Figure 2.1 The standard arrow and spin configurations of the eight-vertex model and their corresponding weights. An equivalent set of spin configurations has all spins reversed.

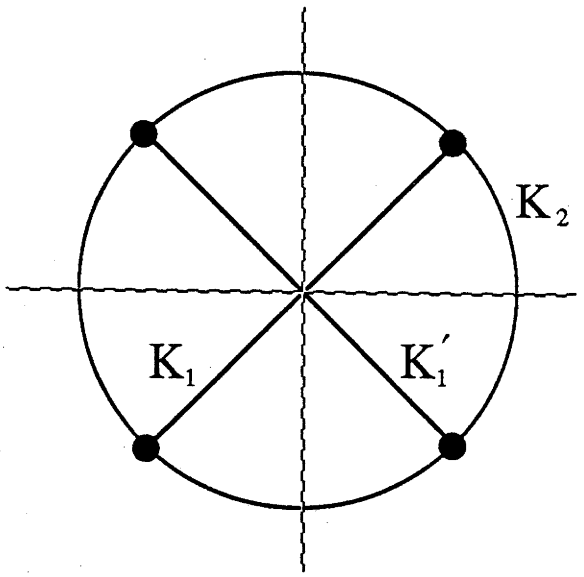

Figure 2.2 Arrangement of spins (filled circles) and associated (reduced) coupling constants around a vertex.

Since we will focus on the transition from the ferromagnetic ground-state we have rearranged the parametrization of the weights compared to Baxter's arrangement (Baxter 1973b). (The interchanges are $a \leftrightarrow c$, $b \leftrightarrow d$). As a result the critical line is given by

$$a = b + c + d \tag{2.2.6}$$

or

$$\sinh 2K_1 \sinh 2K_1' = \exp(-4K_2) . \tag{2.2.7}$$

In the low temperature (ferromagnetic) regime $(a > b + c + d)$ we have

$$0 < q < x^2 < 1 , \quad x < z < x^{-1} . \tag{2.2.8}$$

The symmetric case $K_1 = K_1'$ is given by $z = 1$, here $c = d$. The Ising limit $K_2 = 0$ is given by $q = x^4$, where $ab = cd$. The parametrization (2.2.4) is such that $q = 0$ in the low temperature limit and $q = 1$ at criticality.

All eigenvalues $T(z)$ of the row-to-row transfer matrix (Baxter 1972) are implicitly defined through the functional relation

$$(-)^{v'+v''} T(z)\, Q(z) = P(xz)\, Q(x^{-2}z) + P(x^{-1}z)\, Q(x^2 z) \tag{2.2.9a}$$

where

$$P(z) = \left[\frac{x\, f(z,q)}{\sqrt{z}\, f(x^2,q)} \right]^N , \quad N = 2n , \tag{2.2.9b}$$

$$Q(z) = z^{-(n+v)/2} \prod_{j=1}^{n} f\left(\frac{z}{z_j}, q\right) . \tag{2.2.9c}$$

The condition on the n zeros is

$$\left(\frac{1}{2} i v \Gamma' - \sum_{j=1}^{n} v_j\right) / \Gamma = n + v'' + \text{even integer} , \tag{2.2.10}$$

which can also be written

$$\prod_{j=1}^{n} z_j = (-)^{n+v''} q^{v/2} . \tag{2.2.11}$$

The quantum numbers ν' and ν'' satisfy the following rules :

$\nu' = 0(1)$ if the number of down arrows in a row is even(odd)

$\nu'' = 0(1)$ if the corresponding eigenvector is symmetric(antisymmetric) with respect to arrow reversal.

A further quantum number ν is defined via the condition

$$\nu + \nu' + n = \text{even integer}, \tag{2.2.12}$$

implying that we can choose $\nu = \nu'$ for n even, and for n odd; ν and ν' to differ by one. For convenience, in all subsequent numerical computations we take n to be even, and thus N to be a multiple of four.

The generalized Bethe ansatz equations provide the zeros of the function $Q(z)$. These equations are obtained by setting $z = z_j$, $j = 1,..., n$ in equation (2.2.9a); the left hand side vanishes, resulting in a set of n coupled nonlinear equations:

$$\left[\frac{f(x\, z_j, q)}{f(x^{-1} z_j, q)}\right]^N = -x^{-2\nu} \prod_{k=1}^{n} \frac{f(x^2 \frac{z_j}{z_k}, q)}{f(x^{-2} \frac{z_j}{z_k}, q)}, \quad j = 1,\ldots,n . \tag{2.2.13}$$

The logarithmic form of the eight-vertex equations has been discussed by Johnson, Krinsky and M^c Coy (1973) (see also Takhtadzhan and Faddeev 1979). In our notation we may write the equations as

$$N\Phi_1(\phi_j) = -2\pi l_j - 2\nu\, \ell n x + \sum_{k=1}^{n} \Phi_2(\phi_j - \phi_k), \quad j = 1, \ldots, n . \tag{2.2.14}$$

Here we have further defined $z_j = \exp i\phi_j$. In (2.2.14) the l_j are half-integers and

$$\Phi_p(\phi) = \varphi(\phi, x^p) \tag{2.2.15}$$

where

$$\varphi(\phi, x) = -\pi - \phi - 2\sum_{m=1}^{\infty} \frac{(x^m - x^{-m} q^m) \sin m\phi}{m(1 - q^m)} . \tag{2.2.16}$$

The function $\Phi_p(\phi)$ converges absolutely for q and x in the domain (2.2.8).

2.2.2 Solution on a finite lattice

Equations (2.2.13) and (2.2.14) have not been solved for general values of q, x, and n. In this chapter we are only interested in their solution as a means of providing the two largest eigenvalues from which we define a suitable mass gap. For even n, the maximum eigenvalue $T_0(z)$ has $\nu'' = 0$ while the next largest, $T_1(z)$, has $\nu'' = 1$. Both eigenvalues are in the sector with $\nu' = \nu = 0$.

Bootstrapping in temperature

The first order approximation $(q << x^2 << 1)$ has been carried out by Baxter (1972). In this limit (2.2.13) reduces to

$$z_j^n + (-)^{\nu''} = 0\,, \qquad j = 1,\ldots, n \tag{2.2.17}$$

i.e. the zeros characterizing $T_0(z)$ and $T_1(z)$ are the interlacing nth roots of $\pm$ unity. The corresponding limit in (2.2.14) indicates the following choice for the numbers l_j :

$$T_0(z): \qquad l_j = j - 1/2\,, \qquad j = 1,\ldots, n \tag{2.2.18a}$$

$$T_1(z): \qquad l_j = j + 1/2\,, \qquad j = 1,\ldots, n \tag{2.2.18b}$$

The distribution of zeros in the complex z-plane for each eigenvalue is shown in Figures 2.3(a) and 2.3(c) for $N = 32$. These zeros can be used as initial starting points in the numerical solution for either (2.2.13) or (2.2.14). Given a value of $x(\eta)$, the zeros are obtained by incrementing q and solving the thus modified set of equations for the new distribution of zeros. This distribution is used as input for another increment in q and so on ... . In this way we "bootstrap" the zeros through their finite temperature distributions. The zeros for $T_0(z)$ and $T_1(z)$ at $q = 0.1$ with $q = x^3$ $(\eta = iI'/3)$ are shown in Figures 2.3(b) and 2.3(d). We observe that the sets of zeros remain interlaced.

The most convenient set of equations to solve numerically is the real system (2.2.14). In finding the n zeros we have used a standard library package implementing a Newton-type method (specifically, NAG routine C05NBF). We have checked, for

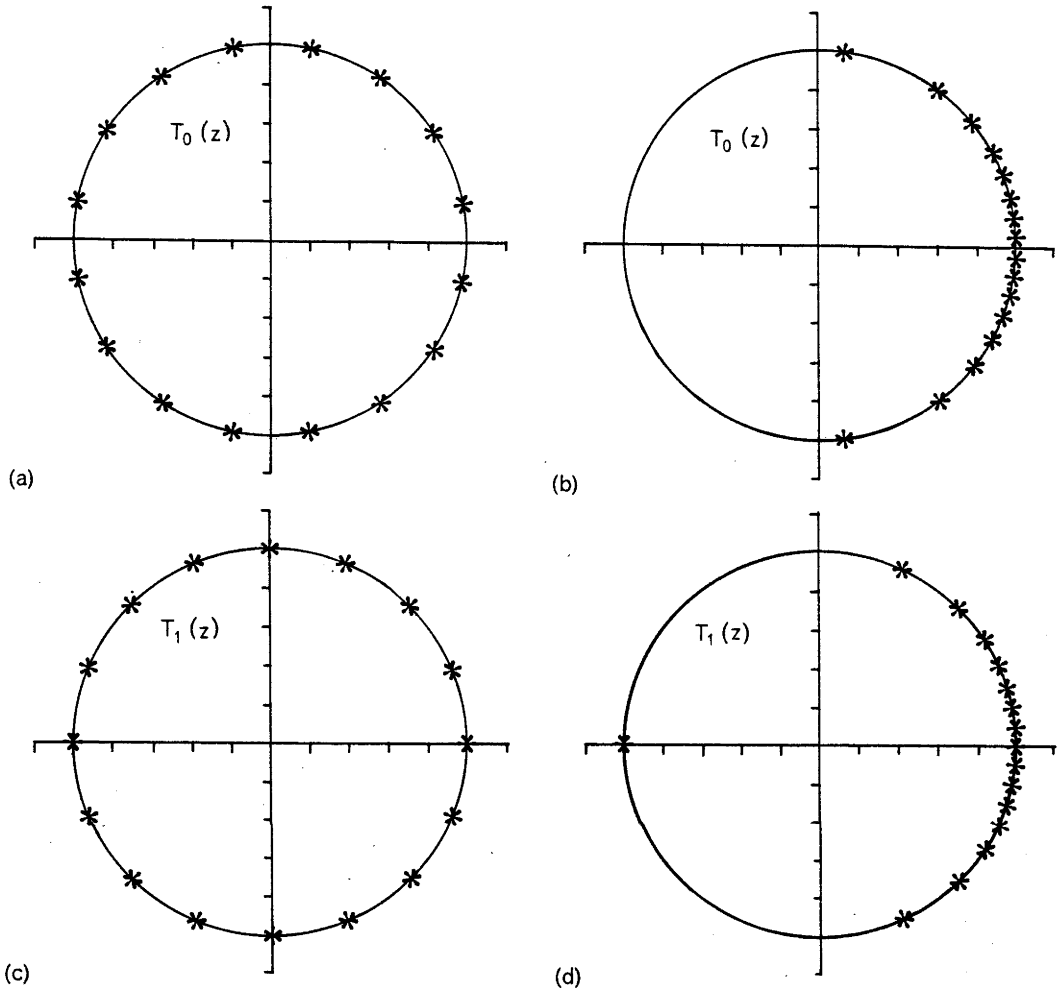

Figure 2.3 Distributions of zeros on the unit circle in the complex z-plane for eigenvalues $T_0(z)$ and $T_1(z)$ on a strip of width N = 32.

(a) and (c): distributions at $q = 0$.

(b) and (d): distributions at $q = 0.1$ with $\eta = i\Gamma/3$ $(q = x^3)$.

lattice sizes $N = 4$ and $N = 8$, the eigenvalues obtained in this way with the results of a "brute-force" diagonalization of the transfer matrix. In practice, as the zeros z_j occur in complex conjugate pairs, the number of zeros and equations can be reduced to $n/2$ for $T_0(z)$, and $n/2 - 1$ for $T_1(z)$ where we further factor out the stationary zeros at $\phi_1 = 0$ and $\phi_n = \pi$.

Exact solutions in the Ising limit

As an alternative to bootstrapping from the low temperature limit, for a given value of q, the incremention can be in the variable x away from the exact Ising solutions. When $q = x^4$, the Bethe ansatz equations decouple and the solutions can be written in closed form. The simplest approach is via (2.2.14), which reduces to

$$N\Phi_1(\phi) = -2\pi l_j - n(\pi + \phi_j) + \sum_{k=1}^{n} \phi_k \quad , \quad j = 1,\ldots, n \, . \tag{2.2.19}$$

On rearranging, this can be written

$$\frac{2\pi}{N} l_j - \frac{\pi}{2} - \frac{1}{N} \sum_{k=1}^{n} \phi_k = \mathrm{am}(\tilde{I}\phi_j/\pi, \tilde{k}) \, , \tag{2.2.20}$$

where $\mathrm{am}(u,k)$ is the elliptic amplitude function of argument u and modulus k (see, *e.g.* Gradshteyn and Ryzhik 1980) satisfying

$$u = \mathfrak{F}(\mathrm{am}(u,k),k) \tag{2.2.21}$$

where $\mathfrak{F}(\theta,k)$ is the elliptic integral of the first kind:

$$\mathfrak{F}(\theta,k) = \int_0^{\theta} \frac{d\alpha}{\sqrt{1 - k^2 \sin^2 \alpha}} \, . \tag{2.2.22}$$

In (2.2.20) nome $\tilde{q} = x$. From (2.2.20) and (2.2.21) we have the following results,

$$T_0(z): \quad \phi_j = \pi \tilde{I}^{-1} \mathfrak{F}\left(\frac{2\pi}{N} l_j - \frac{\pi}{2}, \tilde{k} \right) , \qquad j = 1, \ldots, n \, , \tag{2.2.23a}$$

$$T_1(z): \quad \phi_j = \pi \tilde{I}^{-1} \mathfrak{F}\left(\frac{2\pi}{N} l_j - \frac{\pi}{2} - \frac{\pi}{N}, \tilde{k} \right) , \quad j = 1, \ldots, n \, . \tag{2.2.23b}$$

In practice, to evaluate these zeros we first compute $\tilde{k}$ and $\tilde{I}$ using the formulæ (Gradshteyn and Ryzhik 1980)

$$\tilde{I} = \frac{\pi}{2}\left(1 + 2\sum_{m=1}^{\infty} x^{m^2}\right)^2, \tag{2.2.24}$$

$$\tilde{k} = \frac{2\pi}{\tilde{I}}\, x^{1/2}\left(\sum_{m=1}^{\infty} x^{m(m-1)}\right)^2. \tag{2.2.25}$$

Initial approximation of zeros

For the largest eigenvalue, an initial approximation to the zeros for any values of q and x, increasing in accuracy with system size, can be obtained by generalizing the method outlined by Grieger (1984) in the computation of the ground-state of the isotropic XXZ antiferromagnet. Here we appropriately sample the known (Johnson *et al.* 1973 and Takhtadzhan and Faddeev 1979) distribution of zeros for $T_0(z)$ to provide approximations to the zeros of both leading eigenvalues. To derive the necessary result, we follow Hamer (1986b) and introduce the quantity

$$Z_N(\phi) = -\frac{1}{2\pi}\left[\Phi_1(\phi) - \frac{1}{N}\sum_{k=1}^{n}\Phi_2(\phi_j - \phi_k)\right] \tag{2.2.26}$$

so that, from (2.2.14), at the zeros ϕ_j we have

$$Z_N(\phi_j) = l_j/N\,. \tag{2.2.27}$$

Also define

$$R_N(\phi) = \frac{dZ_N(\phi)}{d\phi} \tag{2.2.28}$$

then (Johnson *et al.* 1973 and Takhtadzhan and Faddeev 1979)

$$R_\infty(\phi) = \frac{1}{4\pi}\sum_{m=-\infty}^{\infty}\frac{\exp(im\phi)}{\mathrm{coshm}\lambda} = \frac{\tilde{I}}{2\pi^2}\,\mathrm{dn}(\tilde{I}\phi/\pi,\tilde{k}) \tag{2.2.29}$$

where dn(u,k) is a standard elliptic function (Gradshteyn and Ryzhik 1980). In (2.2.29), modulus $\tilde{k}$ is defined by

$$\tilde{I}'/\tilde{I} = \lambda/\pi = -i\eta/I \tag{2.2.30}$$

and thus with associated nome $\tilde{q} = x$. Using Eqs. (2.2.28) and (2.2.29) we have

$$Z_\infty(\phi) = \frac{1}{2\pi}\,\mathrm{am}\left(\tilde{I}\,\phi/\pi\,,\,\tilde{k}\right). \tag{2.2.31}$$

Finally from Eqs. (2.2.21), (2.2.27) and (2.2.31),

$$\phi_j = \pi\,\tilde{I}^{-1}\,\Im\left(\frac{2\pi}{N}\,l_j\,,\,\tilde{k}\right) \tag{2.2.32}$$

should be a good approximation to the zeros ϕ_j, becoming exact as $N \to \infty$. Realize however, that (2.2.32) is the result (2.2.23a) obtained in the Ising case. Both of the Ising results (2.2.23a) and (2.2.23b) are thus excellent approximation formulas for all values of q and x. In Table 2.1 the values obtained from these formulæ for $q = x^3 = 0.1$ and $N = 32$ are compared with the exact, numerical, results. As can be seen, the agreement is close, resulting in rapid convergence to the exact zeros.

2.2.3 Comparison with bulk results

For the symmetric case ($z = 1$) (2.2.9a) simplifies to give the largest eigenvalue in the form

$$T_0(1) = 2\left[\frac{f(x,q)}{f(x^2,q)}\right]^N \prod_{j=1}^{n} \frac{f(x^2 z_j,q)}{f(z_j,q)} \tag{2.2.33}$$

where we have exploited the fact that the zeros occur in unimodular complex conjugate pairs. However, for $\nu'' = 1$, (2.2.9a) reduces to the identity "zero = zero". An expression for $T_1(1)$ can be obtained by differentiating (2.2.9a) with respect to z and *then* setting $z = 1$ (this was a suggestion of Michael Barber). The result is

$$T_1(1) = -\left[\frac{f(x,q)}{f(x^2,q)}\right]^N \frac{f(x^2,q)}{g(1,q)}\,F(x,q)\prod_{j=2}^{n} \frac{f(x^2 z_j,q)}{f(z_j,q)} \tag{2.2.34a}$$

in which

$$F(x,q) = \sum_{j=1}^{n}\left[\frac{g(x^{-2}z_j^{-1},q)}{f(x^2 z_j,q)} - \frac{g(x^2 z_j^{-1},q)}{f(x^{-2}z_j,q)}\right] - \frac{N}{f(x,q)}\left[g(x^{-1},q) + x\,g(x,q)\right] \tag{2.2.34b}$$

Table 2.1 Approximate and exact (numerical) zeros ϕ_j characterizing the eigenvalues $T_0(z)$ and $T_1(z)$ on a strip of width $N = 32$ for $\eta = i\Gamma/3$ ($q = x^3$) and $q = 0.1$.

$T_0(z)$		$T_1(z)$	
approx.	exact	approx.	exact
0.048 047	0.048 023	0.096 562	0.096 609
0.146 037	0.145 959	0.197 011	0.197 114
0.250 106	0.249 957	0.306 071	0.306 257
0.365 844	0.365 583	0.430 653	0.430 980
0.502 181	0.501 708	0.582 855	0.583 482
0.676 405	0.675 428	0.789 042	0.790 538
0.932 371	0.929 549	1.132 394	1.139 276
1.471 868	1.446 502		

(2.2.34b)

and the function $g(z,q)$ is defined by

$$g(z,q) = \frac{d}{dz} f(z,q) \ . \tag{2.2.35}$$

In Eqn. (2.2.34) we are to agree that $z_1 = 1$. There are *no* such cancellation problems in the nonsymmetric case.

Given $T_0(z)$ and $T_1(z)$, the free energy per site f_N and the interfacial tension σ_N can be defined on a strip of width N as (see, *eg.* Baxter 1982)

$$-\beta f_N = \frac{1}{N} \ln T_0(z) \ , \tag{2.2.36}$$

$$-\beta \sigma_N = \frac{1}{N} \ln \ln \frac{T_0(z)}{T_1(z)} \ . \tag{2.2.37}$$

The exact results derived by Baxter (1972, 1973b, 1982), valid in the thermodynamic limit, are

$$-\beta f_\infty = \ln a + \sum_{m=1}^{\infty} \frac{\left(x^m + x^{-m} - z^m - z^{-m}\right)\left(x^{2m} - q^m\right)^2}{m x^m \left(1 - q^{2m}\right)\left(1 + x^{2m}\right)} \ , \tag{2.2.38}$$

$$-\beta \sigma_\infty = \frac{1}{2} \ln \left[4x \prod_{m=1}^{\infty} \left(\frac{1 + x^{4m}}{1 + x^{4m-2}} \right)^4 \right] \ . \tag{2.2.39}$$

In Table 2.2 we show the values of (2.2.36) and (2.2.37) for $z = 1$, $q = x^3 = 0.1$ and $q = x^6 = 0.01$ on finite strips of width $N = 2^l$, $l = 2, 3, \ldots, 8$. For comparison we show also the bulk limits given in (2.2.38) and (2.2.39). The slow convergence of the interfacial tension is presumably a result of the double logarithm in its definition.

It should be noted that the only real limit imposed on the evaluation of $T_0(z)$ and $T_1(z)$ with increasing system size is in the resolution of zeros as q tends to its critical value (as can be seen from Figures 2.3(b) and 2.3(d), the non-stationary zeros will coalesce at $z = 1$ in this limit). For this reason, to examine the critical region in detail, we have derived an alternative parametrization of the vertex weights (2.2.4) and the functional equation (2.2.9).

Table 2.2 Finite lattice estimates (2.2.36) and (2.2.37) of the eight-vertex model free-energy per site and interfacial tension. Also shown is the quantity $-\beta f_N^{(1)} = N^{-1} \ell n\, T_1(z)$.

	$q = x^3 = 0.1$			$q = x^6 = 0.01$		
N	$-\beta f_N^{(0)}$	$-\beta f_N^{(1)}$	$-\beta\sigma_N$	$-\beta f_N^{(0)}$	$-\beta f_N^{(1)}$	$-\beta\sigma_N$
4	0.335 068	0.274 637	0.3550	0.111 023	–0.005 419	0.1910
8	0.311 680	0.295 782	0.2578	0.088 066	0.059 143	0.1830
16	0.305 641	0.301 653	0.1720	0.082 064	0.075 222	0.1383
32	0.304 114	0.303 143	0.1085	0.080 553	0.079 016	0.0941
64	0.303 732	0.303 507	0.0663	0.080 181	0.079 862	0.0608
128	0.303 638	0.303 592	0.0401	0.080 092	0.080 035	0.0385
256	0.303 616	0.303 609	0.0248	0.080 073	0.080 066	0.0245
∞	0.303 612...		0.0064...	0.080 069...		0.0064...

2.2.4 Reformulation at criticality

The limit $q \to 1$ can be handled by using the conjugate nome identities outlined in Appendix 2B. In terms of the conjugate variables

$$\zeta = \exp(iw)\ ,\ \chi = \exp(i\mu)\ ,\ p = \exp(-2\pi^2/\varepsilon) \tag{2.2.40}$$

with $w = -i2\pi v/\Gamma'$ and $\mu = -i2\pi\eta/\Gamma'$, the vertex weights (2.2.4) may be written

$$a = \rho\sqrt{\frac{\chi}{\zeta}}\ \frac{f(-\sqrt{\chi\zeta}\ ,p)\ f(-\sqrt{\zeta/\chi}\ ,p)}{f(-\chi,p)\ f(-1,p)} \tag{2.2.41a}$$

$$b = \rho\sqrt{\frac{\chi}{\zeta}}\ \frac{f(\sqrt{\chi\zeta}\ ,p)\ f(\sqrt{\zeta/\chi}\ ,p)}{f(-\chi,p)\ f(-1,p)} \tag{2.2.41b}$$

$$c = \rho\sqrt{\frac{\chi}{\zeta}}\ \frac{f(\sqrt{\chi\zeta}\ ,p)\ f(-\sqrt{\zeta/\chi}\ ,p)}{f(\chi,p)\ f(-1,p)} \tag{2.2.41c}$$

$$d = -\rho\sqrt{\frac{\chi}{\zeta}}\ \frac{f(-\sqrt{\chi\zeta}\ ,p)\ f(\sqrt{\zeta/\chi}\ ,p)}{f(\chi,p)\ f(-1,p)}\ . \tag{2.2.41d}$$

The normalization factor ρ is given by

$$\rho = \exp\left[\frac{\pi}{2\Pi'}(\eta^2 - v^2)\right]\ . \tag{2.2.42}$$

In the ferromagnetic regime, the new variables (2.2.40) satisfy

$$|z| = |\chi| = 1\ ,\ 0 < p < 1\ ,\ |w| < \mu < \pi \tag{2.2.43}$$

and the square root is taken so that

$$-\frac{\pi}{2} < \arg\left(\zeta^{1/2}\right) \le \frac{\pi}{2}\ . \tag{2.2.44}$$

The functional equation (2.2.9) transforms to

$$(-)^{v'+v''}T(\zeta)Q(\zeta) = P(\chi\zeta)Q(\chi^{-2}\zeta) + P(\chi^{-1}\zeta)Q(\chi^{2}\zeta) \tag{2.2.45a}$$

with

$$P(\zeta) = \left[\rho\frac{\chi}{\sqrt{\zeta}}\ \frac{f(\zeta,p^2)}{f(\chi^2,p^2)}\right]^N \tag{2.2.45b}$$

$$Q(\zeta) = \zeta^{-(\nu''+n+ev)/2} \prod_{j=1}^{n} f\left(\frac{\zeta}{\zeta_j}, p^2\right) . \qquad (2.2.45c)$$

Finally, the condition on the zeros (2.2.10) reads

$$\prod_{j=1}^{n} \zeta_j = (-)^{\nu} p^{\nu''+n+ev} . \qquad (2.2.46)$$

The symmetric case $(K_1 = K_1')$ is now given by $w = 0$ and the Ising limit $(\eta = iI'/4)$ by $\mu = \pi/2$. Duality is given by the simple interchange $p \leftrightarrow -p$, criticality occurring at $p = 0$. From (2.2.45a) the zeros specifying a given eigenvalue are now solutions of

$$\left[\frac{f(\chi\zeta_j, p^2)}{f(\chi^{-1}\zeta_j, p^2)}\right]^N = -\chi^{-2\nu''} \prod_{k=1}^{n} \frac{f\left(\chi^2 \zeta_j \zeta_k^{-1}, p^2\right)}{f\left(\chi^{-2} \zeta_j \zeta_k^{-1}, p^2\right)} , \quad j = 1,\ldots, n \qquad (2.2.47)$$

where, for n even, we have chosen $ev = -n$. For the symmetric case, the analogous relations to (2.2.33) and (2.2.34) are

$$T_0(1) = 2\left[\rho \frac{f(\chi, p^2)}{f(\chi^2, p^2)}\right]^N \prod_{j=1}^{n} \frac{f(\chi^2\zeta_j, p^2)}{f(\zeta_j, p^2)} , \qquad (2.2.48)$$

$$T_1(1) = -\left[\rho \frac{f(\chi, p^2)}{f(\chi^2, p^2)}\right]^N \chi F(\chi, p^2) \frac{f(\chi^2, p^2)}{g(1, p^2)} \prod_{j=2}^{n} \frac{f(\chi^2\zeta_j, p^2)}{f(\zeta_j, p^2)} , \qquad (2.2.49)$$

in which $F(\chi, p^2)$ is as defined in (2.2.34b), only now with z_j, x and q replaced by ζ_j, χ and p^2. Here the zeros $z_1 = 1$ and $z_2 = -1$ map to the values $\zeta_1 = 1$ and $\zeta_2 = p$.

In deriving a logarithmic form of the equations (2.2.47) it is convenient to seperately consider the zeros for $T_0(\zeta)$ and $T_1(\zeta)$.

Zeros for $T_0(\zeta)$

On setting $\zeta_j = \exp(-2\alpha_j)$ and using the definition (2.2.1) we may write for example

$$\frac{f(\chi\zeta_j, p^2)}{f(\chi^{-1}\zeta_j, p^2)} = e^{i\mu} \frac{\sinh(\alpha_j - i\mu/2)}{\sinh(\alpha_j + i\mu/2)} \prod_{m=1}^{\infty} \frac{1 + p^{4m} - p^{2m}\cosh(2\alpha_j - i\mu)}{1 + p^{4m} - p^{2m}\cosh(2\alpha_j + i\mu)} . \tag{2.2.50}$$

Subsequently on taking logarithms in (2.2.47) we introduce the quantities φ and Φ defined by

$$\exp(i\varphi) \equiv -\frac{\sinh(\alpha - i\mu/2)}{\sinh(\alpha + i\mu/2)} , \tag{2.2.51}$$

$$\exp(i\Phi) \equiv \frac{1 + p^2 + 2p\cosh(2\alpha - i2\mu)}{1 + p^2 - 2p\cosh(2\alpha + i2\mu)} , \tag{2.2.52}$$

with

$$\varphi(\alpha,\mu) = 2\tan^{-1}(\cot\mu \tanh\alpha) , \tag{2.2.53}$$

$$\Phi(\alpha,\mu,p) = 2\tan^{-1}\left(\frac{2p\sinh 2\alpha \sin 2\mu}{1 + p^2 - 2p\cosh 2\alpha \cos 2\mu}\right) . \tag{2.2.54}$$

For $T_0(\zeta)$ the Bethe ansatz equations can then be written in the form

$$N\Psi(\alpha_j, \mu/2) = 2\pi I_j + \sum_{k=1}^{n} \Psi(\alpha_j - \alpha_k, \mu) \qquad j = 1,\ldots,n \tag{2.2.55}$$

where

$$\Psi(\alpha,\mu) = \varphi(\alpha,\mu) + \sum_{m=1}^{\infty} \Phi(\alpha,\mu,p^{2m}) . \tag{2.2.56}$$

and the I_j are half-integers given by

$$I_j = (2j - n - 1)/2 , \quad j = 1,\ldots,n . \tag{2.2.57}$$

Zeros for $T_1(\zeta)$

The zero $\zeta_1 = p$ trivially satisfies the first of the equations (2.2.47). On re-labelling, the remaining $n-1$ zeros satisfy

$$\left[\frac{f(\chi\zeta_j,p^2)}{f(\chi^{-1}\zeta_j,p^2)}\right]^N = -\chi^2\frac{f(p\chi^2\zeta_j,p^2)}{f(p\chi^{-2}\zeta_j,p^2)}\prod_{k=1}^{n-1}\frac{f\left(\chi^2\zeta_j\zeta_k^{-1},p^2\right)}{f\left(\chi^{-2}\zeta_j\zeta_k^{-1},p^2\right)}\ ,\quad j=1,\ldots,n-1 \tag{2.2.58}$$

and subsequently, on taking logarithms,

$$N\Psi(\alpha_j,\mu/2) = 2\pi I_j + \sum_{m=1}^{\infty}\Phi(\alpha_j,\mu,p^{2m-1}) + \sum_{k=1}^{n-1}\Psi(\alpha_j-\alpha_k,\mu)\ ,\quad j=1,\ldots,n-1 \tag{2.2.59}$$

with integers I_j given by

$$I_j = j-n+2\ ,\quad j=1,\ldots,n-1. \tag{2.2.60}$$

Approximation of zeros

Rather than repeating the working in Section 2.2.2 and inverting appropriate elliptic functions, the shortest path to the desired formula is the direct transformation of the final result (2.2.32). Using the identity

$$\frac{\tilde{I}}{I} = \frac{2\pi}{\mu}\frac{\tilde{I}'}{I'}\ , \tag{2.2.61}$$

(2.2.32) can be used to write

$$\alpha_j = \frac{\mu}{2\tilde{I}'}\,\mathcal{F}\left(\frac{2\pi I_j}{N},\left(1-\tilde{k}'^2\right)^{1/2}\right) \tag{2.2.62}$$

with nome $\tilde{q}' = p^{\pi/\mu}$. In this case the zeros (2.2.62) provide excellent initial approximations to the zeros of the systems (2.2.55) and (2.2.59).

2.2.5. Bethe ansatz equations and eigenvalues at criticality

At $p = 0$ the equations (2.2.55), with the choice of the numbers I_j in (2.2.57), reduce to the Bethe ansatz equations describing the leading eigenvalue of either the 6-vertex model or the XXZ chain (Lieb and Wu 1972, Yang and Yang 1966a,b). Correspondingly, the equations (2.2.59) with (2.2.60) describe the leading eigenvalue in the next-largest sector of either model. Defining

$$\alpha_j = \tanh^{-1}\left(\tan\mu/2 \tan\theta_j/2\right), \tag{2.2.63}$$

the equations for $T_0(\zeta)$ and $T_1(\zeta)$ can thus be written as

$$N\theta_j = 2\pi I_j - \sum_{k=1}^{r} \Theta(\theta_j,\theta_k) , \quad j = 1,\ldots,r \tag{2.2.64}$$

where

$$\Theta(\theta,\theta') = 2\tan^{-1}\left[\frac{\Delta \sin(\theta-\theta')/2}{\cos(\theta+\theta')/2 - \Delta\cos(\theta-\theta')/2}\right] \tag{2.2.65}$$

in which we make the identification $\Delta = -\cos\mu$. In (2.2.64), $r = n$ for $T_0(\zeta)$ and $r = n-1$ for $T_1(\zeta)$.

Finally, in this limit equation (2.2.62) can be evaluated to give the result

$$\alpha_j = \frac{\mu}{\pi} ln \tan\pi\left(\frac{I_j}{N} + \frac{1}{4}\right). \tag{2.2.66}$$

This last approximation formula will be used in Section 3.2.4 for the discussion of the numerical solution of the XXZ Bethe ansatz equations. In this limit the expressions for the two largest eigenvalues, (2.2.48) and (2.2.49), reduce to

$$T_0(1) = 2\left[\frac{\rho}{2\cos\mu/2}\right]^N \prod_{j=1}^{n/2} \frac{\cosh 2\alpha_j - \cos 2\mu}{\cosh 2\alpha_j - 1} , \tag{2.2.67}$$

$$T_1(1) = 2E\left[\frac{\rho}{2\cos\mu/2}\right]^N \prod_{j=1}^{n/2-1} \frac{\cosh 2\alpha_j - \cos 2\mu}{\cosh 2\alpha_j - 1} \tag{2.2.68}$$

where

$$E = 2N\cos^2\mu/2 - \cos\mu - \sum_{j=1}^{n/2-1} \frac{2\sin\mu \sin 2\mu}{\cosh 2\alpha_j - \cos 2\mu} \qquad (2.2.69)$$

Here we have written the eigenvalues in terms of the zeros on $(0,\infty)$ which we can solve for separately (see also Appendix 2D).

In Figure 2.4 we show the zeros ζ_j characterizing the eigenvalues $T_0(\zeta)$ and $T_1(\zeta)$ at criticality. In the limit $p = 1$ all of the zeros are at the point $\zeta = 1$. As p decreases, apart from the stationary zero at $\zeta = 1$, the zeros all move smoothly to the left until at criticality they occupy the positions shown in the figure.

2.3 FINITE-SIZE SCALING

The numerical solution of the eight-vertex model Bethe ansatz equations, described in the preceding section, allows the mass gap

$$\kappa_N = \ell n\left(T_0/T_1\right), \qquad (2.3.1)$$

to be easily evaluated for strips up to $N \approx 256$ for general couplings and up to $N \approx 512$ at criticality. These values of N far exceed the lattice sizes ($N \sim 16$) available in previous finite lattice studies of the eight-vertex model (Nightingale 1977, 1979 and Barber 1985). As mentioned in Section 2.1, this allows a non-trivial test of finite-size scaling and a detailed investigation of *convergence* rates (Privman and Fisher 1983, Barber 1983a). We begin by considering the free energy and mass gap *at* criticality for which the expected behaviour is predicted by conformal invariance (Cardy 1986a).

2.3.1 Free energy at criticality

For a finite strip with periodic boundary conditions, conformal invariance predicts (Blöte *et al.* 1986, Affleck 1986) the free energy per site, f_N, to approach its limiting value, f_∞, as

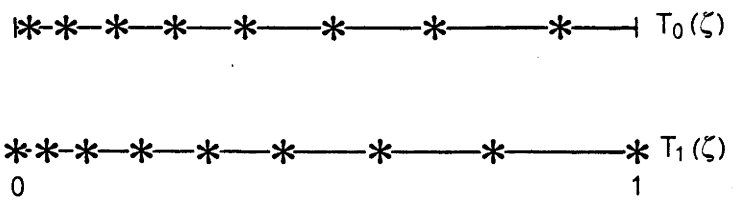

Figure 2.4 Critical distributions of zeros on the real axis in the complex ζ-plane for eigenvalues $T_0(\zeta)$ and $T_1(\zeta)$ on a strip of width N = 32 with $\eta = iI'/3$ ($\mu = 2\pi/3$). Each zero on the open interval (0,1) has a reciprocal on $(1,\infty)$.

$$f_N = f_\infty - \frac{\pi c}{6} N^{-2} + o(N^{-2}), \qquad (2.3.2)$$

where c is the conformal anomaly (note that we have neglected a factor β here). For a model with a line of continuously varying exponents c is expected to be unity (Friedan *et al.* 1984). This prediction has been tested by Blöte *et al.* (1986) using data from strips of up to 16 sites. Excellent agreement was found for $-0.3 < K_2 \le 0.4$ ($0.3 < \mu/\pi \le 0.7$) but for K_2 outside this range the convergence deteriorated significantly.

From (2.2.36) and (2.2.67) the free energy of the eight-vertex model on a finite strip is

$$-\beta f_N = \ell n\left(\frac{\rho}{2\cos\mu/2}\right) + \frac{1}{N}\left[\ell n 2 + \sum_{j=1}^{n/2} \ell n\left(\frac{\cosh 2\alpha_j - \cos 2\mu}{\cosh 2\alpha_j - 1}\right)\right]. \qquad (2.3.3)$$

Taking the thermodynamic limit, we have (Lieb and Wu 1972, Baxter 1982)

$$-\beta f_\infty = \ell n\left(\frac{\rho}{2\cos\mu/2}\right) + \int_{-\infty}^{\infty} \frac{d\alpha}{4\mu\cosh(\pi\alpha/\mu)} \ell n\left(\frac{\cosh 2\alpha - \cos 2\mu}{\cosh 2\alpha - 1}\right). \qquad (2.3.4a)$$

The integral appearing in this result also occurs in the exact solution of the F model (Lieb and Wu 1972) and has been tabulated by Temperley and Lieb (1971) for several values of $\cos\mu$. In particular, at $\mu = \pi/3$, $\pi/2$ and $2\pi/3$, the exact (Temperley and Lieb 1971) results are, respectively, $\ell n 2$, $2/\pi \times$ Catalan's constant, and $3/2\ \ell n(4/3)$. However, as pointed out by Temperley and Lieb, the integral is awkward to evaluate numerically because of the logarithmic singularity at $\alpha = 0$. In our case, it is more convenient to use the result (Baxter 1972, 1984).

$$-\beta f_\infty = \ell n\left(\frac{\rho}{\cos\mu/2}\right) + \int_{-\infty}^{\infty} \frac{[\cosh(\pi-2\mu)t - \cosh\mu t]\,[\cosh\mu t - 1]}{2t\,\sinh\pi t\,\cosh\mu t}\,dt\,. \qquad (2.3.4b)$$

To estimate c, we define estimators

$$c_N = \frac{6}{\pi}\left[f_\infty - f_N\right] N^2, \qquad (2.3.5)$$

which from (2.3.2), should tend to $c = 1$ as $N \to \infty$. In Table 2.3 we show the sequence (2.3.5) for $N = 2^m$, $m = 2, 3, \ldots, 9$ at several values of μ. For all values of

Table 2.3 Finite lattice estimates (2.3.5) of the conformal anomaly ($c = 1$) of the eight-vertex model as a function of the parameter μ.

N	μ: $\pi/12$	$\pi/6$	$\pi/3$	$\pi/2$	$2\pi/3$	$5\pi/6$	$11\pi/12$
4	0.957 470	0.956 599	0.949 226	0.942 761	0.961 539	1.361 967	2.462 339
8	0.992 158	0.991 221	0.985 873	0.983 256	0.987 381	1.111 180	2.260 590
16	1.000 772	0.999 861	0.996 486	0.995 589	0.996 591	1.012 555	1.359 595
32	1.001 997	1.001 164	0.999 164	0.998 881	0.999 130	1.002 391	1.030 141
64	1.001 691	1.000 959	0.999 804	0.999 719	0.999 781	1.000 572	1.005 016
128	1.001 239	1.000 616	0.999 954	0.999 930	0.999 945	1.000 142	1.001 205
256	1.000 886	1.000 367	0.999 990	0.999 982	0.999 986	1.000 035	1.000 299
512	1.000 638	1.000 213	0.999 998	0.999 996	0.999 997	1.000 009	1.000 075

μ, the estimates are clearly seen to approach the value $c = 1$ as N increases. The convergence does appear to be slower, however, for μ less than $\pi/3$. We note also that the convergence is non-monotonic for $\mu = \pi/6$ and $\pi/12$.

To quantify the convergence rate we assume

$$c_N = 1 + aN^{-\lambda}, \quad N \to \infty \tag{2.3.6}$$

and define estimators

$$L_m = \frac{\ell n \left[(c_{2^m} - 1) / (c_{2^{m+1}} - 1) \right]}{\ell n\, 2} \to \lambda \text{ as } m \to \infty . \tag{2.3.7}$$

This sequence converges rapidly with increasing m ; in Figure 2.5 we show the estimator L_8 as a function of μ together with the value

$$\lambda = \begin{cases} \dfrac{4\mu}{\pi - \mu}, & 0 < \mu < \dfrac{\pi}{3}; \\ 2, & \dfrac{\pi}{3} < \mu < \pi , \end{cases} \tag{2.3.8}$$

which appears to account for the observed convergence over the whole range except at $\mu = \pi/3$. The value, (2.3.8), also agrees with the result obtained for the XXZ chain (Hamer 1986a, Woynarovich and Eckle 1987, Alcaraz, Barber and Batchelor 1987a,b). For $\mu = \pi/3$, as in the XXZ chain, we find that the convergence can be accounted for by assuming that $c_N \approx 1 + O((\ell n\, N)/N^2)$, where the amplitude is estimated to be approximately 0.83. The physical significance of these results will be discussed in Section 2.3.5.

2.3.2 Mass gap amplitude at criticality

Turning now to the mass gap, (2.3.1), we expect that at criticality (Cardy 1986a)

$$N\kappa_N = 2\pi x_p + o(1) \text{ as } N \to \infty , \tag{2.3.9}$$

where x_p is the anomalous dimension of the operator linking the two states $|0\rangle$ and $|1\rangle$. Since we are working in the arrow formulation of the eight-vertex model, this operator is

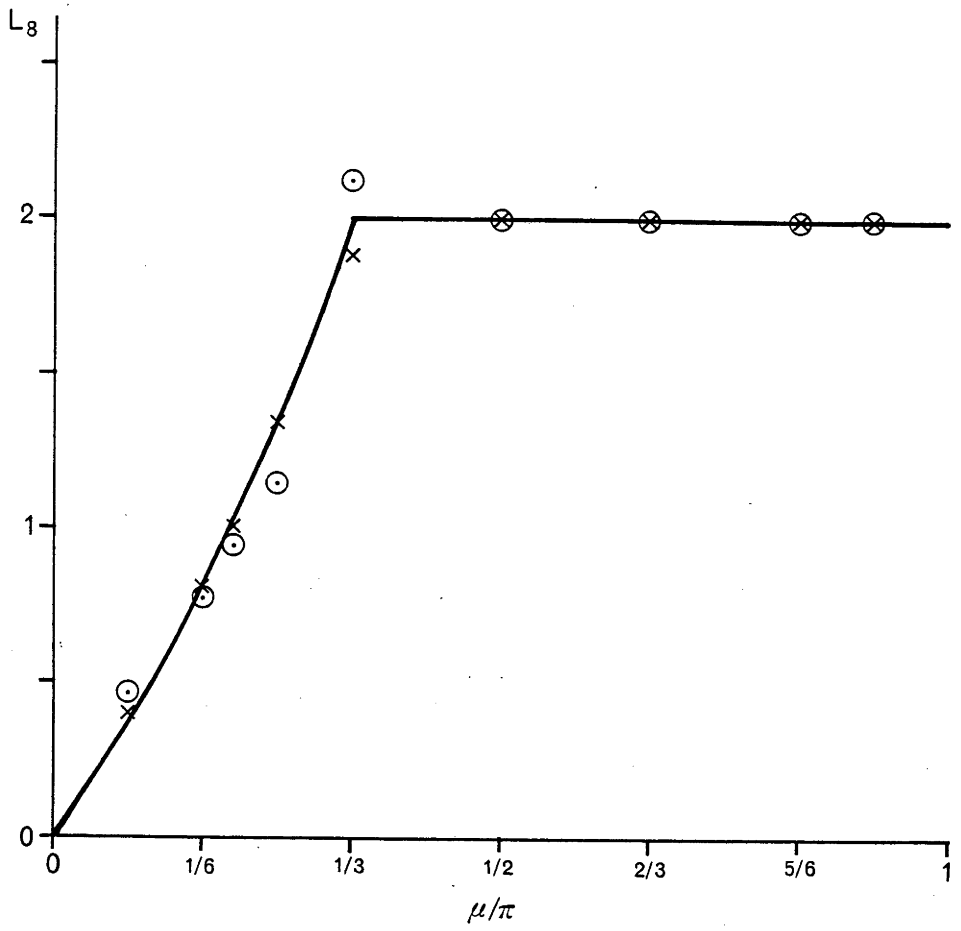

Figure 2.5 The (negated) exponent of the leading correction to the conformal anomaly estimates (2.3.6) and the polarization mass gap (2.3.9) as a function of μ. The estimators L_8 (Eqn. (2.3.7)) are indicated by the symbol $\odot$ while $\times$ indicates the corresponding estimate for the mass gap (2.3.9). The anomalous convergence at $\mu = \pi/3$ can be attributed to a logarithmic correction (see text).

associated with the polarization and hence we expect

$$x_p = \frac{\pi - \mu}{2\pi} \,. \tag{2.3.10}$$

This result was first established by Nightingale and Blöte (1983) using strips of up to 16 sites. Again, poor convergence was observed at both extremes of K_2 (this is particularly evident in Nightingale and Blöte's Figure 1(c)). The result is further supported by the values tabulated in Table 2.4. The corresponding states in the XXZ chain (*i.e.* states characterized by the same Bethe ansatz zeros), not surprisingly, yield the same exponent (see Section 3.3.2). The results of a similar analysis, as described above for c, to quantify the convergence in (2.3.9), are shown in Figure 2.5, also from strips of width $N = 256$ and 512. The leading correction to (2.3.9) is again proportional to $N^{-\lambda}$ with λ given by (2.3.8). Again at $\mu = \pi/3$, the correction is logarithmic but now of order $(\ell n\, N)/N^2$.

2.3.3 Phenomenological renormalization - location of T_c

Given data for κ_N from two different width strips, the critical line can be located by phenomenological or finite-size renormalization (Barber 1983a, Nightingale 1982); namely by solving the equation

$$N\kappa_N(\beta^* \mathbf{J}_0) = N'\kappa_{N'}(\beta^* \mathbf{J}_0) \,, \tag{2.3.11}$$

where $\mathbf{J}_0$ is a fixed direction in the parameter space $\mathbf{K} = \beta\mathbf{J}$. From the point of view of the Bethe ansatz, the most natural implementation of (2.3.11) for the symmetric eight-vertex model involves the variables p and μ with $w = 0$. Thus we estimate p^* $(= 0)$ from the solution p_N^* of

$$N\kappa_N(p^*,\mu) = N'\kappa_{N'}(p^*,\mu) \,. \tag{2.3.12}$$

The resulting estimates for several values of N with $N' = N - 4$ are shown in Figure 2.6 as a function of μ.

The choice of variables (p,μ) is rather advantageous since as we shall discuss further in Section 3.4 they correspond closely to the actual non-linear scaling fields of

Table 2.4 Finite lattice estimates $N\kappa_N/2\pi$ of the anomalous dimension x_p of the eight-vertex model polarization operator as a function of the parameter μ.

N	μ: $\pi/12$	$\pi/6$	$\pi/3$	$\pi/2$	$2\pi/3$	$5\pi/6$	$11\pi/12$
4	0.388 924	0.373 731	0.317 639	0.239 657	0.154 393	0.063 194	0.019 819
8	0.414 303	0.394 662	0.328 363	0.246 999	0.163 237	0.078 204	0.031 844
16	0.428 880	0.405 138	0.331 895	0.249 212	0.165 774	0.082 220	0.039 639
32	0.437 706	0.410 434	0.332 933	0.249 800	0.166 441	0.083 060	0.041 346
64	0.443 422	0.413 217	0.333 223	0.249 950	0.166 610	0.083 265	0.041 591
128	0.447 325	0.414 727	0.333 304	0.249 987	0.166 653	0.083 316	0.041 648
256	0.450 090	0.415 567	0.333 325	0.249 997	0.166 663	0.083 329	0.041 662
512	0.452 101	0.416 039	0.333 331	0.249 999	0.166 666	0.083 332	0.041 666
x_p	0.458 333	0.416 667	0.333 333	0.25	0.166 667	0.083 333	0.041 667

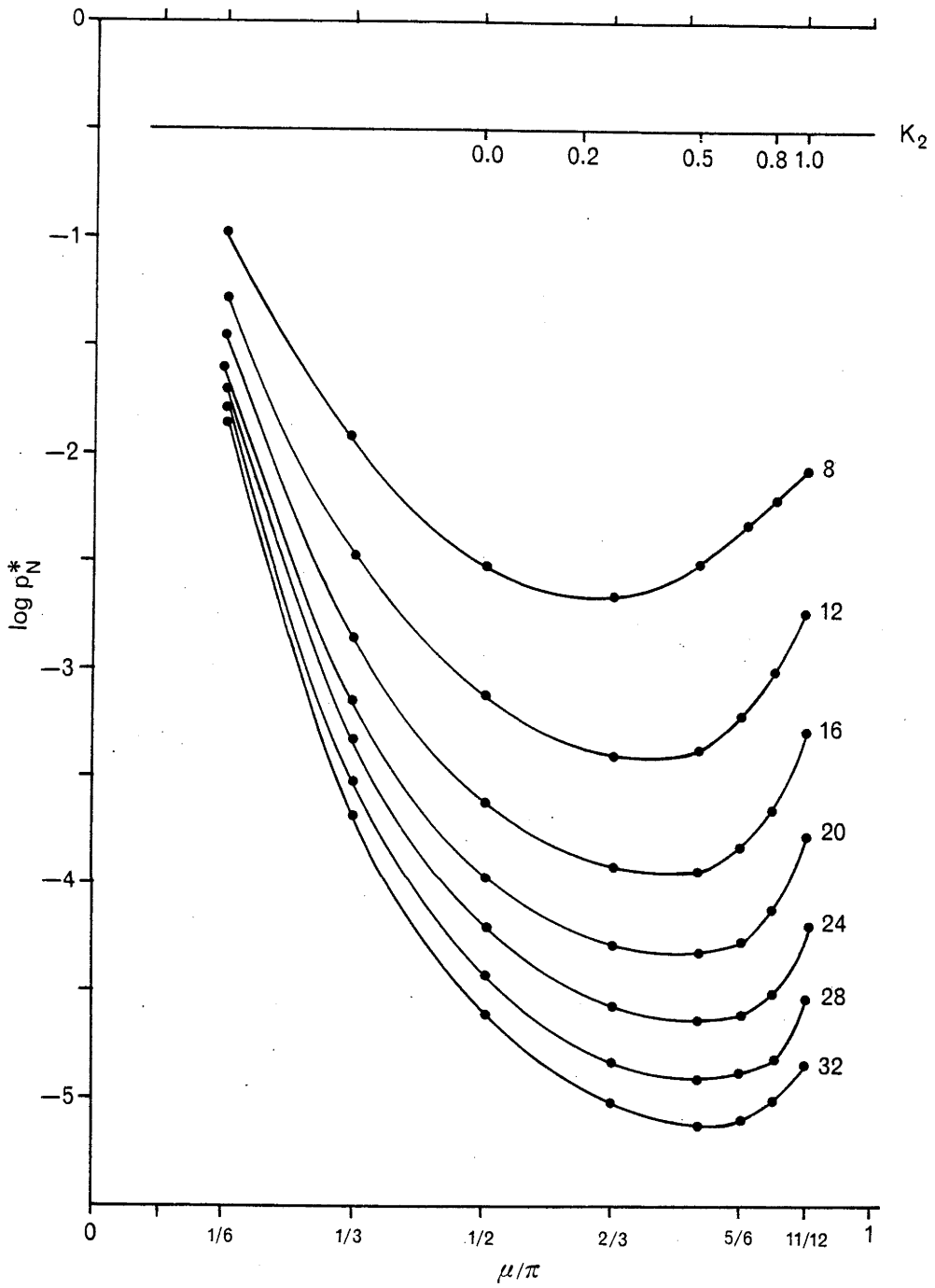

Figure 2.6 Finite lattice estimates p_N^* of the bulk critical temperature, $p^* = 0$, with increasing N as a function of the variable μ. Also shown are the corresponding values of the four-spin coupling constant K_2 at criticality.

the theory and hence minimize correction terms that would normally be expected in any realistic finite lattice calculation. A more realistic test is to revert to the magnetic spin formulation and write (2.3.12) as

$$N\kappa_N\Big(\beta^*J_1(1,\alpha)\Big) = N'\kappa_{N'}\Big(\beta^*J_1(1,\alpha)\Big)\,, \tag{2.3.13}$$

where $\alpha = K_2/K_1$ is fixed. This conforms with Nightingale's approach (Nightingale 1977, 1979, 1982), although we are using a different gap.

From the parametrization of the vertex weights given in (2.2.41) and their relation to the spin couplings in (2.2.3), the connection between the two formulations can be written

$$\exp(4K_1) = -\frac{f^2(-\sqrt{\chi^{-1}\zeta}\,,p)}{f^2(\sqrt{\chi^{-1}\zeta}\,,p)}\,, \tag{2.3.14a}$$

$$\exp(4K_1') = -\frac{f^2(-\sqrt{\chi\zeta}\,,p)}{f^2(\sqrt{\chi\zeta}\,,p)}\,, \tag{2.3.14b}$$

$$\exp(4K_2) = -\frac{f^2(\chi,p)}{f^2(-\chi,p)}\,. \tag{2.3.14c}$$

At criticality, these equations reduce to

$$\exp(2K_1) = \cot(\mu/4 - w/4)\,, \tag{2.3.15a}$$

$$\exp(2K_1') = \cot(\mu/4 + w/4)\,, \tag{2.3.15b}$$

$$\exp(2K_2) = \tan\mu/2\,. \tag{2.3.15c}$$

Thus for a given value of K_2 along the critical line, solving (2.3.13) is equivalent to solving (2.3.12) at the corresponding value of μ given in (2.3.15c). The subsequent value of p_N^* then gives the estimate $\beta_N^*J_1$ through equation (2.3.14a). The resulting estimates for the critical line converge rapidly to the exact curve (2.2.7) in agreement with the earlier studies (Nightingale 1977, 1979).

2.3.4 Phenomenological renormalization - estimate of ν

Let us now turn to the question of estimating the critical exponent ν from the phenomenological renormalization group. We have (Barber 1983a,b, 1985)

$$\left(\frac{d\beta'}{d\beta}\right)^* = r^{1/\nu} = \frac{r\left(\mathbf{J}_0 \cdot \nabla\kappa_N\right)^*}{\left(\mathbf{J}_0 \cdot \nabla\kappa_{N/r}\right)^*} , \tag{2.3.16}$$

where the asterix indicates that the expressions are to be evaluated at criticality and the gradients are with respect to $\mathbf{K}$. Again choosing $N' = N/r = N - 4$, we have the estimators

$$\nu_N^{-1} = 1 + \frac{\ell n\left[\left(\mathbf{J}_0 \cdot \nabla\kappa_N\right)^* / \left(\mathbf{J}_0 \cdot \nabla\kappa_{N-4}\right)^*\right]}{\ell n\,[N/(N-4)]} . \tag{2.3.17}$$

To extend and clarify the previous finite lattice estimates of ν, we consider (2.3.17) as (Nightingale 1982)

$$\nu_N^{-1} = 1 + \frac{\ell n\left[D_1(N)/D_1(N-4)\right]}{\ell n\,[N/(N-4)]} , \tag{2.3.18}$$

with, in general, derivatives $D_i(m)$ defined by

$$D_i(m) = \left(\frac{\partial\kappa_m}{\partial K_i}\right)^* , \quad i = 1, 2 . \tag{2.3.19}$$

The exact result for the thermal exponent can be written as (Baxter 1972, 1982)

$$y_T = \nu^{-1} = \frac{4}{\pi}\tan^{-1}\left(\exp 2K_2\right) = \frac{2\mu}{\pi} . \tag{2.3.20}$$

One of the early achievements of phenomenological renormalization was the success of Nightingale (1977, 1979) in reproducing this behaviour quantitatively. Now, in order to compare our results with those obtained in the spin formalism, it is necessary to write the derivatives in (2.3.19) in terms of the more convenient variables (p,μ). The necessary working is straightforward and is outlined in Appendix 2C. Using results (2C.3), (2C.4) and (2C.5) with $w = 0$ we have

$$D_1(m) = \frac{1}{2\sin\mu\,\sin\mu/2}\left(\frac{\partial\kappa_m}{\partial p}\right)^* + \frac{2\cos\mu}{\sin\mu/2}\left(\frac{\partial\kappa_m}{\partial\mu}\right)^*, \qquad (2.3.21a)$$

$$D_2(m) = \frac{1}{4\sin^2\mu/2}\left(\frac{\partial\kappa_m}{\partial p}\right)^* + 2\cot\mu/2\left(\frac{\partial\kappa_m}{\partial\mu}\right)^*. \qquad (2.3.21b)$$

Evaluation of critical derivatives

Let us briefly consider the evaluation of the derivatives appearing in (2.3.21). We begin by noting that the derivatives with respect to the variable μ are simply derivatives *along* the critical line, *i.e. marginal* derivatives. It is thus convenient to evaluate these derivatives *numerically* using for example the two-sided, four-point formula

$$h'(x) = \frac{h(x-2\Delta x) - 8h(x-\Delta x) + 8h(x+\Delta x) - h(x+2\Delta x)}{12\,\Delta x} + O(\Delta x)^4. \qquad (2.3.22)$$

The derivatives with respect to the temperature-like variable p are however, derivatives *across* the critical line (we shall refer to these as *thermal* derivatives). To use a two-sided derivative as in (2.3.22) we thus need to be able to calculate $T_0(\zeta)$ and $T_1(\zeta)$ *above* the critical temperature.

Fortunately in this formalism, the simple interchange $p \leftrightarrow -p$ represents the duality transformation between the low- and high-temperature phases of the model. Consider first, the largest eigenvalue $T_0(\zeta)$. The Bethe ansatz equations (2.2.47) involve elliptic functions of nome p^2. As none of the zeros characterizing $T_0(\zeta)$ are explicitly dependent on p then the duality transformation leaves $T_0(\zeta)$ unchanged. We must have

$$\left(\frac{\partial T_0}{\partial p}\right)^* = 0\,, \qquad (2.3.23)$$

and so only the derivative of $T_1(\zeta)$ need be considered. Recall that this eigenvalue has an exact zero at $\zeta_1 = p$. Duality dictates that $T_1(\zeta)$ maps to an eigenvalue with an exact zero given by $\zeta_1 = -p$, the remaining zeros being invariant under the transformation.

This is indeed the case, the eigenvalue $T_1(\zeta)$ *crosses* at criticality with the leading eigenvalue in the other sector. We observe that the zero $\zeta_1 = -p$ in fact corresponds, in this language, to a 0-string excitation (Johnson *et al.* 1973). Thus in evaluating the derivative $T_1(\zeta)$ at criticality using (2.3.22) we also compute the leading 0-string eigenvalue. This eigenvalue has associated quantum numbers $\nu = \nu' = \nu'' = 1$ and in terms of the original variables in Section 2.2.2 has an exact zero at $z_1 = -q^{1/2}$ (the zero at $z_1 = -1$ is excited to this position). This level gives in fact, in the spin language, the largest eigenvalue with *antiperiodic* boundary conditions†. In Figure 2.7 we show these levels schematically as a function of the variable p. We have observed that, in this formalism, quite literally, the *whole* spectrum can be 'folded over' the vertical line through $p = 0$.

Alternatively, exact expressions can be derived for the derivatives appearing in (2.3.21), although such expressions involve solving a further set of linear simultaneous equations for the derivatives of the zeros characterizing $T_0(\zeta)$ and $T_1(\zeta)$. However, for large N in particular, we have chosen to evaluate the derivatives of the mass gap in this manner. This necessitates only the computation of the zeros characterizing $T_0(\zeta)$ and $T_1(\zeta)$ *at* criticality. We derive these equations in Appendix 2D. Finally we mention that we have compared our results for the derivatives in (2.3.21) with the exact "brute force" results for lattice sizes $N = 4$ and $N = 8$. We proceed now to our estimates of the critical exponent ν.

Numerical Results

As an illustrative example of our results, we show in Figure 2.8a the finite lattice estimates (2.3.18) as a function of the four-spin coupling K_2 for the particular value $N = 64$. Also shown is the direction in which the finite lattice estimates converge to the

---

† Using (2.2.36), (2.3.1), (2.3.2) and (2.3.8) then gives $(5\pi/6 - \mu)N^{-2}$ as the leading correction to the free-energy per site of the eight-vertex model with anti-periodic boundary conditions in the spin formulation.

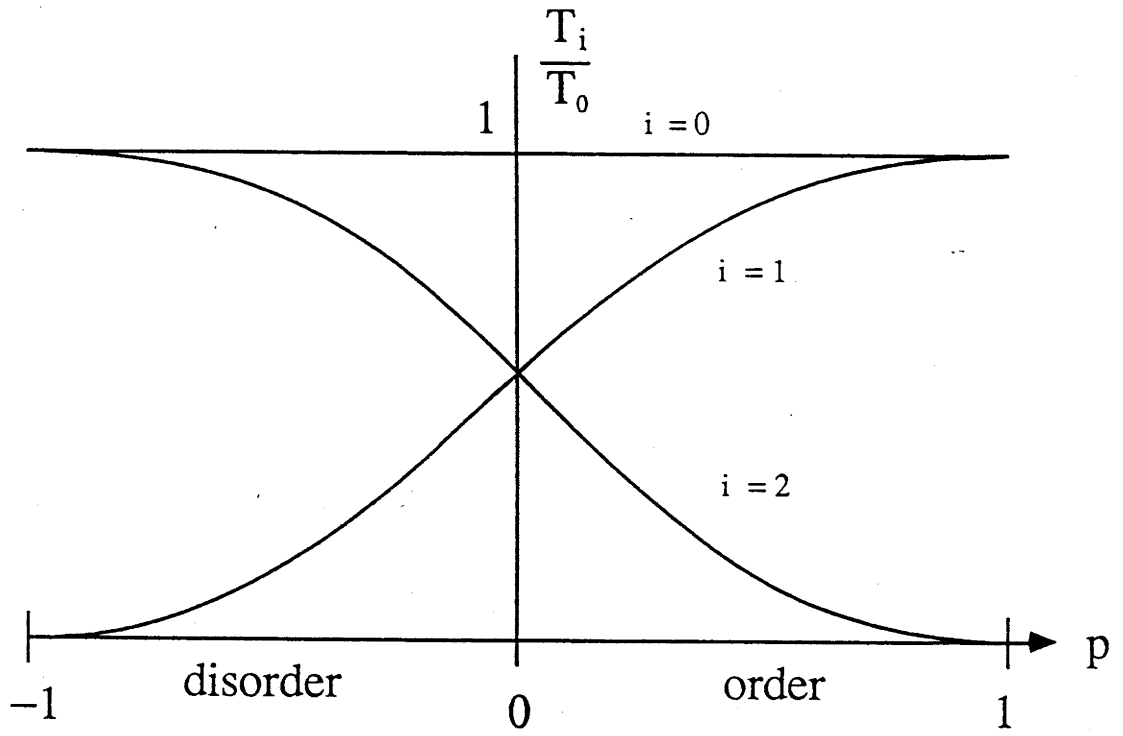

Figure 2.7 Schematic illustration of the three leading eigenvalues of the eight-vertex model on a finite lattice. Eigenvalue $T_1(\zeta)$ crosses at criticality with the leading 0-string eigenvalue, $T_2(\zeta)$.

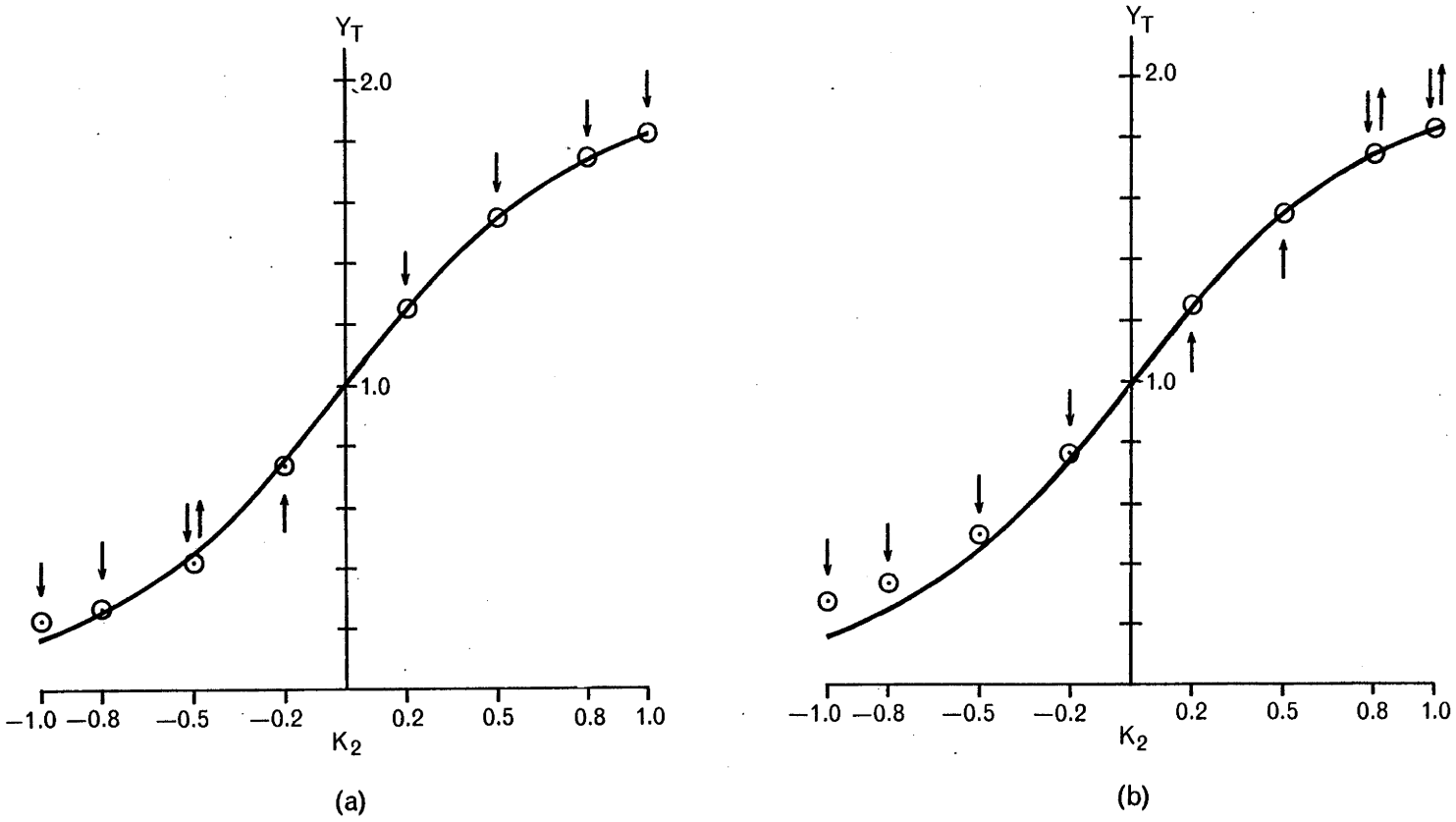

Figure 2.8 Estimates of the thermal exponent y_T of the eight-vertex model as a function of the four-spin coupling K_2 obtained from strips of width N = 64 and N' = 60. The solid line is the exact value of y_T. The arrows indicate the direction of convergence (see text). The mass gaps defined in (2.3.1) and (2.3.24) are used, respectively, for (a) and (b).

exact result (2.3.20); a downward pointing arrow indicating convergence from above *etc.* For the mass gap (2.3.1), the convergence is *monotonic* for large values of the four-spin coupling. At the particular point $K_2 = -0.5$, however, the estimates successively decrease from above the critical temperature until at $N = 60$ they begin to converge uniformly from below (the exact value lies between the $N = 12$ and $N = 16$ estimates).

At first glance these results appear somewhat surprising as the previous results (Nightingale 1977, 1979, Barber 1985) for strips of width up to $N = 16$ showed non-monotonic convergence for $K_2 \geq 0.5$. Recall however, that we are using a different gap. We can readily define a further gap by

$$\kappa_N^{(2)} = \ell n\left(T_0/T_2\right), \qquad (2.3.24)$$

with T_2 the leading eigenvalue in the sector with $\nu = \nu' = 1$ (as discussed above). The critical derivatives of this gap are easily obtained from those of κ; the derivative with respect to μ is the same, but the thermal derivative has opposite sign (recall Figure 2.7).

The finite lattice estimates (2.3.18) using the gap (2.3.24) are shown in Figure 2.8b, also for $N = 64$. Again the convergence is monotonic with now the estimates at $K_2 = 0.8$ and $K_2 = 1.0$ the exceptions. As for the previous gap, such estimates initially approach the bulk critical line from above but "overshoot" the exact values. Here this occurs at $N = 20$ for $K_2 = 0.8$ and $N = 48$ for $K_2 = 1.0$. The trend in convergence changes direction at, respectively, $N = 32$ and $N = 72$.

The common factor in Figure 2.8 is the poor convergence for $K_2 \leq -0.5$. In the next section, we will relate this to the change (recall (2.3.8)) found for estimates of c and the mass gap amplitude in Sections 2.3.1 and 2.3.2 . (In spin language, the value $\mu = \pi/3$ corresponds to $K_2 = -0.274\ldots$.) As we have seen, however, the convergence rate can also be 'distorted' by the behaviour of the derivatives in (2.3.21). In particular, for the mass gap (2.3.24) in which the thermal derivative is negative, the initial overshooting of the exact critical temperatures for large K_2 is reminiscent of the non-monotonic behaviour seen by Nightingale (1977, 1979) and Barber (1985).

Unfortunately, the direct extension of Nightingale's results, by using the same gap, is beyond the scope of this paper. The recovery of this gap from the arrow formulation of the eight-vertex model appears to require imposing *anti-periodic* boundary conditions on the arrows as has recently been pointed out by Davies (1987).

2.3.5 Convergence Rates

In Section 2.3.2, we found that *at* criticality

$$N\kappa_N = 2\pi x_p + O(N^{-\lambda}) , \tag{2.3.25}$$

where λ is given by (2.3.8). On the basis of conformal invariance, Cardy (1986a) has shown that the correction terms in (2.3.25) arise since the physical critical Hamiltonian differs from the conformally invariant fixed point Hamiltonian by terms involving irrelevant operators†.

Writing

$$H_c = H^* + \sum_i \alpha_i O_i , \tag{2.3.26}$$

Cardy showed that a gap, such as κ_N, should behave at criticality as

$$\kappa_N \sim \frac{2\pi}{N}\left(x_p + \sum_i \alpha_i C_{ppi} \left(\frac{2\pi}{N}\right)^{2-x_i} + \ldots \right) , \tag{2.3.27}$$

where x_i (>2) is the anomalous dimension of the operator O_i and C_{ppi} is the relevant (universal) operator algebra coefficient.

A naive interpretation of our conclusion (2.3.25) would identify $\lambda + 2$ with the dimension of the dominant irrelevant operator (the so-called correction-to-scaling exponent). In the XXZ chain, this identification is, however, incorrect since the

---

† The role of irrelevant operators in the corrections to finite-size scaling were pointed out by Barber (1983a) and discussed in detail by Privman and Fisher (1983). (See also Reinicke 1987a.)

eigen-spectrum contains no gaps that can be related to the existence of an operator with such a dimension (see Section 3.3). While we have not made a similar exhaustive search of the eigen-spectrum of the eight-vertex model transfer matrix, the close similarity of the two problems at criticality suggests that the corections to scaling should be of the same origin. In the XXZ model, these can be explained (Barber 1983a, Alcaraz, Barber and Batchelor 1987a,b; see also Section 3.6) by assuming that two irrelevant operators are involved: O_I with dimension $x_I = 4$ and O_{II} with dimension $x_{II} = 1/x_p = 2\pi/(\pi-\mu)$. The operator O_I belongs to the conformal block of the identity operator and gives rise to "analytic" corrections. On the other hand, O_{II} leads to non-analytic corrections but only couples to the relevant operators in *second* order, *i.e.* $C_{ppII} = 0$. As a result

$$N\kappa_N \approx 2\pi x_p + A_I N^{-2} + A_{II} N^{2x_{II}-4}, \qquad (2.3.28)$$

If we accept that this assumption is also valid for the eight-vertex model we are able to account, not only for the convergence of κ_N and c_N, but also for the convergence of the phenomenological renormalization estimators p_N^* and ν_N^*. To do so, we assume that $\kappa_N(p,\mu)$ has the generalized finite-size scaling form

$$\kappa_N(p,\mu) \sim N^{-1} Q(g_T N^{y_T}, g_m, g_I N^{-2}, g_{II} N^{-y}), \qquad (2.3.29)$$

where $g_T \sim p \sim T - T_c$ is the thermal field, $g_m \sim K_2 \sim \mu - \pi/2$ is marginal and we have set $y = x_{II} - 2 = 2\mu/(\pi-\mu)$. To recover (2.3.28), we require

$$Q(0, g, u, v) = 2\pi x_p + A_I(g)u + A_{II}(g)v^2 + \ldots \qquad (2.3.30)$$

as $u, v \to 0$. Prediction of the asymptotic behaviour of p_N^* and ν_N^* requires also the behaviour of $Q(x,\ldots)$ for small x. Since this limit involves a relevant variable, it appears, at first site, that conformal invariance can no longer be used to determine the leading behaviour. However, (2.3.27) remains, in fact, valid for relevant perturbations†.

---

† This has also been realized recently by Reinicke (1987b), who showed that it was possible, given the knowledge of certain correlation functions, to explicitly compute the coefficients of the scaling function at small argument. It would be interesting to extend Reinicke's calculations to the eight-vertex model.

Hence we find that

$$Q(x,g,u,v) = 2\pi x_p + A_0(g)\,x\left[1 + b_I(g)u + b_{II}(g)v^2 + \ldots\right] + A_I(g)u + A_{II}(g)v^2 + \ldots \qquad (2.3.31)$$

as $x, u, v \to 0$, where the absence of a term of order xv is due to the same selection rule that prevented a term of order v in (2.3.30).

With this result, it is straightforward to extend the analysis of Privman and Fisher (1983) (see also Barber 1985) to show that (these results have been derived solely by Michael Barber)

$$p_N^* \sim DN^{-y_T-\lambda}, \quad N \to \infty \qquad (2.3.32)$$

while

$$\nu_N^{-1}{}^* \sim \nu^{-1} + D'N^{-y_T}, \quad N \to \infty \qquad (2.3.33)$$

The occurence of logarithmic factors at $\mu = \pi/3$ can also be understood. At this value, $y_I = 2 - x_I$ and $y_{II} = 2 - x_{II}$ satisfy a linear relation, namely $y_I = 2y_{II}$, which results in additional logarithmic factors (Wegner 1972).

We now turn to the numerical confirmation of the results (2.3.32) and (2.3.33). From (2.3.32), we assume

$$p_N^* \sim DN^{-\omega}, \quad N \to \infty \qquad (2.3.34)$$

and define estimators

$$\omega_N = \frac{\ell n\left(p_{N-4}^* / p_N^*\right)}{\ell n[N/(N-4)]} \to \omega \text{ as } N \to \infty . \qquad (2.3.35)$$

Figure 2.9 shows this sequence for $N = 16$, 32 and 64. Also shown is the value $\omega = y_T + \lambda$, with the exponent λ defined in (2.3.8). Unfortunately the sequence (2.3.35) cannot in general be calculated for larger N as $p_N{}^*$ rapidly approaches the numerical precision of our solutions. Nevertheless, the results shown clearly point to the validity of (2.3.32).

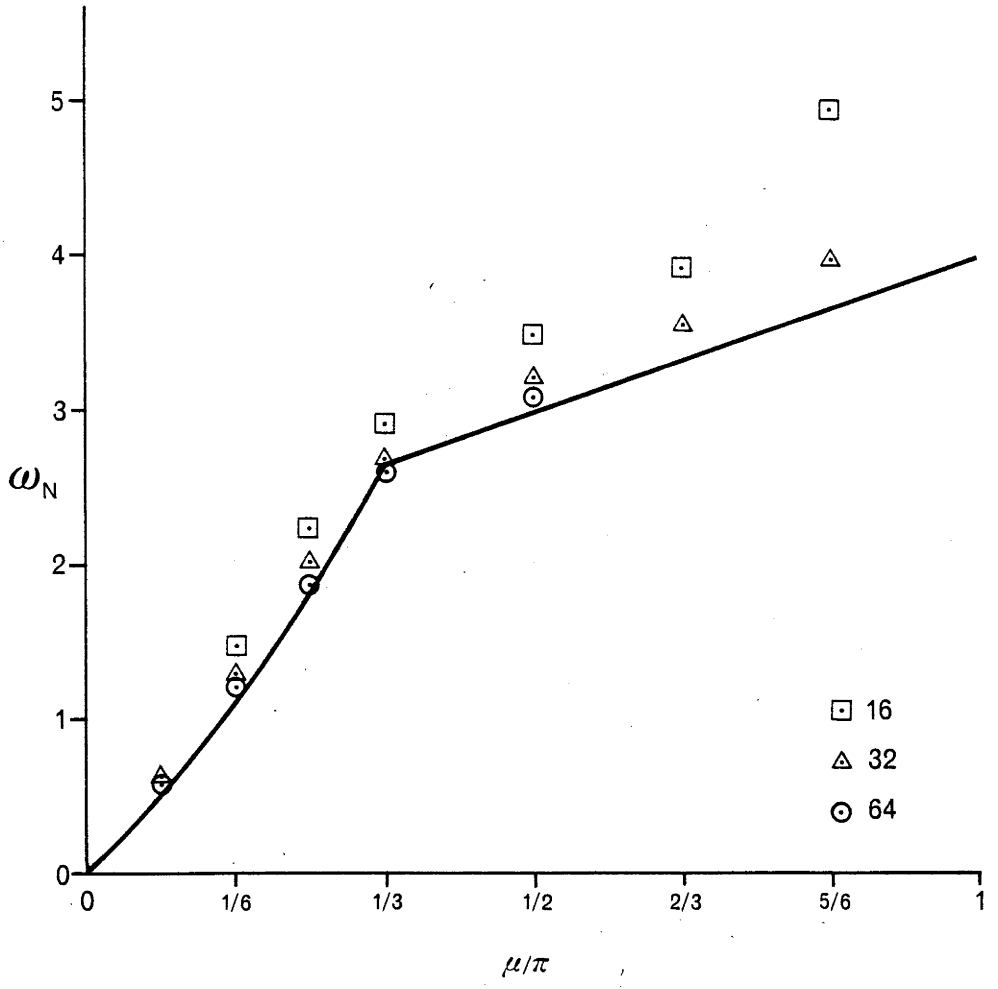

Figure 2.9 Estimates ω_N (Eqn. (2.3.35)) of the leading correction to the finite lattice estimates of the critical temperature as a function of μ. The solid line is the exact value $y_T + \lambda$.

To test (2.3.33), we set $y = \nu^{-1}$, assume

$$y_N^* \sim y + D'N^{-\theta}, \quad N \to \infty \tag{2.3.36}$$

and define the estimators

$$\theta_m = \frac{\ell n\left(\Delta y_{2^m}^* / \Delta y_{2^{m+1}}^*\right)}{\ell n\, 2} \to \theta \text{ as } N \to \infty, \tag{2.3.37}$$

where $\Delta y_N^* = y_N^* - y$. Figure 2.10 shows this sequence as a function of K_2 for the particular values $m = 4, 6$ and 8. For $K_2 > 0$ and $K_2 < 0$ we have used, respectively, the mass gaps (2.3.1) and (2.3.24). The estimators in (3.37) are amenable to extrapolation (Barber 1983a) and in all cases we find excellent agreement with the predictions in (2.3.33).

The result (2.3.33) can be reproduced exactly in the Ising limit. Using the results of Appendix 2D, the derivatives of the mass gaps (2.3.1) and (2.3.24) assume the simple form

$$\left(\frac{\partial \kappa}{\partial K_1}\right)^* = -2\sqrt{2}, \qquad \left(\frac{\partial \kappa}{\partial K_2}\right)^* = -2\left(1 + \frac{1}{N}\right), \tag{2.3.38}$$

$$\left(\frac{\partial \kappa^{(2)}}{\partial K_1}\right)^* = 2\sqrt{2}, \qquad \left(\frac{\partial \kappa^{(2)}}{\partial K_2}\right)^* = 2\left(1 - \frac{1}{N}\right). \tag{2.3.39}$$

Thus for both gaps, the estimators (2.3.18) yield the exact thermal exponent for all N. However, the corresponding estimators with K_2 derivatives are seen to converge as N^{-1}, in agreement with (2.3.33).

2.3.6 Scaling function

Finally, it is of interest to numerically compute the scaling function for κ. Neglecting corrections due to the irrelevant fields, (2.3.29) implies that

$$\kappa_N(p,\mu) \sim N^{-1} Q(pN^{1/\nu};\mu), \tag{2.3.40}$$

as $N \to \infty$ and $p \to 0$ with $pN^{1/\nu}$ order unity. Hence for fixed μ, a plot of $N\kappa_N$

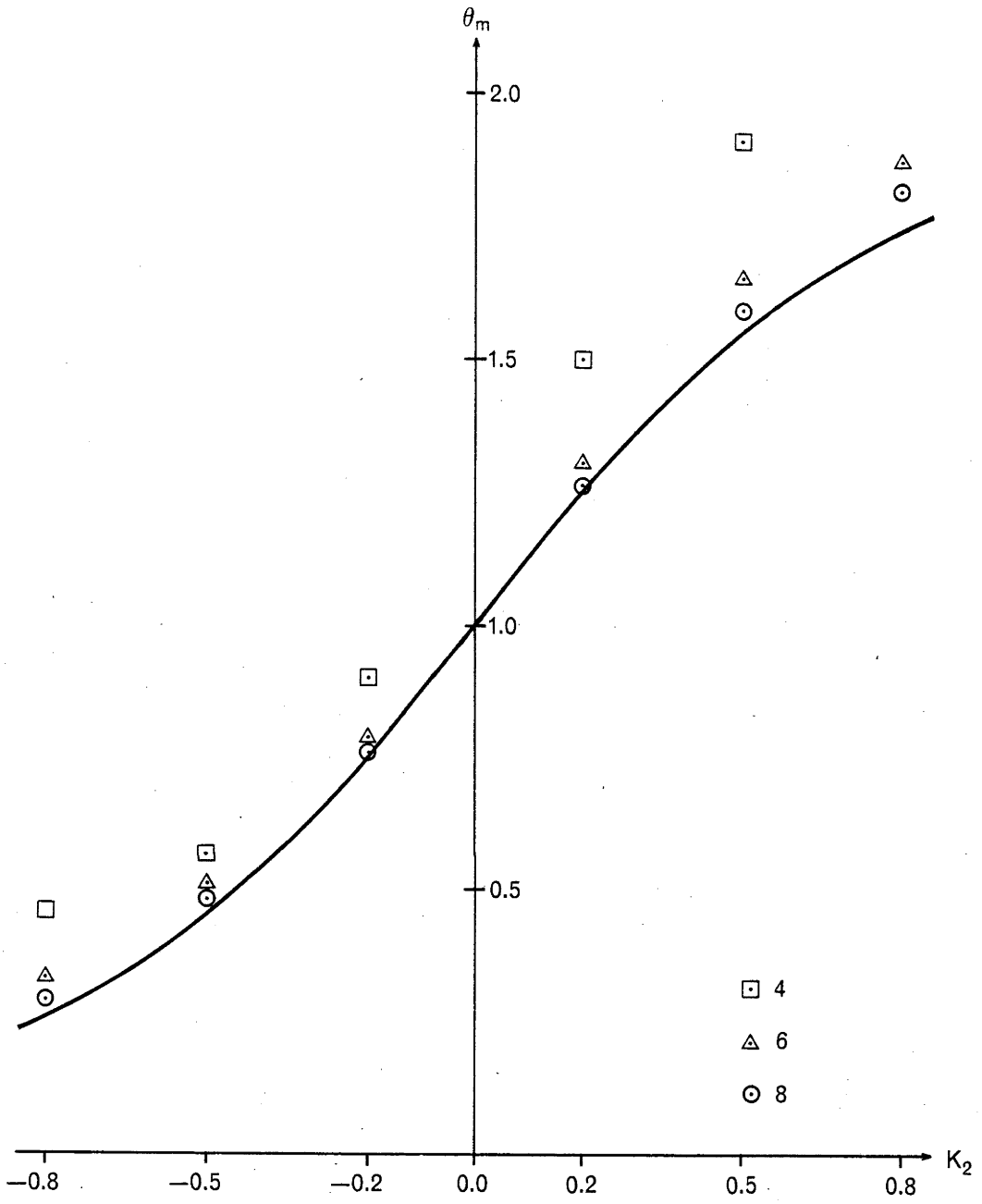

Figure 2.10 Estimates θ_m (Eqn. (2.3.37)) of the leading correction to the finite lattice estimates of the thermal exponent as a function of the four-spin coupling K_2. The solid line is the exact value y_T.

versus $pN^{1/\nu}$ should reduce to a single curve. In Figure 2.11 we show such a plot for the particular values $\mu = \pi/3$ and $\mu = 2\pi/3$. We show only the curve obtained from a strip of width $N = 128$; the error is expected to be no greater than the width of each line.

Two asymptotic regimes of the scaling function (2.3.40) are known. From (2.3.30) we observe that

$$Q(x;\mu) = \pi - \mu + O(x), \quad x \to 0, \tag{2.3.41}$$

while to recover the bulk behaviour we require, as usual in finite-size scaling, that

$$Q(x;\mu) = Q_\infty x^{-\nu} , \quad x \to \infty . \tag{2.3.42}$$

Figure 2.11 clearly demonstrates the cross-over between these two asymptotic regimes.

2.4 LINEAR SCALING FIELDS

It is very apparent from the discussion in Section 2.3.5 that criticality in the eight-vertex model involves several scaling fields. On the other hand, conventional phenomenological renormalization, unlike a microscopic renormalization group, gives no direct information on the scaling field structure of a model. Two methods of estimating linear scaling fields and their critical exponents from finite-lattice data have been recently proposed by Barber (1983b, 1985). To formulate these methods, recall (Fisher 1974, Barber 1977) that for a system described by a set $\mathbf{K}$ of coupling constants the critical exponents and related linear scaling fields are associated with the fixed points $\mathbf{K}^*$ of some microscopic renormalization of the couplings

$$\mathbf{K} \to \mathbf{K}' = \mathfrak{R}_r(\mathbf{K}) , \tag{2.4.1}$$

in which r (>1) is the spatial rescaling factor in the transformation. By linearizing (2.4.1) around a particular fixed point, the exponents are given by the eigenvalues $\Lambda_\alpha = r^{y_\alpha}$, $y_\alpha = 2 - x_\alpha$, of the matrix

$$T_{i,j} = \left(\frac{\partial K'_i}{\partial K_j} \right)^* , \tag{2.4.2}$$

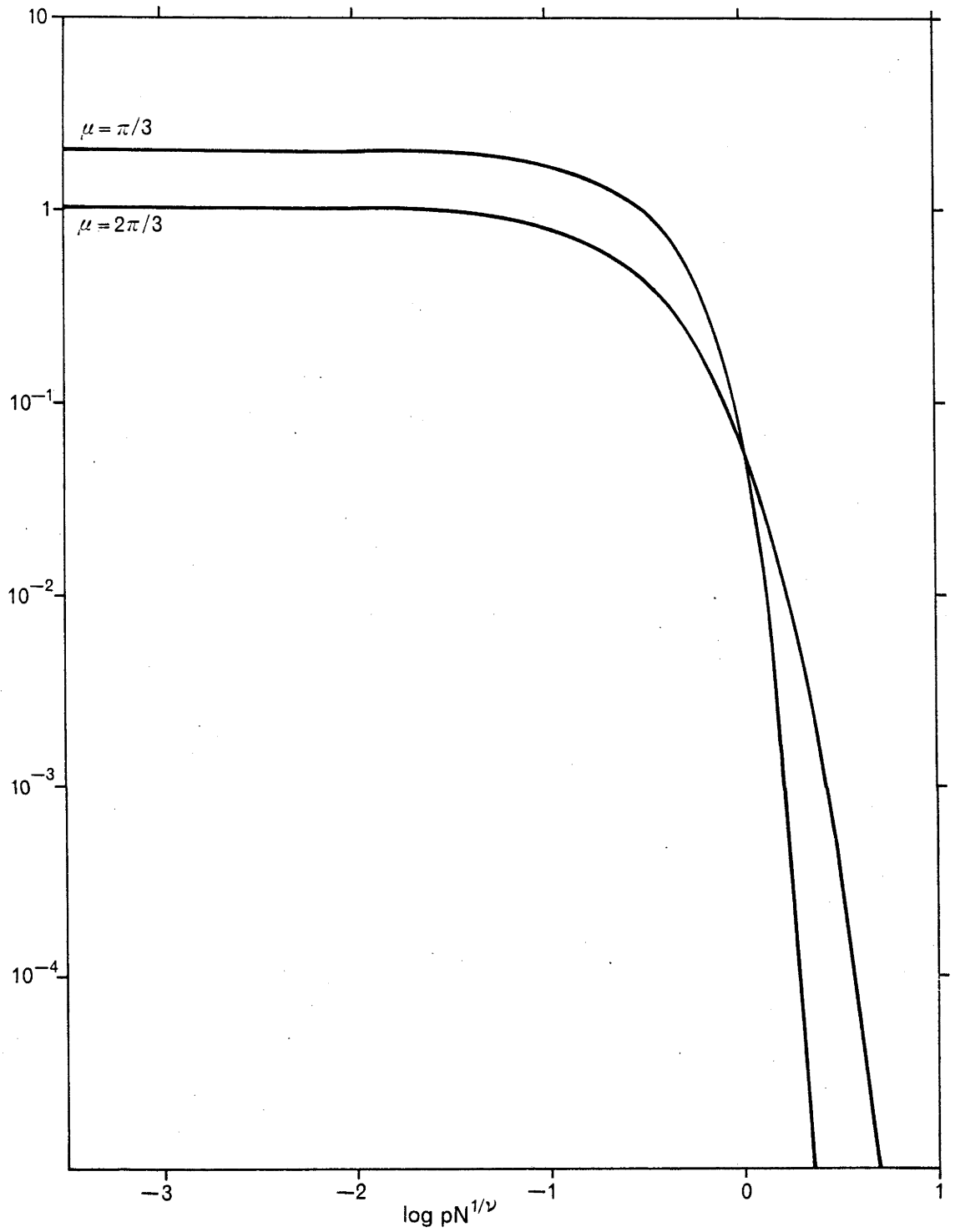

Figure 2.11 Scaling function $Q(pN^{1/\nu};\mu)$ for the eight-vertex model mass gap κ at the particular values $\mu = \pi/3$ and $\mu = 2\pi/3$.

where the derivative is evaluated at $\mathbf{K} = \mathbf{K}^*$. The associated linear scaling fields are given by

$$u_\alpha = \mathbf{f}_\alpha \cdot (\mathbf{K} - \mathbf{K}^*) , \tag{2.4.3}$$

where $\mathbf{f}_\alpha$ is the left eigenvector of $\mathbf{T}$ with eigenvalue Λ_α. We now proceed to derive exact expressions for the amplitudes appearing in (2.4.3).

2.4.1 Linear scaling fields for the eight-vertex model - exact results

Exact expressions for the linear scaling fields of the eight-vertex model, in the spin formulation (2.4.3), can be extracted from equations (2.3.14a-c) by considering the quantities (Paul Pearce showed me how to get at the exact results)

$$u_p \approx (\nabla p)^* \cdot (\mathbf{K} - \mathbf{K}^*) , \tag{2.4.4a}$$

$$u_\mu \approx (\nabla \mu)^* \cdot (\mathbf{K} - \mathbf{K}^*) , \tag{2.4.4b}$$

$$u_w \approx (\nabla w)^* \cdot (\mathbf{K} - \mathbf{K}^*) , \tag{2.4.4c}$$

where the derivatives are with respect to $\mathbf{K}$ and are to be evaluated at criticality. As remarked previously, the variables (p,μ,w) correspond closely to the actual nonlinear scaling fields of the theory (see, *e.g.* the expression for the bulk free energy in Eqn. (10.12.12) of Baxter 1982). The derivatives in (2.4.4) are given in Appendix 2C. Normalizing the fields so that

$$u_1 = (K_1 - K_1^*) + a(1,1')\,(K'_1 - K'^*_1) + a(1,2)\,(K_2 - K_2^*) , \tag{2.4.5a}$$

$$u'_1 = (K'_1 - K'^*_1) + a(1',1)\,(K_1 - K_1^*) + a(1',2)\,(K_2 - K_2^*) , \tag{2.4.5b}$$

$$u_2 = (K_2 - K_2^*) + a(2,1)\,(K_1 - K_1^*) + a(2,1')\,(K'_1 - K'^*_1) , \tag{2.4.5c}$$

we obtain

$$a(1,1') = \frac{\sin(\mu/2+w/2)}{\sin(\mu/2-w/2)} , \quad a(1,2) = \frac{\sin\mu}{\sin(\mu/2-w/2)} , \tag{2.4.6a}$$

$$a(1',1) = -\frac{\sin(\mu/2-w/2)}{\sin(\mu/2+w/2)} , \quad a(1',2) = \frac{\sin 2\mu \sin w}{\sin(\mu/2+w/2)\left[\sin 2\mu - 2\sin(\mu-w)\right]} , \tag{2.4.6b}$$

$$a(2,1) = \frac{\cos\mu \sin(\mu/2-w/2)}{\sin\mu \cos w}, \quad a(2,1') = \frac{\cos\mu \sin(\mu/2+w/2)}{\sin\mu \cos w} . \qquad (2.4.6c)$$

These results simplify considerably in the following two special limits.

Anisotropic Ising limit $\mu = \pi/2$

In this limit the variable w varies the strength of the anisotropic nearest neighbour couplings on the two independent sublattices. The linear scaling fields (2.4.5a-c) reduce to

$$u_1 = (K_1 - K_1^*) + \frac{\cos w/2 + \sin w/2}{\cos w/2 - \sin w/2} (K_1' - K_1'^*) , \qquad (2.4.7a)$$

$$u_1' = (K_1' - K_1'^*) - \frac{\cos w/2 - \sin w/2}{\cos w/2 + \sin w/2} (K_1 - K_1^*) , \qquad (2.4.7b)$$

$$u_2 = 0 . \qquad (2.4.7c)$$

Recalling (2.3.15a) and (2.3.15b), the amplitudes may be written as $a_1 = \sinh 2K_1$ and $a'_1 = -1/a_1$, agreeing with the results derived by Barber (1985). The corresponding exponents are $y_1 = 1$ and $y'_1 = 0$.

Isotropic eight-vertex limit $w = 0$

Here the variable μ alters the strength of the spin coupling constants through (2.3.15a) and (2.3.15c). The linear scaling fields are

$$u_1 = 2 (K_1 - K_1^*) + 2 \cos\mu/2 (K_2 - K_2^*) , \qquad (2.4.8a)$$

$$u_1' = 0 , \qquad (2.4.8b)$$

$$u_2 = (K_2 - K_2^*) + \frac{\cos\mu}{\cos\mu/2} (K_1 - K_1^*) . \qquad (2.4.8c)$$

Renormalizing as in Barber (1985), we define amplitudes $a_1 = \cos(\mu/2)$ and $a_2 = \cos\mu / \cos(\mu/2)$, which in terms of the four-spin coupling constant K_2, may be written

$$a_1 = \frac{1}{\sqrt{1+e^{4K_2}}} , \qquad a_2 = \frac{1-e^{4K_2}}{\sqrt{1+e^{4K_2}}} . \tag{2.4.9}$$

The amplitude a_1 of the thermal field agrees with Barber's result (a minus sign is in fact missing from the result quoted in Barber (1985)), while the amplitude a_2 of the subdominant (marginal) field was previously unknown. In this case $y_1 = y_T$ with y_T given in (2.3.20) and, as for the anisotropic Ising model (Barber 1985), $y_2 = 0$.

2.4.2 Numerical Results

Here we implement and fully test Barber's Method A. Using finite-lattice data, this method explicitly constructs the transformation matrix defined in (2.4.2) from which the scaling fields and exponents readily follow. Specifically, in the isotropic limit we define 2×2 matrices $\mathbf{L}$ and $\mathbf{M}$ by

$$L_{i,j} = D_j(l_i) , \qquad M_{i,j} = D_j(m_i) . \tag{2.4.10}$$

The matrix $\mathbf{T}$ can then be written as (Barber 1983b, 1985)

$$\mathbf{T} = r\,\mathbf{M}^{-1}\mathbf{L} , \tag{2.4.11}$$

where the two pairs of strips (l_1,m_1) and (l_2,m_2) are such that $l_i = r\,m_i$. The linear scaling fields defined in (2.4.3) can then be found from the right eigenvectors of $\mathbf{T}$,

$$\mathbf{e}_i = (\cos\theta_i , \sin\theta_i) , \quad i = 1, 2 \tag{2.4.12}$$

with the result that $a_1 = -\cot\theta_2$ and $a_2 = -\tan\theta_1$. As indicated above, the related exponents follow from the eigenvalues through $\Lambda_i = r^{y_i}$, $i = 1, 2$.

In Table 2.5 we show sequences of finite lattice estimates obtained from the mass gaps (2.3.1) and (2.3.24) at $K_2 = 0.2$, 0.5, 0.8 and 1.0 . (Here quantities obtained from (2.3.1) and (2.3.24) are denoted by, respectively, (1) and (2)). For convenience we have used triplets of lattice sizes. For a given triplet, a different matrix $\mathbf{T}$ is constructed from each gap, yet both matrices are seen to have common eigenvalues and thus produce the same exponent estimates.

Table 2.5a Phenomenolgical renormalization estimates of the exponents $y_1 = y_T$, $y_2 = y_m$ and linear scaling field amplitudes $a_1 = a_T$, $a_2 = a_m$ of the eight-vertex model at (i) $K_2 = 0.2$ and (ii) $K_2 = 0.5$.

r	lattices	y_1	$a_1^{(1)}$	$a_1^{(2)}$	y_2	$a_2^{(1)}$	$a_2^{(2)}$
(i)							
2	(4,8,16)	1.242 628	0.588 362	0.555 239	–0.055 390	–1.088	–0.377
	(8,16,32)	1.246 684	0.556 942	0.556 656	–0.011 898	–0.914	–0.487
	(16,32,64)	1.247 755	0.556 814	0.556 785	–0.002 875	–0.816	–0.562
	(32,64,128)	1.248 026	0.556 801	0.556 798	–0.000 713	–0.760	–0.609
	(64,128,256)	1.248 094	0.556 799	0.556 799	–0.000 178	–0.728	–0.638
	(128,256,512)	1.248 111	"	"	–0.000 044	–0.709	–0.656
4/3	(288,384,512)	1.248 115	"	"	–0.000 016	–0.701	–0.664
8/7	(392,488,512)	1.248 115	"	"	–0.000 016	–0.698	–0.667
	exact	1.248 117	0.556 799		0	–0.682	
(ii)							
2	(4,8,16)	1.534 152	0.347 120	0.343 404	–0.176 223	–10.83	–0.237
	(8,16,32)	1.547 583	0.345 415	0.345 101	–0.037 280	–5.703	–0.731
	(16,32,64)	1.550 483	0.345 263	0.345 252	–0.004 215	–4.044	–1.138
	(32,64,128)	1.551 003	0.345 258	0.345 257	–0.000 904	–3.405	–1.390
	(64,128,256)	1.551 126	"	0.345 258	–0.000 218	–3.028	–1.584
	(128,256,512)	1.551 156	"	"	–0.000 054	–2.783	–1.735
4/3	(288,384,512)	1.551 162	"	"	–0.000 019	–2.652	–1.826
8/7	(392,488,512)	1.551 163	"	"	–0.000 014	–2.616	–1.853
	exact	1.551 166	0.345 258		0	–2.206	

Table 2.5b Phenomenolgical renormalization estimates of the exponents $y_1 = y_T$, $y_2 = y_m$ and linear scaling field amplitudes $a_1 = a_T$, $a_2 = a_m$ of the eight-vertex model at (i) $K_2 = 0.8$ and (ii) $K_2 = 1.0$.

r	lattices	y_1	$a_1^{(1)}$	$a_1^{(2)}$	y_2	$a_2^{(1)}$	$a_2^{(2)}$
(i)							
2	(4,8,16)	1.744 949	0.195 969	0.199 856	0.139 950	23.77	1.198
	(8,16,32)	1.730 084	0.198 175	0.197 632	–0.182 414	17.92	1.528
	(16,32,64)	1.744 552	0.197 917	0.197 890	–0.025 515	–83.54	–0.084
	(32,64,128)	1.746 145	0.197 903	0.197 903	–0.001 312	–17.49	–1.135
	(64,128,256)	1.746 302	"	"	–0.000 241	–13.02	–1.586
	(128,256,512)	1.746 336	"	"	–0.000 056	–10.75	–1.956
4/3	(288,384,512)	1.746 342	"	"	–0.000 020	–9.587	–2.211
8/7	(392,488,512)	1.746 344	"	"	–0.000 014	–9.271	–2.291
	exact	1.746 347	0.197 903		0	–0.682	
(ii)							
2	(4,8,16)	1.944 347	0.130 026	0.138 325	0.579 105	27.96	2.061
	(8,16,32)	1.806 340	0.134 140	0.134 085	–0.114 101	12.80	4.368
	(16,32,64)	1.820 475	0.134 146	0.134 080	–0.119 200	15.18	3.699
	(32,64,128)	1.828 338	0.134 113	0.134 112	–0.005 446	129.6	0.548
	(64,128,256)	1.828 677	"	"	–0.000 305	–88.90	–0.468
	(128,256,512)	1.828 715	"	"	–0.000 060	–48.51	–0.968
4/3	(288,384,512)	1.828 722	"	"	–0.000 020	–37.14	–1.304
8/7	(392,488,512)	1.828 723	"	"	–0.000 014	–34.55	–1.412
	exact	1.828 726	0.134 113		0	–7.188	

As was borne out in the earlier results (Barber 1985), the agreement of the thermal field and its exponent with the exact values is excellent for all K_2. Further we observe that for $K_2 \geq 0.5$ the initial estimates in the sequence for y_1 are non-monotonic. As we saw in Section 2.3 however, the sequences settle down into monotonic behaviour as they enter into the asymptotic regime. For the triplet of largest lattice sizes the exponent estimates are of similar accuracy for all of the K_2 values shown. In agreement with the earlier results, the estimates of the amplitude of the sub-dominant (marginal) scaling field and its exponent are poor for the lattice sizes normally available to direct diagonalization. Unfortunately, the amplitude of the marginal field is *still* poorly determined for large values of K_2, even for the *largest* lattice sizes.

Finally, we consider a general triplet of lattice sizes (N, rN, r^2N) in the Ising limit. Using the exact results (2.3.38) and (2.3.39) to construct the matrices defined in (2.4.10), we find both gaps give

$$\mathbf{T} = \begin{bmatrix} r & (r-1)/\sqrt{2} \\ 0 & 1 \end{bmatrix} \tag{2.4.13}$$

independent of N. Thus, in the isotropic Ising limit, we construct the *exact* transformation matrix, from which we obtain the exact exponents and scaling field amplitudes: $y_1 = 1$, $y_2 = 0$, $a_1 = 1/\sqrt{2}$ and $a_2 = 0$.

2.5 SUMMARY AND CONCLUSION

In this chapter we have reformulated and numerically solved the Bethe ansatz equations of the eight-vertex model on a finite lattice. An approximation scheme, increasing in accuracy with system size, has been used to provide accurate starting points in the numerical solution of the finite system of equations. By using this method, we have obtained the three largest eigenvalues, and subsequently two mass gaps, on infinitely long strips of up to width $N = 512$.

Our discussion in Section 2.3 of the convergence of finite lattice estimates with increasing system size has helped to clarify the anomalous behaviour seen in earlier studies. We find that the free energy per site approaches its bulk limit as

$$f_N = f_\infty - \frac{\pi}{6} N^{-2} + O(N^{-2-\lambda}) , \tag{2.5.1}$$

and for the mass gap (2.3.1);

$$N\kappa_N = 2\pi x_p + O(N^{-\lambda}) , \tag{2.5.2}$$

with x_p the scaling dimension (2.3.10) of the polarization operator.

In (2.5.1) and (2.5.2) the exponent λ is defined by

$$\lambda = \min\left(2, \frac{4\mu}{\pi-\mu}\right) . \tag{2.5.3}$$

This behaviour is the same as for the XXZ chain (Hamer 1986, Woynarovich and Eckle 1987, Alcaraz, Barber and Batchelor 1987a,b). Finite lattice estimates of the critical temperature (p = 0) converge as

$$p_N^* = O(N^{-y_T-\lambda}) , \tag{2.5.4}$$

where $y_T = 1/\nu$ is the thermal exponent (2.3.20). On the other hand, estimates of the exponent ν were found to converge as

$$\nu_N^* = \nu + O(N^{-y_T}) . \tag{2.5.5}$$

The corrections in (2.5.1), (2.5.2), (2.5.4) and (2.5.5) account for the deterioration in convergence seen for four-spin coupling K_2 in the range $K_2 < -0.3$ (Nightingale 1977, 1979, Nightingale and Blöte 1983, Barber 1985 and Blöte *et al.* 1986). For large positive values of the four-spin coupling, however, the above results predict that the convergence should be more rapid than for small values of K_2. The poor convergence seen for the lattice sizes ($N \sim 16$) normally available to direct diagonalization can be attributed to relatively large amplitudes in the correction terms, and also for the estimates of ν, the behaviour of the derivatives appearing in the finite lattice estimators.

In Section 2.4 we have derived exact expressions for the amplitudes of the linear scaling fields and compared the results with a recently proposed method (Barber 1983b, 1985) of estimating linear scaling fields from finite lattice data. This involved the explicit (phenomenological) construction of the transformation matrix (2.4.2) appearing in the renormalization group formalism. Apart from the large K_2 estimates of the subdominant (marginal) scaling field, which becomes large in magnitude, the results obtained were in excellent agreement with the exact values.

Our calculations can be extended in several directions. The observed slow convergence for the interfacial tension defined by (2.2.37) should be obviated by using a definition incorporating a sum over the relevant *band* of eigenvalues. Also, we mention that the calculations presented in this paper can be repeated in the *full* parameter space of the model. This would allow a further test of the methods proposed for extracting linear scaling fields and an investigation of the effect of anisotropy on finite-size scaling and its corrections in the eight-vertex model.

Appendix 2A

Three useful identities involving the ellipitc function f(z,q) defined in (2.2.1) are:

$$f(z^{-1},q) = -z^{-1}f(z,q) \tag{2A.1}$$

$$f(qz^{-1},q^2) = f(qz,q^2) \tag{2A.2}$$

$$\frac{f(z,q)\,f(z,-q)}{f(w,q)\,f(w,-q)} = \frac{f(z^2,q^2)}{f(w^2,q^2)}\,. \tag{2A.3}$$

Appendix 2B *Conjugate Modulus Transformations*

To find a conjugate modulus identity for the elliptic function f(z,q) we need the standard (apart from an irrelevant factor) elliptic theta function (see, *e.g.* Gradshteyn and Rhyzik 1980; Baxter 1982)

$$\theta(u,q) = \sin u \prod_{m=1}^{\infty}(1-2q^m\cos 2u + q^{2m})(1-q^m) = \frac{1}{2}ie^{-iu}\,f(e^{2iu},q). \tag{2B.1}$$

This function is also related to f(z,q) by the conjugate modulus identity (Baxter 1982)

$$\theta(u,e^{-\varepsilon}) = -\frac{1}{2}\left(\frac{2\pi}{\varepsilon}\right)^{1/2}\exp\left[\frac{\varepsilon}{8}-\frac{\pi^2}{2\varepsilon}-\frac{2u(\pi+u)}{\varepsilon}\right]f\left(e^{4\pi u/\varepsilon},e^{-4\pi^2/\varepsilon}\right)\,. \tag{2B.2}$$

Comparison of (2B.1) and (2B.2) results in

$$f\left(e^{2iu},e^{-\varepsilon}\right) = i\left(\frac{2\pi}{\varepsilon}\right)^{1/2}\exp\left[iu+\frac{\varepsilon}{8}-\frac{\pi^2}{2\varepsilon}-\frac{2u(\pi+u)}{\varepsilon}\right]f\left(e^{4\pi u/\varepsilon},e^{-4\pi^2/\varepsilon}\right). \tag{2B.3}$$

Since the parametrization of the weights (2.2.4) and the functional relations (2.2.9) involve only ratios of elliptic functions, we may use (2B.3) to define transformation rules:

$$f\left(e^{i\pi u/I},q^2\right) \sim \exp\left(\frac{i\pi u}{2I}-\frac{\pi u}{2I'}-\frac{\pi u^2}{4II'}\right)f\left(e^{\pi u/I},p\right) \tag{2B.4}$$

$$f\left(e^{i\pi u/I},q\right) \sim \exp\left(\frac{i\pi u}{2I}-\frac{\pi u}{I'}-\frac{\pi u^2}{2II'}\right)f\left(e^{2\pi u/I'},p^2\right)\,. \tag{2B.5}$$

Appendix 2C

In this appendix we give the details in the derivation of the derivatives of the variables (p,μ,w) with respect to the spin coupling constants $\mathbf{K} = (K_1, K_1', K_2)$. The connection between the sets of variables is given in equations (2.3.14a-c). Recalling the definition (2.2.1) of the elliptic function $f(z,q)$ we have, to first oder in p,

$$\exp(2K_1) = \cot(\mu/4-w/4)\left[1 + 4p\cos(\mu/2-w/2)\right], \tag{2C.1a}$$

$$\exp(2K_1') = \cot(\mu/4+w/4)\left[1 + 4p\cos(\mu/2+w/2)\right], \tag{2C.1b}$$

$$\exp(2K_2) = \tan\mu/2\left(1 - 4p\cos\mu\right). \tag{2C.1c}$$

By differentiating these equations, first with respect to K_1, we obtain

$$\left(\frac{\partial\mu}{\partial K_1}\right)^* = 4\sin\mu\cos\mu\left(\frac{\partial p}{\partial K_1}\right)^*, \tag{2C.2a}$$

$$0 = \sin(\mu+w)\left(\frac{\partial p}{\partial K_1}\right)^* - \frac{1}{4}\left[\left(\frac{\partial\mu}{\partial K_1}\right)^* + \left(\frac{\partial w}{\partial K_1}\right)^*\right], \tag{2C.2b}$$

$$\sin(\mu/2-w/2) = \sin(\mu-w)\left(\frac{\partial p}{\partial K_1}\right)^* - \frac{1}{4}\left[\left(\frac{\partial\mu}{\partial K_1}\right)^* - \left(\frac{\partial w}{\partial K_1}\right)^*\right]. \tag{2C.2c}$$

Now (2C.2) simply represents a system of three equations in three unknowns, from which we can readily solve for the derivatives;

$$\left(\frac{\partial p}{\partial K_1}\right)^* = \frac{\sin(\mu/2-w/2)}{2\sin\mu\,(\cos w - \cos\mu)}, \tag{2C.3a}$$

$$\left(\frac{\partial\mu}{\partial K_1}\right)^* = \frac{2\cos\mu\,\sin(\mu/2-w/2)}{\cos w - \cos\mu}, \tag{2C.3b}$$

$$\left(\frac{\partial w}{\partial K_1}\right)^* = \frac{2\sin(\mu/2-w/2)}{\cos w - \cos\mu}\left[\frac{\sin(\mu+w)}{\sin\mu} - \cos\mu\right]. \tag{2C.3c}$$

In a similar manner we obtain the remaining derivatives,

$$\left(\frac{\partial p}{\partial K_1'}\right)^* = \frac{\sin(\mu/2+w/2)}{2\sin\mu\,(\cos w - \cos\mu)}, \tag{2C.4a}$$

$$\left(\frac{\partial\mu}{\partial K_1'}\right)^* = \frac{2\cos\mu\,\sin(\mu/2+w/2)}{\cos w - \cos\mu}, \tag{2C.4b}$$

$$\left(\frac{\partial w}{\partial K_1'}\right)^* = \frac{2\sin(\mu/2+w/2)}{\cos w - \cos\mu}\left[\cos\mu - \frac{\sin(\mu-w)}{\sin\mu}\right] . \qquad (2C.4c)$$

$$\left(\frac{\partial p}{\partial K_2}\right)^* = \frac{1}{2(\cos w - \cos\mu)} , \qquad (2C.5a)$$

$$\left(\frac{\partial \mu}{\partial K_2}\right)^* = \frac{2\cos w - \sin\mu}{\cos w - \cos\mu} , \qquad (2C.5b)$$

$$\left(\frac{\partial w}{\partial K_2}\right)^* = \frac{2\sin w \cos\mu}{\cos w - \cos\mu} . \qquad (2C.5c)$$

Appendix 2D *Derivatives of the mass gap*

In this appendix we derive expressions for the derivative of the mass gap (2.3.1) with respect to the variables p and μ. These expressions are to be evaluated at criticality. We consider first the derivative with respective to p.

Thermal derivative

Using (2.3.23) we have

$$\left(\frac{\partial \kappa}{\partial p}\right)^* = -\left(\frac{1}{T_1}\frac{\partial T_1}{\partial p}\right)^* . \qquad (2D.1)$$

It suffices to consider the eigenvalue equation (2.2.49) in the form

$$T_1(1) = F(\chi)\frac{f(p\chi^2)}{f(p)}\prod_{j=1}^{n-2}\frac{f(\chi^2\zeta_j)}{f(\zeta_j)} , \qquad (2D.2)$$

as the neglected prefactors can be seen to make no contribution to the derivative in the limit $p = 0$. In (2D.2), for ease of notation, we have dropped the explicit functional dependence on nome p^2.

The logarithmic derivative of (2D.2), and subsequently equation (2D.1), can be written as a sum of three terms, A, B, and C, with

$$A = \frac{1}{f(p\chi^2)}\frac{\partial f(p\chi^2)}{\partial p} - \frac{1}{f(p)}\frac{\partial f(p)}{\partial p}\,, \tag{2D.3a}$$

$$B = \frac{1}{F(\chi)}\frac{\partial F(\chi)}{\partial p}\,, \tag{2D.3b}$$

$$C = \sum_{j=1}^{n-2}\left[\frac{1}{f(\chi^2\zeta_j)}\frac{\partial f(\chi^2\zeta_j)}{\partial p} - \frac{1}{f(\zeta_j)}\frac{\partial f(\zeta_j)}{\partial p}\right]. \tag{2D.3c}$$

Given the definitions (2.2.1), (2.2.34b) and (2.2.35) of the functions appearing in (2D.2), and the knowledge that none of the $n-2$ zeros appearing in the summation for C are explicitly dependent on p, the evaluation of the terms in (2D.3) in the limit $p = 0$ is relatively straightforward; care need only be taken with the exact zero at p appearing in the function $F(\chi)$. The results are

$$A^* = 4\sin^2\mu\,, \tag{2D.4a}$$

$$B^* = 4\sin 2\mu\,\frac{B_1}{B_2}\,, \tag{2D.4b}$$

$$C^* = \sum_{j=1}^{n/2-1}\left[\frac{\zeta_j - \zeta_j^{-1}}{1+\zeta_j^2 - 2\zeta_j\cos 2\mu} + \frac{1}{\zeta_j}\left(\frac{1+\zeta_j}{1-\zeta_j}\right)\right]\left(\frac{\partial\zeta_j}{\partial p}\right)^*\,, \tag{2D.4c}$$

with

$$B_1 = -1 + \sum_{j=1}^{n/2-1}\frac{\zeta_j^2 - 1}{(1+\zeta_j^2 - 2\zeta_j\cos 2\mu)^2}\left(\frac{\partial\zeta_j}{\partial p}\right)^*\,, \tag{2D.5a}$$

$$B_2 = \left[1 + 2(N-1)\cos^2\mu/2\right]/\sin\mu - 4\sin 2\mu\sum_{j=1}^{n/2-1}\frac{\zeta_j}{1+\zeta_j^2 - 2\zeta_j\cos 2\mu}\,. \tag{2D.5b}$$

Here again we have used the fact that the zeros are in reciprocal pairs, apart from the zero at p and the stationary zero at 1 (recall also that n is even).

A system of equations for the derivatives of the zeros is readily derived from the Bethe ansatz equations (2.2.47). As remarked in Section 2.2.4, the zero at p satisfies one of the equations, leaving the system given in (2.2.58). The stationary zero satisfies

one of these equations (again, the key point is that the zeros are in reciprocal pairs) and this system can further be written

$$\chi^{-4}\left[\frac{f(\chi\zeta_j)}{f(\chi^{-1}\zeta_j)}\right]^N \frac{f(\chi^{-2}\zeta_j)\, f(p\chi^{-2}\zeta_j)}{f(\chi^2\zeta_j)\, f(p\chi^2\zeta_j)} \prod_{\substack{k=1 \\ \neq j}}^{n-2} \frac{f(\chi^{-2}\zeta_j/\zeta_k)}{f(\chi^2\zeta_j/\zeta_k)} = 1 \ , \quad j = 1,\ldots,n-2 \tag{2D.6}$$

On taking a logarithmic derivative, each zero must satisfy

$$NE_1 + E_2 + E_3 + E_4 = 0 \ , \tag{2D.7}$$

where

$$E_1 = \frac{1}{f(\chi\zeta_j)}\frac{\partial f(\chi\zeta_j)}{\partial p} - \frac{1}{f(\chi^{-1}\zeta_j)}\frac{\partial f(\chi^{-1}\zeta_j)}{\partial p} \ , \tag{2D.8a}$$

$$E_2 = \frac{1}{f(\chi^{-2}\zeta_j)}\frac{\partial f(\chi^{-2}\zeta_j)}{\partial p} - \frac{1}{f(\chi^2\zeta_j)}\frac{\partial f(\chi^2\zeta_j)}{\partial p} \ , \tag{2D.8b}$$

$$E_3 = \frac{1}{f(p\chi^{-2}\zeta_j)}\frac{\partial f(p\chi^{-2}\zeta_j)}{\partial p} - \frac{1}{f(p\chi^2\zeta_j)}\frac{\partial f(p\chi^2\zeta_j)}{\partial p} \ , \tag{2D.8c}$$

$$E_4 = \sum_{k=1}^{n-2}\left[\frac{1}{f(\chi^{-2}\zeta_j/\zeta_k)}\frac{\partial f(\chi^{-2}\zeta_j/\zeta_k)}{\partial p} - \frac{1}{f(\chi^2\zeta_j/\zeta_k)}\frac{\partial f(\chi^2\zeta_j/\zeta_k)}{\partial p}\right] . \tag{2D.8d}$$

On defining the quantity

$$u_j = \left(\frac{\partial\zeta_j}{\partial p}\right)^* \ , \tag{2D.9}$$

equations (2D.8), in the limit $p = 0$, reduce to

$$E_1^* = \frac{-2i\sin\mu\, u_j}{1 + \zeta_j^2 - 2\zeta_j\cos\mu} \ , \tag{2D.10a}$$

$$E_2^* = \frac{2i\sin 2\mu\, u_j}{1 + \zeta_j^2 - 2\zeta_j\cos 2\mu} \ , \tag{2D.10b}$$

$$E_3^* = 2i\sin 2\mu\,(\zeta_j - \zeta_j^{-1}) \ , \tag{2D.10c}$$

$$E_4^* = 2i\sin 2\mu \sum_{k=1}^{n-2} \frac{\zeta_k u_j - \zeta_j u_k}{\zeta_j^2 + \zeta_k^2 - 2\zeta_j \zeta_k \cos 2\mu} . \qquad (2D.10d)$$

Insertion of these results into (2D.7) leads to a linear, nonhomogeneous system of equations for the u_j. Specifically, this system of equations can be written in the form

$$G_j u_j + \sum_{k=1}^{n/2-1} H_{jk} u_k = 2\cos\mu \, (\zeta_j^{-1} - \zeta_j) \ , \ j = 1,\ldots,n-2 \ , \qquad (2D.11)$$

where

$$G_j = G_j^{(1)} + G_j^{(2)} \ , \qquad (2D.12a)$$

$$H_{jk} = 2\,\zeta_j \cos\mu \left(\frac{1}{1 + \zeta_j^2 \zeta_k^2 - 2\zeta_j \zeta_k \cos 2\mu} - \frac{1}{\zeta_j^2 + \zeta_k^2 - 2\zeta_j \zeta_k \cos 2\mu} \right) , \qquad (2D.12b)$$

with

$$G_j^{(1)} = \frac{2\cos\mu}{1 + \zeta_j^2 - 2\zeta_j \cos 2\mu} - \frac{N}{1 + \zeta_j^2 - 2\zeta_j \cos\mu} + \frac{4\zeta_j \cos\mu}{1 + \zeta_j^4 - 2\zeta_j^2 \cos 2\mu} \ , \qquad (2D.12c)$$

$$G_j^{(2)} = 2\cos\mu \sum_{k=1}^{n/2-1} \zeta_k \left[\frac{1}{\zeta_j^2 + \zeta_k^2 - 2\zeta_j \zeta_k \cos 2\mu} - \frac{1}{1 + \zeta_j^2 \zeta_k^2 - 2\zeta_j \zeta_k \cos 2\mu} \right] . \qquad (2D.12d)$$

The system (2D.11) is invariant under the transformation $\zeta_j \to \zeta_j^{-1}$, so that half of the equations are redundant; we need only consider solving (2D.11) for u_j with $j = 1,\ldots, n/2 - 1$. Note that all of the u_j vanish in the Ising limit $\mu = \pi/2$ and the only contribution to (2D.1) is from the term (2D.4a).

Finally we remark that the above equations can be written in perhaps a more elegant form by setting $\zeta_j = \exp(-2\alpha_j)$. In this case one could alternatively consider the Bethe ansatz equations in the form (2.2.59). We adopt this approach for the derivatives with respect to μ.

Marginal derivatives

Here we are actually *at* criticality (we suppress the * notation for convenience). We can consider eigenvalues (2.2.67) and (2.2.68) in the form

$$T_0 = \prod_{j=1}^{n/2} \frac{\cosh 2\alpha_j - \cos 2\mu}{\cosh 2\alpha_j - 1} , \tag{2D.13}$$

$$T_1 = E \prod_{j=1}^{n/2-1} \frac{\cosh 2\alpha_j - \cos 2\mu}{\cosh 2\alpha_j - 1} , \tag{2D.14}$$

where the quantity E is defined in (2.2.69). The logarithmic derivatives are

$$\frac{1}{T_0}\frac{\partial T_0}{\partial \mu} = \sum_{j=1}^{n/2} R_j , \tag{2D.15}$$

$$\frac{1}{T_1}\frac{\partial T_1}{\partial \mu} = \frac{1}{E}\frac{\partial E}{\partial \mu} + \sum_{j=1}^{n/2-1} R_j , \tag{2D.16}$$

where we have set

$$R_j = 2\left[\frac{w_j \sinh 2\alpha_j + \sin 2\mu}{\cosh 2\alpha_j - \cos 2\mu} - \frac{w_j \sinh 2\alpha_j}{\cosh 2\alpha_j - 1}\right] , \tag{2D.17}$$

and defined the derivative w_j by

$$w_j = \frac{\partial \alpha_j}{\partial \mu} . \tag{2D.18}$$

From (2.2.69) we have

$$\frac{\partial E}{\partial \mu} = (1-N)\sin\mu - \sum_{j=1}^{n/2-1} \frac{4 \sin\mu\,(3\cos^2\mu - 1)}{\cosh 2\alpha_j - \cos 2\mu}$$

$$+ \sum_{j=1}^{n/2-1} \frac{4 \sin\mu \sin 2\mu\,(w_j \sinh 2\alpha_j + \sin 2\mu)}{(\cosh 2\alpha_j - \cos 2\mu)^2} . \tag{2D.19}$$

To derive equations for the w_j we consider the Bethe ansatz equations (2.2.58) and (2.2.59) with $p = 0$. In particular, we write these equations as, respectively,

$$N\varphi(\alpha_j,\mu/2) = 2\pi I_j + \sum_{k=1}^{n/2}\Big[\varphi(\alpha_j-\alpha_k,\mu)+\varphi(\alpha_j+\alpha_k,\mu)\Big]$$

$$j=1,\ldots,n/2 \qquad (2D.20)$$

$$N\varphi(\alpha_j,\mu/2) = 2\pi I_j + \varphi(\alpha_j,\mu) + \sum_{k=1}^{n/2-1}\Big[\varphi(\alpha_j-\alpha_k,\mu)+\varphi(\alpha_j+\alpha_k,\mu)\Big]$$

$$j=1,\ldots,n/2-1 \qquad (2D.21)$$

We wish to differentiate these equations with respect to μ. From the definition (2.2.53) of the function $\varphi(\alpha,\mu)$ we have, after some algebra, the intermediate results

$$\frac{\partial\varphi(\alpha,\mu)}{\partial\mu} = \left[\sin 2\mu\,\frac{\partial\alpha}{\partial\mu} - \sinh 2\alpha\right]\Omega(\alpha,\mu)\,, \qquad (2D.22a)$$

$$\frac{\partial\varphi(\alpha,\mu/2)}{\partial\mu} = \left[\sin\mu\,\frac{\partial\alpha}{\partial\mu} - \frac{1}{2}\sinh 2\alpha\right]\Omega(\alpha,\mu/2)\,, \qquad (2D.22b)$$

where we have defined the quantity $\Omega(\alpha,\mu)$ by

$$\Omega(\alpha,\mu) = \frac{1}{\cosh^2\alpha - \cos^2\mu}\,. \qquad (2D.23)$$

Given these results, the system of equations associated with the eigenvalue T_0 can be written in the form

$$U_j w_j + \sum_{\substack{k=1\\ \neq j}}^{n/2} V_{jk} w_k = W_j\,, \qquad j=1,\ldots,n/2\,, \qquad (2D.24)$$

where

$$U_j = N\sin\mu\,\Omega(\alpha_j,\mu/2) - 2\sin 2\mu\,\Omega(2\alpha_j,\mu) - \sin 2\mu\sum_{\substack{k=1\\ \neq j}}^{n/2}\Big[\Omega(\alpha_j-\alpha_k,\mu)+\Omega(\alpha_j+\alpha_k,\mu)\Big]\,, \qquad (2D.25a)$$

$$V_{jk} = \sin 2\mu\Big[\Omega(\alpha_j-\alpha_k,\mu)-\Omega(\alpha_j+\alpha_k,\mu)\Big]\,, \qquad (2D.25b)$$

and

$$W_j = \frac{1}{2} N \sinh 2\alpha_j \, \Omega(\alpha_j, \mu/2) - \sinh 4\alpha_j \, \Omega(2\alpha_j, \mu)$$

$$- \sum_{\substack{k=1 \\ \neq j}}^{n/2} \left[\sinh 2(\alpha_j - \alpha_k) \, \Omega(\alpha_j - \alpha_k, \mu) + \sinh 2(\alpha_j + \alpha_k) \, \Omega(\alpha_j + \alpha_k, \mu) \right] . \qquad (2D.25c)$$

The equations associated with T_1 are of the same form as (2D.24) except with $j, k = 1, \ldots, n/2 - 1$. However, slight modifications arise from the extra term in (2D.21). Rather than writing the equations out in full, we mention only that the quantities $-\sin 2\mu \, \Omega(\alpha_j, \mu)$ and $-\sinh 2\alpha_j \, \Omega(\alpha_j, \mu)$ need to be added to, respectively, equations (2D.25a) and (2D.25c).

Finally we remark that the solution of the systems (2D.11) and (2D.24) has posed no numerical problems; again we chose to use a standard library package (specifically, F04ATF of Numerical Algorithms Group).

3

CONFORMAL INVARIANCE, THE XXZ CHAIN AND THE OPERATOR CONTENT OF TWO-DIMENSIONAL CRITICAL SYSTEMS

3.1 INTRODUCTION

The first suggestion that critical fluctuations in statistical systems should be conformally invariant was made by Polyakov (1970). However, nearly fifteen years were to pass before it was realized (Belavin *et al.* 1984, Friedan *et al.* 1984) that conformal invariance places such severe constraints on the structure of two-dimensional theories to essentially completely determine their critical behaviour (see Cardy 1987). In particular, the possible classes of critical behaviour are indexed by a single dimensionless real number c, the conformal anomaly or central charge. If $c < 1$, unitarity (Friedan *et al.* 1984) further restricts c to the countable set of values

$$c = 1 - \frac{6}{m(m+1)}, \qquad m = 3, 4, \ldots . \tag{3.1.1}$$

In addition, if m is finite the number of critical operators of the theory is also finite; the anomalous dimensions of the operators being given in terms of c by the Kac (1979) formula. Physical universality classes correspond to subsets of the conformal operators and can be determined by modular invariance (Cardy 1986a, Cappelli *et al.* 1987, Di Francesco *et al.* 1987, Gepner 1987).

In parallel with these formal developments, Cardy showed (1984a,b, 1986a,b) that the spectrum of the transfer matrix of a critical theory in a strip of large but finite width was also determined by conformal invariance. If we write the transfer matrix as $T = e^{-a\mathcal{H}}$, where a is the lattice spacing, then in a strip of width L with periodic

boundary conditions, the ground-state energy, $E_0(L)$, of $\mathcal{H}$ behaves for large L as (Blöte *et al.* 1986, Affleck 1986)

$$E_0(L)/L = e_\infty - \frac{\pi c \zeta}{6} L^{-2} + o(L^{-2}); \qquad (3.1.2)$$

where e_∞ is the ground-state energy in the infinite lattice limit. The structure of the higher energy states is determined by the critical operators of the theory (Cardy 1986a, 1987). For each operator O_α with anomalous dimension x_α and spin s_α, there exists a tower of states in the spectrum of $\mathcal{H}$ with energies $E^\alpha_{j,j'}(L)$ and momenta $P^\alpha_{j,j'}(L)$ given by

$$E^\alpha_{j,j'}(L) = E_0(L) + 2\pi\zeta(x_\alpha + j + j')L^{-1} + o(L^{-1}) \quad j, j' = 0, 1, \ldots \qquad (3.1.3a)$$

and

$$P^\alpha_{j,j'}(L) = 2\pi(s_\alpha + j - j')L^{-1} \quad j, j' = 0, 1, \ldots . \qquad (3.1.3b)$$

The factor ζ, appearing in (3.1.2) and (3.1.3a), is (usually) unity in the transfer matrix formulation. However, these results may also be extended (von Gehlen *et al.* 1986) to quantum Hamiltonians describing (1+1)-dimensional field theories. In this formulation, ζ is not known *a priori* but must be determined, usually numerically, to ensure that the resulting equations of motion are conformally invariant (von Gehlen *et al.* 1986). The asymptotic predictions, (3.1.2) and (3.1.3), allow the conformal anomaly, c, and the anomalous dimensions of the theory to be computationally determined from finite lattice calculations of its transfer matrix or quantum Hamiltonian spectrum. This procedure has been applied successfully to many models of physical interest (see, *e.g.* von Gehlen *et al.* 1986, von Gehlen and Rittenberg 1987, Alcaraz and Drugowich de Felício 1984, Alcaraz and Barber 1987a,b, Balbão and Drugowich de Felício 1987 and also Cardy 1987, 1986d and references therein).

In this chapter, we apply these ideas to the one-dimensional quantum XXZ-model:

$$\mathcal{H}_{xxz} = -\tfrac{1}{2}\sum_{m=1}^{M} (\sigma^x_m \sigma^x_{m+1} + \sigma^y_m \sigma^y_{m+1} + \Delta\, \sigma^z_m \sigma^z_{m+1}) \qquad (3.1.4)$$

regarded as a (1+1)-dimensional field theory. Here σ^x, σ^y, σ^z are Pauli matrices, $\Delta = -\cos\gamma$ is a coupling constant with $\gamma \in [0, \pi)$ and we have applied periodic boundary conditions. For this Hamiltonian the constant

$$\zeta = \zeta_x = \frac{\pi \sin\gamma}{\gamma} \tag{3.1.5}$$

can be inferred (Hamer 1985, 1986a) from the known (Johnson *et al.* 1973) energy-momentum dispersion relation.

From the point of view of conformal invariance, the XXZ model is particularly interesting. In the bulk limit, $L \to \infty$, $\mathcal{H}_{xxz}$ is massless with critical exponents varying continuously with Δ (see, *e.g.* Baxter 1982). Hence one would expect (Friedan *et al.* 1984) that $c = 1$. This is confirmed by analytical and numerical calculations (Hamer 1985, 1986a, Avdeev and Dörfel 1986) (see also Section 3.3.1). Furthermore, since $\mathcal{H}_{xxz}$ describes criticality in the eight-vertex model its spectrum should contain levels corresponding to the anomalous dimensions of the eight-vertex model. On the other hand, $\mathcal{H}_{xxz}$ is believed to describe criticality in a number of other two-dimensional models including for example the Potts models. However, the Potts models are examples of conformal theories with $c < 1$, *e.g.* $c = 4/5$ for the 3-state Potts model. How is c changed from the value $c = 1$ as we move through the critical Potts models? Do the Potts critical operators show up in the spectrum of the XXZ chain on a finite lattice? These are some of the questions that motivated the work discussed in this chapter. A brief summary of some of our results has appeared (Alcaraz, Barber and Batchelor 1987a).

The chapter is organized as follows. In the next Section we discuss the spectrum of (3.1.4) for both periodic boundary conditions and a special class of "twisted" boundary conditions:

$$\sigma^x_{M+1} \pm \sigma^y_{M+1} = e^{\pm i\phi}(\sigma^x_1 \pm \sigma^y_1), \quad \sigma^z_{M+1} = \sigma^z_1, \tag{3.1.6}$$

where ϕ is an arbitrary angle. The novel feature of the calculations described in this section is the use of the Bethe anstaz to compute eigen-energies of a finite chain. With these techniques we were able to handle chains of up to 1024 sites. In Section 3.3 we

use this finite lattice data, together with the conformal invariance predictions (3.1.2) and (3.1.3), to identify the operator content of the XXZ chain. Sections 3.4 and 3.5 are concerned with the Ashkin-Teller and Potts models, respectively; both of which can be related to the XXZ model at criticality. Here we *exactly* relate the eigenspectra of the conventional quantum Hamiltonians of both models to that of $\mathcal{H}_{xxz}$ and then use the XXZ results to identify the anomalous dimensions of the relevant operators.

3.2 THE BETHE ANSATZ AND THE SPECTRUM OF THE XXZ CHAIN

In this section we examine, using the Bethe ansatz, the eigenvalue spectrum of the XXZ chain, (3.1.4). Initially, we restrict discussion to periodic boundary conditions and assume M to be even. Since $\mathcal{H}_{XXZ}$ commutes with the total spin operator

$$S_z = \sum_{m=1}^{M} \sigma_m^z \,, \tag{3.2.1}$$

its eigen-space can be decomposed into M+1 disjoint sectors labelled by a quantum number $r = 0, 1, 2, \ldots, M$, defined as the state with the number of spins reversed from the state with all spins down, *i.e.* the state with $S_z = -M$. Because of spin-reversal symmetry, the sectors $r = M/2 - j$ and $r = M/2 + j$, $j = 1, \ldots, M/2$, are degenerate; we can thus restrict our attention to those sectors with $r \leq M/2$.

The Bethe ansatz for the XXZ chain with periodic boundary conditions has been discussed in detail by Yang and Yang (1966a,b); see also Appendix 3A, where the Bethe ansatz solution of the XXZ chain for the more general boundary condition (3.1.6) is outlined. If we let the r down spins be at sites,

$$1 \leq x_1 < x_2 \ldots < x_r \leq M, \tag{3.2.2}$$

the amplitudes of the wave functions can be written, following Bethe (1931)

$$a(x_1, \ldots, x_r) = \sum_P \delta_P \exp\left[i \left(\sum_{k=1}^{r} \theta_{Pk} x_k - \sum_{k<\ell} \Theta(\theta_{Pk}, \theta_{P\ell}) \right) \right]. \tag{3.2.3}$$

Here $\theta_1, \ldots, \theta_r$ are quasi-momenta and P denotes a permutation of $1,\ldots, r$ with $\delta_P = +1(-1)$ if the signature of the permutation is even(odd). The wave functions (3.2.3) are unnormalized; the normalization sum has been discussed by Gaudin *et al.* (1981).

The momenta θ_j are determined from the periodic boundary condition, leading to the r equations

$$M\theta_j = 2\pi I_j - \sum_{k=1}^{r} \Theta(\theta_j, \theta_k), \quad j = 1,\ldots, r, \tag{3.2.4}$$

where the two-particle scattering phase is given by

$$\Theta(\theta,\theta') = 2\tan^{-1}\left\{\frac{\Delta \sin[(\theta-\theta')/2]}{\cos[(\theta+\theta')/2] - \Delta\cos[(\theta-\theta')/2]}\right\}. \tag{3.2.5}$$

and

$$I_j = \text{integer}, \quad \text{if } r = \text{odd}$$

$$I_j + \tfrac{1}{2} = \text{integer}, \quad \text{if } r = \text{even}. \tag{3.2.6}$$

The eigenvalues of the Hamiltonian (3.1.4), in the sector r, follow from

$$E = -\tfrac{1}{2}M\Delta + 2\sum_{j=1}^{r}(\Delta - \cos\theta_j), \tag{3.2.7}$$

while the total momemtum is

$$P = \sum_{j=1}^{r}\theta_j = \frac{2\pi}{M}\sum_{j=1}^{r} I_j. \tag{3.2.8}$$

In the limit $\Delta = -1$, it is more convenient to introduce the variable (see, *e.g.* Yang and Yang 1966a)

$$\lambda = \tfrac{1}{2}\tan\frac{\theta}{2} \tag{3.2.9}$$

in terms of which (3.2.4) can be written

$$\pi I_j = M\tan^{-1}(2\lambda_j) - \sum_{k=1}^{r}\tan^{-1}(\lambda_j - \lambda_k), \quad j = 1,\ldots, r \tag{3.2.10}$$

with (3.2.7) reducing to

$$E = \tfrac{1}{2}M - \sum_{j=1}^{r} \frac{1}{\lambda_j^2 + \frac{1}{4}} . \qquad (3.2.11)$$

3.2.1 Exact solution in the limit $\Delta = 0$

At $\gamma = \pi/2$ ($\Delta = 0$), the Hamiltonian (3.1.4) reduces to the isotropic version of the XY model, first studied (in general) by Lieb, Schultz and Mattis (1961) and Katsura (1962) with the aid of annihilation and creation operators. From the point of view of the Bethe ansatz, (3.2.4) and (3.2.7) give the eigenvalues in each sector r as

$$E = -2\sum_{j=1}^{r} \cos \frac{2\pi I_j}{M} . \qquad (3.2.12)$$

All ${}^{M}C_{r}$ eigenvalues in sector r can be recovered by choosing r distinct values for the I_j from the M possible values

$$\left\{0, \pm 1, \ldots, \pm(\tfrac{M}{2} - 1), \tfrac{M}{2}\right\} \quad \text{for } r = \text{odd} \qquad (3.2.13a)$$

$$\left\{\pm\tfrac{1}{2}, \pm\tfrac{3}{2}, \ldots, \pm\tfrac{M-1}{2}\right\} \quad \text{for } r = \text{even.} \qquad (3.2.13b)$$

For the XXZ model, it is known rigorously (Yang and Yang 1966a) that the state of lowest energy in a given sector r is obtained by restricting the set of I_j in (3.2.13) to the r values

$$I_j = -\frac{r-1}{2} + j, \quad j = 0, 1, \ldots, r-1. \qquad (3.2.14)$$

We shall refer to this state as the *minimum energy state*. At this point it is convenient to relabel the sectors, $r = 0, 1, \ldots, M$, by

$$n = \tfrac{1}{2}M - r; \qquad (3.2.15)$$

the ground-state occuring in the sector $n = 0$. (Here n is related to Yang and Yang's (1966a) magnetization per site, y, by $y = 2n/M$ and represents the number of spins flipped from the *anti-ferromagnetic* ground-state.)

It is useful to picture the basic set (3.2.14) as a sea of particles with the remaining possible values in the wider set (3.2.13) as vacancies; the occupation of a given vacancy by any particle producing a "backflow" or relaxation in the sea of particles. For $\Delta = 0$ however, the scattering phase (3.2.5) is zero (free particles) and consequently there is no backflow in this limit.

From (3.2.12), the choice (3.2.14) can be seen to give

$$E_0(n) = -2 \cos\frac{n\pi}{M} \operatorname{cosec}\frac{\pi}{M} \tag{3.2.16}$$

as the lowest energy state in each sector n. Thus, for fixed n/M,

$$e_\infty(n) = \lim_{M\to\infty}\left(\frac{E_0(n)}{M}\right) = -\frac{2}{\pi}\cos\frac{n\pi}{M}, \tag{3.2.17}$$

which is a well known result (Lieb *et al.* 1961, Katsura 1962, Yang and Yang 1966b).

The particle/sea picture of the leading excitations in a given sector n is shown in Table 3.1. The particles, corresponding to the I_j in (3.2.14), are indicated by $\otimes$'s while vacancies, each associated with the remaining values in (3.2.13), are indicated by $\times$'s. The "barrier" shown between the two species can be thought of as the system's "Fermi level", as the leading excited states involve particles both leaving the sea and entering a vacancy as near to this level as possible. Physically, this is understandable as the larger the value of I_j in (3.2.12), the less favourable is the contribution to the system's total energy. The momentum of each excitation, through (3.2.8), is also shown in Table 3.1.

Each of the excitations in group I share the same energy, which can be written

$$E_I(n) = E_0(n) + 4\cos\frac{n\pi}{M}\sin\frac{\pi}{M}. \tag{3.2.18}$$

Similarly for group II we have

$$E_{IIa}(n) = E_0(n) + 4\cos\frac{(n+1)\pi}{M}\sin\frac{2\pi}{M}. \tag{3.2.19a}$$

$$E_{IIb}(n) = E_0(n) + 4\cos\frac{(n-1)\pi}{M}\sin\frac{2\pi}{M}. \tag{3.2.19b}$$

The remaining excitation listed in Table 3.1 has energy

Table 3.1 Particle/sea picture of the leading excitations at $\Delta = 0$. In this limit, each excitation in a given group produces the same energy. P is the total momentum of the configuration in sector n.

	states	P
	minimum energy state	
O	$\ldots \times\times\times \,\vert\otimes\otimes\otimes \ldots \otimes\otimes\otimes\vert\, \times\times\times \ldots$	0
	leading excitations	
I	$\ldots \times\times\times \,\vert\otimes\otimes\otimes \ldots \otimes\otimes\times \,\vert\otimes\times\times \ldots$	$2\pi/M$
	$\ldots \times\times\otimes\vert\, \times\otimes\otimes \ldots \otimes\otimes\otimes\vert\, \times\times\times \ldots$	$-2\pi/M$
	$\ldots \times\times\otimes\vert\otimes\otimes\otimes \ldots \otimes\otimes\times \,\vert\, \times\times\times \ldots$	$-\pi + 2n\pi/M$
	$\ldots \times\times\times \,\vert\, \times\otimes\otimes \ldots \otimes\otimes\otimes\vert\otimes\times\times \ldots$	$\pi - 2n\pi/M$
IIa	$\ldots \times\times\times \,\vert\otimes\otimes\otimes \ldots \otimes\times\otimes\vert\otimes\times\times \ldots$	$4\pi/M$
	$\ldots \times\times\otimes\vert\otimes\times\otimes \ldots \otimes\otimes\otimes\vert\, \times\times\times \ldots$	$-4\pi/M$
	$\ldots \times\times\otimes\vert\otimes\otimes\otimes \ldots \otimes\times\otimes\vert\, \times\times\times \ldots$	$-\pi + 2(n+1)\pi/M$
	$\ldots \times\times\times \,\vert\otimes\times\otimes \ldots \otimes\otimes\otimes\vert\otimes\times\times \ldots$	$\pi - 2(n+1)\pi/M$
IIb	$\ldots \times\times\times \,\vert\otimes\otimes\otimes \ldots \otimes\otimes\times \,\vert\times\otimes\times \ldots$	$4\pi/M$
	$\ldots \times\otimes\times\vert\, \times\otimes\otimes \ldots \otimes\otimes\otimes\vert\, \times\times\times \ldots$	$-4\pi/M$
	$\ldots \times\otimes\times\vert\otimes\otimes\otimes \ldots \otimes\otimes\times \,\vert\, \times\times\times \ldots$	$-\pi + 2(n-1)\pi/M$
	$\ldots \times\times\times \,\vert\times\otimes\otimes \ldots \otimes\otimes\otimes\vert\times\otimes\times \ldots$	$\pi - 2(n-1)\pi/M$
III	$\ldots \times\times\otimes\vert\, \times\otimes\otimes \ldots \otimes\otimes\times \,\vert\otimes\times\times \ldots$	0

$$E_{III}(n) = E_0(n) + 8\cos\frac{n\pi}{M}\sin\frac{\pi}{M}. \qquad (3.2.20)$$

Note however that $E_{IIb}(0) = E_{IIa}(0)$, $E_{IIb}(1) = E_{III}(1)$ and $E_{IIb}(n) > E_{III}(n)$ for $n \geq 2$ (this last inequality holds for $M \geq 6$). This behaviour indicates that the excitation *structure* is *not* the same for all sectors. We have seen already that a given particle/sea excitation can produce a total momemtum dependent on the value of n. Finally, we remark that, apart from the $n = 1$ sector, the energy level (3.2.20) is unique and, within each sector, is the leading zero-momentum excitation.

For comparison, the above excitations in the sectors $n = 0$, 1 and 2 are shown in Figure 3.1 for $M = 16$. The ordering of levels is the same for all values of M.

3.2.2 Exact solution for $r = 2$ and $M = 4$

The Bethe ansatz equations (3.2.4) have not been solved in general for arbitrary values of Δ and, in particular, finite values of r and M. As it turns out, however, more than an inkling of the nature of the leading excitations for arbitrary Δ can be found by looking at the simple case $r = 2$ and $M = 4$, *i.e.* the 6×6 ground-state sector of a four-site chain. Here the exact eigenvalues and corresponding eigenvectors can be found by using appropriate symmetries and thus, perhaps not surprisingly, the Bethe ansatz equations can also be solved exactly. (I am indebted to Rodney Baxter for showing me how to do this.) Here we define $z = e^{i\theta}$, $z' = e^{i\theta'}$ and write the two equations in (3A19) (with $\phi = 0$) as

$$z^4 = -\frac{1 - 2\Delta z + z\,z'}{1 - 2\Delta z' + z\,z'}, \qquad (3.2.21a)$$

$$z'^4 = -\frac{1 - 2\Delta z' + zz'}{1 - 2\Delta z + z\,z'}. \qquad (3.2.21b)$$

These two equations imply that $(zz')^4 = 1$ so we set $zz' = \tau$, where $\tau = e^{iP}$ with $P = \theta + \theta'$ the total momentum. For $P = \pm\pi$ (3.2.21) reduce to

$$z^4 = -\frac{z}{z'}, \qquad z'^4 = -\frac{z'}{z}, \qquad (3.2.22)$$

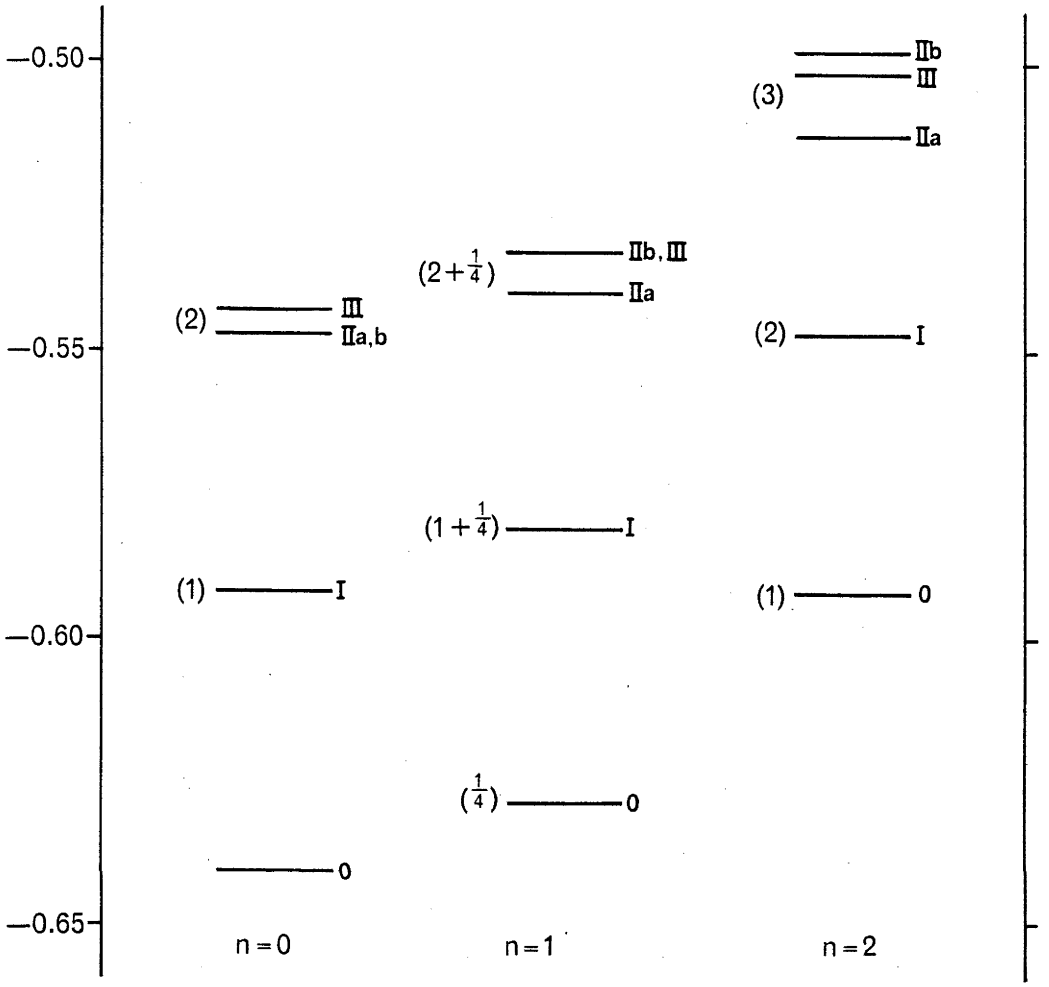

Figure 3.1 The leading energy levels (E/16) of the XXZ chain at $\Delta = 0$ for $M = 16$. Exact expressions for the levels are given in the text. Numbers in parentheses are discussed in Section 3.3.

with solutions

$$z = 1, \quad z' = -1 \tag{3.2.23a}$$

$$z \sim 0, \quad z' \sim \infty \quad \text{such that} \quad zz' = -1. \tag{3.2.23b}$$

The remaining solutions can be found upon setting $z' = \tau/z$. This allows, for example, (3.2.21a) to be written as a polynomial in z,

$$(1+\tau)(1+z^4) = 2\Delta z(1+\tau z^2). \tag{3.2.24}$$

For $P = 0$, the two pairs of solutions to this equation are

$$\begin{aligned} 4z &= \Delta + \sqrt{\Delta^2+8} + i\sqrt{2}\sqrt{4-\Delta^2-\Delta\sqrt{\Delta^2+8}}, \\ 4z' &= \Delta + \sqrt{\Delta^2+8} - i\sqrt{2}\sqrt{4-\Delta^2-\Delta\sqrt{\Delta^2+8}}, \end{aligned} \tag{3.2.25a}$$

and

$$\begin{aligned} 4z &= \Delta - \sqrt{\Delta^2+8} + i\sqrt{2}\sqrt{4-\Delta^2+\Delta\sqrt{\Delta^2+8}}, \\ 4z' &= \Delta - \sqrt{\Delta^2+8} - i\sqrt{2}\sqrt{4-\Delta^2+\Delta\sqrt{\Delta^2+8}}. \end{aligned} \tag{3.2.25b}$$

The remaining zeros are

$$\begin{aligned} 2z &= \Delta + \sqrt{2-\Delta^2} + i\left(\Delta - \sqrt{2-\Delta^2}\right), \\ 2z' &= \Delta - \sqrt{2-\Delta^2} + i\left(\Delta + \sqrt{2-\Delta^2}\right), \end{aligned} \tag{3.2.26a}$$

with $P = \pi/2$ and

$$\begin{aligned} 2z &= \Delta + \sqrt{2-\Delta^2} - i\left(\Delta - \sqrt{2-\Delta^2}\right), \\ 2z' &= \Delta - \sqrt{2-\Delta^2} - i\left(\Delta + \sqrt{2-\Delta^2}\right). \end{aligned} \tag{3.2.26b}$$

with $P = -\pi/2$.

Apart from the stationary zeros in (3.2.23), the above zeros move smoothly in the complex plane as a function of Δ. For the region of interest ($-1 \le \Delta \le 1$) they are confined to the unit circle, as shown in Figure 3.2. The six sets of zeros, when inserted into the wavefunction (3A15), do indeed yield the (six) correct eigenvectors of the problem. Due care has to be taken, however, with the solution (3.2.23b) (R. J. Baxter

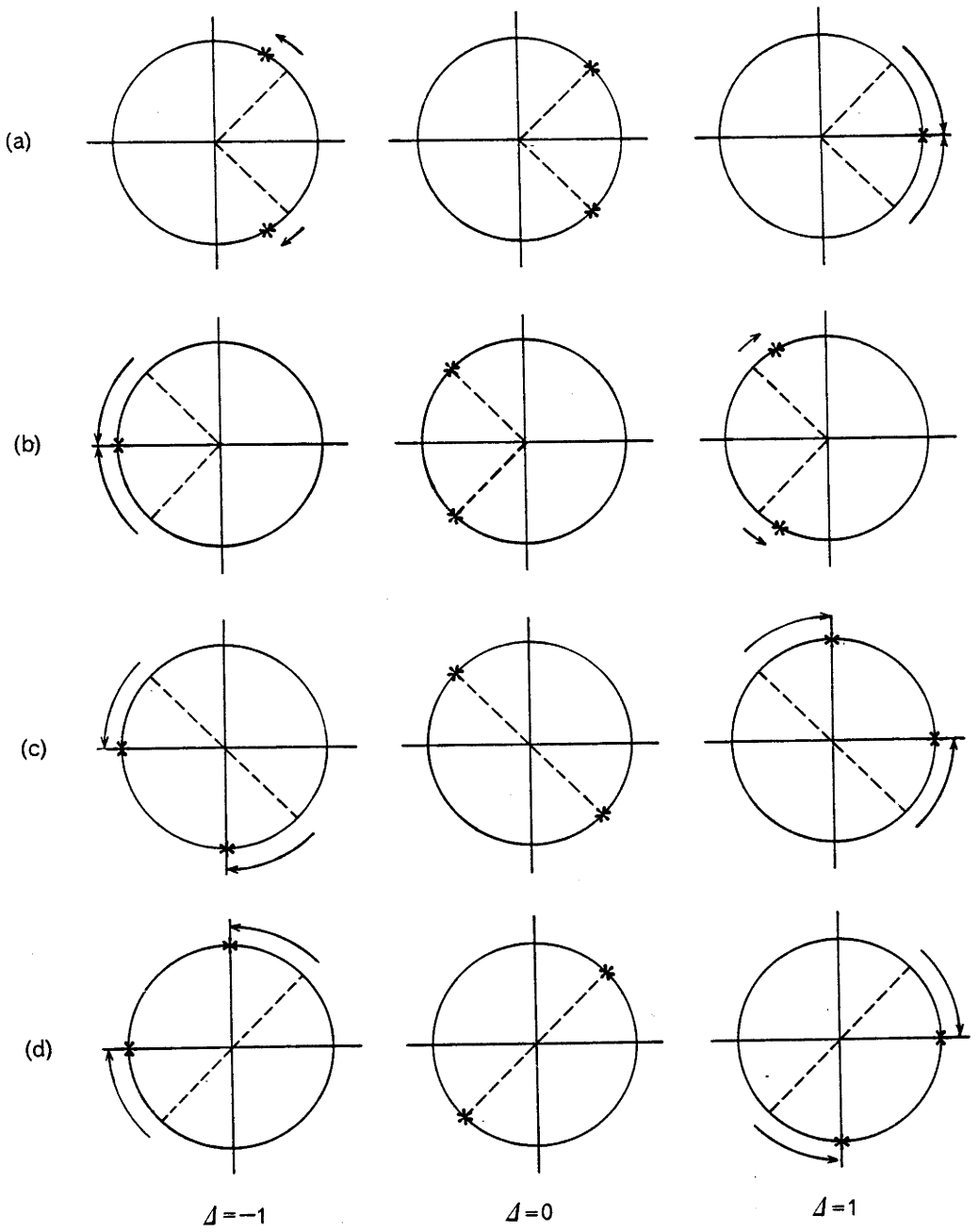

Figure 3.2 Distributions of zeros on the unit circle as a function of Δ in the ground-state sector for $M = 4$. Here the Bethe ansatz equations can be solved exactly. (a) Zeros for the ground-state. The exact values at $\Delta = -1$ are $\exp(\pm i\pi/3)$. (b) The group III excitation. The exact values at $\Delta = 1$ are $\exp(\pm i2\pi/3)$. (c) and (d) Two group I excitations with, respectively, $P = \pi/2$ and $P = -\pi/2$. For each figure, the arrows indicate the movement of the zeros as Δ tends to the limits shown.

and M. T. Batchelor, unpublished).

For completeness, the corresponding energies (e = E/4) are

$$e = \frac{1}{4}\left(\Delta - \sqrt{\Delta^2 + 8}\right), \tag{3.2.27a}$$

for (3.2.25a),

$$e = \frac{1}{2}\Delta, \tag{3.2.27b}$$

for (3.2.23a) and

$$e = \frac{1}{4}\left(\Delta + \sqrt{\Delta^2 + 8}\right), \tag{3.2.27c}$$

for (3.2.25b), while each of (3.2.23b), (3.2.26a) and (3.2.26b) gives $e = 0 \quad \forall\Delta$. These levels are shown in Figure 3.3 as a function of Δ. We remark that each of the four degenerate levels at $\Delta = 0$ belong to group I of Section 3.2.1. For $M = 4$, the effect of non-zero Δ is to shift the energy of one of these levels from that of its group I partners. The highest level in Figure 3.3 is the group III excitation. Before considering larger values of M, we turn now to solution of equations (3.2.4) in the thermodynamic limit.

3.2.3 The infinite chain

Originally Hulthén (1936), following up the earlier work of Bethe (1931), developed a method to obtain the ground-state energy per site of $\mathcal{H}_{xxz}$ in the limit $M \to \infty$ for the isotropic case $\Delta = -1$. This method, involving a tranformation of the equations (3.2.9) to an integral equation with a diffence kernel, was subsequently generalized by Yang and Yang (1966a,b) to provide the ground-state energy per site for arbitrary Δ. The result of interest to us here is

$$e_\infty(\gamma) = \frac{1}{2}\cos\gamma - 2\sin^2\gamma \int_0^\infty \frac{dx}{\cosh(\pi x)\,[\cosh(2\gamma x) - \cos\gamma]}. \tag{3.2.28a}$$

with

$$e_\infty(0) = \frac{1}{2} - 2\ell n 2\,. \tag{3.2.28b}$$

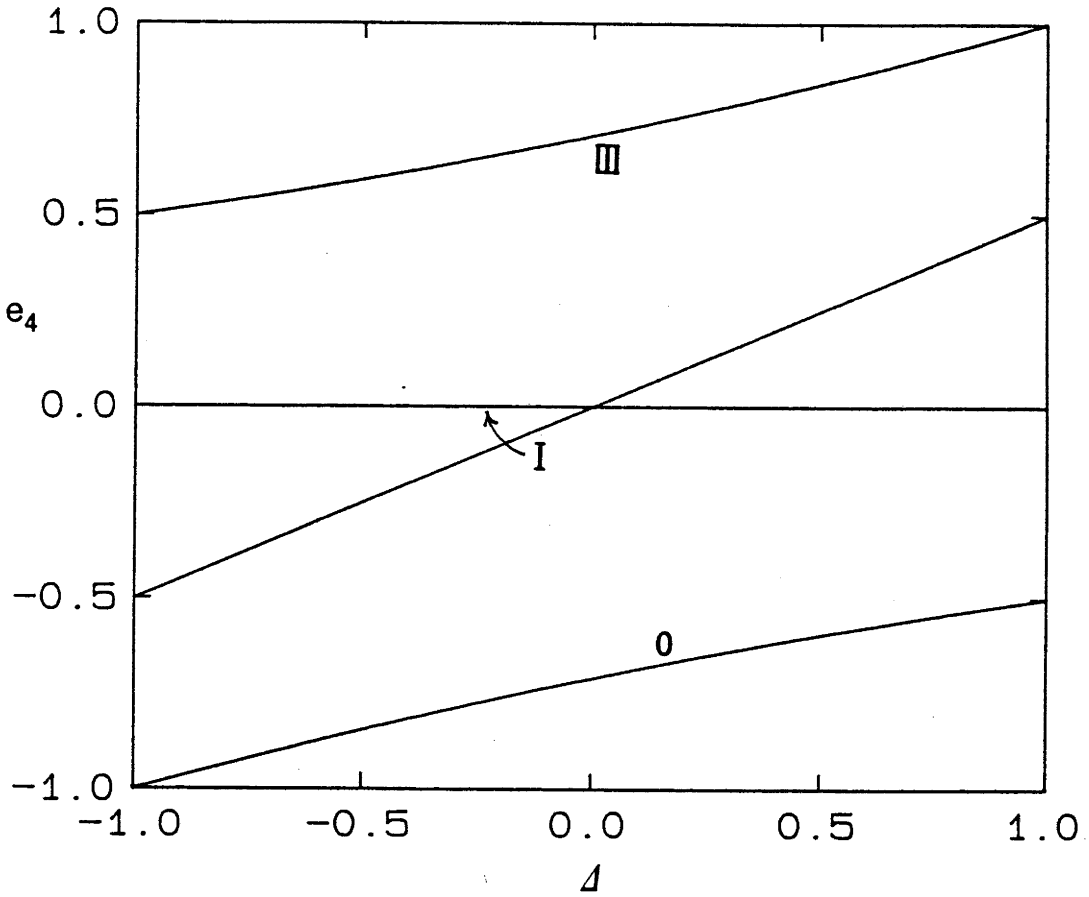

Figure 3.3 Energy levels ($e_4 = E/4$) as a function of Δ in the ground-state sector for M = 4. Shown also is the "group" of the excitation. The zeros corresponding to O, I and III are those shown in Figure 3.2.

Hamer (1981) has evaluated a related integral for several values of γ; we list the results for (3.2.28a) in Table 3.2.

3.2.4 Numerical solution on a finite chain

The little numerical work on the solution of the Bethe ansatz equations (3.2.4) for finite M that has been reported previously is mainly confined to the isotropic ($\Delta = -1$) limit. Des Cloizeaux and Pearson (1962) analyzed the energies of the lowest lying "spin waves" while Grieger (1984), Borysowicz *et al.* (1985) and Kaplan *et al.* (1987) have calculated ground-state correlation functions. Avdeev and Dörfel (1986), in an investigation of the leading correction to e_∞ for finite M, computed the ground-state on chains of up to $M = 256$. More recently, the lowest lying state in the sectors $n = 0$ and $n = 1$ for $-1 \le \Delta \le 0$ has been computed by Woynarovich and Eckle (1987).

We begin by first considering the *minimum energy states* with the numbers I_j given in (3.2.14). For given values of n and M, we have solved the system (3.2.4) for the θ_j by using a Newton-type method (as in the previous chapter). For arbitrary Δ, starting points in the iteration process can be provided by either the trivial $\Delta = 0$ solution or from a generalization of the method used by Grieger (1984). In the notation of Hamer (1985,1986a), we have

$$\theta_\infty(x) = 2\tan^{-1}\left[\cot\tfrac{\gamma}{2}\,\tanh\gamma\lambda_\infty(x)\right] \tag{3.2.29}$$

for the distribution of ground-state zeros on an infinite chain, where

$$\lambda_\infty(x) = \frac{1}{\pi}\ell n\tan\pi\left(x+\tfrac{1}{4}\right). \tag{3.2.30}$$

(This is precisely result (2.2.26), derived from the critical ground-state distribution of zeros in the eight-vertex model.) To obtain starting points, the continuous distribution in (3.2.29) is sampled at the discrete points $x_j = I_j/M$. As a typical example, the starting points $\theta_\infty(x_j)$ and solutions θ_j for the ground-state at $\Delta = -\sqrt{3}/2$ ($\gamma = \pi/6$) for $M = 16$ are listed in Table 3.3. As can be seen, the initial approximation, even for

Table 3.2 Exact results for the ground-state energy per site $e_\infty(\gamma)$ (Eqn. (3.2.28a)) of the quantum XXZ chain.

γ	$e_\infty(\gamma)$	
$\pi/2$	$-2/\pi$	$= -0.6366\ldots$
$\pi/3$	$-3/4$	
$\pi/4$	$-\frac{\sqrt{2}}{\pi} - \frac{1}{2\sqrt{2}}$	$= -0.8037\ldots$
$\pi/6$	$-\frac{1}{\pi} - \frac{11}{12\sqrt{3}}$	$= -0.8475\ldots$
0	$\frac{1}{2} - 2\ell n 2$	$= -0.8862\ldots$

Table 3.3 Inititial iteration points $\theta_\infty(x_j)$ and solutions θ_j for the ground-state energy zeros on a 16-site chain at $\gamma = \pi/6$ ($\Delta = -\sqrt{3}/2$).

$\pm\theta_\infty(x_j)$	$\pm\theta_j$	% difference
0.244 532	0.245 235	0.29
0.740 617	0.742 942	0.31
1.264 227	1.269 200	0.39
1.883 313	1.897 256	0.73

such a relatively small value of M, is excellent. These zeros are shown on the unit circle ($z = e^{i\theta}$) in Figure 3.4(a). As the zeros occur in conjugate pairs, the number of zeros can be halved by solving, for example, for only those zeros of positive sign. For r even we can write (3.2.4) as

$$M\theta_j = 2\pi I_j - \sum_{k=1,k\neq j}^{r/2} [\Theta(\theta_j, \theta_k) + \Theta(\theta_j, -\theta_k)], \quad j = 1,\ldots,\frac{r}{2} \tag{3.2.31}$$

and for r odd;

$$M\theta_j = 2\pi I_j - \Theta(\theta_j, 0) - \sum_{k=1,k\neq j}^{(r-1)/2} [\Theta(\theta_j, \theta_k) + \Theta(\theta_j, -\theta_k)], \quad j = 1,\ldots,\frac{(r-1)}{2}. \tag{3.2.32}$$

In this last result, we have factored out the zero at the origin (*i.e.* we no longer solve for it). In both cases the I_j in (3.2.14) are restricted to positive values.

3.2.5 **Excited states**

The preceding discussion has focused on the lowest lying energy state in each sector r. This state is characterized by real solutions to the equations (3.2.31) and (3.2.32). The characterization of excited states can be more complex and, indeed, several configurations of zeros have been proposed as candidates for the leading excitations; see, *e.g.* Destri and Lowenstein (1982), Woynarovich (1982), Babelon *et al.* (1983) and references therein. From a numerical point-of-view two problems are particularly significant. Firstly, (3.2.4) are non-linear equations and the number of solutions is unknown. Moreover, some of these solutions may correspond to complex values of the θ's making a numerical solution more difficult.

Physically, of course, we expect to find ${}^{M}C_{r}$ eigenvalues in each sector r. However, we are only interested in a few of the lowest lying energy states but require these states to be sequentially ordered. Unfortunately, even if we know a solution of (3.2.4) with energy given by (3.2.7), the Bethe ansatz provides little information on the

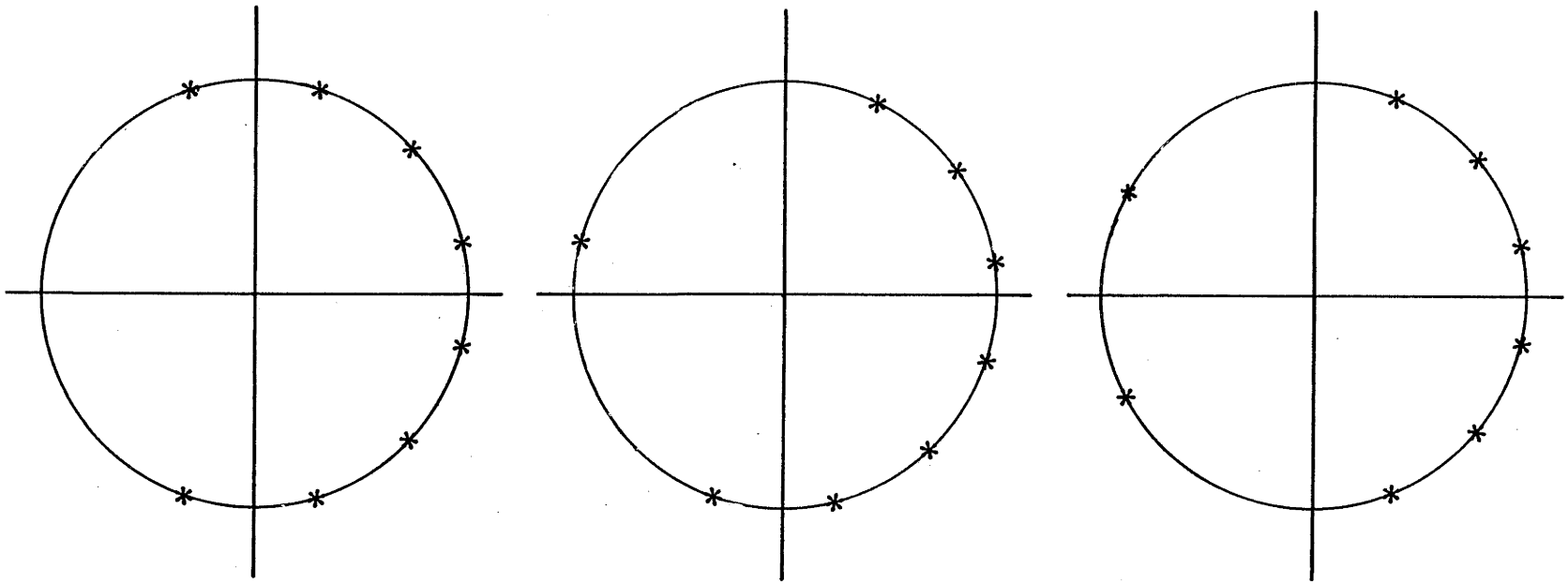

Figure 3.4 Distributions of zeros on the unit circle for $M = 16$ and $r = 8$ at $\gamma = \pi/6$ ($\Delta = -\sqrt{3}/2$). The distributions characterize: (a) the ground-state, (b) the leading state of lowest non-zero momentum ($P = 2\pi/16$), and (c) the so-called marginal state.

ordinal location of this state in the complete spectrum (we could only try to guess the location by judging the relative importance of the corresponding excitation in the particle/ sea picture). To overcome this problem, we have supplemented the numerical solution of the Bethe anstaz equations with the use of more standard methods for small chains, $M \leq 16$. In particular, iteration of the Lanczos algorithm sequentially yields the leading eigenvalues given appropriately chosen initial starting vectors (Cullum and Willoughby 1981). Here Francisco Alcaraz has provided me with some excellent programs, the most general of which gives the leading eigenvalues for all possible values of the momentum. Given these eigenvalues, we then match them to the values of E obtained by finding numerical solutions of (3.2.4). In particular, we identify the corresponding *distribution* of the θ's in the complex plane. Once this is achieved, the relevant levels in the eigen-spectrum can be obtained for large values of M, where the Lanczos algorithm is no longer feasible, by assuming that this distribution remains qualitatively the same. We now proceed to describe some of these excitations.

Lowest momentum state

This state is two-fold degenerate. On the unit circle the two responsible sets of zeros are related to each other by complex conjugation. Here the zero with I_j value $(r-1)/2$ is excited to one with value $(r+1)/2$ to give the total momentum in (3.2.8) as $P = 2\pi/M$. For $M = 16$ and $r = 8$ these zeros are shown in Figure 3.4(b) for $\gamma = \pi/6$. The same eigenvalue is obtained by exciting the zero with I_j value $-(r-1)/2$ to one with $-(r+1)/2$ giving $P = -2\pi/M$. These excitations correspond to the first two states shown in group I of Table 3.1. Such an excitation destroys the symmetry of the zeros around the origin and the full set of equations in (3.2.4) has to be solved.

Marginal state*

This state is characterized by *both* of the above excitations, leaving the symmetry around the origin preserved. In the particle/sea picture this is the group III excitation. For $M = 16$, $r = 8$ and $\gamma = \pi/6$ this set of zeros is shown in Figure 3.4(c). As γ tends to zero the two largest zeros in magnitude coalesce at the point $z = e^{i\theta} = -1$, as happened for $M = 4$ and $r = 2$ (recall Figure 3.2).

Further excited states

The above two levels have been obtained with relative ease. However, attempting to solve equations (3.2.4) for the two remaining group I configurations in a similar manner (by incrementing in Δ away from the known $\Delta = 0$ solutions) leads to *failure*. This can be understood by applying the twisted boundary condition (3.1.6). The Bethe anstaz equations for this system are derived in Appendix 3A. The main result is that the boundary angle ϕ effectively replaces the numbers I_j in (3.2.4) by I_j' where

$$I_j' = I_j + \frac{\phi}{2\pi}. \tag{3.2.33}$$

Subsequently the total momentum (2.7) is "shifted" and can be written

$$P' = \frac{r}{M}\phi + P. \tag{3.2.34}$$

For $0 \le \phi \le \pi$, comparison with the Lanczos results indicates the I_j for the minimum energy states to be again given by (3.2.14) (we would expect this from a *continuity*-type argument). We consider first the third group I state in Table 3.1. Here

$$I_j = -\frac{r-1}{2} + j - 1, \quad j = 0,1,\ldots, r-1, \tag{3.2.35}$$

with $P = -\pi + 2n\pi/M$. In Figure 3.5(a) we show the corresponding zeros for $M = 16$, $r = 8$ and $\gamma = \pi/6$ with $\phi = \pi/2$. Also shown are the initial $\gamma = \pi/2$ ($\Delta = 0$) starting points and the directions in which the zeros move as γ is incremented from $\pi/2$ to $\pi/6$.

---

* This nomenclature anticipates the identification of this state with the marginal operator of the eight-vertex model (see Section 3.3, below).

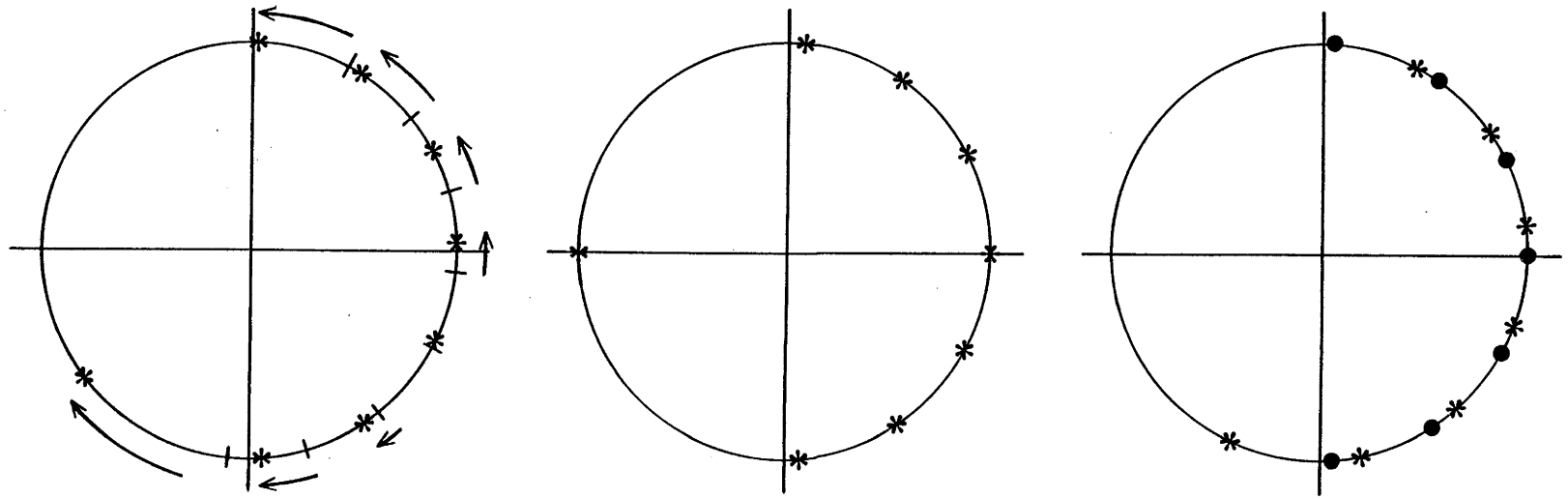

Figure 3.5 (a) Distribution of zeros on the unit circle for the choice (3.2.35) of the numbers I_j with $M = 16$, $r = 8$, $\gamma = \pi/6$ and $\phi = \pi/2$. Marks indicate the positions of the zeros at $\gamma = \pi/2$ ($\Delta = 0$) while the arrows indicate the movement of the zeros as γ is incremented to $\pi/6$. (b) The corresponding distribution in the limit $\phi = 0$, here the zeros, apart from those at $\theta = 0$ and $\theta = \pi$, are in reciprocal pairs. This configuration represents the first excited state in the ground-state sector. The zeros interlace those of the ground-state, shown in Figure 3.4(a). (c) Distribution of zeros for the first excited state in the sector $r = 7$, again for $M = 16$ and $\gamma = \pi/6$ ($\phi = 0$). The corresponding numbers I_j are given in (3.2.35). Filled circles indicate the corresponding minimum energy solution.

At the particular value $\gamma = \phi/2 = \pi/4$, these zeros were observed to be in complex conjugate pairs; apart from the zeros at the exact positions $\theta = 0$ and $\theta = -3\pi/4$. For $n = 0$ this was found to be true for all M whenever $\phi = 2\gamma$, except when $M/2$ is odd, in which case there is no zero at $\theta = 0$.

Figure 3.5(b) shows the position of the zeros of Figure 3.5(a) in the limit $\phi = 0$. Here the zeros again form into complex conjugate pairs. This distribution of zeros characterizes the *first* excited state in the $n = 0$ (ground-state) sector. For the same couplings and chain size, the zeros characterizing the first excited state in the sector $n = 1$ are shown in Figure 3.5(c). Here the I_j are as given in (3.2.35) and the equations (3.2.4) can be solved directly without recourse to switching on and off the "field" ϕ as described above to locate the position of the zeros in the limit $\phi = 0$.

Returning to Figure 3.5(b), we note the two exact zeros at $\theta = 0$ and $\theta = \pi$. This distribution of zeros corresponds to the solution (3.2.23a) for $M = 4$, which *also* gives the first excited state in the $n = 0$ sector at $\gamma = \pi/6$ (see Figure 3.3). For $M/2$ odd and $n = 0$ there is only the one exact zero, at $\theta = \pi$. For convenience in working with larger chain sizes, we have chosen $M/2$ to be even. In this case the zeros at $\theta = 0$ and $\theta = \pi$ can be factored out of the equations (3.2.4) and the remaining zeros determined numerically as for the minimum energy distribution. In particular, for these zeros we may choose

$$I_j = -\frac{r-3}{2} + j, \quad j = 0, 1, \ldots, r-3. \tag{3.2.36}$$

This choice does not exactly agree with (3.2.35), but nevertheless it reproduces the correct eigenvalue.

The remaining group I excitation listed in Table 3.1 has

$$I_j = -\frac{r-1}{2} + j + 1, \quad j = 0, 1, \ldots, r-1, \tag{3.2.37}$$

with $P = \pi - 2n\pi/M$. This distribution of zeros is shown in Figure 3.6(a) for $M = 16$, $r = 8$ and $\gamma = \pi/2.39$ at $\phi = \pi/3$. Also shown are the initial $\gamma = \pi/2$ ($\Delta = 0$) starting points. As γ is further decreased, the two zeros largest in magnitude move closer

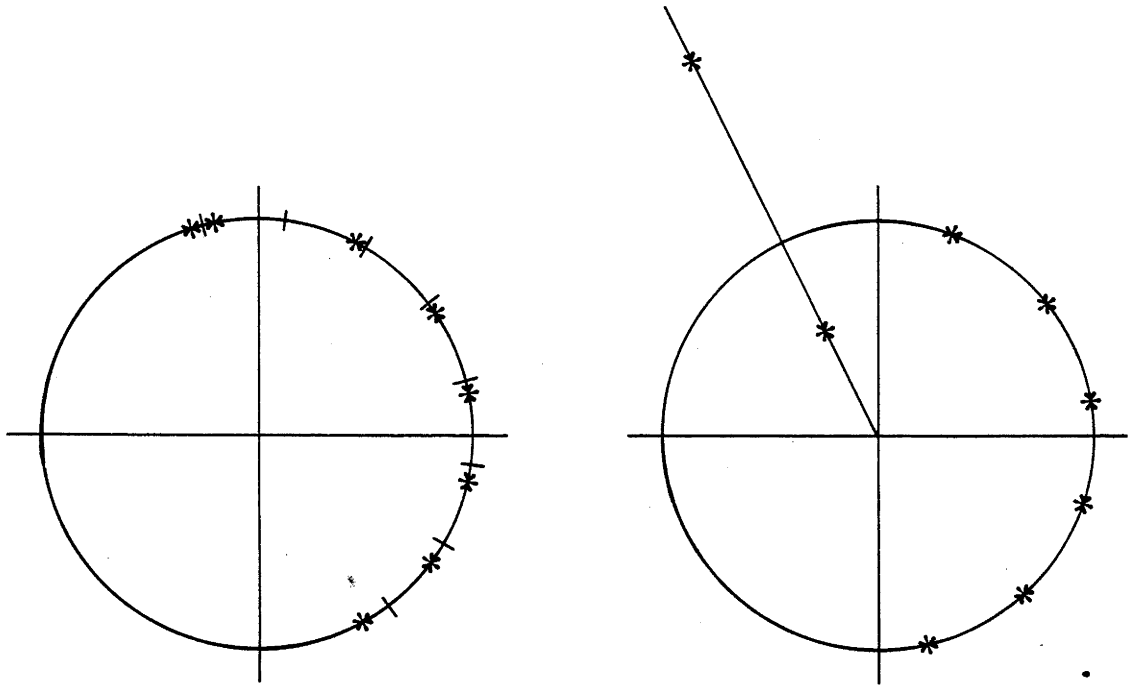

(a) (b)

Figure 3.6 (a) Distribution of zeros on the unit circle for the choice (3.2.37) of the numbers I_j with $M = 16$, $r = 8$, $\gamma = \pi / 2.39$ and $\phi = \pi/3$. Marks indicate the positions of the zeros at $\gamma = \pi/2$ ($\Delta = 0$). (b) The corresponding distribution at $\gamma = \pi/6$ showing a 2-string off the unit circle (see text).

together, until at a critical γ value they actually "collide". At this point the remaining zeros are in conjugate pairs and the total momentum (3.2.33) is given by $P' = \pi + \phi/2$. This momentum is shared by the two colliding zeros; implying that each zero collides at $\theta_c = \pi/2 + \phi/4$. Upon further decreasing γ, these two zeros move off on a ray in such a manner that the product of their moduli is always unity. In Figure 3.6(b) we show this distribution of zeros at $\gamma = \pi/6$.

This process represents the birth of the so-called 2-string (see, *e.g.* Takahashi and Suzuki 1972, Johnson *et al.* 1973). Unfortunately, the equations become difficult to solve, particularly so for large M, once the 2-string zeros leave the unit circle. However, in the limit $\phi = 0$, the 2-string configuration can be obtained with relative ease. To illustrate this it is convenient to write the Bethe ansatz equations in a different form.

3.2.6 Alternative formulation

The Bethe anstaz equations (3.2.4) can be written (Takahashi and Suzuki, 1972)

$$\left[\frac{\sinh\gamma(\lambda_j - i/2)}{\sinh\gamma(\lambda_j + i/2)}\right]^M = -\prod_{k=1}^{r}\frac{\sinh\gamma(\lambda_j - \lambda_k - i)}{\sinh\gamma(\lambda_j - \lambda_k + i)}, \quad j = 1,\ldots,r, \tag{3.2.38}$$

where the relationship between the new and original variables is

$$\theta = 2\tan^{-1}\left(\cot\tfrac{\gamma}{2}\tanh\gamma\lambda\right). \tag{3.2.39}$$

Similarly the energy expression (3.2.7) is

$$E = \tfrac{1}{2}M\cos\gamma - 2\sin^2\gamma\sum_{j=1}^{r}\frac{1}{\cosh(2\gamma\lambda_j) - \cos\gamma}. \tag{3.2.40}$$

In this formalism, the ground-state zeros in Figure 3.4(a) for $M = 16$, $r = 8$ and $\gamma = \pi/6$ map to the positions shown in Figure 3.7(a). For the first excited state in this sector, the exact zeros at $\theta = 0$ and $\theta = \pi$ are given by, respectively, $\lambda = 0$ and $\lambda = i\pi/(2\gamma)$. In this case, the zeros in Figure 3.4(b) occupy the positions shown in

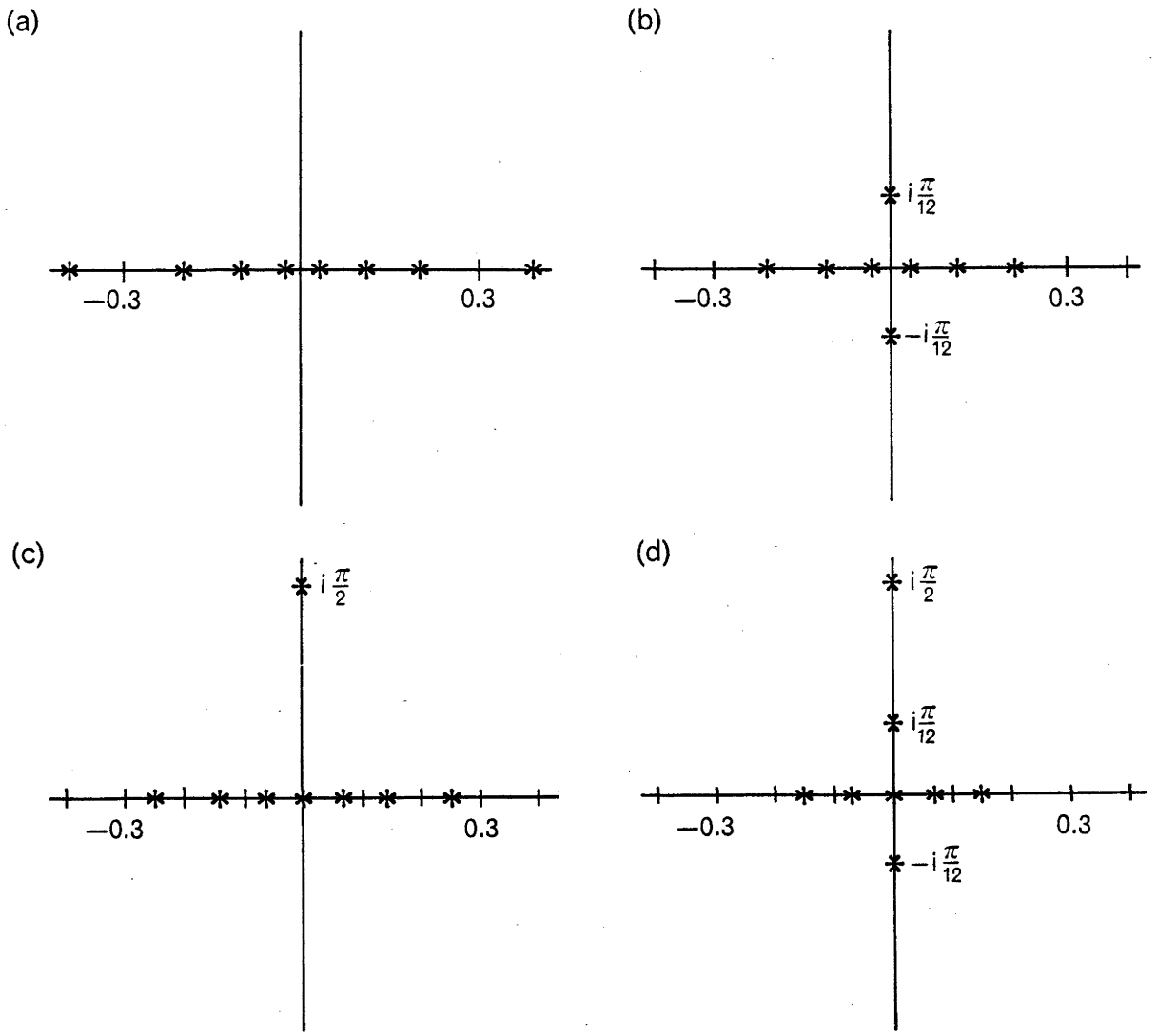

Figure 3.7 Typical distributions of zeros in the complex $\alpha = \gamma\lambda$ plane for $M = 16$ and $r = 8$ at $\gamma = \pi/6$. The configuration (a) characterizes the ground-state while the zeros in (c) and (b) give, respectively, the first and second excited states in the ground-sate sector. The zeros shown in (d) give a level higher in the spectrum. In each case all of the real zeros are symmetric about the origin. The vertical axis is schematic.

Figure 3.7(c). For later reference we refer to this set of zeros, and the I_j configurarion (3.2.35), as a 1-type solution.

2-string

As indicated in the previous Section, the distribution of zeros for the choice of the numbers I_j in (3.2.37) is the 2-string configuration. The zeros in the string have the I_j values $(r-1)/2$ and $(r+1)/2$ with the remaining numbers given in (3.2.36). In terms of the λ-variables, the 2-string corresponds to an *exact* pair of zeros at $\lambda_\pm = \pm i/2$, each of which satisfies one of the equations in (3.2.38). This configuration of zeros, for $M = 16$, $r = 8$ and $\gamma = \pi/6$, is shown in Figure 3.7(b). Here again, the outer-most pair of zeros in the mimimum energy distribution can be thought of as being excited, this time to the string positions. As for all excitations, the remaining zeros "relax".

To obtain the energy of the 2-string solution form (3.2.40) an appropriate limit has to be taken. We set $\lambda_\pm = x \pm i/2$ and then

$$\lim_{x \to 0} \left[\frac{1}{\cosh(2\gamma\lambda_+) - \cos\gamma} + \frac{1}{\cosh(2\gamma\lambda_-) - \cos\gamma} \right] = \frac{\cos\gamma}{\sin^2\gamma}, \qquad (3.2.41)$$

so that the contribution to the energy (3.2.40) of the 2-string is $-2\cos\gamma$.

In terms of the unit circle variables, the 2-string manifests itself as zeros at the origin and infinity. However, the product of these zeros is such that $z_+z_- = -1$ with $\cos p_+ + \cos p_- = -\cos\gamma$. We have already seen this pair of zeros in (3.2.23b) for $M = 4$. This solution can be understood for example, by attempting to "bootstrap" the zeros shown in Figure 3.6(b) to the limit $\phi = 0$. In this limit, the "collision angle" is $\theta_c = \pi/2$ and the momentum associated with the 2-string configuration is $P = \pi$.

In a given sector n, where n is even, we have found the 1-type solution to be the first excited state. The second excited state is the 2-string. (We emphasize however, that we have only examined the nature of the low-lying excitations for $\gamma \leq \pi/2$ $(\Delta \leq 0)$.) The corresponding I_j distributions are given by (3.2.35) and (3.2.27). In a given sector, for n odd, both choices give the first excited state. The two sets of zeros are related to each other by complex conjugation with the zeros confined to the unit

circle; as in Figure 3.5(c). However, for n odd, we *have* found an exact 2-string solution producing a level higher in the spectrum. For example, in the r = 3 sector, the exact solution $\lambda = 0, \pm i/2$ gives the exact energy $E = -2 + (M/2 - 4)\cos\gamma$ which is the *second* excited state in the ground-state (n = 0) sector for M = 6, but a *higher* level in the n = 1 sector for M = 8.

Related and more exotic excitations

Rather than exciting-off the zeros largest in magnitude to the positions $\lambda = 0$ and $\lambda = i\pi/(2\gamma)$ or to the 2-string configuration, pairs of zeros can be excited from positions closer to the origin in the minimum energy distribution to the same excitation positions but at a cost of higher energy. A further and, particularly, relevant excitation that we have found is a combination of the 1-type and 2-string excitations. The simplest example of this type of excitation for r even occurs in the r = 4 sector. Here the exact energy of this zero momentum excitation is $E = (M/2 - 6)\cos\gamma$ and all four zeros of largest magnitude (in this case *all* zeros) are excited from their ground-state positions. The corresponding distribution of zeros, for M = 16, r = 8 and $\gamma = \pi/6$, are shown in Figure 3.7(d). As can be seen for the excitations shown in this figure, the relaxation of the remaining zeros on the real axis is relatively slight, enabling the minimum energy distribution (3.2.29) to be used to provide initial starting points, as in the solution for the ground-state itself. Since all of the excitation positions shown are exact for all finite M, the zeros can be mapped to the unit circle formulation and factored from Eqs. (3.2.4), leaving again, a real system of equations to be solved for real unknowns.

As $M \to \infty$, the zeros on the real axis close up to form a dense set, while the excited imaginary zeros remain fixed at their bulk positions. Previously it was believed that the 2-string zeros for a finite system would only be *near* (exponentially close in M) their bulk positions. This idea can be traced back to Bethe (1931); we have seen however, that *some* excitations are exact for finite M – our 2-string solution is even exact for M = 4! It is interesting to observe that the next string-like solution of (3.2.38) is a 6-string with zeros at $\pm i/2, \pm 3i/2, \pm 5i/2$.

In order to summarize the results of this Section, we show in Figure 3.8 some of the particular levels in the periodic XXZ spectrum that we have obtained via the Bethe ansatz. Specifically, we show, as a function of Δ, the minimum energy (ground-state), group I (1-type, 2-string, lowest momentum) and group III (marginal) states for $n = 0$ and $M = 16$. For comparison, we show also the minimum energy and first excited states in the $n = 1$ sector. The $n = 1$ minimum energy state is is clearly seen to be the first excited state, although at $\Delta = -1$, the 1-type configuration gives the same energy. Recalling Figure 3.1, we see that, apart from the lowest momentum state, the degeneracy of the group I excitations is lifted for finite Δ. Further, we have observed that the marginal state remains a unique level in the spectrum $\forall\gamma$.

It should be emphasized that we have *not*, to this point, discussed any of the group II excitations; though the procedure for examining these levels should by now be quite clear. For again, attempting to insert the corresponding I_j into the *periodic* Bethe ansatz equations (3.2.4) and "bootstrap" the zeros away from the exact $\Delta = 0$ solutions results in failure. By "switching on and off" the field ϕ, as described above, these distributions of zeros should be similarly locatable in the complex plane. In this regard, it is worth mentioning an ingeneous method of locating the zeros suggested by Rodney Baxter (unpublished). Here one can *extract* the zeros from the eigenvectors. For example, in the $r = 3$ sector the expressions for the eigenvectors (in the $z = e^{i\theta}$ formulation) can be manipulated in such a way as to yield a cubic equation involving key components of the eigenvectors as co-efficients; the zeros are the roots of this equation. This method was seen to work well in practice and could be used to extract for example *all* of the zeros on relatively short chains where the exact eigenvectors can be found by conventional methods.

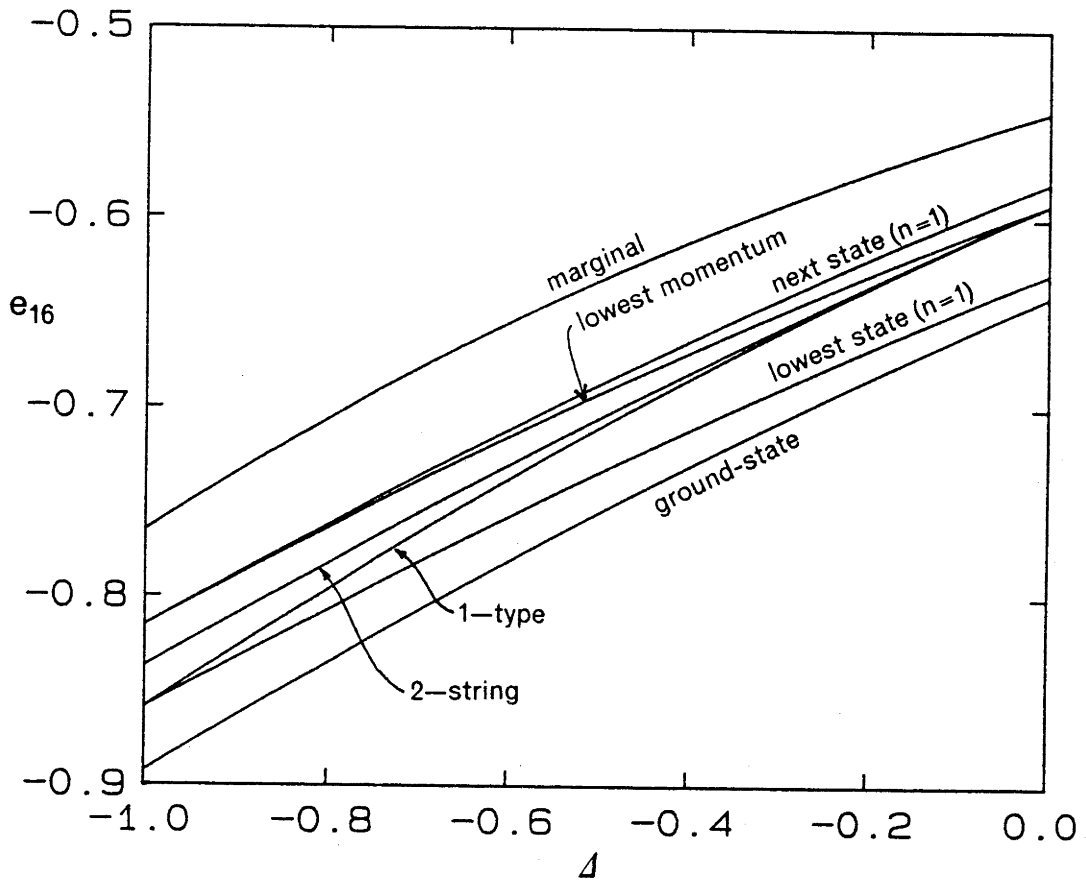

Figure 3.8 Energy levels, E/M for M = 16, as a function of Δ in the periodic XXZ eigen-spectrum, obtained via the Bethe ansatz. All of the levels shown have been discussed in the text and the corresponding zeros at the particular coupling $\gamma = \pi/6$ are to be found in the various figures: The ground-state zeros are shown in Figs. 3.4(a) and 3.7(a). The 1-type solution is shown in Figs. 3.5(b) and 3.7(c). The 2-string solution is shown in Fig. 3.7(b). One of the degenerate lowest momemtum states is shown in Fig. 3.4(b) with the marginal configuration shown in Fig. 3.4(c). Both the lowest and one of the degenerate next-lowest states in the n = 1 sector are shown in Fig. 3.5(c).

3.2.7 Eigen-spectrum for twisted boundaries

The effect of the boundary angle ϕ on the eigen-energies is readily illustrated by returning to the $\Delta = 0$ limit. Here the eigen-energies (3.2.12) are replaced by

$$E = -2\sum_{j=1}^{r}\cos\left(\frac{2\pi I_j}{M} + \frac{\phi}{M}\right), \tag{3.2.42}$$

The choice (3.2.14) corresponding to the *minimum energy state* is seen to give

$$E_0(n,\phi) = -2\cos\frac{\phi}{M}\cos\frac{n\pi}{M}\operatorname{cosec}\frac{\pi}{M}. \tag{3.2.43}$$

This is the generaliztion of the periodic ($\phi = 0$) result (3.2.16). We now proceed to work our way through the list of excitations in Table 3.1. Here we list below the quantities $\delta E(n,\phi) \equiv E(n,\phi) - E_0(n,\phi)$. The group I excitations yield, respectively,

$$4\cos\left(\frac{n\pi}{M} - \frac{\phi}{M}\right)\sin\frac{\pi}{M}, \tag{3.2.44a}$$

$$4\cos\left(\frac{n\pi}{M} + \frac{\phi}{M}\right)\sin\frac{\pi}{M}, \tag{3.2.44b}$$

$$4\cos\left(\frac{n\pi}{M}\right)\sin\left(\frac{\pi}{M} - \frac{\phi}{M}\right), \tag{3.2.44c}$$

$$4\cos\left(\frac{n\pi}{M}\right)\sin\left(\frac{\pi}{M} + \frac{\phi}{M}\right). \tag{3.2.44d}$$

And similarly for group IIa:

$$2\sin\left(\frac{n\pi}{M} + \frac{3\pi}{M} - \frac{\phi}{M}\right) - 2\sin\left(\frac{n\pi}{M} - \frac{\pi}{M} - \frac{\phi}{M}\right), \tag{3.2.45a}$$

$$2\sin\left(\frac{n\pi}{M} + \frac{3\pi}{M} + \frac{\phi}{M}\right) - 2\sin\left(\frac{n\pi}{M} - \frac{\pi}{M} + \frac{\phi}{M}\right), \tag{3.2.45b}$$

$$2\sin\left(\frac{n\pi}{M} + \frac{3\pi}{M} - \frac{\phi}{M}\right) - 2\sin\left(\frac{n\pi}{M} - \frac{\pi}{M} + \frac{\phi}{M}\right), \tag{3.2.45c}$$

$$2\sin\left(\frac{n\pi}{M} + \frac{3\pi}{M} + \frac{\phi}{M}\right) - 2\sin\left(\frac{n\pi}{M} - \frac{\pi}{M} - \frac{\phi}{M}\right). \tag{3.2.45d}$$

In IIb there are two degenerate levels:

$$2\sin\left(\frac{n\pi}{M} + \frac{\pi}{M} + \frac{\phi}{M}\right) - 2\sin\left(\frac{n\pi}{M} - \frac{3\pi}{M} - \frac{\phi}{M}\right), \tag{3.2.46a}$$

$$2 \sin\left(\frac{n\pi}{M} + \frac{\pi}{M} - \frac{\phi}{M}\right) - 2 \sin\left(\frac{n\pi}{M} - \frac{3\pi}{M} + \frac{\phi}{M}\right). \qquad (3.2.46b)$$

Finally, the group III excitation gives

$$8 \cos\frac{\phi}{M} \cos\frac{n\pi}{M} \sin\frac{\pi}{M}. \qquad (3.2.47)$$

These levels were shown in Figure 3.1 at $\phi = 0$ for $n = 0, 1, 2$ and $M = 16$. The corresponding levels, now as a function of ϕ, are shown in Figure 3.9. Several comments are in order. Firstly, the figure indicates that $\phi = \pi$ is a special point. Here many of the sets of I_j' in (3.2.33) are related to each other by negation, giving rise to the degeneracy of levels. For $M = 8$ we have observed, by diagonalizing the complete Hamiltonian, that the eigenspectrum is in fact *symmetric* about the line through $\phi = \pi$. The same calculations also indicate this to be true for non-zero Δ. The effect of the boundary angle ϕ on the two lowest states in the $n = 0$ sector for $M = 16$ and $\gamma = \pi/6$ is shown in Figure 3.10, further indicating the symmetry about $\phi = \pi$.

We have seen in this Section that the angle ϕ is capable of dramatically *shifting* the eigen-spectrum of the periodic chain. We will show in the following Sections that it is *precisely* this behaviour that enables us to recover the anomalous dimensions of the critical Potts models. Here we remark that we have found (numerically) the ground-state energy to be given by $E_0 = -3M/4$ for *all* even M at the particular couplings $\gamma = \pi/3$ and $\phi = 2\pi/3$. This observation provides a very useful check on the accuracy of the numerical solution of the Bethe ansatz equations. This effect is somewhat similar to the disorder-type solutions found in various models where convenient values of the coupling constants are chosen to yield a constant free-energy per site. As in those cases, it suggests that the associated eigenvector should have a simple product form, although we have been unable to find such a representation.

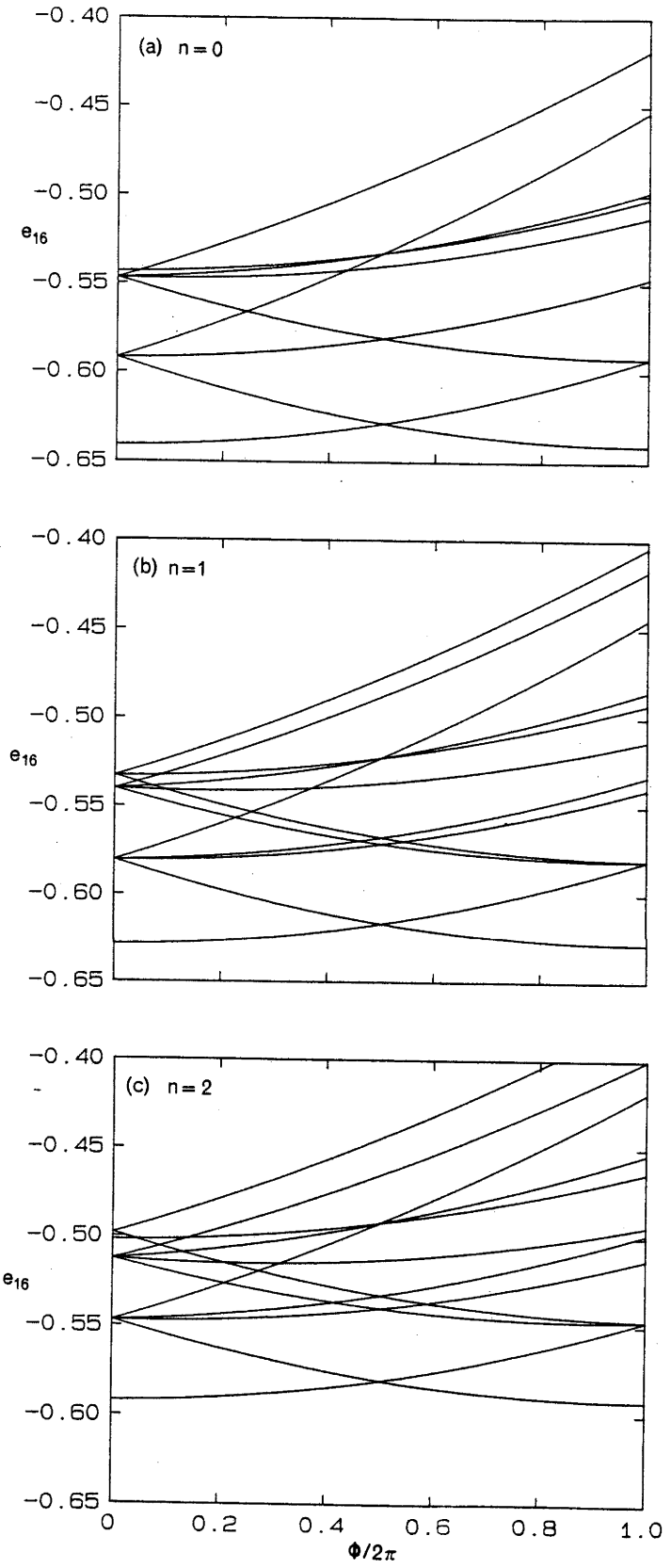

Figure 3.9 The leading $\Delta = 0$ energy levels ($e_{16} = E/16$), calculated in the text, as a function of ϕ for $M = 16$. In general, the levels are symmetric about $\phi = \pi$.

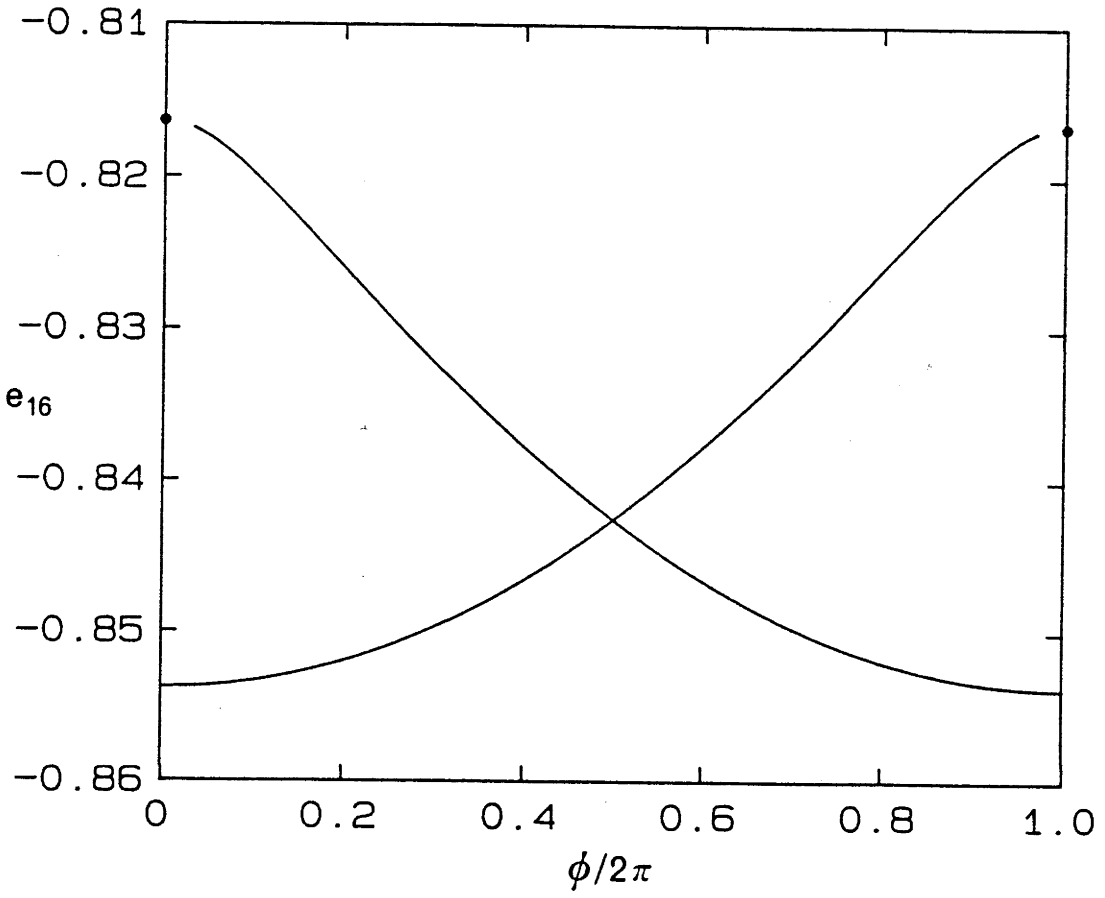

Figure 3.10 The two lowest states, obtained via the Bethe ansatz, in the sector $r = 8$ for $M = 16$ and $\gamma = \pi/6$ as a function of the boundary angle ϕ. The two levels are symmetric about $\phi = \pi$. The lines terminate where an attempt at numerical solution fails.

3.3 OPERATOR CONTENT OF THE PERIODIC XXZ CHAIN

In this Section, we make use of the predictions, (3.1.2) and (3.1.3), of conformal invariance, to interpret the eigen-spectrum of $\mathcal{H}_{XXZ}$ on a periodic chain revealed by the numerical results of the preceding section. From these relations and the numerical solution of equations (3.2.4) for large M we are able to estimate with very high precision various anomalous dimensions.

We begin by recalling that for even M, the ground-state of $\mathcal{H}_{XXZ}$ is antiferromagnetic, non-degenerate and corresponds to the mimimum energy solution of (3.2.4) in the sector $n = 0$. On the other hand, if M is odd, the ground-state is two-fold degenerate; the degenerate eigenvectors corresponding to the minimum energy solutions in the two sectors $n = \pm 1/2$. These states are not truly antiferromagnetic and hence the interpretation of the eigen-spectrum of (3.1.4) for odd M is qualitatively different; we defer consideration of this case to Section 3.3.4.

In Section 3.3.5, we briefly examine the role of the boundary angle ϕ in the operator content of the XXZ chain.

3.3.1 Ground-state energy and the conformal anomaly

If M is even, the value of the conformal anomaly follows from the behaviour of the ground-state energy $E_0(\gamma,M)$ for periodic boundary conditions as $M\to\infty$. This has been computed analytically by Hamer (1985, 1986a), who found that

$$E_0(\gamma,M)/M = e_\infty(\gamma) - \frac{\pi}{6}\zeta_x M^{-2} + o(M^{-2}), \qquad (3.3.1)$$

where the bulk limit e_∞ is given in (3.2.28) and the conformal scale, ζ_x by (3.1.5). Comparison with (3.1.2) implies

$$c = 1. \qquad (3.3.2)$$

In Table 3.4 we list the raw estimators

$$c_M(\gamma) \equiv \frac{6\,M}{\pi\,\zeta_x}\left[e_\infty(\gamma)\,M - E_0(\gamma,M)\right] \tag{3.3.3}$$

for several values of γ and $M = 4, 8, 16, \ldots, 512$. The values of $E_0(\gamma,M)$ were obtained by solving system (3.2.31) as described above with $r = M/2$. For those values of γ for which $e_\infty(\gamma)$ is not listed in Table 3.2, the integral in (3.2.28a) was evaluated numerically. Rapid convergence of the estimators (3.3.3) to the exact value (3.3.2) is apparent for all γ.

At $\gamma = \pi/2$ ($\Delta = 0$), the ground-state energy for finite M is given exactly by (3.2.16) with $n = 0$:

$$E_0(\tfrac{\pi}{2}, M) = -2\,\mathrm{cosec}\,\frac{\pi}{M}. \tag{3.3.4}$$

Expanding in powers of M^{-1} gives

$$c_M(\tfrac{\pi}{2}) = 1 + \frac{7\pi^2}{60}M^{-2} + O(M^{-4}), \tag{3.3.5}$$

which explains the excellent convergence seen in Table 3.4 at this value of γ.* We shall return to the convergence of the estimators (3.3.3) and thus the next correction term in (3.3.1) for general γ in Section 3.6.

3.3.2 Excited states

As mentioned in the introduction to this chapter, we expect the anomalous dimensions of at least some operators associated with the eigenspectrum of $\mathcal{H}_{xxz}$ to vary with γ. It will turn out that the natural parametrization of this variation is by

$$x_p = \frac{\pi - \gamma}{2\pi}. \tag{3.3.6}$$

---

* Note that at $\gamma = \pi/2$ the model is equivalent to a *doubled* Ising chain; hence we obtain $c = 1$ instead of $c = 1/2$ as might have been anticipated.

Table 3.4 Conformal anomaly estimators $c_M(\gamma)$ (Eqn. (3.3.3)) with increasing M as a function of γ.

M	γ: 0	$\pi/6$	$\pi/3$	$\pi/2$	$2\pi/3$
4	1.105 996	1.104 853	1.094 664	1.076 962	1.035 786
8	1.030 227	1.029 152	1.023 200	1.018 289	1.009 759
16	1.010 452	1.009 435	1.005 937	1.004 516	1.002 473
32	1.004 496	1.003 560	1.001 535	1.001 126	1.000 620
64	1.002 395	1.001 558	1.000 397	1.000 281	1.000 155
128	1.001 496	1.000 765	1.000 103	1.000 070	1.000 039
256	1.001 032	1.000 404	1.000 027	1.000 018	1.000 010
512	1.000 756	1.000 223	1.000 007	1.000 004	1.000 002

Table 3.5 Scaling dimension estimators $\Lambda_M(\gamma; 1)$ (Eqn. (3.3.7)) with increasing M as a function of γ.

M	γ: $\pi/6$	$\pi/3$	$\pi/2$	$2\pi/3$
8	0.397 934	0.333 262	0.253 263	0.170 367
16	0.405 936	0.333 149	0.250 806	0.167 578
32	0.410 630	0.333 248	0.250 201	0.166 894
64	0.413 265	0.333 303	0.250 050	0.166 723
128	0.414 739	0.333 323	0.250 013	0.166 681
256	0.415 569	0.333 330	0.250 003	0.166 670
512	0.416 040	0.333 332	0.250 001	0.166 668
x_p	0.416 667	0.333 333	0.25	0.166 667

Minimum energy levels

We first discuss the energy levels corresponding to the minimum energy solutions in each sector. Define

$$\Lambda_M(\gamma; n) \equiv \frac{M}{2\pi \zeta_x} \left[E_n(\gamma, M) - E_0(\gamma, M) \right], \tag{3.3.7}$$

where E_n is the lowest energy in sector n. Table 3.5 lists the sequence $\Lambda_M(\gamma; 1)$ for several values of γ and $M = 8, 16, \ldots, 512$. Also shown are the corresponding values of the quantity x_p defined in (3.3.6). Accordingly, in Figure 3.11 we show $\Lambda_{256}(\gamma; n)$ for $n = 1, 2, 3$ and 4 as a function of x_p. In each case, convergence to the limit

$$x_{n,0} = n^2 x_p \tag{3.3.8}$$

is apparent and can be confirmed by numerical extrapolation of the sequences by standard acceleration techniques (see, *e.g.* Barber 1983)*. For each n, the level has zero momentum and is specified by $s_\alpha = 0$ with $j = j' = 0$ in (3.1.3).

At $\gamma = \pi/2$ (3.3.8) can be verified exactly. From (3.2.16),

$$E_n - E_0 = -2\left(\cos \frac{n\pi}{M} - 1 \right) \operatorname{cosec} \frac{\pi}{M}. \tag{3.3.9}$$

On expanding this result in powers of M^{-1}, the definition (3.3.7) yields

$$\Lambda_M(\tfrac{\pi}{2}; n) = n^2 \tfrac{1}{4} \left[1 - \frac{(n^2 - 2)\pi^2}{12M^2} + O(M^{-4}) \right], \tag{3.3.10}$$

explaining the rapid convergence seen at this point in Table 3.5. Also, as we would expect, the convergence is seen to be slower for large values of n (*i.e.* for levels higher in the spectrum), though still dominated by the same correction to scaling exponent.

These results suggest the existence of a set of operators $O_{n,0}$ with scaling dimensions $x_{n,0}$. The operators $O_{1,0}$ and $O_{2,0}$ correspond (den Nijs 1981) to the polarization and energy operators, respectively, of the eight-vertex model. This identification of $O_{1,0}$ confirms that made by Hamer (1985, 1986a) from an analytical

---

* Throughout this chapter we list only the "raw" estimates of various anomalous dimensions.

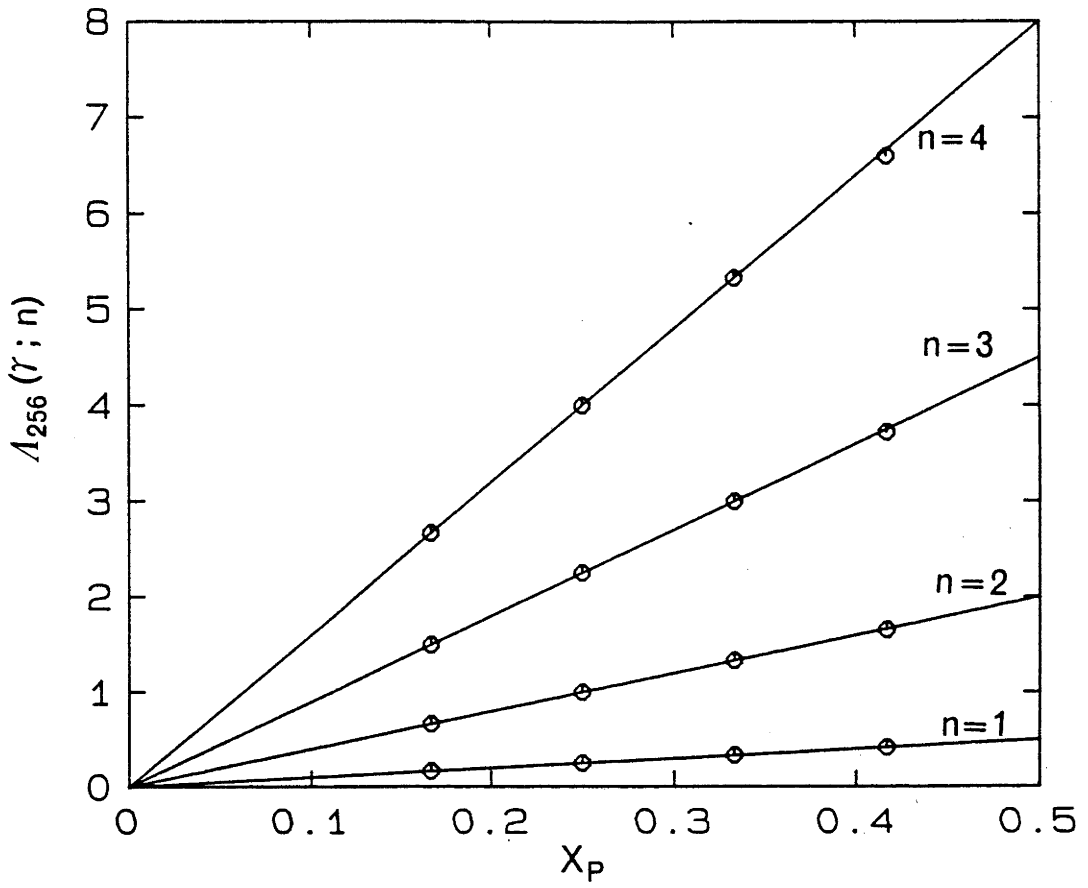

Figure 3.11 The minimum energy solution scaling dimension estimators $\Lambda_{256}(\gamma; n)$ (Eqn. (3.3.7)) as a function of x_p. The solid lines are given by $n^2 x_p$.

treatment of the Bethe ansatz equations.

Hamer's analysis can be easily extended to the other minimum energy solutions of (3.2.4); see also Woynarovich and Eckle (1987). Specifically, Hamer's results show that for large M the gap $E_n - E_0$ can be approximated to leading order by

$$E_n - E_0 \approx M\left[f(\gamma, \tfrac{2n}{M}) - f(\gamma, 0)\right], \tag{3.3.11}$$

where

$$f(\gamma, y) = \lim_{M\to\infty} E_M(y)/M \tag{3.3.12}$$

is the smallest eigenvalue of $\mathcal{H}_{XXZ}$ with magnetization per spin,

$$y = \lim_{M\to\infty} \left(\frac{1}{M} \sum_{m=1}^{M} \sigma_m^z \right), \tag{3.3.13}$$

on an *infinite* lattice. This has been calculated by Yang and Yang (1966a,b). From their results*

$$f(\gamma, y) - f(\gamma, 0) = \frac{\pi - \gamma}{4} \zeta_x y^2 + o(y^2) \quad \text{as } y \to 0. \tag{3.3.14}$$

Substituting this result in (3.3.11) yields precisely (3.3.8) and confirms our numerical results.

The lowest momentum and marginal states

As described in Section 3.2.5, from the point of view of the Bethe ansatz the simplest excited state in a given sector is the lowest state with momemtum $P = \pm 2\pi/M$. In the $n = 0$ sector, its energy implies the existence of an operator with anomalous dimension $x = 1$ for all γ, as indicated for various γ in Table 3.6. In (3.1.3), this result suggests the assignments $x_\alpha = 1$, $s_\alpha = \pm 1$ with $j = j' = 0$. The physical significance of this dimension is discussed in Section 3.3.3.

---

* Note that f as defined here differs from that in Yang and Yang (1966a,b) by a factor of two.

Table 3. 6 Scaling dimension estimates for the lowest state with momentum $P = \pm 2\pi/M$.

M	γ: $\pi/6$	$\pi/3$	$\pi/2$	$2\pi/3$
8	0.960 486	0.955 183	0.974 495	1.062 337
16	0.996 034	0.989 095	0.993 587	1.017 373
32	1.002 320	0.997 381	0.998 394	1.004 465
64	1.002 428	0.999 374	0.999 598	1.001 124
128	1.001 650	0.999 850	0.999 900	1.000 281
256	1.001 006	0.999 964	0.999 975	1.000 070

Table 3.7 Scaling dimension estimates for the marginal state.

M	γ: $\pi/6$	$\pi/3$	$\pi/2$	$2\pi/3$
8	1.569 939	1.765 226	1.948 991	2.242 794
16	1.752 223	1.924 394	1.987 174	2.060 717
32	1.853 806	1.977 894	1.996 789	2.015 157
64	1.912 551	1.993 790	1.999 197	2.003 788
128	1.947 734	1.998 287	1.999 799	2.000 947
256	1.969 020	1.999 533	1.999 950	2.000 237
512	1.981 809	1.999 873	1.999 987	2.000 059

The analogous distributions of zeros in the sectors $n = 1, 2, \ldots$ yield scaling dimensions $x_{n,0} + 1$. Evidence for this is presented in Figure 3.12(a) where we show the estimators $\Lambda_{256}(\gamma\,;\,n)$, $n = 1 \rightarrow 4$ as a function of x_p (here and for subsequent levels we redefine (3.3.7) accordingly). Such values correspond to the *first* level in the conformal tower associated with the operators $O_{n,0}$ ($s_\alpha = 0$ with $j = 0, j' = 1$ or $j = 1, j' = 0$).

In the $n = 0$ sector, the "marginal" configuration of zeros also predicts a γ-independent anomalous dimension, namely $x = 2$, as shown in Table 3.7. The associated operator is thus marginal corresponding to the four-spin coupling of the eight-vertex model. Its presence in $c = 1$ theories results in the appearance of a line of critical points; the operator itself governing motion along the critical line (Kadanoff and Brown 1979, den Nijs 1981). This state has zero momemtum and in (3.1.3) corresponds to $x_\alpha = 2$, $s_\alpha = 0$ with $j = j' = 0$.

The analogous distribution of zeros in the other sectors yield scaling dimensions $x_{n,0} + 2$ as indicated in Figure 3.12(b). Such values correspond to the *second* level in the conformal tower associated with the operators $O_{n,0}$ ($s_\alpha = 0$ with $j = j' = 1$).

Again, these results can be verified *exactly* at $\gamma = \pi/2$. The anomalous dimensions associated with each of the excitations listed in Table 3.1 at this point are indicated on the energy levels shown in Figure 3.1. Looking back at this figure, we see that even for $M = 16$, the low-lying levels in the eigen-spectrum appear to be well "ordered". Recall that the lowest momentum state is in group I while the "marginal" configuration constitutes group III. We turn now to the two remaining group I excitations.

1-type and 2-string solutions

As seen from Table 3.8A, in the $n = 0$ sector, both the 1-type and 2-string excitations appear to correspond to an operator $O_{0,1}$ with dimension $x_{0,1} \equiv (4x_p)^{-1}$. The operator $O_{0,1}$ can be identified (den Nijs 1981) with the crossover operator of the eight-vertex model or equivalently the energy operator of the Ashkin-Teller model (see

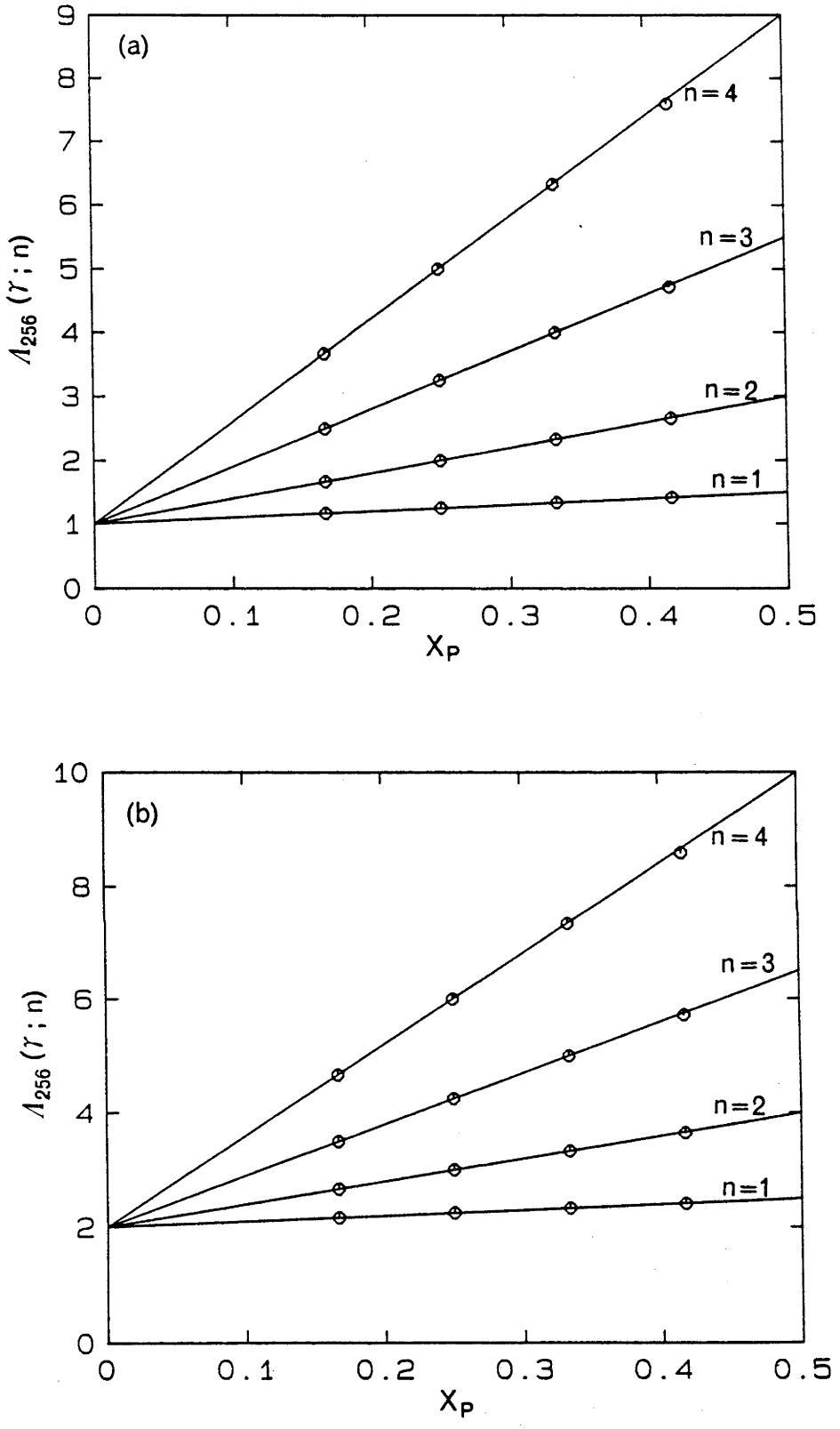

Figure 3.12 Scaling dimension estimators, analogous to (3.3.7), as a function of x_p for (a) the lowest state with momentum $P = \pm 2\pi/M$ and (b) The marginal configuration. The solid lines are given by (a) $1 + n^2 x_p$ and (b) $2 + n^2 x_p$.

Table 3.8 A: Anomalous dimensions associated with the 1-type and 2-string excitations in the ground-state (n = 0) sector. Also shown are the corresponding values of $x_{0,1} = (4x_p)^{-1}$. B: As for above, but with the "holes" at the second-most outer pair of zeros. Here the estimates converge to the limit $x_{0,1} + 2$.

	γ:	$5\pi/12$		$\pi/3$		$\pi/4$	
	M	1-type	2-string	1-type	2-string	1-type	2-string
A							
	8	0.801 564	0.868 600	0.659 420	0.811 150	0.552 107	0.783 910
	16	0.837 994	0.864 500	0.704 764	0.785 743	0.592 327	0.744 140
	32	0.850 617	0.860 625	0.727 867	0.769 180	0.619 128	0.715 883
	64	0.854 889	0.858 623	0.739 166	0.759 948	0.636 459	0.697 639
	128	0.856 351	0.857 740	0.744 666	0.755 075	0.647 536	0.686 125
	256	0.856 860	0.857 376	0.747 359	0.752 567	0.654 574	0.678 895
	512	0.857 041	0.857 233	0.748 688	0.751 292	0.659 033	0.674 356
	$x_{0,1}$	0.857 142		0.75		0.666 667	
B							
	8	2.141 106	2.345 764	2.045 547	2.344 147	2.006 331	2.343 304
	16	2.617 468	2.753 516	2.448 128	2.722 538	2.344 594	2.710 612
	32	2.784 062	2.841 103	2.624 220	2.782 303	2.497 869	2.756 912
	64	2.834 932	2.856 763	2.695 968	2.778 101	2.571 134	2.739 357
	128	2.850 022	2.858 389	2.725 700	2.767 202	2.609 759	2.716 635
	256	2.854 910	2.857 952	2.738 631	2.759 442	2.631 810	2.699 306
	512	2.856 399	2.857 530	2.744 534	2.754 947	2.645 018	2.687 571
	$x_{0,1} + 2$	2.857 142		2.75		2.666 667	

Section 3.4). We have found that the *second* level in the conformal tower associated with this operator is located by considering the 1-type and 2-string excitations in which the "holes" are now at the second-most outer pair of zeros. In Table 3.8B we list the successive estimates of the scaling dimensions for these levels. They correspond to the choice $j = j' = 1$ in (3.1.3), giving an "effective" scaling dimension $x = x_{0,1} + 2$.

Let us define a general set of operators $O_{n,m}$ with dimensions

$$x_{n,m} = n^2 x_p + \frac{m^2}{4x_p} , \qquad (3.3.15)$$

where $n, m = 0, 1, \ldots ; (n, m) \neq (0, 0)$. Evidence is presented below indicating that the equivalent excitations (namely 1-type and 2-string) in other sectors correspond to operators $O_{n,1}$. For example, in the $n = 1$ sector, the first excited state, obtained by directly choosing either of the distributions (3.2.35) or (3.2.37), gives dimension $x_{1,1}$, corresponding to an operator $O_{1,1}$. The numerical estimates of the anomalous dimension are given in Table 3.9. On the other hand, we have already observed that the exact 2-string configuration in this sector produces an energy level higher in the spectrum. This level, in fact, yields a scaling dimension $x_{1,1} + 1$, as shown in Table 3.10, corresponding to the *first* level in the conformal tower associated with the operator $O_{1,1}$.

The finite-size estimates of the scaling dimension of the level associated with the choices (3.2.35) or (3.2.37) in sector $n = 3$ are shown in Table 3.11. These results are clearly seen to fit the value $x_{3,1}$ in (3.3.15), thus indicating the presence of an operator $O_{3,1}$. In a similar manner we locate the anomalous dimensions $x_{n,1}$ associated with the operaors $O_{n,1}$.

We have also located a state in the XXZ eigenspectrum corresponding to an operator $O_{0,2}$ with dimension $x_{0,2} = 2\pi / (\pi - \gamma)$, which is irrelevant for $\gamma > 0$ but becomes marginal at $\gamma = 0$. We find that this operator is, in fact, *the main determinant* of the finite-size corrections appearing in the XXZ model and plays an important role in the finite-size behaviour of the Ashkin-Teller and Potts models (Alcaraz, Barber and Batchelor 1987a,b). This state is a combination of the leading 1-type and 2-string excitations described in Section 3.2.6. For $M = 16$, $n = 0$ and $\gamma = \pi/6$, the

Table 3.9 Scaling dimension estimates for the first excited state in the n = 1 sector. Also shown is $x_{1,1} = x_p + (4x_p)^{-1}$.

M	γ: $5\pi/12$	$\pi/3$	$\pi/4$	$\pi/6$
8	1.066 477	1.013 921	0.985 412	0.972 295
16	1.127 636	1.065 689	1.029 291	1.011 322
32	1.143 470	1.078 909	1.039 313	1.018 577
64	1.147 471	1.082 227	1.041 372	1.018 962
128	1.148 474	1.083 057	1.041 709	1.018 269
256	1.148 726	1.083 264	1.041 723	1.017 653
$x_{1,1}$	1.148 809	1.083 333	1.041 667	1.016 667

Table 3.10 Scaling dimension estimates for the 2-string excitation in the n = 1 sector. The estimates converge to $x_{1,1} + 1$.

M	γ: $5\pi/12$	$\pi/3$	$\pi/4$
8	2.028 721	2.045 547	2.079 608
16	2.134 060	2.130 461	2.163 770
32	2.150 799	2.124 661	2.145 892
64	2.151 402	2.108 783	2.115 141
128	2.150 235	2.097 366	2.090 327
256	2.149 455	2.090 709	2.073 089
512	2.149 078	2.087 120	2.061 725
$x_{1,1} + 1$	2.148 809	2.083 333	2.041 667

Table 3.11 Scaling dimension estimates for the first excited state in the $n = 3$ sector. Also shown is $x_{3,1} = 9x_p + (4x_p)^{-1}$.

M	γ: $5\pi/12$	$\pi/3$	$\pi/4$	$\pi/6$
8	2.634 756	2.822 694	2.979 924	3.098 340
16	3.248 052	3.479 528	3.695 062	3.870 702
32	3.422 004	3.677 194	3.933 074	4.157 436
64	3.466 990	3.730 878	4.006 925	4.263 841
128	3.478 345	3.745 019	4.030 094	4.307 412
256	3.481 193	3.748 707	4.037 643	4.327 466
$x_{3,1}$	3.482 142	3.75	4.041 667	4.35

Table 3.12 Scaling dimension estimates for the "combined" 1-type and 2-string excitation in the $n = 0$ sector. The estimates converge to the limit $x_{0,2} = 1/x_p$.

M	γ: $5\pi/12$	$\pi/3$	$\pi/4$
8	2.842 881	2.535 617	2.343 304
16	3.263 390	2.849 612	2.564 743
32	3.386 198	2.955 371	2.634 274
64	3.417 929	2.987 281	2.655 986
128	3.425 910	2.996 450	2.662 991
256	3.427 906	2.999 022	2.665 351
512	3.428 405	2.999 733	2.666 181
$x_{0,2}$	3.428 571	3.0	2.666 667

corresponding zeros are those of Figure 3.7(d). Estimates of the anomalous dimension, at various γ, are given in Table 3.12 and are clearly seen to fit the value $x_{0,2}$.

Finally, we remark that we have not persued the location of further (higher) levels in the eigen-spectrum in order to further justify the general result (3.3.15). As we shall see below, it can even be "derived".

3.3.3 **Relation to the Gaussian model**

The anomalous dimensions revealed by the above analysis of the eigen-spectrum of the XXZ model are remarkably similar to those of the Gaussian model derived by Kadanoff and Brown (1979) and Kadanoff (1979). (See also Knops (1980).) In particular, there exists in the Gaussian model a set of operators with anomalous dimensions having the same structure as (3.3.15), namely

$$x^{G}_{n,m} = \frac{n^2}{4\pi K} + \pi K m^2 , \tag{3.3.16}$$

where K is the coupling. This similarity is, in fact, no coincidence.

As discussed above, $O_{1,0}$ is the polarization operator of the eight-vertex model. Hence identifying $x_{1,0} = x_p$ with the electric field exponent of the eight-vertex model gives an explicit mapping of the interval $[0,\pi)$ of γ-values for which the XXZ model is massless to the critical line of the eight-vertex model, parametrized by the four-spin coupling, K_4 (den Nijs 1981):†

$$\gamma = \cos^{-1}(-\tanh 2K_4) . \tag{3.3.17}$$

On the other hand, Kadanoff and Brown (1979) argued that the critical line of the eight-vertex model maps to the Gaussian model through the transformation

$$\tanh 2K_4 = \cos\left(\frac{1}{2K}\right) . \tag{3.3.18}$$

---

† Note that through (2.3.15c), we have $\gamma \equiv \mu$.

Eliminating K_4 between (3.3.17) and (3.3.18) gives the direct map

$$\gamma = \pi - \frac{1}{2K} \tag{3.3.19}$$

from the XXZ model to the Gaussian model. Recalling the definition (3.3.6) of x_p, we immediately find that (3.3.15) maps directly to (3.3.16) under (3.3.19). Hence we can identify the XXZ operators $O_{n,m}$ as the analogs of Gaussian model operators (Kadanoff and Brown 1979) composed of spin wave excitation of index n and a "vortex" excitation of vorticity m.

We can now carry the identification of the XXZ operators one step further. We have already remarked that $O_{1,0}$ is the cross-over operator of the eight-vertex model (den Nijs 1981). This in turn is known (den Nijs 1979) to be the energy operator of the Ashkin-Teller model (Ashkin and Teller 1943). The precise mapping from the XXZ model with coupling $\Delta = -\cos\gamma$ to the critical line of the Ashkin-Teller model, parametrized by the four-spin coupling K_4^{AT} follows if we accept the mapping (Kadanoff and Brown 1979)

$$\tanh 2K_4^{AT} = \frac{\cos(\pi^2 K/2)}{\cos(\pi^2 K/2) - 1} \tag{3.3.20}$$

of the Ashkin-Teller model to the Gaussian model. Composing this result with (3.3.15) gives the equivalence

$$\cos\gamma = -\frac{\tanh 2K_4^{AT}}{\tanh 2K_4^{AT} - 1} . \tag{3.3.21}$$

Since the Ashkin-Teller model is also expected (Friedan *et al.* 1984, Cardy 1987) to have $c = 1$, it is not surprising that there should exist a close ralation between it and $\mathcal{H}_{XXZ}$. On the other hand, we do not appear to have all of the Ashkin-Teller operators. In particular, Kadanoff and Brown (1979) argued that the dimension of the polarization operator of the Ashkin-Teller model is given by

$$x_p^{AT}(K_4^{AT}) = x^G_{0,\frac{1}{2}}(K) , \tag{3.3.22}$$

where K and K_4^{AT} are related by (3.3.20) and $x^G_{0,1/2}$ is given by (3.3.16) with m

extended to half integral values. The resolution of this problem is presented in Section 3.4, where we will see that to recover this dimension in the XXZ model requires a modified boundary condition.

Before leaving this discussion of the relation between the XXZ model and the Gaussian model, we need to comment on the γ-independent dimensions we found, namely $x = 1$ and $x = 2$. The latter, as discussed earlier, is the dimension of the marginal operator responsible for the existence of the critical line with continuously varying exponents. In the Gaussian model such non-varying dimensions are associated with the operators, in Kadanoff's (1979) notation, $F_{N,M}$ constructed from gradients of the basic Gaussian field $\phi(r)$; the dimension of $F_{N,M}$ being $x_{N,M} = N + M$. The operators $F_{2,0}$, $F_{0,2}$ and $F_{1,1}$ are, hence, marginal, while $F_{1,0}$ and $F_{0,1}$ are examples of so-called redundant operators (see, *e.g.* Fisher 1974); they generate a trivial shift of the Gaussian field by a constant, $\phi \rightarrow \phi + b$. The analog of these operators in the XXZ model has been discussed by den Nijs (1981), who showed that redundant operators should arise from the fact that the free energy of the eight-vertex model is regular with respect to anisotropy of the two-spin interaction (see, *e.g.* Baxter 1982). Our observations are a direct confirmation of den Nijs's arguments.

3.3.4 **XXZ chain on an odd number of sites**

Ground-state

As discussed above, the ground-state for odd M is two-fold degenerate, occuring as the lowset eigenvalue in each of the two sectors with $n = \pm 1/2$ or $r = (M \pm 1)/2$. Proceeding as in Section 3.3.1 we find the leading correction to the ground-state to be of the form

$$E_0(\gamma, M)/M = e_\infty(\gamma) - \frac{\pi \tilde{c}}{6} M^{-2} + o(M^{-2}) \qquad (3.3.23)$$

where

$$\tilde{c} = -\frac{1}{2} + \frac{3\gamma}{2\pi} \,. \tag{3.3.24}$$

Evidence for this result is presented in Table 3.13. It can be explained if we regard the ground-state for odd M as not being the true ground-state (vacuum) of the theory but rather one associated with a "defect" consisting of a spin wave index 1/2. The ground-state (3.3.1) is effectivley "boosted" by the presence of an operator $O_{1/2,0}$. If we now use the associated scaling dimension $x_{1/2,0}$ as a "correction" in (3.3.1), we readily derive the results (3.3.23) and (3.3.24).

One interseting consequence of the result (3.3.24) is that the leading correction vanishes at $\gamma = \pi/3$. Numerically, we find that, in fact, *all* corrections in M vanish at this point: $E_0(\pi/3, M) = -3M/4$ for all odd M. This observation provides another useful check on the accuracy of the numerical solution of the Bethe ansatz equations. (Recall that we found a similar point in Section 3.2.7; here again we have been unable to find a simple product form for the wave-function.)

Excited states

In general we find that the same operators $O_{n,m}$ are present in the theory for M odd as for even M but "corrected" by the presence of the operator $O_{1/2,0}$. In particular, the scaling dimensions corresponding to these operators now appear as

$$x_{n+1/2,\,m} - x_{1/2,0} \qquad n, m = 0, 1, \ldots , \tag{3.3.25}$$

where we extend the index n in (3.3.15) to fractional values. The scaling dimensions in (3.3.25) have been confirmed with similar accuracy to those for M even. Typical estimates of several anomalous dimensions are shown for $\gamma = \pi/3$ in Table 3.14. In each case the estimates are seen to converge to the values given by (3.3.25). In addition, as for even M, the lowest state with momentum $P = \pm 2\pi/M$ and the "marginal" state produce γ-independent dimensions in the ground-state (n = 0) sector. However, the corresponding states for different n produce, respectively, the first and second levels in the conformal tower associated with the operator $O_{n,0} - O_{1/2,0}$, *i.e.* as for even M, but "corrected" by $O_{1/2,0}$.

Table 3.13 Conformal anomaly estimators (Eq. (3.3.3)) with increasing odd chain size as a function of γ. The exact values shown are given by (3.3.24) (see text).

M	γ:	$\pi/6$	$\pi/4$	$\pi/2$	$2\pi/3$
5		−0.220 881	−0.119 906	0.252 909	0.487 833
9		−0.230 864	−0.122 309	0.250 891	0.496 989
17		−0.238 177	−0.123 726	0.250 249	0.499 206
33		−0.242 958	−0.124 439	0.250 066	0.499 793
65		−0.245 885	−0.124 763	0.250 017	0.499 947
129		−0.247 618	−0.124 903	0.250 004	0.499 987
257		−0.248 627	−0.124 961	0.250 001	0.499 997
513		−0.249 210	−0.124 984	0.250 000	0.499 999
exact		−0.25	−0.125	0.25	0.5

Table 3.14 Various anomalous dimension estimates for odd M at the particular value $\gamma = \pi/3$ (see text).

M	(n,m): (1,0)	(0,1)	(1,1)	lowest P	marginal
9	0.645 922	0.720 462	1.291 283	0.939 823	1.808 721
17	0.659 744	0.740 874	1.381 221	0.982 827	1.934 549
33	0.664 543	0.747 371	1.407 350	0.995 418	1.979 815
65	0.666 047	0.749 271	1.414 301	0.998 817	1.994 117
129	0.666 491	0.749 802	1.416 076	0.999 700	1.998 338
257	0.666 618	0.749 947	1.416 520	0.999 924	1.999 539
exact	0.666 667	0.75	1.416 667	1.0	2.0

Group IIa excitations

Recall that for n odd, the sector's first excited state is obtained by directly solving equations (3.2.4) with either the choice (3.3.35) or (3.3.37) for the numbers I_j; otherwise these choices give rise to the leading 1-type and 2-string solutions. For M odd, however, the first excited state in *any* sector is given by directly solving (3.2.4) with *either* of the above choices, *i.e.* without recourse to the either the 1-type or 2-string configurations. This gives us a strong hint that the nature of the zeros may well be different for odd M, even though the basic I_j configuration is the same. It turns out, in fact, that we *can*, for example, *easily* solve equations (3.2.4) for the "group IIa" excitations shown schematically Table 3.1 when M is odd. This is indeed fortuitous, as we can then find the anomalous dimensions of these states and subsequently, through (3.3.25), *deduce* the corresponding operators.

In Table 3.15 we show the estimates of the anomalous dimension associated with the first two group IIa excitations; as for the $P = \pm 2\pi/M$ state both possible distributions are seen to produce the same eigenvalue. These estimates clearly converge to $x = 2$, suggesting that the states are associated with the *first* level in the conformal tower of the operator with associated anomalous dimension $x_\alpha = 1$ ($s_\alpha = \pm 1$ with $j = 0$, $j' = 1$ or $j = 1$, $j' = 0$) with presumabley the first two group IIb excitations corresponding to the same assignments.

Conversely, the scaling dimension estimates shown in Table 3.16 for the two remaining group IIa excitations vary with γ. Working "backwards" as indicated above, we see that the values are clearly consistent with $x_{0,1} + 1$. The eigenvalues associated with these choices of I_j thus produce the *first* level in the conformal tower associated with the operator $O_{0,1}$. Recall that we had previously located the *second* level in the tower.

Table 3.15 Scaling dimension estimates for the first two group IIa excitations shown in Table 3.1.

M γ:	$5\pi/12$	$\pi/3$	$\pi/4$
9	1.535 906	1.493 539	1.462 984
17	1.861 694	1.848 292	1.837 261
33	1.962 657	1.958 964	1.955 286
65	1.990 331	1.989 368	1.988 146
129	1.997 543	1.997 297	1.996 880
257	1.999 381	1.999 319	1.999 171

Table 3.16 Scaling dimension estimates for the remaining two group IIa excitations shown in Table 3.1.

M γ:	$5\pi/12$	$\pi/3$	$\pi/4$
9	1.486 574	1.406 170	1.349 054
17	1.747 276	1.646 455	1.570 778
33	1.827 503	1.721 562	1.639 862
65	1.849 468	1.742 504	1.659 309
129	1.855 192	1.748 061	1.664 631
257	1.856 651	1.749 503	1.666 088
exact	1.857 143	1.75	1.666 667

3.3.5 Effect of the boundary angle ϕ

In Section 3.2.7, we discussed the *shifting* of the eigen-spectrum due to the angle ϕ (recall Figs. 3.9 and 3.10). Here we examine the role of ϕ in the operator identification established in the preceding sections. We point out however, that we have examined only those states of relevance to subsequent sections. We begin with the leading correction to the ground-state.

Ground-state

Proceeding again as in Section 3.3.1, we find the leading corrections to the ground-state energy per site (more specifically, for the numbers I_j given in (3.2.14); recall that this choice gives the lowest state only for $0 \le \phi \le \pi$) to be of the form

$$E_0(\gamma, \phi, M)/M = e_\infty(\gamma) - \frac{\pi \zeta \hat{c}(\phi)}{6M^2} + o(M^{-2}), \tag{3.3.26}$$

where

$$\hat{c}(\phi) = 1 - 12 x_{0, \frac{\phi}{2\pi}}$$

$$= 1 - \frac{3\phi^2}{2\pi(\pi - \gamma)} . \tag{3.3.27}$$

Evidence for this result is presented in Table 3.17 where we show the estimates of $\hat{c}$ for $\phi = \pi/3$ and various γ. In each case the result (3.3.27) is shown for comparison. In Table 3.18 we further show estimates of $\hat{c}$ for $\gamma = \pi/3$ and various ϕ. Here we recall that at the particular value $\phi = 2\pi/3$, $\hat{c} = 0$ and, in fact, *all* corrections in M were seen to vanish.

Excited states

Here we consider the I_j configurations given in (3.2.35) and (3.2.37), *i.e.* those obtained by shifting, respectively, the basic configuration (3.2.14) to the "left" and to the "right" by one unit. We saw that the choice (3.2.35) gives rise to the first excited state in

Table 3.17 Conformal anomaly estimators (Eq. (3.3.3)) for $\phi = \pi/3$ with increasing chain size as a function of γ. The exact values shown are given by (3.3.27).

M	γ: $\pi/4$	$\pi/3$	$5\pi/12$	$2\pi/3$
8	0.795 958	0.766 039	0.727 461	0.496 095
16	0.782 779	0.754 079	0.717 536	0.499 101
32	0.779 228	0.751 048	0.715 096	0.499 780
64	0.778 221	0.750 270	0.714 488	0.499 945
128	0.777 921	0.750 069	0.714 336	0.499 986
256	0.777 826	0.750 018	0.714 298	0.499 997
$\hat{c}$	0.777 778	0.75	0.714 286	0.5

Table 3.18 Conformal anomaly estimators (Eq. (3.3.3)) for $\gamma = \pi/3$ with increasing chain size as a function of ϕ. The exact values shown are given by (3.3.27).

M	ϕ: $2\pi/9$	$\pi/2$	π	$4\pi/3$
8	0.908 795	0.445 857	−1.257 973	−2.975 946
16	0.893 970	0.439 605	−1.251 619	−2.991 849
32	0.890 199	0.438 035	−1.250 315	−2.997 444
64	0.889 227	0.437 636	−1.250 057	−2.999 233
128	0.888 976	0.437 535	−1.250 009	−2.999 776
256	0.888 911	0.437 509	−1.250 001	−2.999 936
$\hat{c}$	0.888 889	0.4375	−1.25	−3.0

the ground-state sector (our "1-type" solution) while (3.2.37) gives the second excited state (our "2-string"). However, both configurations give the first excited state in the $n = 1$ sector. In Table 3.19, we show the anomalous dimensions associated with the choice (3.2.35) in the ground-state sector for $\phi = \pi/3$ and various γ. This level corresponds to the excited state shown in figure 3.10 as a function of ϕ. For the same state, we show in Table 3.20 the anomalous dimensions for $\gamma = \pi/3$ and various ϕ. In particular, at $\phi = 4\pi/3$ we have $E/M = -3/4$ for all M; a consequence of the symmetry of the eigen-spectrum about $\phi = \pi$ (as discussed in Section 3.2.7).

In each table we show also the values obtained from

$$x_{0,1-\frac{\phi}{2\pi}} = \frac{\pi}{2(\pi-\gamma)}\left(1-\frac{\phi}{2\pi}\right)^2 . \tag{3.3.28}$$

In each case this is clearly seen to be the exact result. On the other hand, it is difficult to solve the Bethe ansatz equations, for large M, with the choice (3.2.37) for arbitrary ϕ (recall this is a 2-string in the complex z-plane). Rather, we shall infer the associated anomalous dimension indirectly by considering the corresponding distribution of zeros in the $n = 1$ sector where there are no such difficulties.

In Table 3.21 we show the anomalous dimensions associated with the choice (3.3.35) for $n = 1$, $\phi = \pi/3$ and various γ. In each case convergence is to the value

$$x_{1,1-\frac{\phi}{2\pi}} = \frac{\pi-\gamma}{2\pi} + \frac{\pi}{2(\pi-\gamma)}\left(1-\frac{\phi}{2\pi}\right)^2 . \tag{3.3.29}$$

The corresponding estimates for the choice (3.3.37) are shown in Table 3.22 and converge to

$$x_{1,1+\frac{\phi}{2\pi}} = \frac{\pi-\gamma}{2\pi} + \frac{\pi}{2(\pi-\gamma)}\left(1+\frac{\phi}{2\pi}\right)^2 . \tag{3.3.30}$$

Given these results we conclude that the anomalous dimension associated with the 2-string in the $n = 0$ sector is

$$x_{0,1+\frac{\phi}{2\pi}} = \frac{\pi}{2(\pi-\gamma)}\left(1+\frac{\phi}{2\pi}\right)^2 . \tag{3.3.31}$$

which can be verified exactly in the $\Delta = 0$ limit (recall also Fig. 3.9).

Table 3.19 Anomalous dimensions associated with the I_j in (3.2.35) in the n = 0 sector for $\phi = \pi/3$ with increasing chain size as a function of γ. The exact values shown are given by (3.3.28).

M γ:	$\pi/6$	$\pi/4$	$\pi/3$	$5\pi/12$
8	0.397 934	0.445 277	0.508 912	0.587 774
16	0.405 936	0.455 296	0.517 215	0.593 378
32	0.410 630	0.459 803	0.519 792	0.594 777
64	0.413 265	0.461 688	0.520 541	0.595 124
128	0.414 739	0.462 453	0.520 752	0.595 210
256	0.415 569	0.462 760	0.520 811	0.595 231
exact	0.416 667	0.462 963	0.520 833	0.595 238

Table 3.20 Anomalous dimensions associated with the I_j in (3.2.35) in the n = 0 sector for $\gamma = \pi/3$ with increasing chain size as a function of ϕ. The exact values shown are given by (3.3.28).

M ϕ:	$2\pi/9$	$\pi/2$	π	$4\pi/3$
8	0.571 332	0.417 718	0.190 098	0.085 267
16	0.586 226	0.420 502	0.188 130	0.083 828
32	0.590 799	0.421 455	0.187 654	0.083 461
64	0.592 099	0.421 751	0.187 538	0.083 366
128	0.592 458	0.421 840	0.187 509	0.083 342
256	0.592 556	0.421 865	0.187 502	0.083 336
exact	0.592 593	0.421 875	0.1875	0.083 333

Table 3.21 Anomalous dimensions associated with the I_j in (3.2.35) in the n = 1 sector for $\phi = \pi/3$ with increasing chain size as a function of γ. The exact values shown are given by (3.3.29).

M γ:	$\pi/6$	$\pi/4$	$\pi/3$	$5\pi/12$
8	0.805 020	0.805 427	0.814 530	0.839 404
16	0.829 516	0.831 392	0.844 445	0.874 822
32	0.834 160	0.836 963	0.851 805	0.883 869
64	0.834 521	0.837 967	0.853 594	0.886 145
128	0.834 180	0.838 064	0.854 028	0.886 715
256	0.833 856	0.838 028	0.854 133	0.886 857
exact	0.833 333	0.837 963	0.854 167	0.886 905

Table 3.22 Anomalous dimensions associated with the I_j in (3.2.37) in the n = 1 sector for $\phi = \pi/3$ with increasing chain size as a function of γ. The exact values shown are given by (3.3.30).

M γ:	$\pi/6$	$\pi/4$	$\pi/3$	$5\pi/12$
8	1.159 951	1.187 932	1.239 331	1.324 616
16	1.221 926	1.259 367	1.323 939	1.423 584
32	1.234 610	1.277 070	1.346 383	1.449 547
64	1.236 001	1.281 249	1.352 175	1.456 129
128	1.235 340	1.282 188	1.353 658	1.457 781
256	1.234 602	1.282 380	1.354 037	1.458 195
exact	1.233 333	1.282 407	1.354 167	1.458 333

3.4 THE XXZ CHAIN AND THE CRITICAL BEHAVIOUR OF THE ASHKIN-TELLER MODEL

In Section 3.3.3 we argued that we could identify the XXZ operator $O_{0,1}$ with the energy operator of the Ashkin-Teller model. In this Section, we derive the equivalence between these two models directly, by showing that the eigen-spectrum of the quantum Ashkin-Teller Hamiltonian on a *finite* chain can be obtained exactly from that of $\mathcal{H}_{XXZ}$ provided we consider more general boundary conditions on the XXZ chain. We shall see that it is precisely this generalization that allows the identification of the complete operator content of the Ashkin-Teller Hamiltonian from the eigen-spectrum of $\mathcal{H}_{XXZ}$.

3.4.1 Equivalence between the Eigen-spectra of the XXZ and Quantum Ashkin-Teller Hamiltonians

The specific quantum Ashkin-Teller Hamiltonian that we shall study is that obtained (Kohmoto *et al.* 1981) by the particular time continuous limit of the classical Ashkin-Teller model which preserves the self-dual nature of the classical model. This Hamiltonian describes the dynamics of two commuting sets of spin-1/2 Pauli matrices: $\{\sigma^a_i, \tau^a_i\ ;\ a = x, y, z\}$. On a chain of L sites, we write the Hamiltonian (Kohmoto *et al.* 1981) as

$$\mathcal{H}_{AT} = \mathcal{H}_V + \mathcal{H}_S \tag{3.4.1a}$$

where

$$\mathcal{H}_V = -\sum_{j=1}^{L-1}\left[\left(\sigma_j^z\,\sigma_{j+1}^z + \tau_j^z\,\tau_{j+1}^z\right) + \varepsilon\,\sigma_j^z\,\sigma_{j+1}^z\,\tau_j^z\,\tau_{j+1}^z\right]$$

$$-\lambda\sum_{j=1}^{L}\left(\sigma_j^x + \tau_j^x + \varepsilon\,\sigma_j^x\,\tau_j^x\right) \tag{3.4.1b}$$

and $\mathcal{H}_S$ is a "surface" term determined by the boundary condition imposed on the ends

of the chain.

Four types of boundary condition will be of interest:

a1) Periodic ($\tilde{Q} = 0$)

$$-\mathcal{H}_S^{(0)} = \sigma_L^z \sigma_1^z + \tau_L^z \tau_1^z + \varepsilon \sigma_L^z \sigma_1^z \tau_L^z \tau_1^z \tag{3.4.2a}$$

a2) Antiperiodic ($\tilde{Q} = 2$)

$$-\mathcal{H}_S^{(2)} = -\left(\sigma_L^z \sigma_1^z + \tau_L^z \tau_1^z\right) + \varepsilon \sigma_L^z \sigma_1^z \tau_L^z \tau_1^z \tag{3.4.2b}$$

a3) Twisted ($\tilde{Q} = 1$)

$$-\mathcal{H}_S^{(1)} = \sigma_L^z \tau_1^z - \tau_L^z \sigma_1^z - \varepsilon \sigma_L^z \sigma_1^z \tau_L^z \tau_1^z \tag{3.4.2c}$$

a4) Free

$$-\mathcal{H}_S^{(F)} = 0\,. \tag{3.4.2d}$$

The parameter λ plays the role of a temperature and $\varepsilon = \cos\gamma$ is a coupling constant. In the thermodynamic limit ($L \to \infty$) the Hamiltonian (3.4.1) is self-dual for all ε along the line $\lambda = 1$. The limiting cases $\varepsilon = 0$ and $\varepsilon = 1$ correspond to a doubled Ising model in a transverse field and the 4-state quantum Potts model, respectively. The phase diagram in the (λ, ε)-plane is reasonably well understood (Kohmoto *et al.* 1981, Alcaraz and Drugowich de Felício 1984). Our interest centres on the line

$$\lambda = 1, \quad -\frac{1}{\sqrt{2}} \le \varepsilon \le 1 \tag{3.4.3}$$

along which exponents vary continuously with ε (or γ). For $-1/2 \le \varepsilon \le 1$, this line is related to the critical line of the classical isotropic model (Ashkin and Teller 1943) are related by the correspondence

$$\varepsilon = \frac{1}{2}\left[\exp(4K_4^{AT}) - 1\right], \tag{3.4.4a}$$

with

$$\sinh 2K^{AT} = \exp(-2K_4^{AT})\,. \tag{3.4.4.b}$$

Another line, separating anitiferromagnetic and paramagnetic phases, has K^{AT} negated (see, *e.g.* Baxter 1982).

Kohmoto *et al.* (1981) mapped the Hamiltonian (3.4.1) to a *staggered* XXZ chain. At criticality, the staggering disappears and $\mathcal{H}_{XXZ}$ is recovered. This discussion, however, neglected the role of boundary conditions. We shall see that these are crucial for a complete identification of operators. Here we establish the equivalence between $\mathcal{H}_{AT}$ and $\mathcal{H}_{XXZ}$ by showing that the two Hamiltonians are simply different representations of the same operator.

Except for boundary a3) ($\tilde{Q} = 1$), $\mathcal{H}_{AT}$ commutes independently with the parity operators

$$\mathcal{P}_1 = \prod_{j=1}^{L} \sigma_j^x \quad \text{and} \quad \mathcal{P}_2 = \prod_{j=1}^{L} \tau_j^x . \tag{3.4.5}$$

Consequently, the Hilbert space can be separated into four disjoint sectors labelled by the eigenvalues of $\mathcal{P}_1$ and $\mathcal{P}_2$, namely $Q = 0$ ($\mathcal{P}_1 = +$, $\mathcal{P}_2 = +$), $Q = 1$ (+, −), $Q = 2$ (−, −) and $Q = 3$ (−, +). By symmetry of $\mathcal{H}_{AT}$ under the interchange $\sigma \leftrightarrow \tau$, the sectors $Q = 1$ and $Q = 3$ are degenerate. For boundary a3), $\mathcal{H}_{AT}$ commutes only with the product $\mathcal{P}_1 \cdot \mathcal{P}_2$ and the Hilbert space divides into only two disjoint sectors, $Q = 0$ ($\mathcal{P}_1 \cdot \mathcal{P}_2 = +$) and $Q = 1$ ($\mathcal{P}_1 \cdot \mathcal{P}_2 = -$). We denote the sectors of $\mathcal{H}_{AT}$ subject to the various boundary conditions by $\mathcal{H}_{AT}^{(Q,\tilde{Q})}$ with $Q = 0, 1, 2, 3$ and $\tilde{Q} = 0, 1, 2, F$.

Let us, for the sake of simplicity, concentrate initially on the periodic and antiperiodic cases ($\tilde{Q} = 0$ and $\tilde{Q} = 2$). Define two sets of *link* variables $\{\rho_j, \eta_j ; j = 1, 2, \ldots, 2L\}$:

$$\rho_{2j-1} \equiv \sigma_j^x , \qquad \eta_{2j-1} \equiv \tau_j^x \qquad j = 1, 2, \ldots, L \tag{3.4.6a}$$

$$\rho_{2j} \equiv \sigma_j^z \sigma_{j+1}^z , \qquad \eta_{2j} \equiv \tau_j^z \tau_{j+1}^z \qquad j = 1, 2, \ldots, L-1 \tag{3.4.6b}$$

$$\rho_{2L} \equiv i^{\tilde{Q}} \sigma_L^z \sigma_1^z , \qquad \eta_{2L} \equiv i^{\tilde{Q}} \tau_L^z \tau_1^z . \tag{3.4.6c}$$

It is easy to show, from these definitions, that

$$\rho_j^2 = \eta_j^2 = 1, \qquad j = 1, 2, \ldots, 2L , \tag{3.4.7a}$$

$$[\rho_j , \eta_k] = 0, \qquad j , k = 1, 2, \ldots , 2L , \tag{3.4.7b}$$

$$\{\rho_j , \rho_k\} = \{\eta_j , \eta_k\} = 0 \quad \text{for} \quad |j-k| = 1 \text{ or } j = 1, k = 2L \tag{3.4.7c}$$

and

$$[\rho_j , \rho_k] = [\eta_j , \eta_k] = 0 \qquad \text{otherwise.} \tag{3.4.7d}$$

These new operators are not, however, independent but should satisfy the constraint

$$\prod_{j=1}^{L} \rho_{2j} = \prod_{j=1}^{L} \eta_{2j} = i^{\tilde{Q}} . \tag{3.4.8}$$

In terms of these varibales, $\mathcal{H}_{AT}^{(Q,\tilde{Q})}$ for $\tilde{Q} = 0$ and $\tilde{Q} = 2$ can be written

$$-\mathcal{H}_{AT}^{(Q,\tilde{Q})}(\lambda) = \sum_{j=1}^{2L} \left[\left(\rho_{2j} + \eta_{2j} + \varepsilon \rho_{2j} \eta_{2j} \right) + \lambda \left(\rho_{2j-1} + \eta_{2j-1} + \varepsilon \rho_{2j-1} \eta_{2j-1} \right) \right] . \tag{3.4.9}$$

Note that this Hamiltonian, as well as the algebra (3.4.7) itself, is cyclically invariant. On the other hand, the constraint (3.4.8) is, in general, not cyclically invariant. However, if we restrict attention to the sectors Q = 0 and Q = 2, shifting the lattice by one unit ($i \rightarrow i + 1$) yields the relations

$$\mathcal{H}_{AT}^{(0,0)}(\lambda) = \lambda \, \mathcal{H}_{AT}^{(0,0)}\left(\frac{1}{\lambda}\right) , \tag{3.4.10a}$$

$$\mathcal{H}_{AT}^{(2,2)}(\lambda) = \lambda \, \mathcal{H}_{AT}^{(2,2)}\left(\frac{1}{\lambda}\right) , \tag{3.4.10b}$$

$$\mathcal{H}_{AT}^{(0,2)}(\lambda) = \lambda \, \mathcal{H}_{AT}^{(2,0)}\left(\frac{1}{\lambda}\right) , \tag{3.4.10c}$$

These relations are, in fact, consequences of the self-dual nature of the original Hamiltonian (3.4.1); more generally, it can be proved that

$$\mathcal{H}_{AT}^{(Q,\tilde{Q})}(\lambda) = \lambda \, \mathcal{H}_{AT}^{(\tilde{Q},Q)}\left(\frac{1}{\lambda}\right) , \qquad Q , \tilde{Q} = 0, 1, 2, 3(F). \tag{3.4.11}$$

At the self-dual point ($\lambda = 1$) (3.4.9) reduces to the simple form

$$-\mathcal{H}_{AT}^{(Q,\tilde{Q})}(\lambda) = \sum_{j=1}^{2L} \left(\rho_j + \eta_j + \varepsilon \rho_j \eta_j \right) . \tag{3.4.12}$$

Let us now consider $\mathcal{H}_{xxz}$ on a finite chain of 2L-sites. Here, we write the

Hamiltonian (3.1.4) as

$$\mathcal{H}_{XXZ} = \mathcal{H}_V + \mathcal{H}_S \tag{3.4.13a}$$

where

$$-\mathcal{H}_V = \sum_{j=1}^{2L-1}\left(\sigma_j^x \sigma_{j+1}^x + \sigma_j^y \sigma_{j+1}^y + \Delta \sigma_j^z \sigma_{j+1}^z\right) \tag{3.4.13b}$$

and $\mathcal{H}_S$ is specified by the boundary conditions imposed. Note that we have dropped the prefactor of 1/2 in (3.1.4).

Three general classes of boundary conditions will be of interest. The first class is the twisted boundary condition defined by (3.1.6). This produces a surface term in the Hamiltonian:

$$-\mathcal{H}_S = \cos\phi\left(\sigma_{2L}^x \sigma_1^x + \sigma_{2L}^y \sigma_1^y\right) + \sin\phi\left(\sigma_{2L}^y \sigma_1^x - \sigma_{2L}^x \sigma_1^y\right) + \Delta\, \sigma_{2L}^z \sigma_1^z . \tag{3.4.14}$$

Three particular values of ϕ will be important:

b1) $\phi = 0$, (Periodic boundary conditions)

b2) $\phi = \pi$, (Partially antiperiodic boundary conditions)

b3) $\phi = \pi/2$, (Twisted x – y boundary conditions).

We shall denote these boundary conditions by $\Psi = 0, 2, 1$, respectively. The other two boundary conditions we shall consider are type b4) specified by

$$\sigma_{2L+1}^x = \sigma_1^x, \quad \sigma_{2L+1}^y = -\sigma_1^y, \quad \sigma_{2L+1}^z = \sigma_1^z \tag{3.4.15}$$

and

b5) free boundary conditions ($\mathcal{H}_S = 0$).

As we did for the Ashkin-Teller model, we discuss initially the cases b1) and b2) specified by $\Psi = 0$ and $\Psi = 2$ respectively. We introduce link variables

$$\rho_{2j-1} \equiv \sigma_{2j-1}^x \sigma_{2j}^x, \qquad \eta_{2j-1} \equiv \sigma_{2j-1}^y \sigma_{2j}^y \qquad j = 1, 2, \ldots, L \tag{3.4.16a}$$

$$\rho_{2j} \equiv \sigma_{2j}^y \sigma_{2j+1}^y, \qquad \eta_{2j} \equiv \sigma_{2j}^x \sigma_{2j+1}^x \qquad j = 1, 2, \ldots, L-1 \tag{3.4.16b}$$

$$\rho_{2L} \equiv i^\Psi \sigma_{2L}^y \sigma_1^y, \qquad \eta_{2L} \equiv i^\Psi \sigma_{2L}^x \sigma_1^x, \qquad \Psi = 0, 2. \tag{3.4.16c}$$

It is simple to verify that these variables also satisfy the algebra in (3.4.6) and that, in terms of them, the Hamiltonian (3.4.13) can be written exactly as in (3.4.12), provided we make the identification $\Delta = -\varepsilon$. However, a difference is that from (3.4.16), the constraint (3.4.8) should be replaced by

$$\prod_{j=1}^{L} \rho_{2j-1}\,\eta_{2j} \;=\; \prod_{j=1}^{L} \eta_{2j-1}\,\rho_{2j} \;=\; i^{\Psi}. \tag{3.4.17}$$

Consider now the sector $Q = 0$ ($\mathcal{P}_1 = \mathcal{P}_2 = +$) of the Ashkin-Teller model with boundary conditions a1) and a2), *i.e.* $\tilde{Q} = 0$ and $\tilde{Q} = 2$. In these cases

$$\prod_{j=1}^{L} \rho_{2j-1} \;=\; \prod_{j=1}^{L} \eta_{2j} \;=\; 1\,. \tag{3.4.18}$$

Together with the constraint (3.4.8) we can thus completely satisfy the constraint (3.4.17) in the XXZ model. Consequently, the sector $\mathcal{P}_1 = \mathcal{P}_2 = +$ of $\mathcal{H}_{AT}$ with boundaries of type a1) and a2) should be present in the spectrum of the XXZ model with boundaries b1) and b2), respectively. Similarly the sector $\mathcal{P}_1 = \mathcal{P}_2 = -$ of the Ashkin-Teller model with boundaries a1) and a2) will be present in the XXZ model with boundaries b2) and b1), respectively. On the other hand, eigen-energies in the sectors $\mathcal{P}_1 = -\mathcal{P}_2 = +$ or $\mathcal{P}_1 = -\mathcal{P}_2 = -$ of $\mathcal{H}_{AT}$ with boundaries of type a1) and a2) will not occur in the spectrum of $\mathcal{H}_{XXZ}$ with boundaries b1) and b2) because the restrictions (3.4.8) and (3.4.17) cannot be satisfied simultaneously. It is straightforward to verify that by defining $\rho_{2L} \equiv -\sigma^{y}_{2L}\,\sigma^{y}_{1}$ and $\eta_{2L} \equiv \sigma^{x}_{2L}\,\sigma^{x}_{1}$ intead of (3.4.16c), with boundary b4) $\mathcal{H}_{XXZ}$ contains the sector of the periodic and antiperiodic Ashkin-Teller Hamiltonians.

These equivalences between the two Hamiltonians can be extended to other boundary conditions. For the Ashkin-Teller Hamiltonian subject to the boundary condition a3), i.e. $\tilde{Q} = 1$, the link variables are defined by (3.4.6a), (3.4.6b) and

$$\rho_{2L} \;\equiv\; \sigma^{z}_{L}\,\tau^{z}_{1}\,, \qquad \eta_{2L} \;\equiv\; \tau^{z}_{L}\,\sigma^{z}_{1}\,. \tag{3.4.19}$$

At $\lambda = 1$, $\mathcal{H}_{AT}$ still takes the form (3.4.12) but the algebra of the link variables is now given by

$$\{\rho_i , \eta_j\} = 0 \quad \text{except} \quad \{\rho_{2L} , \eta_1\} = \{\eta_{2L} , \rho_1\} = 0 \tag{3.4.20a}$$

$$\text{if} \begin{cases} |i-j| = 1 & \{\rho_i , \rho_j\} = \{\eta_i , \eta_j\} = 0 \\ \text{otherwise} & [\rho_i , \rho_j] = [\eta_i , \eta_j] = 0 \end{cases} \tag{3.4.20b}$$

while the constraint (3.4.8) is replaced by

$$\prod_{j=1}^{L} \rho_{2j}\, \eta_{2j} = -1 . \tag{3.4.21}$$

On the other hand, introducing link variables through (3.4.16a) and (3.4.16b) and

$$\rho_{2L} \equiv -\sigma^y_{2L}\, \sigma^x_1 , \qquad \eta_{2L} \equiv \sigma^x_{2L} \sigma^y_1 \tag{3.4.22}$$

allows subject to boundary conditions b3), *i.e.* $\phi = \pi/2$ or $\Psi = 1$, to be reduced to (3.4.12), where the link variables satisfy the commutation relations (3.4.20) but the constraint is now

$$\prod_{j=1}^{2L} \rho_j\, \eta_j = -1 . \tag{3.4.23}$$

Consequently we see, using (3.4.21), that the sector $\mathcal{H}_{AT}$ of with boundary a3) is present in the spectrum of the XXZ model with boundary b3), ($\phi = \pi/2$). Finally, for both models with free ends, we can define link variables by (3.4.6a,b) for the Ashkin-Teller model and (3.4.16a,b) for the XXZ model. No constraint applies and the whole spectrum of the Ashkin-Teller model should occur in that of the XXZ model.

All of the equivalences discussed above involve $\mathcal{H}_{XXZ}$ on an even number of lattice sites. Similar arguments can be constructed to relate the eigen-spectrum of $\mathcal{H}_{XXZ}$ on a chain with an odd number of sites to that of $\mathcal{H}_{AT}$ subject to additional boundary conditions specified by

$$\text{a5)} \quad -\mathcal{H}_S = \sigma^x_L \tau^z_L \tau^z_1 + \tau^x_L \sigma^z_L \sigma^z_1 + \varepsilon\, \sigma^x_L \tau^x_L \sigma^z_L \tau^z_L \sigma^z_1 \tau^z_1 \tag{3.4.24a}$$

$$\text{a6)} \quad -\mathcal{H}_S = -\left(\sigma^x_L \tau^z_L \tau^z_1 + \tau^x_L \sigma^z_L \sigma^z_1 \right) + \varepsilon\, \sigma^x_L \tau^x_L \sigma^z_L \tau^z_L \sigma^z_1 \tau^z_1 \tag{3.4.24b}$$

$$\text{a7)} \quad -\mathcal{H}_S = \sigma^y_L \sigma^z_1 + \tau^y_L \tau^z_1 - \varepsilon\, \sigma^y_L \sigma^z_1 \tau^y_L \tau^z_1 . \tag{3.4.24c}$$

Eigenvalues in the sector $\mathcal{P}_1 = \mathcal{P}_2 = +$ ($\mathcal{P}_1 = \mathcal{P}_2 = -$) of $\mathcal{H}_{AT}$ on L sites and with boundaries of types a5) and a6) occur in the spectrum of on (2L–1) sites with boundary conditions b1) and b2) (b2) and b1)), respectively. The corresponding eigenvalues, in the sectors $\mathcal{P}_1 = -\mathcal{P}_2 = \pm$ are present in $\mathcal{H}_{XXZ}$ with boundar b4). Finally, eigenvalues in sectors $\mathcal{P}_1 = \mathcal{P}_2 = \pm$ of $\mathcal{H}_{AT}$ with boundary a7) can be found in the spectrum of $\mathcal{H}_{XXZ}$ on (2L–1) sites with boundary b3).

All of these eigen-spectrum relations derived in this section have been verified from numerical calculations of the complete spectra of $\mathcal{H}_{XXZ}$ and $\mathcal{H}_{AT}$ on small lattices ($L \sim 2-9$). It is important to stress that the related XXZ-Hamiltonian also has many other eigenvalues besides those of the Ashkin-Teller Hamiltonian. The Ashkin-Teller eigen-energies need to be detected by comparing the spectrum of both models for several small lattices. Once this has been done, we can extend the Ashkin-Teller data to very large lattices ($L \sim 512$) by using the extended Bethe ansatz equations derived in Appendix 3A for the XXZ-chain. This procedure is, obviously, possible only for the Ashkin-Teller Hamiltonian subject to boundaries of the type a1) and a2). For boundary conditions a3), the Bethe ansatz appears to fail. On the other hand for free ends, it is possible to derive (Gaudin 1971, 1983; Alcaraz *et al.* 1987) Bethe ansatz equations for the corresponding XXZ-Hamiltonian; we derive the necessary equations and discuss this case in Chapter 4.

In this paper, we focus on the spectrum of $\mathcal{H}_{AT}$ with boundaries of types a1), a2) and a3) and make use of the conformal invariance relations (3.1.2) and (3.1.3) to explore the operator content of the Ashkin-Teller chain. This has also been discussed recently by von Gehlen and Rittenberg (1987) using conventional finite-lattice techniques. However, our ability to obtain energy levels for very large lattices gives much improved estimates of scaling dimensions. It is notationally convenient to order states by increasing energy; we denote the energy of the ℓth state in sector Q of $\mathcal{H}_{AT}$ subject to boundary condition, $\tilde{Q}$, recall (3.4.2a-c), by $E^{(Q,\tilde{Q})}(\ell,p)$, where the momentum of the state is $2\pi p/L$.

3.4.2 Energy scale and Conformal anomaly

To apply the results (3.1.2) and (3.1.3) to Hamiltonian (3.4.1), it is necessary to find the factor ζ_{AT} to ensure that the resulting equations of motion are conformally invariant. Reference to (3.1.5) shows that the appropriate factor is

$$\zeta_{AT} = \frac{\pi \sin\gamma}{\gamma} , \tag{3.4.25}$$

where $\varepsilon = \cos\gamma$. Previously, ζ_{AT} was known only numerically (von Gehlen and Rittenberg 1987). At $\varepsilon = 1$, *i.e.* $\gamma = 0$, $\mathcal{H}_{AT}$ reduces to the Hamiltonian of the 4-state Potts model (Kohmoto *et al.* 1981). At this point, (3.4.25) implies $\zeta_{AT} = \pi = 3.14...$ disproving a previous conjecture (von Gehlen *et al.* 1986) of $\zeta = (4^{4/3})/2 = 3.17...$. For $\gamma = \pi/4$ the quantum Ashkin-Teller model reduces to the Hamiltonian version of the Z(4) self-dual Fateev and Zamolodchikov (1982) model and the value $\zeta = 2\sqrt{2}$ confirms a previous conjecture (Alcaraz 1986a,b).

With ζ_{AT} determined, we can now apply (3.1.2) and (3.1.3). With periodic boundary conditions applied, the ground-state energy of $\mathcal{H}_{AT}$ on a chain of L sites corresponds to the ground-state energy of $\mathcal{H}_{XXZ}$ on $M = 2L$ sites also with periodic boundary conditions. The results of Section 3.3.1 immediately confirm that the conformal anomaly of the Ashkin-Teller model is also $c = 1$.

3.4.3 Operator Content

Thermal operators

Mass gap amplitudes in the ground-state ($Q = 0$) sector are related to the thermal operators. The anomalous dimension x_ε^{AT} of the energy operator can be estimated by extrapolating the sequence

$$X_L^{(0)}(1) \equiv \frac{L}{2\pi\zeta_{AT}}\left[E^{(0,0)}(1,0) - E^{(0,0)}(0,0)\right] = x_\varepsilon^{AT} + o(1) \quad \text{as } L \to \infty . \tag{3.4.26}$$

The scaling dimension $x_{\varepsilon\varepsilon}^{AT}$ of the second thermal operator follows similarly from the sequence

$$X_L^{(0)}(2) \equiv \frac{L}{2\pi\zeta_{AT}}\left[E^{(0,0)}(2,0) - E^{(0,0)}(0,0)\right] = x_{\varepsilon\varepsilon}^{AT} + o(1) \quad \text{as} \quad L \to \infty . \tag{3.4.27}$$

From the equivalence derived in Section 3.4.1, these sequences can be obtained by solving numerically the XXZ model Bethe ansatz equations for periodic boundary conditions. The eigen-energies $E^{(0,0)}(1,0)$ and $E^{(0,0)}(2,0)$ are eigen-states already detected in our earlier analysis of the XXZ model (Section 3.2). Specifically, these energies are obtained from, respectively, the 1-type and marginal configurations. In particular, the gap associated with $E^{(0,0)}(1,0)$ confirms directly the identification of the XXZ operator, $O_{0,1}$, with the Ashkin-Teller energy operator and hence the identification $x_\varepsilon^{AT} = x_{0,1}$. The scaling dimension $x_{\varepsilon\varepsilon}^{AT}$ of the second thermal exponent is 2 for all γ; the associated operator is the marginal operator again governing motion along the critical line.

The energy corresponding to the XXZ operator, $O_{0,2}$, with dimension $x_{0,2}$, is also an eigen-energy of the Ashkin-Teller Hamiltonian. Consequently, the Ashkin-Teller model possesses an irrelevant operator with scaling dimension $4x_\varepsilon^{AT}$. As we shall briefly discuss in Section 3.6, this operator determines the dominant correction-to-scaling in the Ashkin-Teller as well as the XXZ model.

Order parameters

The anomalous dimension x_m^{AT} and x_p^{AT} of the magnetic and electric operators are given by mass gap amplitudes in the sectors $Q = 1$ and $Q = 2$, respectively. Suitable estimators for these dimensions are

$$X_L^{(1)}(0) \equiv \frac{L}{2\pi\zeta_{AT}}\left[E^{(1,0)}(0,0) - E^{(0,0)}(0,0)\right] = x_m^{AT} + o(1) \quad \text{as} \quad L \to \infty . \tag{3.4.28}$$

and

$$X_L^{(2)}(0) \equiv \frac{L}{2\pi\zeta_{AT}}\left[E^{(2,0)}(0,0) - E^{(0,0)}(0,0)\right] = x_p^{AT} + o(1) \quad \text{as } L \to \infty . \tag{3.4.29}$$

Again the energies $E^{(1,0)}(0,0)$ and $E^{(2,0)}(0,0)$ can be obtained from the spectrum of the XXZ Hamiltonian now with boundary conditions b4) and b2), respectively. Unfortunately, for boundary conditions b4), (3.4.15), the total magnetization (3.2.1) no longer commutes with $\mathcal{H}_{XXZ}$ and the Bethe ansatz appears to be inapplicable. The magnetic exponent can be estimated by calculating $E^{(1,0)}(0,0)$ using the Lanczos method (Cullum and Willoughby 1981). This has already been reported in the earlier work of Alcaraz and Drugowich de Felício (1984) and von Gehlen and Rittenberg (1987), who directly diagonalized $\mathcal{H}_{AT}$. While the available data is restricted to small chains of length $L \leq 10$, convergence is good and the value $x_m^{AT} = 1/8$ can be confirmed, confidently, for all γ.

On the other hand, $E^{(2,0)}(0,0)$ can be found by solving the generalized Bethe ansatz equations (see Appendix 3A) for the XXZ Hamiltonian with $\phi = \pi$. In particular, $E^{(2,0)}(0,0)$ is obtained from the lowest state in the ground-state ($n = 0$) sector. In Table 3.23 we list the estimators, (3.4.29) as a function of L for several values of γ (recall that the Ashkin-Teller coupling is given by $\varepsilon = \cos\gamma$). Excellent agreement with the conjecture (den Nijs 1979)

$$x_p^{AT} = \frac{1}{4}\, x_\varepsilon^{AT} \tag{3.4.30}$$

can be observed for all γ. In the notation of Section 3.3.2, this dimension is $x_{0,1/2}$ where, as in the Gaussian model (Kadanoff and Brown 1979), the second index in (3.3.15) is extended to fractional values. We have thus recovered the missing operators discussed in Section 3.3.3.

Table 3.23 Scaling dimension estimates of the Ashkin-Teller polarization operator. Exact values are given by $x_p^{AT} = x_{0,1/2}$.

L	γ: $5\pi/12$	$\pi/3$	$\pi/4$	$\pi/6$
4	0.217 096	0.190 098	0.169 748	0.155 191
8	0.214 978	0.188 130	0.167 513	0.152 165
16	0.214 458	0.187 654	0.166 911	0.151 041
32	0.214 329	0.187 538	0.166 741	0.150 547
64	0.214 296	0.187 509	0.166 691	0.150 301
128	0.214 288	0.187 502	0.166 675	0.150 169
$x_{0,1/2}$	0.214 286	0.187 5	0.166 667	0.15

Parafermions

Since the Ashkin-Teller model has a $Z(2) \otimes Z(2)$ symmetry, it is expected to have *parafermion* (Fradkin and Kadanoff 1980) operators with spin s, where s is a multiple of 1/4. The scaling dimensions of these operators can be estimated from the sequences (von Gehlen and Rittenberg 1987)

$$X_{pf}^{(Q,\tilde{Q})} \equiv \frac{L}{2\pi\,\zeta_{AT}}\left[E^{(Q,\tilde{Q})}(0,0) - E^{(0,0)}(0,0)\right] = x_{pf}(Q,\tilde{Q}) + o(1) \quad \text{as } L \to \infty . \tag{3.4.31}$$

Here $x_{pf}(Q, \tilde{Q})$ is the dimension of the parafermion operator with spin $s = Q\tilde{Q}/4$.

From the equivalences of Section 3.4.1, relevant states for this calculation: $E^{(1,1)}(0,0)$, $E^{(2,2)}(0,0)$ and $E^{(1,3)}(0,0)$ can be obtained from the eigen-spectrum of $\mathcal{H}_{XXZ}$ with the surface term (3.4.14) for, respectively, $\phi = \pi/2$, $\phi = 0$ and $\phi = 3\pi/2$. $E^{(1,1)}(0,0)$ and $E^{(1,3)}(0,0)$ are obtained from the state associated with the minimum energy state (3.2.14) in the $n = 1$ sector. $E^{(2,2)}(0,0)$ corresponds to the "lowest momentum state" of Section 3.2.5. A further state, $E^{(1,2)}(0,0)$, requires the boundary b4) given in (3.4.15). The first three states can be obtained for large lattices by solving the Bethe ansatz equations. In Table 3.24 we show the estimators $X_{pf}^{(1,1)}$ as a function of L for various γ. Similarly in Table 3.25 we show $X_{pf}^{(1,3)}$. From these tables and our previous analysis of the the XXZ Hamiltonian in Section 3.3, we conclude that the anomalous dimension of the spin 1/4 and 3/4 operators are given by

$$x_{pf}(1,1) = \frac{1}{4}\left(\frac{1}{x_{\varepsilon}^{AT}} + x_{p}^{AT}\right), \tag{3.4.32a}$$

$$x_{pf}(1,3) = \frac{1}{4}\left(\frac{1}{x_{\varepsilon}^{AT}} + 9\,x_{p}^{AT}\right) \tag{3.4.32b}$$

and correspond to the XXZ operators $O_{1,1/4}$ and $O_{1,3/4}$ with dimensions $x_{1,1/4}$ and $x_{1,3/4}$. The result (3.4.32a) explains the earlier numerical calculations of von Gehlen and Rittenberg (1987). The spin 1 parafermion corresponds to the spin 1 operator already detected in the XXZ model (Section 3.3) and subsequently

Table 3.24 Scaling dimension estimates of the Ashkin-Teller spin 1/4 parafermion operator. Exact values are given by $x_{pf}(1,1) = x_{1,1/4}$.

L γ:	5π/12	π/3	π/4
4	0.344 783	0.378 155	0.409 734
8	0.345 126	0.379 629	0.413 978
16	0.345 211	0.380 050	0.415 627
32	0.345 231	0.380 165	0.416 263
64	0.345 236	0.380 197	0.416 509
128	0.345 238	0.380 205	0.416 605
$x_{1,1/4}$	0.345 238	0.380 208	0.416 667

Table 3.25 Scaling dimension estimates of the Ashkin-Teller spin 3/4 parafermion operator. Exact values are given by $x_{pf}(1,3) = x_{1,3/4}$.

L γ:	5π/12	π/3	π/4
4	0.738 920	0.726 068	0.725 383
8	0.764 984	0.748 185	0.745 110
16	0.771 597	0.753 531	0.749 293
32	0.773 256	0.754 809	0.750 027
64	0.773 671	0.755 114	0.750 087
128	0.773 775	0.755 186	0.750 054
$x_{1,3/4}$	0.773 810	0.755 208	0.75

$$x_{pf}(2,2) = 1 \qquad (\forall \gamma) . \tag{3.4.32c}$$

At the 4-state Potts point, $\gamma = 0$, we have $x_{pf}(1,1) = 17/32$, $x_{pf}(1,3) = 25/32$ and $x_{pf}(2,2) = 1$ in agreement with existing conjectures (Nienhuis and Knops 1985).

As for the magnetic exponent, the spin 1/2 parfermion, with dimension $x_{pf}(1,2)$ cannot be estimated for large lattices. Using the Lanczos method chains of length up to $L = 10$, we find estimates of $x_{pf}(1,2)$ that converge well to the value of 5/8 for all γ, in agreement with the results of von Gehlen and Rittenberg (1987). We should stress that the earlier numerical calculations of the dimensions x_{pf} in the Ashkin-Teller (von Gehlen and Rittenberg 1987) and 4-state Potts (von Gehlen *et al.* 1986) models did not find the dimension $x_{pf}(1,3)$ corresponding to the spin 3/4 parafermion. Furthermore, the spin 1 operator, with dimension $x_{pf}(2,2)$, was not located in the Potts study while for the Ashkin-Teller model, $x_{pf}(2,2)$ appeared to be unity for $\varepsilon < 0$ and decreased for $\varepsilon > 0$. We believe that this is related to the crossing of levels at $\varepsilon = 0$ ($\gamma = \pi/2$). We find that the states $E^{(1,3)}(0,0)$ and $E^{(2,2)}(0,0)$ are not the lowest state in their respective sectors for all γ. For example, for $\varepsilon < 0$ the lowest state in the sector $Q = 2$ with boundary $\tilde{Q} = 2$ has *momentum* and $E^{(2,2)}(0,0)$ is the *next* leading state.

As mentioned in Section 3.4.2, at $\gamma = \pi/4$ the Ashkin-Teller model is equivalent to the Z(4) self-dual model introduced by Fateev and Zamolodchikov (1982). At this point $x_{pf}(1,1) = 5/12$ and $x_{pf}(1,2) = 5/8$, which confirm the recent conjectures of Alcaraz (1986a,b). The remaining parafermions have dimensions $x_{pf}(1,3) = 3/4$ and $x_{pf}(2,2) = 1$.

Other boundaries

To finalize this section, we consider briefly the spectroscopy of $\mathcal{H}_{AT}$ with boundaries a5), a6) and a7), recall (3.4.24). With these boundaries, $\mathcal{H}_{AT}$ is related to the XXZ Hamiltonian on an odd number of lattice sites. However, unlike $\mathcal{H}_{XXZ}$, $\mathcal{H}_{AT}$ has a non-degenerate ground-state for all γ. The spectroscopic analysis of the XXZ Hamiltonian with an odd number of sites can be translated directly to these Ashkin-Teller

models. The ground-state of the Ashkin-Teller model with boundary condition a5) has one excitation corresponding to a half spin wave in the same way as the odd XXZ Hamiltonian. Taking this into consideration, as for $\mathcal{H}_{XXZ}$ on an odd number of sites, our numerical spectroscopic analysis reveals the same scaling dimensions as obtained with boundaries a1) - a3). As in the XXZ equivalent with $\gamma = \pi/3$, the ground-state per spin of the Ashkin-Teller Hamiltonian with boundary a5) and $\gamma = \pi/3$ also has no finite size correction; we find $E_0/L = 3.0$ for all L.

3.5 THE XXZ CHAIN AND THE CRITICAl BEHAVIOUR OF POTTS MODELS

We turn now to a discussion of the critical behavior and operator content of the Potts models. As with the Ashkin-Teller model, our analysis will be based on exact equivalences between the eigen-spectrum of the critical quantum Hamiltonian of the Potts model and that of $\mathcal{H}_{XXZ}$ with modified boundary conditions.

3.5.1 Free edge boundary conditions

While our main interest in this section is in the eigen-spectrum of the Potts Hamiltonian with periodic boundary conditions, it is convenient to first derive the equivalence for free edge boundary conditions.

The (1+1)-dimensional Hamiltonian field theory of the q-state Potts model was first discussed by Sólyom and Pfeuty (1981) from a τ-continuum limit of the transfer matrix derived by Mittag and Stephen (1971). On a chain of L sites with free ends the Hamiltonian can be written as

$$\mathcal{H}^{f}_{\text{Potts}} = -\sum_{m=1}^{L}\sum_{k=1}^{q-1} \Omega_m^k - \lambda \sum_{m=1}^{L-1}\sum_{k=1}^{q-1} R_m^k R_{m+1}^{q-k} \qquad (3.5.1)$$

where the operators Ω_m and R_m at site m obey a Z(q)-algebra:

$$\Omega_m R_m = \omega^{-1} R_m \Omega_m , \quad \Omega_m R_m^\dagger = \omega R_m^\dagger \Omega_m , \quad \Omega_m^q = R_m^q = 1 \qquad (3.5.2)$$

with $\omega = e^{2\pi i/q}$. Criticality corresponds to $\lambda = \lambda_c = 1$. Following Berkcan (1983) we define operators $U_1, \ldots, U_{2L-1}$ by

$$U_{2\ell-1} = \frac{1}{\sqrt{q}} \sum_{k=0}^{q-1} \Omega_\ell^k , \qquad \ell = 1, 2, \ldots, L \qquad (3.5.3a)$$

$$U_{2\ell} = \frac{1}{\sqrt{q}} \sum_{k=0}^{q-1} R_\ell^k R_{\ell+1}^{q-k} , \qquad \ell = 1, 2, \ldots, L-1. \qquad (3.5.3b)$$

In terms of these operators, we can write (3.5.1) as

$$\mathcal{H}^f_{\text{Potts}} = L + \lambda(L-1) - \sqrt{q}\left[\sum_{\ell=1}^{L} U_{2\ell-1} + \lambda \sum_{\ell=1}^{L-1} U_{2\ell}\right], \qquad (3.5.4)$$

which reduces at criticality to

$$\mathcal{H}^f_{\text{Potts,c}} = 2L - 1 - \sqrt{q} \sum_{\ell=1}^{2L-1} U_\ell . \qquad (3.5.5)$$

The operators U satisfy the Temperley-Lieb algebra (Temperley and Lieb 1971; see also Baxter 1982):

$$U_\ell^2 = \sqrt{q}\, U_\ell \qquad (3.5.6a)$$

$$U_\ell U_{\ell\pm1} U_\ell = U_\ell \qquad (3.5.6b)$$

$$[U_\ell , U_{\ell'}] = 0, \quad |\ell - \ell'| \geq 2 . \qquad (3.5.6c)$$

Temperley and Lieb (1971) give an alternative representation of these operators in terms of Pauli spins:

$$U_\ell = \frac{1}{2}\left(\sigma_\ell^x \sigma_{\ell+1}^x + \sigma_\ell^y \sigma_{\ell+1}^y\right) + \frac{1}{2}\cosh\theta \left(1 - \sigma_\ell^z \sigma_{\ell+1}^z\right) + \frac{1}{2}\sinh\theta \left(\sigma_{\ell+1}^z - \sigma_\ell^z\right) \qquad (3.5.7)$$

where $\cosh\theta = \sqrt{q}/2$. Substitution of this expression in (3.5.5) yields

$$\mathcal{H}^f_{\text{Potts,c}} = (2L-1)(1 - \frac{q}{4}) + \sqrt{q}\, \mathcal{H}^f_{\text{XXZ}} , \qquad (3.5.8)$$

where

$$\mathcal{H}^{f}_{XXZ}(\Delta, p) = -\frac{1}{2}\sum_{\ell=1}^{2L-1}\left(\sigma^{x}_{\ell}\sigma^{x}_{\ell+1} + \sigma^{y}_{\ell}\sigma^{y}_{\ell+1} + \Delta\,\sigma^{z}_{\ell}\sigma^{z}_{\ell+1}\right) + \frac{1}{2}p\left(\sigma^{z}_{1} - \sigma^{z}_{2L}\right) \tag{3.5.9}$$

is the Hamiltonian of an XXZ chain of 2L sites with fields p/2 and – p/2 applied to the two free ends. The coupling $\Delta = -\cosh\theta = -\sqrt{q}/2$, while the "end" field $p = \sinh\theta$. For $q < 4$, θ is pure imaginary. Hence setting $\theta = i\gamma$, we have for the "critical" Potts models (*i.e.* $q \le 4$)

$$\Delta = -\cos\gamma = -\frac{1}{2}\sqrt{q} \tag{3.5.10}$$

and

$$p = i\sin\gamma\,. \tag{3.5.11}$$

Several comments are appropriate. Eq. (3.5.8) is an operator equivalence; both $\mathcal{H}^{f}_{Potts,c}$ and $\mathcal{H}^{f}_{XXZ}$ are, apart from additive and multiplicative constants, simply the sum, ΣU_{ℓ}, of the Temperley-Lieb operators. The possible eigenvalues of $\mathcal{H}^{f}_{Potts,c}$ and $\mathcal{H}^{f}_{XXZ}$ are determined from the algebra (3.5.6). However, degeneracies are not determined by the algebra but by the dimensionality of the specific representation chosen for the Temperley-Lieb operators. Indeed for small q-states, there exist eigen-energies of $\mathcal{H}^{f}_{XXZ}$ (which is a $2^{2L} \times 2^{2L}$ matrix) which do not occur in $\mathcal{H}^{f}_{Potts,c}$ (a $q^{L} \times q^{L}$ matrix). For example, the "trivial" eigenstates of (3.5.9) consist of all "up" or all "down" spins, *i.e.* $\sigma^{z}_{\ell}\,|0\rangle = \pm\,|0\rangle$, for all ℓ with energy $-L\Delta/2$ do not appear in $\mathcal{H}^{f}_{Potts,c}$.

Eigen-energies of (3.5.9) can be found by the Bethe ansatz; see Chapter 4. In that chapter the equivalence (3.5.8) is be used to discuss the operater content of the free surface.

One consequence of (3.5.8) is of relevance to our present analysis of the Potts Hamiltonian with periodic boundary conditions. This concerns the value of the factor ζ_{p} required to ensure that the quantum Hamiltonian Potts model is conformally invariant. From (3.1.5), which gives the corresponding factor for $\mathcal{H}_{XXZ}$, and (3.5.10) we immediately obtain

$$\zeta_p = \frac{1}{2}\sqrt{q}\,\zeta = \frac{\pi\sqrt{q(4-q)}}{4\cos^{-1}\left(\frac{1}{2}\sqrt{q}\right)} . \qquad (3.5.12)$$

For $q = 2, 3, 4$, this reduces to the values $\zeta_p = 2, (3/2)\sqrt{3}, \pi$ respectively. On the basis of a numerical study of $\mathcal{H}^f_{\text{Potts}}$, von Gehlen *et al.* (1986) estimated ζ_p and conjectured that $\zeta_p = q^{q/(q-1)}/2$. For $q = 2$ and 3 we see that this expression is exact but, as already noted in the previous section, yields for $q = 4$ the value $2^{5/3} = 3.17\ldots$ instead of $\pi = 3.14\ldots$.

3.5.2 Periodic boundary conditions

We now return to the quatum Hamiltonian of the Potts model with periodic boundary conditions. Hence we consider

$$\mathcal{H}^0_{\text{Potts}} = -\sum_{m=1}^{L}\sum_{k=1}^{q-1}\left(\Omega_m^k + \lambda R_m^k R_{m+1}^{q-k}\right), \qquad (3.5.13)$$

where the operators Ω_m, R_m satisfy (3.5.2) and $R_{L+1} = R_1$ represents the periodic boundary condition. More generally (von Gehlen *et al.* 1986), we apply a "twisted" boundary with

$$R_{L+1} = \omega^{\tilde{q}} R_1 , \quad \tilde{q} = 0, 1, \ldots, q-1. \qquad (3.5.14)$$

We denote the resulting Hamiltonian by $\mathcal{H}^{\tilde{q}}_{\text{Potts}}$. In a basis that diagonalizes the Ω_m's, these Hamiltonians can be diagonalized into sectors labelled by the eigenvalues of

$$\prod_{m=1}^{L}\Omega_m = \omega^{\hat{q}}, \quad \hat{q} = 0, 1, \ldots, q-1. \qquad (5.3.15)$$

We denote $\mathcal{H}^{\tilde{q}}_{\text{Potts}}$ acting in the sector $\hat{q}$ by $\mathcal{H}^{(\hat{q},\tilde{q})}_{\text{Potts}}$.

We would like to relate the eigenvalues of to those of an XXZ chain as was done in the presceding Section for free ends. However, a direct mapping, through the Temperley-Lieb algebra, is difficult because of the boundary conditions (3.5.14) and sector conditions (3.5.15). The basic difficulty arises from the fact that the set of 2L

operators ($\Omega_1, \ldots, \Omega_L, R_1, \ldots, R_L$) is not independent; (3.5.15) acting as a constraint in exactly the same way as the constraints oposed on the link operators in Section 3.4.1 for the Ashkin-Teller chain. The natural way to impose periodic boundary conditions on the Temperley-Lieb Hamiltonian (3.5.5) is to define U_{2L} by extending (3.5.3b) to $\ell = L$. The difficulty is that we do not now how to express (3.5.15) in terms of the U's.

For periodic boundary conditions ($\tilde{q} = 0$) and the ground-state sector ($\hat{q} = 0$) we can overcome this problem and obtain the required map to the XXZ chain by returning to the Euclidean Potts model and performing a number of transformations. This analysis is essentially that carried out by Hamer (1981) but with explicit care taken of boundary effects to ensure that the mapping is exact for a finite chain.

We begin with the two-dimensional anisotropic q-state Potts model on a square lattice of $L \times L$ sites. The partition function is

$$Z_{\text{Potts}} = \sum_{\{\sigma\}} \exp\left[\sum_{i,j=1}^{L} \left\{ K_s\, \delta(\sigma_{i,j}, \sigma_{i+1,j}) + K_t\, \delta(\sigma_{i,j}, \sigma_{i,j+1}) \right\} \right], \qquad (3.5.16)$$

where K_s and K_t are the coupling constants in the horizontal (space-like) direction and the vertical (time-like) direction, and $\sigma_{i,j}$ is the spin at site (i,j); $\sigma_{i,j}$ taking the values $0, 1, \ldots, q-1$. The overall sum is over all configurations of spins. We assume the lattice is wrapped on a cylinder, *i.e.* we apply periodic boundary conditions ($\sigma_{L+1,j} = \sigma_{i,j}$) in the horizontal direction and free edge boundary conditions ($\sigma_{i,L+1} = 0$) in the vertical direction. In the usual way we can express Z_{Potts} in terms of a transfer matrix (see, *e.g.* Baxter 1982):

$$Z_{\text{Potts}} = \langle 0 |\, T^L \,| 0 \rangle \qquad (3.5.17)$$

where T is a $q^L \times q^L$ dimensional matrix with elements

$$T(\sigma, \sigma') = \exp \sum_{m=1}^{L} \left[\tfrac{1}{2} K_s \left\{ \delta(\sigma_m, \sigma_{m+1}) + \delta(\sigma'_m, \sigma'_{m+1}) \right\} + K_t\, \delta(\sigma_m, \sigma'_m) \right]$$

and $|0\rangle$ is the boundary state. Here $\sigma = \{\sigma_1, \sigma_2, \ldots, \sigma_L\}$ denotes the configuration of a horizontal row of the lattice.

Following Hamer (1981), we now consider the τ-continuum limit:

$$\tau \equiv e^{-K_t} \to 0, \quad K_s = q\lambda\tau . \tag{3.5.19}$$

In this limit,

$$T = e^{LK_t}\left(I - \tau\mathcal{H} + O(\tau^2)\right) \tag{3.5.20}$$

where, apart from an additive constant, $\mathcal{H}$ is the quantum Hamiltonian, (3.5.13), of the Potts model. Explicitly

$$\mathcal{H} = \mathcal{H}^{0}_{\text{Potts}} - \lambda L . \tag{3.5.21}$$

To make the contact with $\mathcal{H}_{XXZ}$, we first express (3.5.16) as a Whitney polynomial (Temperley and Lieb 1971, Baxter *et al.* 1976, Baxter 1982), which gives

$$Z_{\text{Potts}} = \sum_{G} q^{C} v_t^{\ell} v_s^{\ell'} \tag{3.5.22}$$

where

$$v_a = e^{K_a} - 1, \quad a = t, s \tag{3.5.23}$$

and the summation is over all graphs G formed by placing ℓ (ℓ') lines on vertical (horizontal) bonds of the lattice and C is the number of connected components in G (including empty sites). Following Temperley and Lieb (1971), we now express (3.5.22) as a staggered eight-vertex model on an auxiliary lattice $\mathfrak{L}'$ with alternating sublattices A and B as shown in Figure 3.13(a). Explicitly we have

$$Z_{\text{Potts}} = v_s^{L} Z_{8v} \tag{3.5.24}$$

where Z_{8v} is the partition function of the vertex model defined on $\mathfrak{L}'$ with weights (we use Hamer's definition of vertices (see Fig. 3.13(b)))

$$\text{(A)} \quad w_1, \ldots, w_8 = X, X, 1, 1, 0, 0, X + e^{-\theta}, X + e^{\theta}$$

$$\text{(B)} \quad w'_1, \ldots, w'_8 = \frac{X}{\lambda}, \frac{X}{\lambda}, 1, 1, 0, 0, \frac{X}{\lambda} + e^{-\theta}, \frac{X}{\lambda} + e^{\theta} \tag{3.5.25}$$

on the two sub-lattices A and B, where

$$X = x_t = v_t/\sqrt{q}, \quad \lambda = x_t x_s \tag{3.5.26}$$

and $\sqrt{q} = 2\cosh\theta$, as before. The equivalence (3.5.24) is not exact, however, for a finite lattice; polygons that wrap entirely around the cycinder are weighted incorrectly.

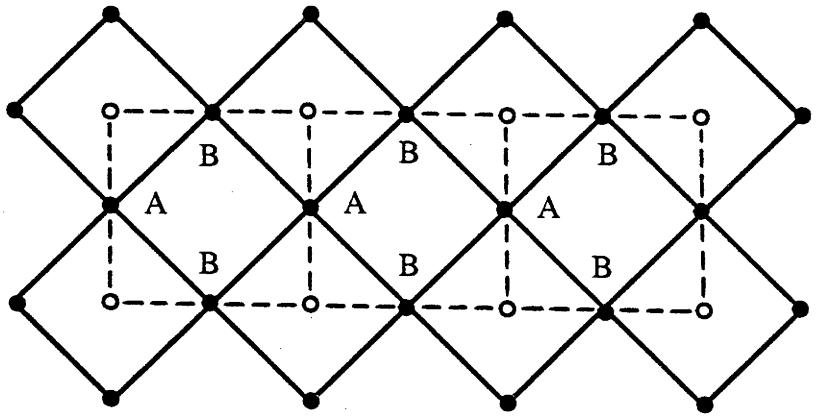

(a)

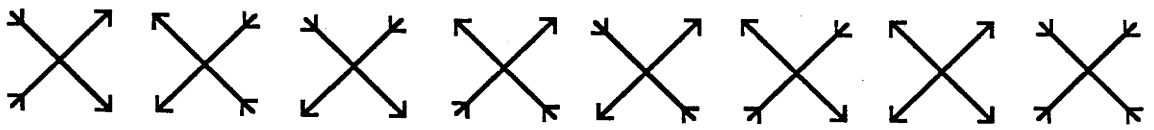

(b)

Figure 3.13 (a) The square lattice $\mathfrak{L}$ (open circles and broken lines) and the auxiliary lattice $\mathfrak{L}'$ (full circles and lines). Also shown is the pattern of A and B vertices on the two sublattices. (b) The arrow representation of the eight possible vertices.

This can be overcome, as was first pointed out by Baxter *et al.* (1976), if we place a vertical "seam" in the lattice and modify the weights along the seam. With our definition of the vertices, the relevant modifications are

$$w_3 \to w'_3 = e^{-2\theta} w_3 , \qquad w_4 \to w'_4 = e^{2\theta} w_4 ,$$

$$w_5 \to w'_5 = e^{-2\theta} w_5 , \qquad w_6 \to w'_6 = e^{2\theta} w_6 . \tag{3.5.27}$$

Introducing operators (Temperley and Lieb 1971, Hamer 1981), $J^{(1)}, J^{(2)}, \ldots, J^{(8)}$ for the vertices of Figure 3.13(b), we can now write the transfer function of the eight-vertex model in operator form:

$$T_{8v} = X^{2L} \prod_{j=1}^{2L-1} \left\{ I + \frac{1}{X}\left[J_j^{(3)} + J_j^{(4)}\right] + \frac{1}{X}\left[e^{-\theta} J_j^{(7)} + e^{\theta} J_j^{(8)}\right] \right\}$$

$$\times \left\{ I + \frac{1}{X}\left[e^{-2\theta} J_{2L}^{(3)} + e^{2\theta} J_{2L}^{(4)}\right] + \frac{1}{X}\left[e^{-\theta} J_{2L}^{(7)} + e^{\theta} J_{2L}^{(8)}\right] \right\} . \tag{3.5.28}$$

Here the product is over a single (diagonal) row of A and B sites in Figure 3.13(a), *i.e.* T is the diagonal-to-diagonal transfer matrix (Temperley and Lieb 1971). In writing (3.5.28), we have also set $\lambda = 1$ and positioned the defect seam between columns 1 and 2L. The second factor in (3.5.28) involves the modified vertices; otherwise (3.5.28) is exactly Eq. (3.18) of Hamer (1981) specialized to criticality. Hence, taking the τ-continuum limit (3.5.19), which amounts to the limit $X \to \infty$, we obtain

$$T_{8v} = X^{2L}\left(I - \tau \mathcal{H}_{8v} + O(\tau^2)\right) , \tag{3.5.29}$$

where

$$\mathcal{H}_{8v} = -\sqrt{q}\left\{ \sum_{j=1}^{2L-1} \left[J_j^{(3)} + J_j^{(4)} + e^{-\theta} J_j^{(7)} + e^{\theta} J_j^{(8)} \right] \right.$$

$$\left. + e^{-2\theta} J_{2L}^{(3)} + e^{2\theta} J_{2L}^{(4)} + e^{-\theta} J_{2L}^{(7)} + e^{\theta} J_{2L}^{(8)} \right\} . \tag{3.5.30}$$

The final step is to express the vertex operators in terms of Pauli operators. We have (Temperley and Lieb 1971, Hamer 1981)

$$J_j^{(3)} + J_j^{(4)} = \frac{1}{2}\left(\sigma_j^x \sigma_{j+1}^x + \sigma_j^y \sigma_{j+1}^y\right), \tag{3.5.31a}$$

$$J_j^{(3)} - J_j^{(4)} = -\frac{1}{2} i\left(\sigma_j^x \sigma_{j+1}^y - \sigma_j^y \sigma_{j+1}^x\right), \tag{3.5.31b}$$

$$J_j^{(7)} + J_j^{(8)} = \frac{1}{2}\left(1 - \sigma_j^z \sigma_{j+1}^z\right), \tag{3.5.31c}$$

$$J_j^{(7)} - J_j^{(8)} = \frac{1}{2}\left(\sigma_{j+1}^z - \sigma_j^z\right). \tag{3.5.31d}$$

Substituting these expressions in (3.5.30) and rearranging gives

$$\mathcal{H}_{8v} = -\frac{1}{2} qL + \sqrt{q}\ \mathcal{H}_{XXZ}(\gamma, 2\gamma), \tag{3.5.32}$$

where

$$\mathcal{H}_{XXZ}(\gamma, \phi) = -\frac{1}{2}\sum_{j=1}^{2L-1}\left(\sigma_j^x \sigma_{j+1}^x + \sigma_j^y \sigma_{j+1}^y - \cos\gamma\ \sigma_j^z \sigma_{j+1}^z\right)$$
$$- \frac{1}{2}\Big[\cos 2\phi\left(\sigma_{2L}^x \sigma_1^x + \sigma_{2L}^y \sigma_1^y\right) + \sin 2\phi\left(\sigma_{2L}^y \sigma_1^x - \sigma_{2L}^x \sigma_1^y\right)$$
$$- \cos\gamma\ \sigma_{2L}^z \sigma_1^z\Big]. \tag{3.5.33}$$

and we have taken $q \le 4$ so that $\theta = i\gamma$ with $2\cos\gamma = \sqrt{q}$. The Hamiltonian (3.5.33) will be recognized as that of the XXZ chain subject to the boundary condition (3.1.6); see also (3.4.14). Finally, collecting constants and other factors, we have the operator equivalence

$$\mathcal{H}_{Potts}^{(0,0)} = (2 - \frac{1}{2} q)L + \sqrt{q}\ \mathcal{H}_{XXZ}(\gamma, 2\gamma). \tag{3.5.34}$$

Note that $\mathcal{H}_{Potts}$ is defined with periodic boundary conditions on L sites, whereas $\mathcal{H}_{XXZ}$ is defined on 2L sites with the twisted boundary condition $\phi = 2\gamma$. Note also that the eigenvalue equivalence implied by (3.5.34) is restricted to states in the ground-state (charge $\hat{q} = 0$) sector of $\mathcal{H}_{Potts}$. A discussion of other sectors will be given in Alcaraz, Barber and Batchelor (1987b).

3.5.3 Conformal anomaly

The equivalence (3.5.34) implies that the ground-state energy per site, $E_0(q\,;L)/L$, of the critical q-state quantum Potts Hamiltonian on a periodic chain of L sites is given by

$$\frac{E_0(q\,;L)}{L} = 2 - \frac{1}{2}q + 2\sqrt{q}\,\frac{E_0(\gamma\,,2\gamma\,;2L)}{2L}\,, \tag{3.5.35}$$

where $\gamma = \cos^{-1}(\sqrt{q}/2)$ and $E_0(\gamma\,,\phi\,;M)/M$ is the ground-state energy of $\mathcal{H}_{XXZ}$ subject to boundary conditions (3.1.6). As discussed in Section 3.2 and Appendix 3A, the Bethe anstaz is applicable to this model. In Section 3.3.5, we argued that

$$E_0(\gamma\,,\phi\,;M) = e_\infty(\gamma)\,M - \frac{\pi\,\zeta\,\hat{c}(\phi)}{6M} + o(M^{-1})\,, \tag{3.5.36}$$

where

$$\hat{c}(\phi) = 1 - \frac{3\phi^2}{2\pi\,(\pi-\gamma)}\,, \tag{3.5.37}$$

and $\zeta = (\pi/\gamma)\sin\gamma$. Accepting this result and allowing for the factor ζ_p in (3.5.12) yields

$$\frac{E_0(q\,;L)}{L} = e'_\infty(q) - \frac{\pi\,\zeta_p\,c(q)}{6L^2} + o(L^{-2})\,, \tag{3.5.38}$$

where

$$e'_\infty(q) = 2 - \frac{1}{2}q + 2\sqrt{q}\;e_\infty\Big(\cos^{-1}(\sqrt{q}/2)\Big)\,, \tag{3.5.39}$$

with $e_\infty(\gamma)$ given in (3.2.28). The exact values of $e_\infty(\gamma)$, corresponding to $q = 0$, 1, 2, 3 and 4, are shown in Table 3.2.

Comparison of (3.5.38) with (3.1.2), identifies the conformal anomaly of the q-state Potts model as

$$c(q) = \hat{c}(2\gamma) = 1 - \frac{3y^2}{2-y}\,, \tag{5.3.40}$$

where, in accord with common paractice, we have set $y = 2\gamma/\pi$. The result (5.3.40) is then precisely of the form predicted by other approaches (Blöte *et al.* 1986, Dotsenko

1984).

3.5.4 Operator content

For this section it is sufficient to label the energies of $\mathcal{H}^{(\hat{q},\tilde{q})}_{\text{Potts}}$ by $E^{(\hat{q},\tilde{q})}(r)$ ($r = 0, 1, \ldots$) with $r = 0$ for the lowest state *etc.* The anomalous dimension $x_\varepsilon^{\text{Potts}}$ of the energy operator can be estimated by extrapolating the sequence

$$X_L^{(0)}(1) \equiv \frac{L}{2\pi\zeta_p}\left[E^{(0,0)}(1) - E^{(0,0)}(0)\right] = x_\varepsilon^{\text{Potts}} + o(1) \quad \text{as} \quad L \to \infty \ . \quad (3.5.41)$$

Similarly, the anomalous dimension x_σ^{Potts} of the magnetic operator can be estimated from the sequence

$$X_L^{(1)}(0) \equiv \frac{L}{2\pi\zeta_p}\left[E^{(1,0)}(0) - E^{(0,0)}(0)\right] = x_\sigma^{\text{Potts}} + o(1) \quad \text{as} \quad L \to \infty \ . \quad (3.5.42)$$

The state $E^{(0,0)}(1)$ is associated with the leading 2-string excitation in the ground-state ($n = 0$) sector of $\mathcal{H}_{XXZ}$. The distribution of zeros for $q = 3$ ($\gamma = \pi/6$, $\phi = \pi/3$) and $L = 8$ is shown in Figure 3.6(b). As discussed in Section 3.2.5, the Bethe ansatz equations become difficult to solve for this particular distribution. At present we have not been able to go beyond $M = 16$ ($L = 8$). However, for $q = 4$ ($\gamma = 0$) we have $\phi = 0$, *i.e.* the periodic case where the position of the actual "string" is exact. On the other hand, $E^{(1,0)}(0)$ is obtained from the lowest state in the ground-state ($n = 0$) sector of $\mathcal{H}_{XXZ}$ with $\phi = \pi$. The estimators (5.3.41) and (5.3.42) are shown in Table 3.26 as a function of L for $q = 3$ and $q = 4$. For $q = 4$, Cardy (1986c) has shown that the estimates converge as $1/(\ell n L)$. Allowing for such a convergence rate yields the "extrapolated" values quoted in the table. From this evidence and the operator identificatiuons of Section 3.3.5, we conclude that the exact results are given by

$$\begin{aligned} x_\varepsilon^{\text{Potts}} &= x_{0,1-\gamma/\pi} - x_{0,\gamma/\pi} \\ &= \frac{\pi + 2\gamma}{2(\pi - \gamma)} \ , \end{aligned} \quad (3.5.43)$$

and

Table 3.26 Scaling dimension estimators $X_L^{(0)}(1)$ and $X_L^{(1)}(0)$ (Eqs. (3.5.41) and (3.5.42)) for the Potts energy and magnetization operators. For $q = 4$, the extrapolated values are obtained by assuming a logarithmic correction of order $1/(\ell nL)$.

	$q = 3$	$q = 4$	
L	x_σ^{Potts}	x_ε^{Potts}	x_σ^{Potts}
4	0.137 537	0.771 229	0.143 407
8	0.135 084	0.722 621	0.139 056
16	0.134 176	0.684 992	0.136 751
32	0.133 776	0.657 247	0.135 233
64	0.133 577	0.636 473	0.134 106
128	0.133 471	0.620 490	0.133 217
256	0.133 412	0.607 858	0.132 493
extrap		0.501± 0.002	0.126 ± 0.002
exact	0.133 333	0.5	0.125

$$x_{\sigma}^{\text{Potts}} = x_{0,1/2} - x_{0,\gamma/\pi}$$

$$= \frac{\pi^2 - 4\gamma^2}{8\pi(\pi - \gamma)} \quad , \tag{3.5.44}$$

in which $\gamma = \cos^{-1}(\sqrt{q}/2)$. These results have been conjectured in the past (see, *e.g.* Wu 1982 and Baxter 1982, and references therein). They further agree with the Coulomb-gas calculations of den Nijs (1983) and the identifications made by Dotsenko (1984).

Parafermions

Like the Ashkin-Teller model, the Potts models are expected to have *parafermion* operators (Fradkin and Kadanoff 1980) with in this case the associated spins being multiples of 1/q. In particular, we have located the corresponding levels in $\mathcal{H}_{XXZ}$ for the parafermions with spin $s = \alpha/q$ for $q = 3$ and $q = 4$ where $\alpha = 1, \ldots, q-1$. In each case, the level in $\mathcal{H}_{XXZ}$ is the lowest state in the $n = 1$ sector with

$$\frac{\phi}{2\pi} = \frac{\alpha}{q} \quad , \quad \alpha = 1, \ldots, q-1 \, . \tag{3.5.45}$$

The scaling dimensions of these operators can be estimated from sequences analogous to (3.4.31) (see von Gehlen *et al.* 1986). From our previous operator identifications (Section 3.3) and the finite lattice estimates shown in Table 3.27 for $q = 3$ and $q = 4$, we conclude that the exact results are given by

$$x_{pf}(\alpha\,;\,q) = x_{1,\alpha/q} - x_{0,\gamma/\pi}$$

$$= \frac{\pi - \gamma}{2\pi} + \frac{\alpha^2\pi^2 - q^2\gamma^2}{2\pi\, q^2(\pi - \gamma)} \, . \tag{3.5.46}$$

The exact values in Table 3.27 are given by $x_{pf}(1\,;\,3) = 7/15$, $x_{pf}(2\,;\,3) = 2/3$, $x_{pf}(1\,;\,4) = 17/32$, $x_{pf}(2\,;\,4) = 5/8$ and $x_{pf}(3\,;\,4) = 25/32$, agreeing with the conjectures of Nienhuis and Knops (1985).

Table 3.27 Finite-size estimates of the anomalous dimensions, $x_{pf}(\alpha ; q)$, associated with the spin α/q parafermion operators of the 3- and 4-state Potts models. The exact values for the continuous q-state models are given in (3.5.44), with the exact values at $q = 3$ and $q = 4$ given further in the text. The extrapolated value shown is obtained by assuming a logarithmic correction of order $1/(\ell nL)$.

L	$x_{pf}(1 ; 3)$	$x_{pf}(2 ; 3)$	$x_{pf}(1 ; 4)$	$x_{pf}(2 ; 4)$	$x_{pf}(3 ; 4)$
4	0.447 856	0.645 034	0.459 772	0.566 387	0.738 308
8	0.457 521	0.661 518	0.474 226	0.582 202	0.759 867
16	0.461 894	0.665 475	0.483 573	0.589 756	0.765 632
32	0.464 063	0.666 400	0.490 105	0.594 410	0.767 625
64	0.465 211	0.666 610	0.494 965	0.597 777	0.768 719
128	0.465 842	0.666 656	0.498 747	0.600 415	0.769 568
256	0.466 196	0.666 665	0.501 786	0.602 567	0.770 312
extrap			0.529 ± 0.003		
exact	0.466 667	0.666 667	0.53125	0.625	0.78125

APPENDIX 3A *Quantum XXZ chain with a twisted boundary*

In this appendix we give the details of the Bethe ansatz solution of an M-site XXZ chain with the "twisted" boundary condition (3.1.6). We define the Hamiltonian

$$\mathcal{H} = -\frac{1}{2}\left[\sum_{m=1}^{M-1}\left(\sigma_m^x \sigma_{m+1}^x + \sigma_m^y \sigma_{m+1}^y + \Delta\, \sigma_m^z \sigma_{m+1}^z\right) + \mathcal{H}_s(\phi)\right] \tag{3A1}$$

where

$$\mathcal{H}_s(\phi) = \cos\phi\left(\sigma_M^x \sigma_1^x + \sigma_M^y \sigma_1^y\right) + \sin\phi\left(\sigma_M^x \sigma_1^y - \sigma_M^y \sigma_1^x\right) + \Delta\sigma_M^z \sigma_1^z \tag{3A2}$$

As for the periodic case ($\phi = 0$), the total spin operator (3.2.1) commutes with $\mathcal{H}$ so that its eigenspace can still be decomposed into sectors labelled by r. As is customary, we build up the full Bethe ansatz formalism by first considering the cases $r = 1$ and $r = 2$, where r is the number of spins reversed from the state with all spins down.

<u>r = 1</u>

We define the wave-function

$$\Psi = \sum_{x=1}^{M} a(x)\,\Phi(x) \tag{3A3}$$

with $\Phi(x) = \beta_1 \ldots \alpha_x \ldots \beta_M$, *i.e.* an upturned spin at site x. The effect of the Hamiltonian (3A1) on $\Phi(x)$ is

$$\begin{aligned}
\mathcal{H}\,\Phi(1) &= -\tfrac{1}{2}(M-4)\,\Delta\Phi(1) - \left[e^{i\phi}\Phi(M) + \Phi(2)\right], \\
\mathcal{H}\,\Phi(x) &= -\tfrac{1}{2}(M-4)\,\Delta\Phi(x) - \left[\Phi(x-1) + \Phi(x+1)\right], \\
\mathcal{H}\,\Phi(M) &= -\tfrac{1}{2}(M-4)\,\Delta\Phi(M) - \left[\Phi(M-1) + e^{-i\phi}\Phi(1)\right].
\end{aligned} \tag{3A4}$$

Substitution of (3A3) with (3A4) into $\mathcal{H}\Psi = E\Psi$ yields

$$E\,a(x) = -\tfrac{1}{2}(M-4)\,\Delta\,a(x) - \left[a(x-1) + a(x+1)\right], \tag{3A5}$$

provided we define the end condition

$$a(x+M) = e^{i\phi} a(x). \tag{3A6}$$

As for the periodic case we also define the amplitudes $a(x) = e^{i\theta x}$ which, when substituted into (3A5) and (3A6), respectively yield

$$E = -\tfrac{1}{2} M\Delta + 2(\Delta - \cos\theta), \tag{3A7}$$

$$\exp i(M\theta - \phi) = 1 . \tag{3A8}$$

From (3A8) we choose $M\theta - \phi = 2\pi I$ with I an integer. These are the solutions of the "Bethe ansatz equation" (3A8), providing the energy eigenvalues through (3A7).

r = 2

Here the wave function is of the form

$$\Psi = \sum_{x<y} a(x,y)\Phi(x,y) . \tag{3A9}$$

There are two cases to consider, (i) $y > x + 1$ and (ii) $y = x + 1$. The effect of the Hamiltonian (3A1) in each case is

(i)

$$\mathcal{H}\,\Phi(1,y) = -\tfrac{1}{2}(M-8)\Delta\Phi(1,y) - \left[e^{i\phi}\Phi(y,M) + \Phi(2,y) + \Phi(1,y-1) + \Phi(1,y+1)\right],$$

$$\mathcal{H}\,\Phi(x,y) = -\tfrac{1}{2}(M-8)\Delta\Phi(x,y) - \left[\Phi(x-1,y) + \Phi(x+1,y) + \Phi(x,y-1) + \Phi(x,y+1)\right],$$

$$\mathcal{H}\,\Phi(x,M) = -\tfrac{1}{2}(M-8)\Delta\Phi(x,M) - \left[\Phi(x-1,M) + \Phi(x+1,M) + \Phi(x,M-1) + e^{-i\phi}\Phi(1,x)\right], \tag{3A10}$$

(ii)

$$\mathcal{H}\,\Phi(1,2) = -\tfrac{1}{2}(M-4)\Delta\Phi(1,2) - \left[e^{i\phi}\Phi(2,M) + \Phi(1,3)\right],$$

$$\mathcal{H}\,\Phi(x, x+1) = -\tfrac{1}{2}(M-4)\,\Delta\Phi(x, x+1) - \Big[\Phi(x-1, x+1) + \Phi(x, x+2)\Big],$$

$$\mathcal{H}\,\Phi(M-1, M) = -\tfrac{1}{2}(M-4)\,\Delta\Phi(M-1, M) - \Big[\Phi(M-2, M) + e^{-i\phi}\,\Phi(1, M-1)\Big]. \qquad (3A11)$$

Substitution of (3A9) with (3A10) and (3A11) into $\mathcal{H}\Psi = E\Psi$ yields the recurrence relations

$$E\,a(x, y) = -\tfrac{1}{2}(M-8)\,\Delta\,a(x, y) - \Big[a(x-1, y) + a(x+1, y) + a(x, y-1) + a(x, y+1)\Big], \qquad (3A12)$$

$$E\,a(x, x+1) = -\tfrac{1}{2}(M-4)\,\Delta\,a(x, x+1) - \Big[a(x-1, x+1) + a(x, x+2)\Big], \qquad (3A13)$$

provided we define

$$a(y, x+M) = e^{i\phi}\,a(x, y). \qquad (3A14)$$

If we now write (Bethe ansatz)

$$a(x, y) = C\,e^{i\theta x}\,e^{i\theta' y} + C'\,e^{i\theta' x}\,e^{i\theta y} \qquad (3A15)$$

then (3A12) reduces to

$$E = -\tfrac{1}{2}M\Delta + 2(2\Delta - \cos\theta - \cos\theta'). \qquad (3A16)$$

To make (3A13) compatible with (3A12) we let $y = x + 1$ in (3A13) and thus require

$$2\Delta\,a(x, x+1) = a(x, x) + a(x+1, x+1). \qquad (3A17)$$

Using (3A15) this "collision" or "meeting" condition gives the ratio of the two co-efficients,

$$\frac{C}{C'} = -\frac{1 - 2\Delta e^{i\theta} + e^{i(\theta+\theta')}}{1 - 2\Delta e^{i\theta'} + e^{i(\theta+\theta')}}. \qquad (3A18)$$

The equations to be solved for θ and θ' now follow from (3A14) and (3A15),

$$\exp i(M\theta - \phi) = C/C'$$

$$\exp i(M\theta' - \phi) = C'/C \,. \tag{3A19}$$

Following Yang and Yang (1966a) we define

$$C/C' = -\exp\left[-i\Theta(\theta,\theta')\right], \tag{3A20}$$

with $\Theta(\theta,\theta')$ defined in (3.2.5). Taking logarithms in (3A19) then gives

$$M\theta - \phi = 2\pi I - \Theta(\theta,\theta') ,$$

$$M\theta' - \phi = 2\pi J - \Theta(\theta',\theta) , \tag{3A21}$$

where I and J are half-odd integers.

general r

From the above special cases, the role of the boundary angle ϕ in the Bethe ansatz formalism is readily apparent. Specifically, for general r we introduce the usual wave-function

$$\Psi = \sum_{x_1<\ldots<x_r} a(x_1,\ldots,x_r)\Phi(x_1,\ldots,x_r) \tag{3A22}$$

in which

$$a(x_1,\ldots,x_r) = \sum_P C_{p1,\ldots,pr}\, e^{i\theta_{p1}x_1} \ldots e^{i\theta_{pr}x_r} , \tag{3A23}$$

where the sum is over all permutations $P = \{p1,\ldots,pr\}$ of the integers $1,\ldots, r$. Here, as again for the periodic case, these amplitudes can be written as in (3.2.3). Similarly, the eigenvalues of $\mathcal{H}$ are given by (3.2.7). However, the usual end condition is replaced by

$$a(x_2,\ldots, x_r, x_1 + M) = e^{i\phi}\, a(x_1,\ldots, x_r) , \tag{3A24}$$

resulting in the θ_j satisfying

$$M\theta_j = 2\pi I_j + \phi - \sum_{k=1}^{r} \Theta(\theta_j,\theta_k) , \quad j = 1,\ldots, r \tag{3A25}$$

with the numbers I_j given in (3.2.6).

4

SURFACE EXPONENTS AND SURFACE ENERGY OF POTTS AND ASHKIN-TELLER QUANTUM CHAINS

4.1 INTRODUCTION

In this chapter we continue the work of the preceding chapter and consider the Ashkin-Teller and Potts quantum chains with *free* boundaries. Recall that in Sections 3.4 and 3.5 we showed that the eigen-spectrum of the quantum Ashkin-Teller and q-state Potts Hamiltonians on chains of L sites, with periodic or twisted boundary conditions, can be obtained exactly at criticality from the eigen-spectrum of a 2L-site quantum XXZ chain with appropriate boundary conditions. By numerically solving the Bethe ansatz equations for the eigen-energies of the XXZ chain we calculated mass gap amplitudes in the Ashkin-Teller and Potts models for chains of up to 512 sites thereby considerably improving previous numerical estimates of the bulk critical exponents.

Now Cardy (1984a) has also derived a set of important relations involving *surface* exponents. In the case of the Hamiltonian formalism these relations can be stated as follows. To each surface exponent x_s of the infinite system (Binder 1983, Cardy 1987) there corresponds a set of states in the finite free boundary Hamiltonian on L sites with energies $\mathcal{E}$, at the bulk critical point, given by

$$\mathcal{E}_s(L,i) = \mathcal{E}_0(L) + \pi\zeta(x_s + i)/L + o(L^{-1}), \qquad i = 0,1,\ldots \tag{4.1.1}$$

Here $\mathcal{E}_0(L)$ is the ground-state energy of the finite chain and ζ is the same conformal invariance preserving constant that we encountered in Chapter 3. In contrast to the result (3.1.2) for periodic boundary conditions, the conformal anomaly c governs the dominant universal finite-size corrections in the ground-state energy per site as (Blöte *et*

al. 1986, Affleck 1986)

$$\mathcal{E}_0(L)/L = e_\infty + \frac{f_\infty}{L} - \frac{\pi\zeta c}{24L^2} + o(L^{-2}) , \qquad (4.1.2)$$

where e_∞ and f_∞ are, respectively, the bulk limits of the ground-state and surface energy per site.

The XXZ chain appropriate for our analysis is defined in (3.5.9), which can be written (recall (3.5.11))

$$\mathcal{H}_{XXZ} = -\frac{1}{2}\left[\sum_{j=1}^{M-1}\left(\sigma_j^x \sigma_{j+1}^x + \sigma_j^y \sigma_{j+1}^y + \Delta\,\sigma_j^z \sigma_{j+1}^z\right) + i\alpha\left(\sigma_1^z - \sigma_M^z\right)\right], \qquad (4.1.3)$$

where $\Delta = -\cos\gamma$ and $\alpha = -\sin\gamma$ are coupling constants with $\gamma \in [0, \pi)$. We observe that although the Hamiltonian (4.1.3) is not Hermitian the eigen-energies are real since (4.1.3) is invariant under complex conjugation and reflection symmetry (relabelling sites from right to left). The eigen-energies of the above Hamiltonian with $M = 2L$ sites and free ends ($\alpha = 0$) are exactly related to those of the self-dual L-site quantum Ashkin-Teller chain with Hamiltonian (3.4.1), which we write here as

$$\mathcal{H}_{AT} = -\frac{1}{2}\sum_{j=1}^{L}\left(\sigma_j^z \sigma_{j+1}^z + \tau_j^z \tau_{j+1}^z + \varepsilon\,\sigma_j^z \sigma_{j+1}^z \tau_j^z \tau_{j+1}^z + \sigma_j^x + \tau_j^x + \varepsilon\,\sigma_j^x \sigma_j^x\right). \qquad (4.1.4)$$

In (4.1.4), $\varepsilon = \cos\gamma$ and $\sigma^z_{L+1} = \tau^z_{L+1} = 0$ for free ends.

On the other hand, we saw that the eigen-energies of a 2L-site XXZ Hamiltonian (4.1.3), with couplings $\gamma = \cos^{-1}(\sqrt{q}/2)$ ($q = 2, 3, 4$) are exactly related to the eigen-energies of an L-site self-dual q-state quantum Potts chain with free ends ($R_{L+1} = 0$), defined by the Hamiltonian (3.5.1), written here as

$$\mathcal{H}_q = -\frac{1}{\sqrt{q}}\sum_{i=1}^{L}\sum_{k=0}^{q-1}\left(R_i^k R_{i+1}^{q-k} + \Omega_i^k\right) + (2L-1)\sqrt{q}/4 . \qquad (4.1.5)$$

For general values of γ, (4.1.5) describes the Hamiltonian analogue of the continuous ($0 \le q \le 4$) q-state Potts model.

The Bethe ansatz equations for the Hamiltonian (4.1.3) with $\alpha = 0$ have been derived by Gaudin (1971,1983). In the next section we derive Bethe ansatz equations for the free XXZ chain with an arbitrary 'surface' field at each end of the chain. By numerically solving these equations for the XXZ chain (4.1.3) we obtain eigen-energies, for L up to 256, of the quantum Ashkin-Teller (4.1.4) and Potts (4.1.5) chains.

4.2 BETHE ANSATZ

Rather than directly considering the Hamiltonian (4.1.3), we define a more general Hamiltonian by

$$\mathcal{H} = -\frac{1}{2}\left[\sum_{j=1}^{M-1}\left(\sigma_j^x \sigma_{j+1}^x + \sigma_j^y \sigma_{j+1}^y + \Delta \sigma_j^z \sigma_{j+1}^z\right) + p\,\sigma_1^z + p'\,\sigma_M^z\right], \quad (4.2.1)$$

where Δ, p and p' are arbitrary constants. Since this Hamiltonian commutes with the total spin operator (3.2.1), the number of down spins r is again a good quantum number. We therefore consider

$$\mathcal{H}\,|r\rangle = \mathcal{E}|r\rangle\,, \quad (4.2.2)$$

where

$$|r\rangle = \sum f(x_1,\ldots,x_r)\;|x_1,\ldots,x_r\rangle\,. \quad (4.2.3)$$

Here the $x_1, \ldots, x_r$ denote the locations of the down spins on the chain, and the summation extends over all sets of the r increasing integers varying between 1 and M, as in (3.2.2) (see, *e.g.* Baxter 1982, Ch. 8):

$$1 \le x_1 < x_2 < \ldots < x_r \le M\,. \quad (4.2.4)$$

r = 1

For one down spin on the chain, the eigenvalue equation (4.2.2) gives

$$\mathcal{E}\,f(x) = -f(x-1) - f(x+1) - \frac{1}{2}\left[(M-5)\,\Delta + p + p'\right] f(x)\,, \quad x = 2,\ldots,M-1\,. \quad (4.2.5)$$

At the boundaries, we get slightly different equations

$$E\, f(1) = -f(2) - \frac{1}{2}\left[(M-3)\,\Delta - p + p'\right] f(1)\,, \tag{4.2.6a}$$

$$\mathcal{E}\, f(M) = -f(M-1) - \frac{1}{2}\left[(M-3)\,\Delta + p - p'\right] f(M)\,. \tag{4.2.6b}$$

We now try as a solution

$$f(x) = A(k)\, e^{ikx} - A(-k)\, e^{-ikx}\,. \tag{4.2.7}$$

Substituting this in equation (4.2.5) we obtain the eigenvalue

$$\mathcal{E} = -2\cos k - \frac{1}{2}\left[(M-5)\,\Delta + p + p'\right]. \tag{4.2.8}$$

We want equation (4.2.5) to be valid for $x = 1$ and $x = M$ also, where $f(0)$ and $f(M+1)$ are defined by (4.2.7). Combining (4.2.5) and (4.2.6) we get the end conditions

$$f(0) = (\Delta - p)\, f(1)\,, \tag{4.2.9a}$$

$$f(M+1) = (\Delta - p')\, f(M)\,. \tag{4.2.9b}$$

Defining the functions $\alpha(k)$ and $\beta(k)$ by

$$\alpha(k) = 1 + (p-\Delta)\, e^{-ik}\,, \tag{4.2.10a}$$

$$\beta(k) = \left[1 + (p'-\Delta)\, e^{-ik}\right] e^{i(M+1)k}\,, \tag{4.2.10b}$$

and substituting (4.2.7) in (4.2.9), we obtain

$$A(k)\,\alpha(-k) - A(-k)\,\alpha(k) = 0\,, \tag{4.2.11a}$$

$$A(k)\,\beta(k) - A(-k)\,\beta(-k) = 0\,. \tag{4.2.11b}$$

Compatibility between (4.2.11a) and (4.2.11b) yields

$$\alpha(k)\,\beta(k) = \alpha(-k)\,\beta(-k)\,, \tag{4.2.12}$$

or, using (4.2.10),

$$e^{i2(M-1)k}\,\frac{\left(e^{ik} + p - \Delta\right)\left(e^{ik} + p' - \Delta\right)}{\left(e^{-ik} + p - \Delta\right)\left(e^{-ik} + p' - \Delta\right)} = 1. \tag{4.2.13}$$

In the special case where the constants satisfy

$$(\Delta - p)\,(\Delta - p') = 1\,, \tag{4.2.14}$$

(4.2.13) reduces to

$$e^{i2Mk} = 1 . \qquad (4.2.15)$$

Given the compatibility relation (4.2.12), the solution of (4.2.11) for A(k) is

$$A(k) = \beta(-k) , \qquad (4.2.16)$$

where it should be noted that A(k) is determined up to a factor that is invariant under $k \leftrightarrow -k$.

r = 2

For two down spins on the chain, we obtain the eigenvalue equation

$$\mathcal{E}\, f(x_1 , x_2) = -f(x_1 - 1, x_2) - f(x_1 + 1, x_2) - f(x_1 , x_2 - 1) - f(x_1 , x_2 + 1)$$
$$- \tfrac{1}{2}\left[(M-9)\,\Delta + p + p'\right] f(x_1 , x_2) . \qquad (4.2.17)$$

We now also get the usual "meeting condition" that arises because the two down spins may be neighbours (see, *e.g.* Gaudin 1983)

$$f(x_1 , x_1) + f(x_1 + 1, x_1 + 1) - 2\Delta\, f(x_1 , x_1 + 1) = 0 . \qquad (4.2.18)$$

In addition to this, as in the case r = 1, we have two conditions to be satisfied at the free ends of the chain

$$f(0 , x_2) = (\Delta - p)\, f(1 , x_2) , \qquad (4.2.19a)$$

$$f(x_1 , M + 1) = (\Delta - p')\, f(x_1 , M) . \qquad (4.2.19b)$$

Guided by the r = 1 case we consider the ansatz

$$f(x_1 , x_2) = \sum_P \varepsilon_P\, A(k_1 , k_2)\, e^{i(k_1 x_1 + k_2 x_2)} , \qquad (4.2.20)$$

where the sum extends over the permutations and the negations of k_1 and k_2, and ε_p is a sign factor (± 1) that changes sign on negation or pair interchange. Substituting this ansatz in (4.2.17) we obtain the eigenvalue

$$\mathcal{E} = -2\cos k_1 - 2\cos k_2 - \tfrac{1}{2}\left[(M-9)\,\Delta + p + p'\right] . \qquad (4.2.21)$$

Defining the function $s(k_1,k_2)$ by

$$s(k_1 , k_2) = 1 - 2\Delta\, e^{ik_2} + e^{i(k_1 + k_2)} , \qquad (4.2.22)$$

necessary conditions for the equations (4.2.18) and (4.2.19) to be satisfied are

$$A(k_1, k_2)\, s(k_1, k_2) - A(k_2, k_1)\, s(k_2, k_1) = 0\,, \tag{4.2.23a}$$

$$A(k_1, k_2)\, \alpha(-k_1) - A(-k_1, k_2)\, \alpha(k_1) = 0\,, \tag{4.2.23b}$$

$$A(k_1, k_2)\, \beta(k_2) - A(k_1, -k_2)\, \beta(-k_2) = 0\,, \tag{4.2.23c}$$

together with nine other equations that can be obtained from (4.2.23) by applying permutations and negations. Using (4.2.23a), (4.2.23c), (4.2.23a) and (4.2.23b) to successively express $A(k_1,k_2)$ in terms of $A(k_2,k_1)$, $A(k_2,-k_1)$, $A(-k_1,k_2)$ and $A(k_1,k_2)$, the fact that the prefactor we pick up along the way is unity leads to

$$\frac{\alpha(k_1)\,\beta(k_1)}{\alpha(-k_1)\,\beta(-k_1)} = \frac{B(-k_1, k_2)}{B(k_1, k_2)}\,, \tag{4.2.24}$$

where $B(k,k')$ is given by

$$B(k, k') = s(k, k')\, s(k', -k)\,. \tag{4.2.25}$$

Using (4.2.10) we may rewrite the compatibility condition (4.2.24) as

$$e^{i2(M-1)k_1}\, \frac{\left(e^{ik_1} + p - \Delta\right)\left(e^{ik_1} + p' - \Delta\right)}{\left(e^{-ik_1} + p - \Delta\right)\left(e^{-ik_1} + p' - \Delta\right)} = \frac{B(-k_1, k_2)}{B(k_1, k_2)}\,. \tag{4.2.26}$$

Since there are eight functions that can be obtained from $A(k_1,k_2)$ by permutations and negations, it follows that there are eight compatibility equations to be satisfied, each analogous to (4.2.26). It is not difficult to see however, that (4.2.26) is invariant under $k_1 \leftrightarrow -k_1$ and $k_2 \leftrightarrow -k_2$ (in fact, if $k_1 \neq 0$, (4.2.26) can be written as a polynomial equation in terms of $\cos k_1$ and $\cos k_2$ only), so permuting k_1 and k_2 results in just one more equation

$$\frac{\alpha(k_2)\,\beta(k_2)}{\alpha(-k_2)\,\beta(-k_2)} = \frac{B(-k_2, k_1)}{B(k_2, k_1)}\,, \tag{4.2.27}$$

Again in the special limit (4.2.14), there is some simplification in these equations; the left hand side of (4.2.24) and (4.2.27) reducing to $\exp(i2Mk_1)$ and $\exp(i2Mk_2)$, respectively.

In principle, the coupled equations (4.2.26) and (4.2.27) give k_1 and k_2 which in turn give the corresponding eigenvalue through (4.2.21). We now turn to the coefficient $A(k_1,k_2)$ in the wave function (4.2.20). From (4.2.23a) we have

$$A(k_1, k_2) = s(k_2, k_1)\, C(k_1, k_2)\,, \tag{4.2.28}$$

where $C(k_1,k_2)$ is symmetric under $k_1 \leftrightarrow k_2$. In order to determine $C(k_1,k_2)$, we substitute (4.2.28) in (4.2.23c), obtaining

$$C(k_1, k_2) = \beta(-k_2)\, v(k_1, k_2)\, g(k_1)\,, \tag{4.2.29}$$

where the symmetric function $v(k_1,k_2)$ is defined by

$$v(k_1, k_2) = e^{-ik_1} + e^{-ik_2} - 2\Delta\,. \tag{4.2.30}$$

The factor $g(k_1)$ is determined from the symmetry of $C(k_1,k_2)$ under $k_1 \leftrightarrow k_2$, resulting in

$$C(k_1, k_2) = \beta(-k_1)\, \beta(-k_2)\, v(k_1, k_2)\,. \tag{4.2.31}$$

Finally, substitution of (4.2.31) into (4.2.28) leads to

$$A(k_1, k_2) = \beta(-k_1)\, \beta(-k_2)\, B(-k_1, k_2)\, e^{ik_2}\,, \tag{4.2.32}$$

where $B(k,k')$ is defined in (4.2.25).

General r

The above can be generalized to arbitrary values of r. The ansatz for the wave function becomes

$$f(x_1, \ldots, x_r) = \sum_P \varepsilon_P\, A(k_1, \ldots, k_r)\, e^{i(k_1x_1 + \ldots + k_rx_r)}\,, \tag{4.2.33}$$

where the sum extends over all permutations and negations of $k_1,\ldots, k_r$ and ε_P changes sign at each such 'mutation'. The coefficients in the wave function are given by

$$A(k_1, \ldots, k_r) = \prod_{j=1}^{r} \beta(-k_j) \prod_{1\le j<\ell\le r} B(-k_j, k_\ell)\, e^{ik_\ell} \tag{4.2.34}$$

where $B(k,k')$ is defined in (4.2.25) and (4.2.22). The parameters $k_1,\ldots, k_r$ satisfy

$$\frac{\alpha(k_j)\,\beta(k_j)}{\alpha(-k_j)\,\beta(-k_j)} = \prod_{\ell=1}^{r} \frac{B(-k_j, k_\ell)}{B(k_j, k_\ell)}, \quad j = 1, \ldots, r. \tag{4.2.35}$$

with $\alpha(k)$ and $\beta(k)$ defined in (4.2.10). The eigenvalues $\hat{\mathcal{E}}$ are given by

$$\hat{\mathcal{E}} = -\tfrac{1}{2}\left[(M-1)\,\Delta + p + p'\right] - 2\sum_{j=1}^{r} (\cos k_j - \Delta). \tag{4.2.36}$$

Returning to the Hamiltonian (4.1.3), the two cases of interest are $p = p' = 0$ and $p = -p' = i\alpha$ with $\Delta = -\cos\gamma$ and $\alpha = \sin\gamma$, $\gamma \in [0,\pi)$. For both cases the eigen-energies are given by

$$\hat{\mathcal{E}} = -\tfrac{1}{2}(M-1)\,\Delta - 2\sum_{j=1}^{r}(\cos k_j - \Delta). \tag{4.2.37}$$

Taking the logarithm of (4.2.35) (see, *e.g.* Baxter 1982), the parameters k_j, $j = 1,\ldots, r$ satisfy

$$(M+1)\,k_j = \pi\ell_j - \Theta(k_j,-k_j) - \frac{1}{2}\sum_{\substack{\ell=1\\ \neq j}}^{r}\left[\Theta(k_j,-k_\ell) + \Theta(k_j,k_\ell)\right] \tag{4.2.38}$$

for the Ashkin-Teller case ($\alpha = 0$) and

$$M k_j = \pi\ell_j - \frac{1}{2}\sum_{\substack{\ell=1\\ \neq j}}^{r}\left[\Theta(k_j,-k_\ell) + \Theta(k_j,k_\ell)\right] \tag{4.2.39}$$

for the Potts case ($\Delta^2 + \alpha^2 = 1$). The phase factor appearing in these equations is the same as that for the periodic case, see (3.2.5).

From the numerical evidence (see below), the lowest state in a given sector is obtained by choosing the integers $\ell_j = j$, $j = 1, \ldots, r$, as earlier surmised by Gaudin (1971, 1983). From these equations, the ground-state energy per site in the thermodynamic limit, $M \to \infty$, has been evaluated in Alcaraz *et al.* 1987; see also Hamer, Quispel and Batchelor (1987). Naturally, we recover the periodic chain result (3.2.28).

4.3 CONFORMAL ANOMALY AND SURFACE ENERGY

The main numerical computations presented in this paper were achieved by solving the equations (4.2.38) and (4.2.39). We obtained, in this way, several eigen-energies in the various sectors of (4.1.3) for chain size up to $M = 512$. These eigen-energies were then identified with the corresponding levels in the models (4.1.4) and (4.1.5) on $L = M/2$ sites. To make this comparison, the Bethe ansatz results for small L were compared with the results obtained by directly diagonalizing (4.1.4) and (4.1.5) with the Lanczos method. (In the case of the q-state Potts model with $q \neq 2, 3, 4$ we simply assume that the corresponding states are the analytic continuation of those occuring in (4.1.5).) For the remainder of this chapter we use the eigen-energies of models (4.1.4) and (4.1.5) calculated through (4.1.3) and the relations (4.1.1) and (4.1.2) in order to obtain the surface exponents and conformal anomaly of all three models.

Before applying (4.1.1) and (4.1.2), however, we need to identify the factor ζ. From the results of the preceding chapter and the normalization of the Hamiltonians (4.1.3), (4.1.4) and (4.1.5), we identify the values

$$\zeta_{XXZ} = \frac{\pi \sin\gamma}{\gamma} \tag{4.3.1}$$

and

$$\zeta_{AT} = \frac{\pi \sin\gamma}{2\gamma}\,, \quad \zeta_q = \frac{\pi\sqrt{4-q}}{4\cos^{-1}\left(\sqrt{q}/2\right)} \;\; (q<4) \;\text{ with }\; \zeta_4 = \frac{\pi}{2}. \tag{4.3.2}$$

It is gratifying to observe that the earlier numerical estimates (von Gehlen *et al.* 1986, von Gehlen and Rittenberg 1986a,b,c; 1987) of ζ_{AT} and ζ_q are in good agreement with the exact values given in (4.3.2).

As typical examples of our numerical computations we show in Table 4.1A the ground-state energy per site for $L = 2^\ell$, $\ell = 2, 3, \ldots, 8$, of the Ashkin-Teller model with couplings $\varepsilon = -\sqrt{3}/2, -1/2, 1/2, 1/\sqrt{2}$, and $\sqrt{3}/2$. The corresponding results for a

2L-site XXZ chain can be simply obtained by exploiting the equivalence between (4.1.3) and (4.1.4) (in particular, $\Delta = -\varepsilon$). In Table 4.1B we similarly show the ground state energy per site of the q-state Potts model for q = 2, 3, 3.414... [$4\cos^2(\pi/8)$], 3.618... [$4\cos^2(\pi/10)$], and 4.

To compute the conformal anomaly from (4.1.2), we need first to estimate the (non-universal) surface energy f_∞. We have done this by simply extrapolating by Vanden Broeck / Schwartz (1979) approximates the sequence

$$f_L \equiv L\left[\mathcal{E}_0(L) - e_\infty\right] \rightarrow f_\infty \quad \text{as } L \rightarrow \infty \tag{4.3.3}$$

with e_∞ obtained from the exact result (3.2.28). The resulting estimates are quoted in Table 4.1 and are believed to be accurate to the number of digits quoted. With f_∞ thus estimated, we can then estimate the conformal anomaly c by similarly extrapolating the sequence

$$c(L) \equiv -\left[\mathcal{E}_0(L) - L\,e_\infty - f_\infty\right]\frac{24\,L}{\pi\,\zeta} \ . \tag{4.3.4}$$

The resulting estimates, again obtained by Vanden Broeck / Schwartz approximates, are shown in Table 4.1. From the table, we clearly see that c = 1, independent of Δ and ε, for the XXZ and Ashkin-Teller models which is expected due to their non-universal behaviour. We also see for the Potts chain that c = 1/2, 4/5, 25/28, 14/15, and 1 for the respective values of q. (The poorer convergence as q nears 4 is a result of the correction terms in (4.1.2) increasing with importance in this limit, in particular at q = 4 logarithmic corrections appear (Cardy 1986c, Woynarovich and Eckle 1987, Alcaraz, Barber and Batchelor 1987a,b.) These values agree with the predicted values from conformal invariance (Dotsenko 1984, Cardy 1987). As in Section 3.5.3, they are well accounted for by the expression

$$c(q) = 1 - \frac{6}{\pi/\gamma\,(\pi/\gamma - 1)} \ , \qquad \gamma = \cos^{-1}\left(\sqrt{q}/2\right) . \tag{4.3.5}$$

The Bethe ansatz equations (4.2.39) decouple at the value $\gamma = \pi/2$ corresponding to the q = 0 limit. This limit further corresponds to the Hamiltonian analogue of a resistor network (see, *e.g.* Wu 1982). From (4.2.37) the ground-state

Table 4.1(a) The ground-state energy per site of the quantum Ashkin-Teller Hamiltonian (4.1.4). Exact values denoted by (*) are given by doubling (3.2.28). The extrapolated results (†) were obtained from the sequence L = 4, 6, 8,..., 60 (see text).

L	$\varepsilon = -\sqrt{3}/2$	$\varepsilon = -1/2$	$\varepsilon = 1/2$	$\varepsilon = 1/\sqrt{2}$	$\varepsilon = \sqrt{3}/2$
4	–0.898 391	–0.999 749	–1.421 625	–1.527 916	–1.613 182
8	–0.955 665	–1.047 739	–1.458 847	–1.565 672	–1.652 109
16	–0.984 695	–1.072 596	–1.478 866	–1.585 976	–1.673 022
32	–0.999 322	–1.085 256	–1.489 283	–1.596 544	–1.683 900
64	–1.006 662	–1.091 646	–1.494 602	–1.601 942	–1.689 456
128	–1.010 339	–1.094 856	–1.497 291	–1.604 672	–1.692 265
256	–1.012 179	–1.096 465	–1.498 643	–1.606 045	–1.693 677
e_∞*	–1.014 020 ...	–1.098 076 ...	–1.5	–1.607 423 ...	–1.695 095 ...
f_∞†	0.471 568	0.412 883	0.348 076	0.353 553	0.363 777
c†	0.999 99(6)	0.999 99(5)	1.000 0(3)	1.000 0(1)	1.00(5)

Table 4.1(b) The ground-state energy per site of the quantum q-state Potts Hamiltonian (4.1.5). Exact values denoted by (*) are given by doubling (3.2.28). The extrapolated results (†) were obtained from the sequence L = 4, 6, 8,..., 60 (see text).

L	q = 2	q = 3	q = 3.414...	q = 3.618...	q = 4
4	−1.459 958	−1.580 754	−1.626 304	−1.647 982	−1.687 466
8	−1.532 473	−1.636 076	−1.675 238	−1.693 900	−1.727 934
16	−1.569 617	−1.665 066	−1.701 131	−1.718 317	−1.749 664
32	−1.588 434	−1.679 942	−1.714 489	−1.730 948	−1.760 964
64	−1.597 906	−1.687 482	−1.721 281	−1.737 379	−1.766 733
128	−1.602 659	−1.691 279	−1.724 706	−1.740 626	−1.769 650
256	−1.605 040	−1.693 185	−1.726 427	−1.742 257	−1.771 116
e_∞*	−1.607 423 ...	−1.695 095 ...	−1.728 152 ...	−1.743 893 ...	−1.772 588 ...
f_∞†	0.610 502	0.489 637	0.442 487	0.419 717	0.377 649
c†	0.500 00(1)	0.799 9(2)	0.89(3)	0.93(5)	0.99(2)
c	0.5	0.8	0.892 857 ...	0.93	1.0

energy per site is exactly given by

$$\mathcal{E}_0/L = -2\sqrt{2}\cos\frac{\pi}{4}\left(1+\frac{1}{L}\right)\operatorname{cosec}\frac{\pi}{4L}\,, \qquad (4.3.6)$$

which on expressing in powers of 1/L and comparing with (4.1.2) yields the exact values $f_\infty = 1$ and $c = -2$. In the $q = 1$ limit (percolation) we have $\gamma = \pi/3$ and although we are unable to solve (4.2.39) analytically our numerical results are reproduced for all L by

$$\mathcal{E}_0/L = -\frac{3}{2}\left(1-\frac{1}{2L}\right), \qquad (4.3.7)$$

which gives $e_\infty = -3/2$, $f_\infty = 3/4$ and $c = 0$. It is interesting to observe that these results also fit the formula (4.3.5). This equation can be expressed as in (3.1.1) by making the identification $\pi/\gamma = m+1$. We see that $c = -2$ and $c = 0$ respectively correspond to the values $m = 1$ and $m = 2$.

4.4 SURFACE EXPONENTS

We now turn to the surface exponents of the models under consideration. Let us consider initially an M-site XXZ model with free boundaries (Eqn. (4.1.3) with $\alpha = 0$). It is again convenient here to label the sectors by the number n, defined in (3.2.15), representing the number of over-turned spins from the antiferromagnetic ground-state ($r = M/2$). Associated with the lowest energy $E_0^{(n)}$ in each sector we have a surface exponent $x_s^{(n)}$, which may be estimated from the sequence (recall Eqn. (4.1.1))

$$x_s^{(n)}(M) \equiv \left[E_0^{(n)} - E_0^{(0)}\right]\frac{M}{\pi\zeta} \qquad n = 1, 2, \ldots \qquad (4.4.1)$$

where $E_0^{(0)}$ is the ground state energy and ζ is given in (4.3.1). For $n = 1, 2, \ldots$ these dimensions govern, respectively, the decay of the spin-spin, energy-energy,... correlations. In Table 4.2 we show, for several values of $\varepsilon = -\Delta$, the extrapolated values of the above sequence. Our results strongly suggest that these exponents are given by

Table 4.2 Extrapolated and expected results for the leading surface exponents of the XXZ and Ashkin-Teller chains.

ε	$x_s^{(1)} \equiv x_s^{(1,+)}$	$x_s^{(2)}$	$x_s^{(3)}$	$x_s^{(1,-)}$	$x_s^{(2,+)}$	$x_s^{(2,-)}$
$-\sqrt{3}/2$	0.166666(9) (1/6)	0.666666(5) (2/3)	1.50000(3) (3/2)	1.16(4) (7/6)	——	——
$-1/2$	0.333333(3) (1/3)	1.33333(8) (4/3)	3.0000(1) (3)	1.33333(5) (4/3)	1.00000(6) (1)	2.00000(4) (2)
$1/2$	0.6666(7) (2/3)	2.666(8) (8/3)	6.000(2) (6)	1.6666(5) (5/3)	1.0000(7) (1)	2.000(2) (2)
$1/\sqrt{2}$	0.75000(7) (3/4)	2.9999(3) (3)	6.749(7) (27/4)	1.7500(4) (7/4)	1.0000(4) (1)	1.9999(9) (2)

$$x_s^{(n)} = 2n^2 x_p \qquad n = 1, 2, \ldots \tag{4.4.2}$$

where $x_p \equiv (\pi - \gamma)/2\pi$ is the anomalous dimension of the bulk polarization operator. In comparison, the corresponding scaling dimensions for the bulk correlation functions are given by $x^{(n)} = n^2 x_p$, n = 1, 2, ... (recall Section 3.3.2).

For the case of the Ashkin-Teller chain the Hamiltonian (4.1.4) is invariant under Z(2)⊗Z(2) internal symmetry as well as possessing reflection symmetry. The Hilbert space decomposes into eight sectors with corresponding energies $E_i^{(Q,P)}$ where Q = 0, 1, 2, 3, P = ± and i = 0, 1, 2, ... The sectors with Q = 1 and Q = 3 are degenerate due to the global symmetry $\sigma \Leftrightarrow \tau$ in (4.1.4). In each of these sectors we identify the corresponding surface exponent $x_s^{(Q,P)}$ from the sequence

$$x_s^{(Q,P)}(L) \equiv \left[E_0^{(Q,P)} - E_0^{(0,0)} \right] \frac{L}{\pi\zeta}, \qquad Q = 1, 2, 3, \quad P = \pm \tag{4.4.3}$$

with ζ given by (4.3.2). These sequences are listed in Table 4.3 for the particular value $\varepsilon = 1/2$ and chain sizes $L = 2^\ell$ for ℓ = 2, 3, ..., 8. Extrapolated results for several ε values are given in Table 4.2. We observe from these results that $x_s^{(Q,-)} = x_s^{(Q,+)} + 1$, implying that for a given charge Q, the ground-state in the positive (negative) parity sector corresponds to the first (second) state in the tower of states given in (4.1.1). In agreement with earlier numerical results (von Gehlen and Rittenberg 1986c,1987), our results clearly show that the surface exponents describing the magnetic and electric correlations $x_s^m = \eta_\parallel^m/2$ and $x_s^e = \eta_\parallel^e/2$, respectively, are given by

$$x_s^m \equiv x_s^{(1,+)}(\infty) = (\pi - \gamma)/\pi = (2x_\varepsilon^{AT})^{-1} \quad \text{for} \quad -1 \le \varepsilon \le 1, \tag{4.4.4}$$

$$x_s^e \equiv x_s^{(2,+)}(\infty) = 1 \quad \text{for} \quad -\frac{1}{\sqrt{2}} \le \varepsilon \le 1, \tag{4.4.5}$$

where x_ε^{AT} is the anomalous dimension of the energy operator. The levels $E_0^{(2,+)}$ and $E_0^{(2,-)}$ are both in the n = 0 (r = L) sector of (4.1.3) with M = 2L and the integers ℓ_j chosen from {1, 2, ..., r−1, r+1} and {1, 2, ..., r−2, r, r+1}, respectively. For both the Ashkin-Teller and Potts models (see below) the levels $E_0^{(1,+)}$ and $E_0^{(1,-)}$ occur in

Table 4.3 Amplitude estimators (Eqn.(4.4.3)) for the Ashkin-Teller chain at $\varepsilon = 1/2$.

L	$x_s^{(1,+)}(L)$	$x_s^{(1,-)}(L)$	$x_s^{(2,+)}(L)$	$x_s^{(2,-)}(L)$
4	0.547 542	1.345 31	0.777 955	1.555 91
8	0.596 800	1.496 16	0.880 264	1.760 53
16	0.626 720	1.574 75	0.935 469	1.870 94
32	0.644 236	1.616 43	0.965 016	1.930 03
64	0.654 243	1.639 07	0.980 990	1.961 98
128	0.659 859	1.651 54	0.989 687	1.979 37
256	0.662 969	1.658 41	0.994 425	1.988 85
exact	2/3	5/3	1	2

the $n = 1$ ($r = L - 1$) sector of (4.1.3) again with $M = 2L$ but with respective integer sets $\{1, 2, \ldots, r\}$ and $\{1, 2, \ldots, r-1, r+1\}$. Unfortunately, due to numerical instabilities we are unable to compute the level in (4.1.3) corresponding to x_s^e inside the critical fan region ($-1 \leq \varepsilon \leq -1/\sqrt{2}$).

In the case of the q-state Potts model ($q \in Z$) the Hamiltonian (4.1.5) is symmetric under global $Z(q)$ transformations and reflections of the lattice. Consequently the Hilbert space separates into $2q$ disjoint sectors with energies $E_i^{(Q,P)}$ ($Q = 0, 1, \ldots, q-1$, $P = \pm$, $i = 0, 1, 2, \ldots$). The ground-state lies in the sector labelled by $Q = 0$, $P = +$, ($i = 0$) while the sectors with $Q \neq 0$ are degenerate. In this case the leading surface exponent can be extracted by extrapolating the estimators (4.4.3) with $Q = 1$ and the corresponding ζ given in (4.3.2). In Table 4.4 we show the sequence $x_s^{(1,+)}(L)$ with $L = 2^\ell$ for $\ell = 2, 3, \ldots, 8$ and $q = 1$, 2, 3, 3.414... [$4\cos^2(\pi/8)$], 3.618... [$4\cos^2(\pi/10)$], and 4. As in the Ashkin-Teller case we have also verified that $x_s^{(1,-)} = x_s^{(1,+)} + 1$ which as before implies that the lowest state in the negative parity sector corresponds to the second level in the tower of states characterizing $x_s = \eta_\parallel/2 \equiv x_s^{(1,+)}(\infty)$. All of the observed values are well accounted for by the expression

$$x_s = 1 - \frac{2\gamma}{\pi}, \qquad q = 4\cos^2\gamma \tag{4.4.6}$$

which agrees with the predicted value (Cardy 1984c) $x_s = (m-1)/(m+1)$, $m = 1, 2, 3, 5, \ldots$ if we again identify $\pi/\gamma = m+1$. In the limit $q = 0$, corresponding to $m = 1$, the Bethe ansatz equation (4.2.39) and (4.2.37) yield the exact equality $E_0^{(0,+)}(L) = E_0^{(1,+)}(L)$ giving $x_s = \eta_\parallel = 0$ in agreement with (4.4.6). Again the convergence of the sequences deteriorates as we approach the limit $q = 4$ where the logarithmic corrections occur. The extrapolated value for $q = 4$ quoted in Table 4.4 is obtained by assuming a logarithmic correction in (4.4.3) of the form predicted by Cardy (1986c).

Table 4.4 Amplitude estimates (Eqn.(4.4.3)), $x_s^{(1,+)}(L)$, for the q-state Potts chain.

L	q = 1	q = 2	q = 3	q = 3.414...	q = 3.618...	q = 4
4	0.310 468	0.442 191	0.546 487	0.585 170	0.603 466	0.636 608
8	0.322 203	0.469 919	0.595 135	0.643 906	0.667 460	0.710 956
16	0.327 900	0.484 665	0.624 763	0.681 940	0.710 179	0.763 490
32	0.330 662	0.492 260	0.642 322	0.706 203	0.738 489	0.800 955
64	0.332 012	0.496 112	0.652 588	0.721 662	0.757 377	0.828 331
128	0.332 677	0.498 051	0.658 548	0.731 552	0.770 131	0.848 934
256	0.333 006	0.499 025	0.661 992	0.737 920	0.778 858	0.864 907
extrap	0.333 33(3)	0.500 00(0)	0.666 66(9)	0.749 (8)	0.799 (6)	0.99(3)
exact	1/3	1/2	2/3	3/4	4/5	1

4.5 EXACT SURFACE ENERGY

The exact suface energy, f_∞, of the free XXZ, Ashkin-Teller and Potts chains has recently been calculated by Hamer (Hamer, Quispel and Batchelor 1987) using the methods of De Vega and Woynarovich (1985) and Woynarovich and Eckle (1987). The results, obtained from the equivalent XXZ Hamiltonian (4.1.3), are

$$f_\infty^{\text{Potts}} = \frac{\pi \sin\gamma}{2\gamma} - \frac{\cos\gamma}{2} - \frac{\sin\gamma}{4}\int_{-\infty}^{\infty} dk \left[1 - \coth\left(\frac{\pi k}{4}\right)\tanh\left(\frac{\gamma k}{2}\right)\right] \quad (4.5.1)$$

for the Potts Hamiltonian (4.1.5), and

$$f_\infty^{\text{AT}} = \frac{\pi \sin\gamma}{2\gamma} - \frac{\cos\gamma}{2} - \frac{\sin\gamma}{4}\int_{-\infty}^{\infty} dk \left[1 - \tanh\left(\frac{\pi k}{4}\right)\tanh\left(\frac{\gamma k}{2}\right)\right] \quad (4.5.2)$$

for the Ashkin-Teller Hamiltonian (4.1.4). The above integrals are easily evaluated numerically and the results are in agreement with the estimates shown in Table 4.1. Furthermore, the values of f_∞^{AT} confirm the numerical estimates of von Gehlen and Rittenberg (1987) obtained by directly diagonalizing $\mathcal{H}_{\text{AT}}$. Both (4.5.1) and (4.5.2) have been evaluated for several γ values by Chris Hamer (unpublished). Let us denote (4.5.1) by $f_\infty^{\text{Potts}}(q)$, then the exact results are: $f_\infty^{\text{Potts}}(0) = 1$, $f_\infty^{\text{Potts}}(1) = 3/4$, $f_\infty^{\text{Potts}}(2) = (3\pi - 4)/(2\pi\sqrt{2})$, $f_\infty^{\text{Potts}}(3) = (6\sqrt{3} - 7)/(4\sqrt{3})$ and $f_\infty^{\text{Potts}}(4) = (\pi - 1)/2 - \ell n 2$.

The surface energy of the Potts Hamiltonian written in the form (3.5.1) is

$$f'_\infty(q) = \sqrt{q}\, f_\infty^{\text{Potts}} - \left(1 - \frac{q}{4}\right). \quad (4.5.3)$$

Using the above value, this formula gives $f'_\infty(3) = 3\sqrt{3}/2 - 2$, confirming a numerical estimate of von Gehlen and Rittenberg (1986a).

5

A FINITE LATTICE STUDY OF THE CRITICAL BEHAVIOUR OF THE BIAXIAL NEXT-NEAREST-NEIGHBOUR ISING MODEL

5.1 INTRODUCTION

Systems with interactions beyond those between nearest-neighbours are now known to be capable of yielding rich and complex critical behaviour. A wide variety of ordered phases at low temperatures, including modulated phases, can be found in Ising systems with competing ferromagnetic and antiferromagnetic interactions (see, *e.g.* Selke 1984). The nature of the phase transition can also vary quite dramatically, with the occurence, in particular cases, of non-universal behaviour, first-order transitions and multicritical points.

The most studied of these systems is the so called axial next-nearest-neighbour Ising (or ANNNI) model. This system was originally introduced by Elliot (1961) as a means of modelling the sinusoidal magnetic structure observed in certain rare earth materials. The ANNNI model exhibits both commensurate and incommensurate modulated phases and an extremely rich phase diagram. Beyond the ferromagnetic nearest-neighbour interactions, the model has antiferromagnetic interactions between next-nearest-neighbour spins in one direction only.

In this chapter we study, in two dimensions, the isotropic version of the ANNNI model. We choose to call the model the "biaxial next-nearest-neighbour Ising" or "BNNNI" model. Our results, presented in this chapter, have been reported in recent publications (Oitmaa *et al.* 1986, 1987).

The model is described by the Hamiltonian ($s_i = \pm 1$)

$$\mathcal{H} = -J\sum_{<ij>} s_i s_j - J'\sum_{[ij]} s_i s_j \qquad (5.1.1)$$

where the summations run over nearest- and next-nearest-neighbour pairs in both axial directions of the square lattice. Without loss of generality, we restrict attention to ferromagnetic nearest-neighbour interaction ($J > 0$).

Depending on the values of the interaction parameters, J and J', the Hamiltonian (5.1.1) has three basic types of ground-state. These are the ferromagnetic (F), antiferromagnetic (AF) and "antiphase" (AP) states, shown in Figure 5.1(a). Three of the degenerate antiphase states are shown in Figure 5.1(b). In each case the (2,2) antiphase state of the ANNNI model is present along both axial directions. The "chessboard" state has an eight-fold degeneracy while the "staircase" configurations are each four-fold degenerate.

The transition from the ferromagnetic ground-state is expected to be of universal $d = 2$ Ising type. For $J' < -1/2\ J$ the nature of the transition, or sequence of transitions from the commensurately modulated chessboard configuration to the high temperature disordered phase is uncertain. The early Monte Carlo work (Hornreich *et al.* 1979, Selke and Fisher, 1980) indicated a transition from the commensurate phase to an incommensurate phase followed by a second transition to the disordered phase, this transition presumably being of Kosterlitz-Thouless type. However, the more recent Monte Carlo study by Landau and Binder (1985) suggests there is no intermediate phase. Rather, the commensurate ordered and the disordered phases are separated by a single first order transition. The series analysis of Oitmaa and Velgakis (1987) tends to support the picture of two transitions, although the evidence is far from conclusive.

To explore the nature of the transitions from the ferromagnetic and anti-phase ground states by a different technique and to hopefully resolve the above conflict, we have applied the finite lattice method. In order to do so, and in particular to make the finite lattice computations feasible, we need to define a suitable transfer matrix.

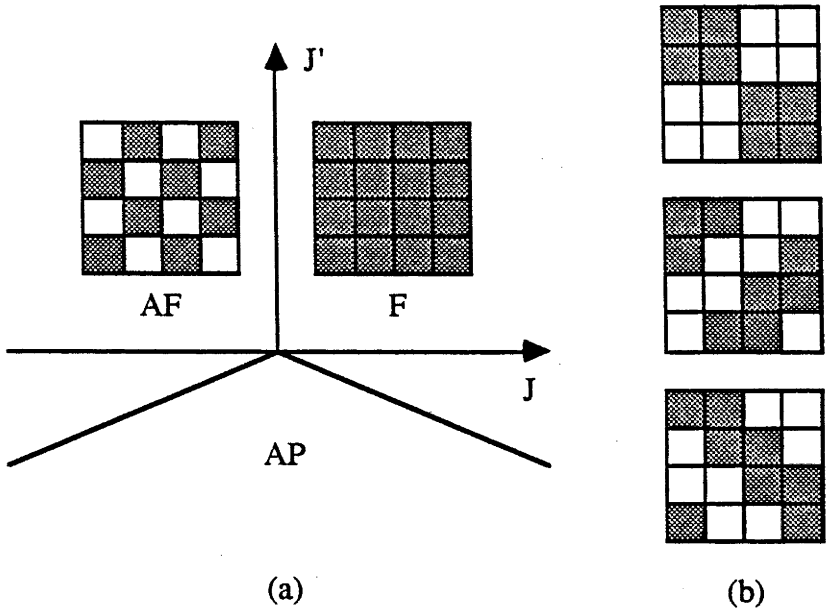

Figure 5.1 (a) Possible ground states of Hamiltonian (5.1.1) as a function of J and J': F-ferromagnetic; AF-antiferromagnetic; AP-antiphase ordered. (b) Three of the possible antiphase ground states. The top figure represents a chessboard configuration while the remaining two figures are each staircase configurations. Here open and shaded squares represent up and down spins.

Transfer Matrix

In defining the transfer matrix, the most convenient choice of strips was suggested by Jaan Oitmaa. As shown in Figure 5.2 we run the transfer matrix in the diagonal direction between successive "zig-zag" rows. This choice has two advantages: firstly only neighbouring rows are coupled by the interactions, and secondly the natural modulation direction lies parallel to the strip direction.

If the spin configurations of two adjacent rows are specified by $\mathbf{s} = (s_1, s_2, \ldots, s_n)$ and $\mathbf{t} = (t_1, t_2, \ldots, t_n)$ then the $2^n \times 2^n$ transfer matrix $\mathbf{T(s,t)}$ can be written

$$\mathbf{T(s,t)} = \varphi_0(\mathbf{s})\, \varphi_1(\mathbf{s,t})\, \varphi_2(\mathbf{s,t}) \tag{5.1.2}$$

where

$$\varphi_0(\mathbf{s}) = \exp\left(K \sum_{i=1}^{n} s_i\, s_{i+1} \right) \tag{5.1.3}$$

$$\varphi_1(\mathbf{s,t}) = \exp\left[K \sum_{i=1}^{n/2} s_{2i} \left(t_{2i-1} + t_{2i+1} \right) \right] \tag{5.1.4}$$

$$\varphi_2(\mathbf{s,t}) = \exp\left[K' \sum_{i=1}^{n} s_i \left(t_{i-2} + t_{i+2} \right) \right] \tag{5.1.5}$$

with the reduced coupling constants $K = \beta J$ and $K' = \beta J'$ where $\beta = (kT)^{-1}$.

Alternatively, each transfer matrix element can be written as a product of Boltzmann weights

$$\mathbf{T(s,t)} = \prod_{i=1}^{n/2} w(s_{2i-1}, s_{2i}, s_{2i+1}, t_{2i-2}, t_{2i-1}, t_{2i}, t_{2i+1}, t_{2i+2}) \tag{5.1.6}$$

where a typical face is shown in Figure 5.3. For the BNNNI model, we define the weight associated with this face as

$$w(a,b,c,d,e,f,g,h) = \exp\left[K(ab+bc+af+cf) + K'(bd+ce+ag+bh) \right] \tag{5.1.7}$$

We impose periodic boundary conditions between the edges of the strip,

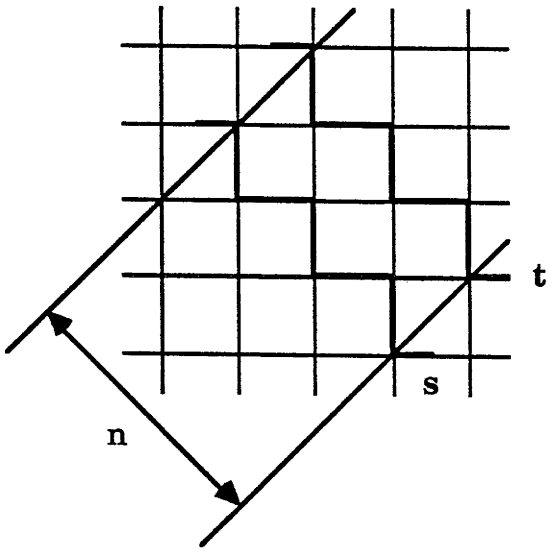

Figure 5.2 Diagonal rows of spins **s** and **t** on the square lattice used to define the transfer matrix **T(s,t)** on a strip of width n.

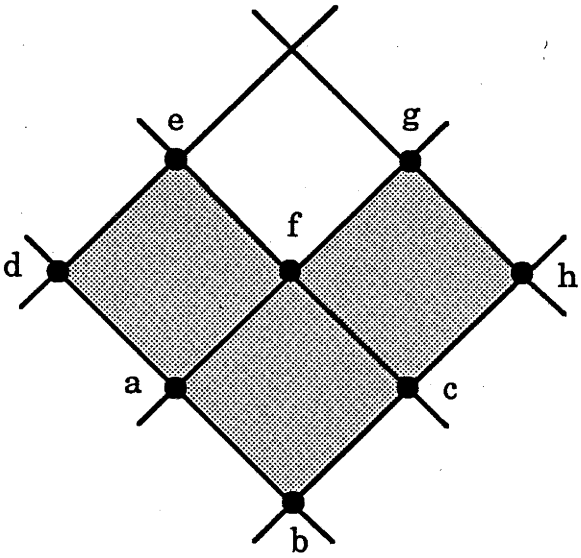

Figure 5.3 Typical face *abcdefgh* on the square lattice, drawn diagonally, corresponding to the Boltzmann weight defined in Eqn. (5.1.7).

requiring that the strip width, n, is even. In addition, for $K' < -1/2\ K$, n must be a multiple of four to incorporate all of the possible antiphase states.

For a specified choice of the reduced coupling constants K and K', we have computed the leading eigenvalues of the transfer matrix by two methods. These methods are described in the following two sections.

5.2 BLOCK DIAGONALIZATION OF THE TRANSFER MATRIX

The computational effort involved in computing the leading eigenvalues of **T** can be reduced by exploiting appropriate symmetries (see, *e.g.* Ree and Chestnut 1966, Runnels and Combs 1966, and Kinzel and Schick 1981). For the BNNNI model, translational symmetries along the "zig-zag" rows enable the transfer matrix to be constructed in block diagonal form. In particular, the two largest blocks are constructed from basis states which are *invariant* under translations along the rows. In general, each block is associated with a given parity which is reflected in the behaviour of the constituent basis states under spin reversal. Under such an operation, basis states with even or odd parity are, respectively, unchanged or change sign.

On the computational side, there are many "tricks-of-the-trade". Jaan Oitmaa wrote the original program and Michael Barber showed me how to speed up the calculations by using bit manipulations and gave me access to his basis state program.

The dominant eigenvalue, λ_0, is contained in the even parity sector, while the odd parity sector contains the first subdominant eigenvalue, λ_1. In Table 5.1 we show the sizes of the matrices involved for increasing values of the strip width n. As can be seen, the storage requirements still become prohibitive; the largest matrix we handled was 356×356 for a strip of width $n = 12$.

Table 5.1 Size of the matrices required to compute the largest eigenvalues, λ_0 and λ_1, of the transfer matrix **T**.

n	λ_0	λ_1
4	6	4
6	12	12
8	38	32
10	104	104
12	356	344
14	1172	1172

5.3 SPARSE FACTORIZATION OF THE TRANSFER MATRIX

The second approach is to factor the full $2^n \times 2^n$ transfer matrix into a product of sparse matrices. Explicit factorizations have been given in the past for the general "Interactions Round a Face" (IRF) Ising model (Baxter 1980). The row to row transfer matrix was considered by Nightingale 1979 while Baxter 1980 introduced a factorization for the diagonal to diagonal transfer matrix. These factorizations have been reviewed by Batchelor (1987). The sparse factors of a more general Ising model containing first, second and third nearest neighbour interactions have also been presented in that paper. The details of this factorization are given in this section.

In Figure 5.4 we show the product of Boltzmann weights in the transfer matrix (5.1.6) between spin sets **s** and **t**. Each of the fundamental units of Figure 5.3 appearing in Figure 5.4 can be thought of as giving rise to a sparse factor of the transfer matrix. To define these factors we develop the diagram shown in Figure 5.5 .

Consider the first wedge shaped face in Figure 5.4, the spins s_1, s_2 and s_3

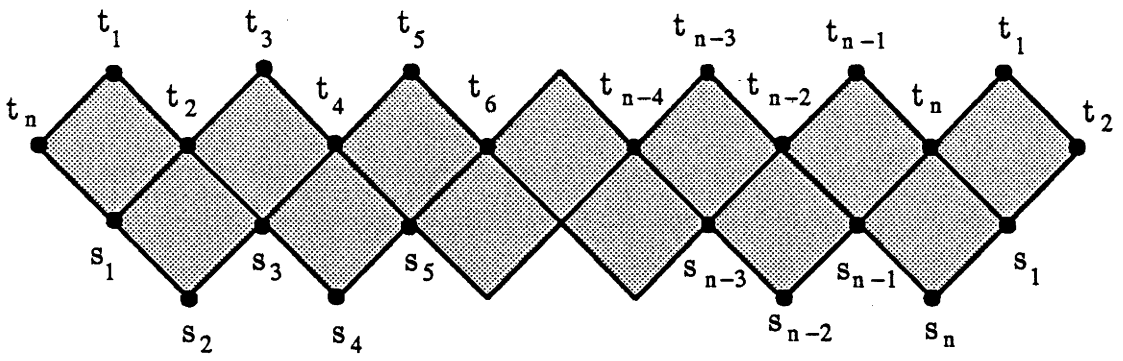

Figure 5.4 Row of Boltzmann weights used in defining the transfer matrix T between spin sets **s** and **t**.

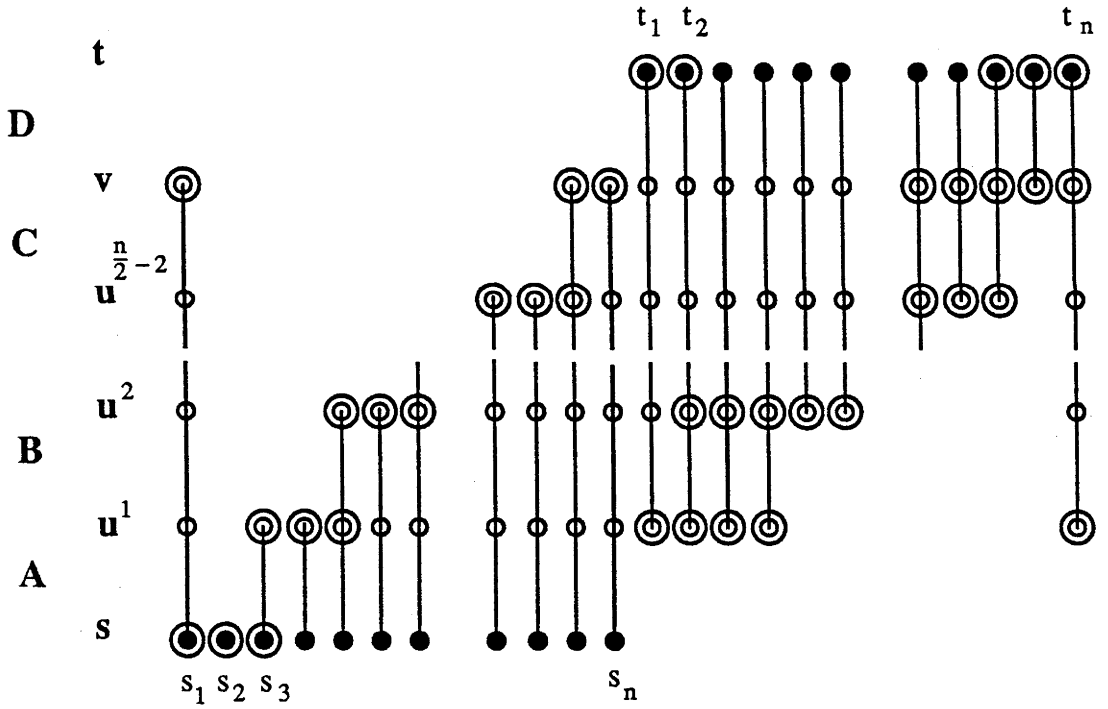

Figure 5.5 Hierarchy of interacting spin sets for the sparse factorization of **T**. Circled spins interact through a Boltzmann weight and solid lines indicate interaction via a delta function. The first weight in Figure 5.4 is represented here between the first three spins in **s** and the last five spins in $\mathbf{u}^1$, defining the factor **A**. In a similar manner, each weight in Figure 5.4 defines a sparse factor, represented in the hierarchy as an interaction between the corresponding circled spins.

interact with spins t_n , t_1, t_2 , t_3 and t_4 ; we indicate this by circling the corresponding spins in Figure 5.5 . For the spins in the set $\mathbf{t}$ we circle the spins directly below in the auxiliary set $\mathbf{u}^1$. This is the first level in the hierarchy. In a similar fashion, the second "wedge" in Figure 5.4 is represented in Figure 5.5 between the levels $\mathbf{u}^1$ and $\mathbf{u}^2$. In general, each fundamental unit in Figure 5.4 corresponds to an interaction between two levels in the hierachy of auxiliary spins.

From Figure 5.5, we are lead to define $n/2 - 1$ sets of spins,

$$\mathbf{u}^p = \{ u_1^p,...,u_{n+4}^p \} \tag{5.3.1}$$

$$\mathbf{v} = \{ v_1,...,v_{n+3} \} \tag{5.3.2}$$

with $p = 1, ..., r$ where $r = n/2 - 2$.

The transfer matrix elements in (5.1.6) can then be written

$$\mathbf{T(s|t)} = \sum_{\{\mathbf{u}^p\},\mathbf{v}} \mathbf{A(s|u}^1\mathbf{)B(u}^1\mathbf{|u}^2\mathbf{)...C(u}^r\mathbf{|v)D(v|t)} \tag{5.3.3}$$

where

$$\mathbf{A(s|u}^1\mathbf{)} = w(s_1,s_2,s_3,u^1_{n+4},u^1_n,u^1_{n+1},u^1_{n+2},u^1_{n+3})\ \delta(s_1,u^1_1)\ \delta(s_3,u^1_2)...\delta(s_n,u^1_{n-1}) \tag{5.3.4}$$

$$\mathbf{B(u}^p\mathbf{|u}^q\mathbf{)} = w(u^p_2,u^p_3,u^p_4,u^q_{n-1},u^q_n,u^q_{n+1},u^q_{n+2},u^q_{n+3})$$
$$\delta(u^p_1,u^q_1)\ \delta(u^p_4,u^q_2)...\delta(u^p_{n+3},u^q_{n+1})\ \delta(u^p_{n+4},u^q_{n+4}) \tag{5.3.5}$$

$$\mathbf{C(u}^r\mathbf{|v)} = w(u^r_2,u^r_3,u^r_4,v_{n-1},v_n,v_{n+1},v_{n+2},v_{n+3})$$
$$\delta(u^r_1,v_1)\ \delta(u^r_4,v_2)...\delta(u^r_{n+3},v_{n+1})\ \delta(u^r_{n+4},v_{n+3}) \tag{5.3.6}$$

$$\mathbf{D(v|t)} = w(v_2,v_3,v_1,t_{n-2},t_{n-1},t_n,t_1,t_2)\ \delta(v_4,t_1)...\delta(v_{n+3},t_n) \tag{5.3.7}$$

in which $q = p + 1$.

The final result, from (5.3.3), is

$$\mathbf{T} = \mathbf{A}\mathbf{B}^{n/2-3}\mathbf{C}\mathbf{D} \ . \tag{5.3.8}$$

This is the required sparse factorization of the transfer matrix.

Structure of A, B, C, D

The structure of these matrices can readily be written down once an ordering of the possible spin configurations is decided upon. We assume the general model possesses spin reversal symmetry, *i.e.* the Boltzmann weights remain unchanged on reversing the signs of the spins. This is true for the BNNNI model and the corresponding weight defined in (5.1.7). We thus order the states according to spin reversal symmetry. This ordering, along with the labelling scheme adopted for the Boltzmanm weights, is outlined in Appendix 5A.

The transfer matrix $\mathbf{T}$ can then be written in block form

$$\mathbf{T} = \begin{bmatrix} \mathbf{T}_1 & \mathbf{T}_2 \\ \mathbf{T}_2 & \mathbf{T}_1 \end{bmatrix} \tag{5.3.9}$$

where both $\mathbf{T}_1$ and $\mathbf{T}_2$ are square matrices of order 2^{n-1}. In this representation the $2^n \times 2^{n+4}$ matrix $\mathbf{A}$, defined in (5.3.4), assumes the form

$$\mathbf{A} = \begin{bmatrix} \mathbf{A}_1 & 0 \\ 0 & \mathbf{A}_1 \end{bmatrix} \tag{5.3.10}$$

with

$$\mathbf{A}_1 = \begin{bmatrix} \mathbf{1}_{n-3} \otimes \mathbf{a}_0 & \mathbf{0} \\ \mathbf{0} & \mathbf{1}_{n-3} \otimes \mathbf{a}_1 \\ \mathbf{1}_{n-3} \otimes \mathbf{a}_2 & \mathbf{0} \\ \mathbf{0} & \mathbf{1}_{n-3} \otimes \mathbf{a}_3 \end{bmatrix} \tag{5.3.11}$$

Here $\mathbf{1}_m$ is the $2^m \times 2^m$ identity matrix, $\mathbf{a}_0$, $\mathbf{a}_1$, $\mathbf{a}_2$ and $\mathbf{a}_3$ are row matrices of

length 32 defined as

$$\mathbf{a}_i = \left[w_{i,0} \; w_{i,16} \; w_{i,1} \; w_{i,17} \; \cdots \; w_{i,15} \; w_{i,31} \right] \tag{5.3.12}$$

The $2^{n+4} \times 2^{n+4}$ matrix $\mathbf{B}$, defined in (5.3.5), assumes the form

$$\mathbf{B} = \begin{bmatrix} \mathbf{B}_1 & 0 \\ 0 & \mathbf{B}_1 \end{bmatrix} \tag{5.3.13}$$

with

$$\mathbf{B}_1 = \begin{bmatrix} \mathbf{1}_{n-4} \otimes \mathbf{b}_0 & \mathbf{0} \\ \mathbf{0} & \mathbf{1}_{n-4} \otimes \mathbf{b}_1 \\ \mathbf{1}_{n-4} \otimes \mathbf{b}_2 & \mathbf{0} \\ \mathbf{0} & \mathbf{1}_{n-4} \otimes \mathbf{b}_3 \\ \mathbf{1}_{n-4} \otimes \mathbf{b}_4 & \mathbf{0} \\ \mathbf{0} & \mathbf{1}_{n-4} \otimes \mathbf{b}_5 \\ \mathbf{1}_{n-4} \otimes \mathbf{b}_6 & \mathbf{0} \\ \mathbf{0} & \mathbf{1}_{n-4} \otimes \mathbf{b}_7 \end{bmatrix} \tag{5.3.14}$$

Each of the 16×64 matrices $\mathbf{b}_i$ are defined as

$$\mathbf{b}_i = \begin{bmatrix} w_{i,0} \; 0 \; w_{i,1} \; 0 \; w_{i,2} \; 0 \; w_{i,3} \; 0 & & 0 \\ 0 \; w_{i,0} \; 0 \; w_{i,1} \; 0 \; w_{i,2} \; 0 \; w_{i,3} & & \\ & \ddots & \\ 0 & & w_{i,28} \; 0 \; w_{i,29} \; 0 \; w_{i,30} \; 0 \; w_{i,31} \; 0 \\ & & 0 \; w_{i,28} \; 0 \; w_{i,29} \; 0 \; w_{i,30} \; 0 \; w_{i,31} \end{bmatrix} \tag{5.3.15}$$

The $2^{n+4} \times 2^{n+3}$ matrix $\mathbf{C}$, defined in (5.3.6), assumes the form

$$\mathbf{C} = \begin{bmatrix} \mathbf{C}_1 & 0 \\ 0 & \mathbf{C}_1 \end{bmatrix} \tag{5.3.16}$$

with

$$\mathbf{C}_1 = \begin{bmatrix} \mathbf{1}_{n-4} \otimes \mathbf{c}_0 & \mathbf{0} \\ \mathbf{0} & \mathbf{1}_{n-4} \otimes \mathbf{c}_1 \\ \mathbf{1}_{n-4} \otimes \mathbf{c}_2 & \mathbf{0} \\ \mathbf{0} & \mathbf{1}_{n-4} \otimes \mathbf{c}_3 \\ \mathbf{1}_{n-4} \otimes \mathbf{c}_4 & \mathbf{0} \\ \mathbf{0} & \mathbf{1}_{n-4} \otimes \mathbf{c}_5 \\ \mathbf{1}_{n-4} \otimes \mathbf{c}_6 & \mathbf{0} \\ \mathbf{0} & \mathbf{1}_{n-4} \otimes \mathbf{c}_7 \end{bmatrix} \tag{5.3.17}$$

where the 16×32 matrices $\mathbf{c}_i$ are defined by

$$\mathbf{c}_i = \begin{bmatrix} w_{i,0} & 0 & w_{i,2} & 0 & & & \mathbf{0} \\ 0 & w_{i,1} & 0 & w_{i,3} & & & \\ & & & & \ddots & & \\ & & & & & & \\ \mathbf{0} & & & & & w_{i,28} \; 0 & w_{i,30} \; 0 \\ & & & & & 0 \; w_{i,29} \; 0 & w_{i,31} \end{bmatrix} \tag{5.3.18}$$

Finally, the $2^{n+3} \times 2^n$ matrix $\mathbf{D}$, defined via equation (5.3.7), can be seen to assume the form

$$\mathbf{D} = \begin{bmatrix} \mathbf{D}_1 & \mathbf{D}_2 \\ \mathbf{D}_2 & \mathbf{D}_1 \end{bmatrix} \tag{5.3.19}$$

in which

$$
\mathbf{D}_1 = \begin{bmatrix}
\mathbf{1}_{n-5} \otimes \mathbf{e}_0 & \mathbf{0} \\
\mathbf{0} & \mathbf{1}_{n-5} \otimes \mathbf{f}_0 \\
\mathbf{0} & \mathbf{0} \\
\mathbf{0} & \mathbf{0} \\
\mathbf{1}_{n-5} \otimes \mathbf{e}_2 & \mathbf{0} \\
\mathbf{0} & \mathbf{1}_{n-5} \otimes \mathbf{f}_2 \\
\mathbf{0} & \mathbf{0} \\
\mathbf{0} & \mathbf{0} \\
\mathbf{1}_{n-5} \otimes \mathbf{e}_4 & \mathbf{0} \\
\mathbf{0} & \mathbf{1}_{n-5} \otimes \mathbf{f}_4 \\
\mathbf{0} & \mathbf{0} \\
\mathbf{0} & \mathbf{0} \\
\mathbf{1}_{n-5} \otimes \mathbf{e}_6 & \mathbf{0} \\
\mathbf{0} & \mathbf{1}_{n-5} \otimes \mathbf{f}_6 \\
\mathbf{0} & \mathbf{0} \\
\mathbf{0} & \mathbf{0}
\end{bmatrix} \qquad (5.3.20)
$$

and

$$
\mathbf{D}_2 = \begin{bmatrix}
0 & & 0 \\
0 & & 0 \\
0 & \mathbf{1}^{A}_{n-5} \otimes \mathbf{g}_0 & \\
\mathbf{1}^{A}_{n-5} \otimes \mathbf{h}_0 & & 0 \\
0 & & 0 \\
0 & & 0 \\
0 & \mathbf{1}^{A}_{n-5} \otimes \mathbf{g}_2 & \\
\mathbf{1}^{A}_{n-5} \otimes \mathbf{h}_2 & & 0 \\
0 & & 0 \\
0 & & 0 \\
0 & \mathbf{1}^{A}_{n-5} \otimes \mathbf{g}_4 & \\
\mathbf{1}^{A}_{n-5} \otimes \mathbf{h}_4 & & 0 \\
0 & & 0 \\
0 & & 0 \\
0 & \mathbf{1}^{A}_{n-5} \otimes \mathbf{g}_6 & \\
\mathbf{1}^{A}_{n-5} \otimes \mathbf{h}_6 & & 0
\end{bmatrix} \tag{5.3.21}
$$

Here we have further defined $\mathbf{1}_m{}^A$ as the $2^m \times 2^m$ matrix in which all elements, except those along the anti-diagonal, vanish. The 8×8 matrices $\mathbf{e}_i$, $\mathbf{f}_i$, $\mathbf{g}_i$ and $\mathbf{h}_i$ are defined as

$$
\mathbf{e}_i = \begin{bmatrix}
w_{i,0} & & & & & & & \\
& w_{i,4} & & & & & 0 & \\
& & \ddots & & & & & \\
& & & \ddots & & & & \\
& & & & \ddots & & & \\
& 0 & & & & w_{i,24} & & \\
& & & & & & w_{i,28}
\end{bmatrix} \tag{5.3.22}
$$

$$\mathbf{f}_i = \begin{bmatrix} w_{i,1} & & & \\ & w_{i,5} & & 0 \\ & & \ddots & \\ & 0 & & w_{i,25} \\ & & & & w_{i,29} \end{bmatrix} \tag{5.3.23}$$

$$\mathbf{g}_i = \begin{bmatrix} & & & w_{i,2} \\ & 0 & & w_{i,6} \\ & & \ddots & \\ & w_{i,26} & & 0 \\ w_{i,30} & & & \end{bmatrix} \tag{5.3.24}$$

$$\mathbf{h}_i = \begin{bmatrix} & & & w_{i,3} \\ & 0 & & w_{i,7} \\ & & \ddots & \\ & w_{i,27} & & 0 \\ w_{i,31} & & & \end{bmatrix} \tag{5.3.25}$$

The matrices $\mathbf{T}_1$ and $\mathbf{T}_2$ in (5.3.9) can also be factored. Inserting the block forms (5.3.10), (5.3.13), (5.3.16) and (5.3.19) into equation (5.3.8) leads to

$$\mathbf{T}_1 = \mathbf{A}_1 \mathbf{B}_1^{n/2-3} \mathbf{C}_1 \mathbf{D}_1 \tag{5.3.26}$$

$$\mathbf{T}_2 = \mathbf{A}_1 \mathbf{B}_1^{n/2-3} \mathbf{C}_1 \mathbf{D}_2 \ . \tag{5.3.27}$$

Leading eigenvalues

The factorizations (5.3.26) and (5.3.27) form the starting point for the leading eigenvalue computations. Following Nightingale (1979), we apply a similarity transformation to the factorization (5.3.8) with

$$\mathbf{U} = \mathbf{U}^{-1} = \frac{1}{\sqrt{2}}\begin{bmatrix} 1 & 1 \\ 1 & -1 \end{bmatrix} . \tag{5.3.28}$$

The new matrix $\hat{\mathbf{T}}$ is given by

$$\hat{\mathbf{T}} = \mathbf{U}\,\mathbf{T}\,\mathbf{U} = \begin{bmatrix} \mathbf{T}^{+} & \mathbf{0} \\ \mathbf{0} & \mathbf{T}^{-} \end{bmatrix} \tag{5.3.29}$$

where

$$\mathbf{T}^{\pm} = \mathbf{T}_1 \pm \mathbf{T}_2 . \tag{5.3.30}$$

This finally leads to the factorization

$$\mathbf{T}^{\pm} = \mathbf{A}_1 \mathbf{B}_1^{n/2-3} \mathbf{C}_1 \left(\mathbf{D}_1 \pm \mathbf{D}_2\right) . \tag{5.3.31}$$

As for the sparse factorization of the IRF model (Nightingale 1979), we find that the largest eigenvalue, λ_0, is the dominant eigenvalue of the matrix $\mathbf{T}^{+}$. Similarly, the next-largest eigenvalue, λ_1, is the leading eigenvalue of $\mathbf{T}^{-}$.

Nightingale has emphasized the significant reduction obtainable in the number of elementary arithmetic operations required in eigenvalue computations by using sparse matrix representations. To see this, consider the direct calculation of $\mathbf{T}_1\varphi$ from the vector φ. This requires $2^{n-1} \times 2^{n-1}$ multiplications. When the factorization (5.3.30) is used (by successively generating $\mathbf{D}_1\varphi$, $\mathbf{C}_1\mathbf{D}_1\varphi$, *etc.*), the number of multiplications needed can be reduced to that of the number of non-zero matrix elements appearing in the sparse factors. From equations (5.3.11), (5.3.14), (5.3.17), (5.3.20) and (5.3.21) this number is seen to be $(32n - 124) \times 2^{n-1}$.

5.4 NATURE OF THE LEADING EIGENVALUES

The transfer matrix $\mathbf{T}$ is in general non-symmetric. To find the dominant eigenvalues, we have used the power algorithm as modified by Faddeev and Fadeeva (1963) to allow for the dominant eigenvalue being a complex conjugate pair. A brief outline of the algorithm is given in Appendix 5B.

The nature of the leading eigenvalues $\lambda_0, \lambda_1, \lambda_2$ ($\lambda_0 > |\lambda_1| \geq |\lambda_2| ...$) is shown schematically in Figure 5.6 as a function of the couplings K and K'. We note four points:

(i) the dominant eigenvalue λ_0 is everywhere real, positive, and non-degenerate.

(ii) for a given K' all eigenvalues are symmetric in K. For λ_0 this reflects the fact that the free energy is an even function of K; for λ_1 it is a consequence of the diagonal direction of the strip - the diagonal correlations are unchanged on changing the sign of K.

(iii) for $K' > 0$, and for part of the region $K' < 0$, the subdominant eigenvalue λ_1 is real, positive and non-degenerate. In the remainder of the region $K' < 0$, separated from the previous part by a "disorder line", the subdominant eigenvalue is a complex conjugate pair with negative real part.

(iv) along the axis $K = 0$, the dominant eigenvalue is symmetric in K' and the subdominant eigenvalue is real and doubly degenerate. In this limit the model consists of four independent, interpenetrating, lattices with nearest neighbour coupling K'.

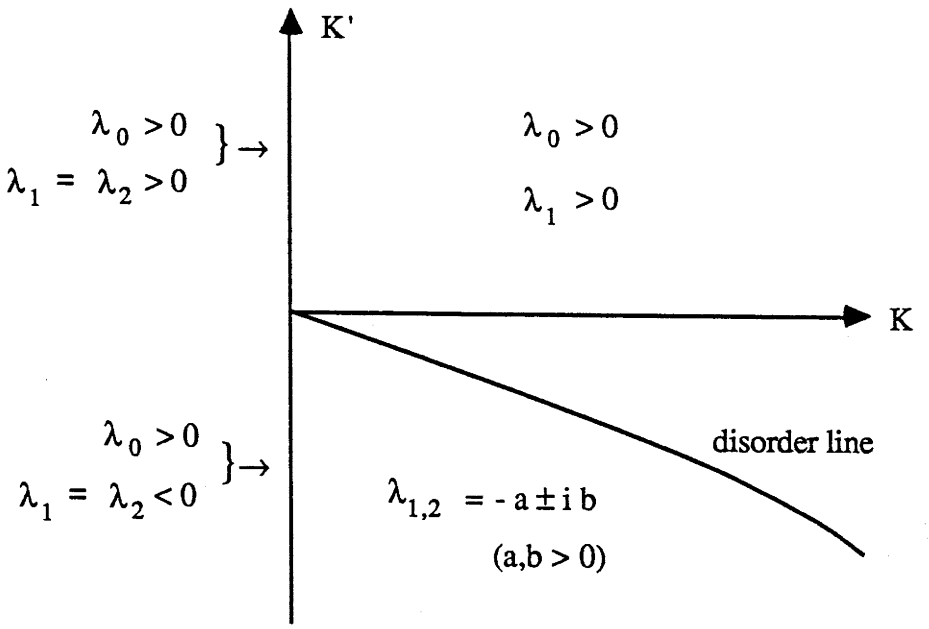

Figure 5.6 Schematic illustration of the nature of the leading eigenvalues of the transfer matrix as a function of the reduced couplings K and K'.

5.5 THE FINITE LATTICE METHOD

As mentioned in the Section 1.1, the method of "phenomenological renormalization" is based on computation from the appropriate transfer matrices, of the correlation length for a sequence of $n \times \infty$ strips, followed by a scaling analysis. This approach has proven to be highly successful for a variety of two-dimensional systems (see, *e.g.* Nightingale 1982 and Barber 1983a). The inverse correlation length, which describes the decay of correlations in the infinite direction of the strip, is obtained as

$$\xi_n^{-1} = ln\left(\lambda_0/|\lambda_1|\right) \qquad (5.5.1)$$

and the finite-size scaling assumption (Nightingale 1976, Barber 1983a) is that, at

criticality, this scales inversely with the width of the strip. Thus the equation

$$n\,\xi_n^{-1}(K,K') = n'\,\xi_{n'}^{-1}(K,K') \tag{5.5.2}$$

gives, for a sequence of values n , n', a sequence of estimates of the critical point.

More generally, to allow for the possibility of anisotropic scaling, one considers the quantities (Domany and Kinzel 1981, Barber 1983a)

$$Y_{n,n'} = \frac{ln\left(\xi_n / \xi_{n'}\right)}{ln\left(n/n'\right)} \tag{5.5.3}$$

and obtains estimates of the critical point from intersections of successive Y's. In regions where the correlations are oscillatory, the scaling behaviour of the modulation wavevector can also yield useful information (Duxbury *et al.* 1984). The appropriate quantity is

$$Z_{n,n'} = \frac{ln\left(\delta q_{n'} / \delta q_n\right)}{ln\left(n/n'\right)} \tag{5.5.4}$$

with

$$\delta q_n = \frac{1}{2\pi}\tan^{-1}\left[\frac{\Im m(\lambda_1)}{\Re e(\lambda_1)}\right] - q_0 \tag{5.5.5}$$

and where q_0 is the characteristic wavevector of the ground-state.

Estimates of the correlation length exponent ν can be obtained from finite lattice estimates of the quantities

$$\omega_n \equiv \frac{\partial \xi_n^{-1}}{\partial T} \tag{5.5.6}$$

since standard scaling arguments (Barber 1983a) imply that (recall Eqn. (1.1.8))

$$\frac{ln\left[n\omega_n(T_c)/n'\omega_{n'}(T_c)\right]}{ln\left(n/n'\right)} \to \nu^{-1} \quad \text{as} \quad n \to \infty \ . \tag{5.5.7}$$

We now proceed to describe and discuss our results.

5.6 THE FERROMAGNETIC REGION

In the ferromagnetic region ($\alpha > -0.5$) a single Ising-like transition is expected and this is borne out by our results. In Figure 5.7(a) we show a plot of the quantities $Y_{n,n-2}$ (Eqn. (5.5.3)) versus temperature, for the case $\alpha = -0.2$. The curves clearly show the expected scaling behaviour with a common crossover point at $kT/J \approx 1.41$. Furthermore, the scaling appears to be isotropic, so that the phase boundary can be determined by solving the equation

$$n\,\xi_n^{-1}(K,\alpha K) = (n-2)\,\xi_{n-2}^{-1}(K,\alpha K) \qquad (5.6.1)$$

numerically, for a fixed α. The sequences of finite lattice estimates obtained in this way, for $\alpha = 0.5, 0.0, -0.2, -0.4,$ are shown in Table 5.2(a). In all cases, the estimates for $n > 8$ appear to be converging at a rate close to n^{-3} in accord with the expected convergence rate for an Ising system (Barber 1985). The extrapolated value listed in the table was obtained by fitting estimates from two successive lattice pairs to the form $a + bn^{-3}$; the error bar being a (subjective) indication of the reliability of this extrapolation.

The critical temperatures obtained in this way are in agreement with the Monte Carlo results of Landau and Binder (1985) and with the series estimates obtained by Oitmaa and Velgakis (1987). However, the transfer matrix method used here is able to handle the region near the multiphase point $\alpha = -0.5$, where the series method is unsuccessful. The critical line is shown in Figure 5.8. We also show the approximate phase boundary obtained by Hornreich *et al.* (1979), using the method of Müller-Hartmann and Zittartz (1977), which gives

$$kT/J = \frac{2(1+2\alpha)}{ln\left(1+\sqrt{2}\right)} \qquad (5.6.2)$$

Estimates of the correlation length exponent ν obtained from the finite lattice estimators (5.5.7) are shown in Table 5.2(b), and are clearly consistent with a limiting value of $\nu = 1$, confirming the universal nature of the transition throughout the

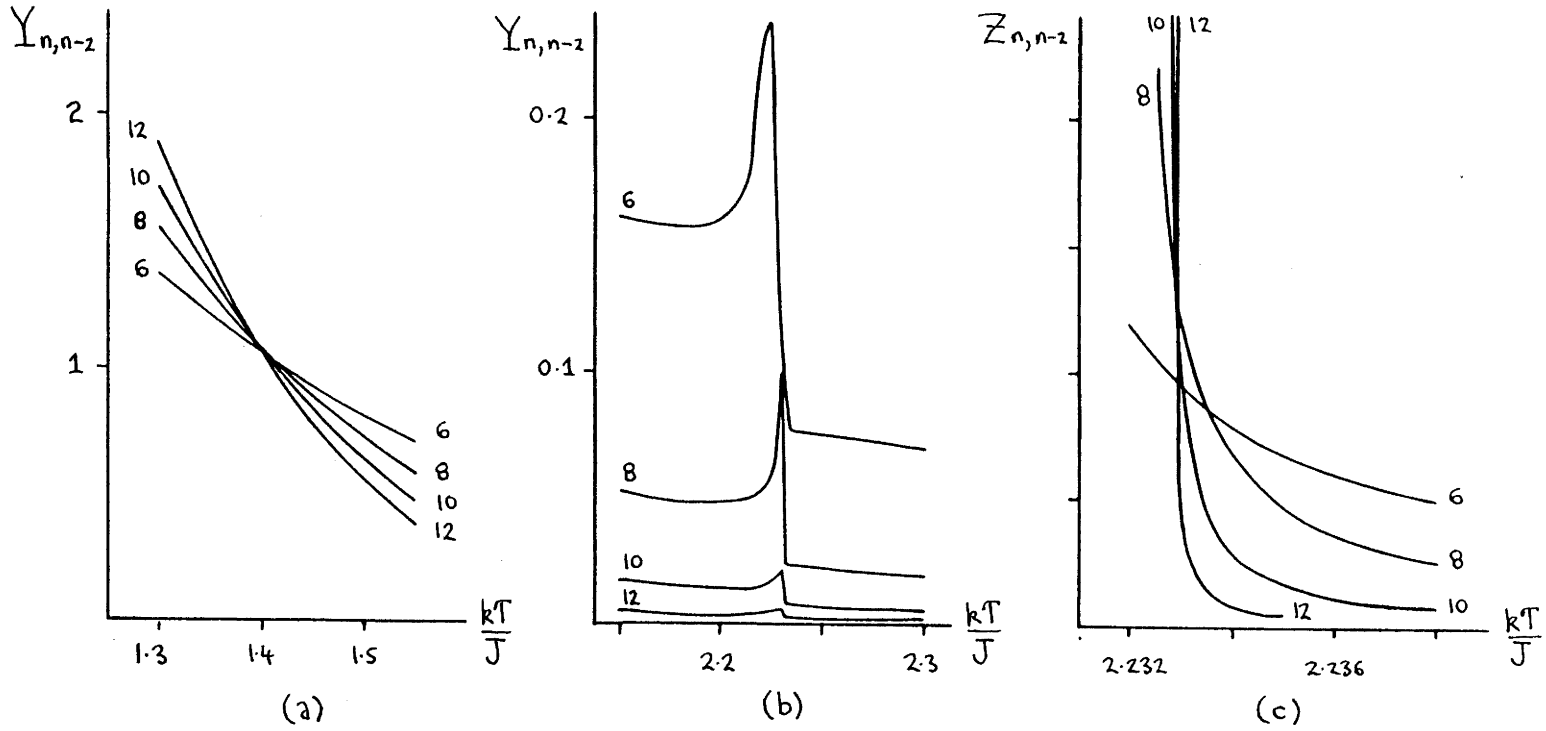

Figure 5.7 ·The scaling estimators $Y_{n,n-2}$ and $Z_{n,n-2}$ as functions of temperature for $\alpha = -0.2$ for the indicated values of n. (a) The correlation length estimator $Y_{n,n-2}$. Successive curves cross at the finite-lattice estimates of the transition temperature. (b) Peaks in $Y_{n,n-2}$ at higher temperature indicating the presence of a disorder point. (c) The wavevector estimator $Z_{n,n-2}$. Successive curves cross at the finite-lattice estimates of the disorder temperature.

Table 5.2

(a) Estimates of the critical temperature kT_c/J, obtained from the finite lattice method.

n/n'	α : 0.5	0.0	− 0.2	− 0.4
6/4	4.06014	2.23833	1.42477	0.51466
8/6	4.05958	2.25696	1.42013	0.50514
10/8	4.09361	2.26319	1.41619	0.49852
12/10	4.10340	2.26583	1.41398	0.49467
14/12	4.10967	2.26712	1.41275	0.49237
extrapolation	4.120 ± 0.0006	2.2691 ± 0.0002	1.4105 ± 0.0005	0.488 ± 0.001
		exact = 2.26918...		

(b) Estimates of the critical exponent ν

n/n'	α : 0.5	0.0	− 0.2	− 0.4
6/4	0.9908	1.039	1.107	1.575
8/6	0.9952	1.021	1.048	1.229
10/8	0.9968	1.013	1.024	1.096
12/10	0.9974	1.009	1.013	1.041
14/12	0.9986	1.007	1.007	1.014

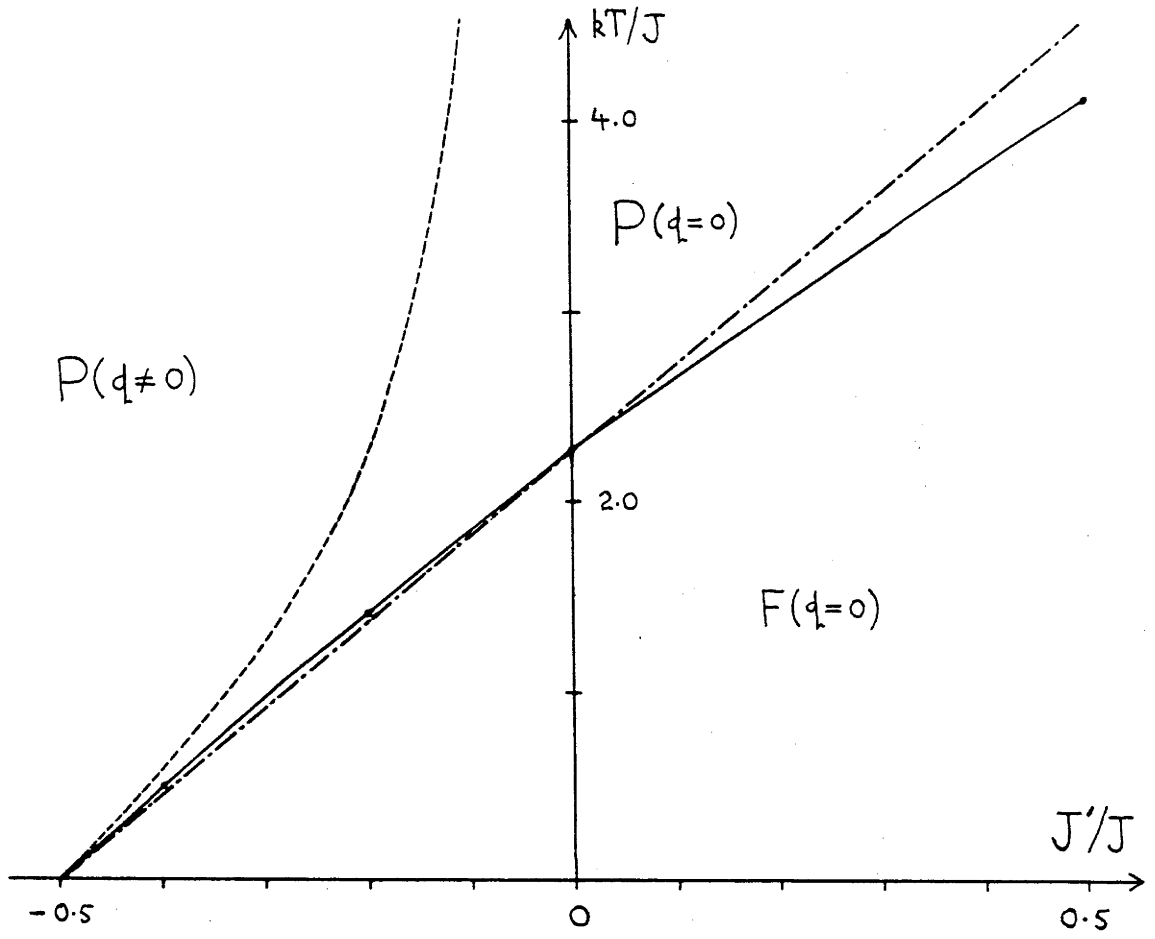

Figure 5.8 The ferromagnetic phase boundary of the BNNNI model. Curves: (———) transition temperatures as determined from finite width strips, (– – – –) the disorder line (see text) and (—·—·—) the approximation (Eqn. (5.6.2) of Hornreich *et al.* (1979).

ferromagnetic region.

Most systems with competing interactions exhibit a disorder line (Stephenson 1970), which separates regions of monotonically decaying and oscillatory correlations in the paramagnetic phase. In the present case we have used two related methods to locate the disorder line. The crossover from monotonic to oscillatory decay of correlations corresponds to the merging of the second and third largest eigenvalues of the transfer matrix into a complex conjugate pair. Thus, for a given value of α, the disorder point corresponds to the K value at which these eigenvalues merge. This gives a rapidly converging sequence of estimates with increasing strip width.

The location of the disorder line can also be obtained from the quantities $Y_{n,n'}$ and $Z_{n,n'}$ defined in the previous section. In this we follow the work of Beale *et al.* (1985), who used this approach to locate the disorder line for the two-dimensional ANNNI model. For given α, the disorder line is expected to lead to a sharp peak in the $Y_{n,n-2}$ at the disorder temperature, and this is clearly seen in Figure 5.7(b) for the case $\alpha = -0.2$. However, the height of the peak decreases rapidly for increasing strip width, and it is more convenient to examine the quantities $Z_{n,n-2}$. These are shown in Figure 5.7(c) and are seen to scale at the disorder temperature. The location of the disorder line is shown in Figure 5.8.

Conformal Invariance

To conclude this section we briefly discuss the applicability of consequences of conformal invariance to the BNNNI model along the ferromagnetic critical line. Isotropic, translationally invariant systems with short-range interactions are believed to be conformally invariant at criticality. In two dimensions, this has a number of significant implications (for a recent review see Cardy 1987). In particular, for a transfer matrix of a strip of finite width n, conformal invariance predicts (Cardy 1984a)

$$\text{i)} \qquad \varepsilon_0 \equiv \lim_{n\to\infty} n\,\xi_n^{-1} = \frac{a_t}{a_x}\,\pi\eta \qquad (5.6.3)$$

and (Blöte *et al.* 1986, Affleck 1986)

$$\text{ii)} \quad \delta_0 \equiv \lim_{n\to\infty} \left(\beta f_\infty - \beta f_n\right) n^2 = \frac{a_t}{a_x}\,\frac{\pi c}{6} \tag{5.6.4}$$

where

$$\beta f_n = -\frac{1}{n} \ln \lambda_0 \tag{5.6.5}$$

is the free energy per site. In (5.6.3) and (5.6.4), a_t and a_x are, respectively, the units of length along and perpendicular to the strip direction and c is the conformal anomaly.

In the present case, we have $a_t = \sqrt{2}$ and $a_x = 1/\sqrt{2}$ from the orientation of the strip (recall Fig. 5.2). Hence, on assuming that the ferromagnetic transition of the BNNNI model is Ising-like, so that $c = 1/2$ and $\eta = 1/4$ we obtain the predictions

$$\delta_0 = \frac{\pi}{6} \quad \text{and} \quad \varepsilon_0 = \frac{\pi}{2} \,. \tag{5.6.6}$$

Finite lattice estimates of δ_0 were obtained from successive strips using a simple two-point fit to $-\beta f_n$ as a linear function of $1/n^2$. The resulting estimates versus $1/n$ are shown in Figure 5.9(a) for $\alpha = 0.5,\ 0.0,\ -0.2$ and -0.4, where in each case we have used the corresponding (central) estimate of the bulk critical temperature shown in Table 5.2(a). These estimates are not particularly sensitive to variations of the temperature within the errors quoted in Table 5.2(a). Clearly, the trend with increasing n is consistent with the expected limit for all α, although for $\alpha = -0.4$ the approach to ths limit is evidently quite slow.

The corresponding trend in estimates of the quantities $n\xi_n^{-1}$ at the (estimated) bulk critical temperatures results in either over- or under-estimation of the expected limit for ε_0. This reflects on over- or under- estimation of the bulk critical temperature and clearly *assuming* (5.6.3) could be used as a means of sharpening our estimates of T_c. A better test of (5.6.3) is obtained if $n\xi_n^{-1}$ is computed at the $n/(n-2)$ estimate of the critical temperature. These quantities are plotted against $1/n$ in Figure 5.9(b) and illustrate a clear trend towards the expected universal limit.

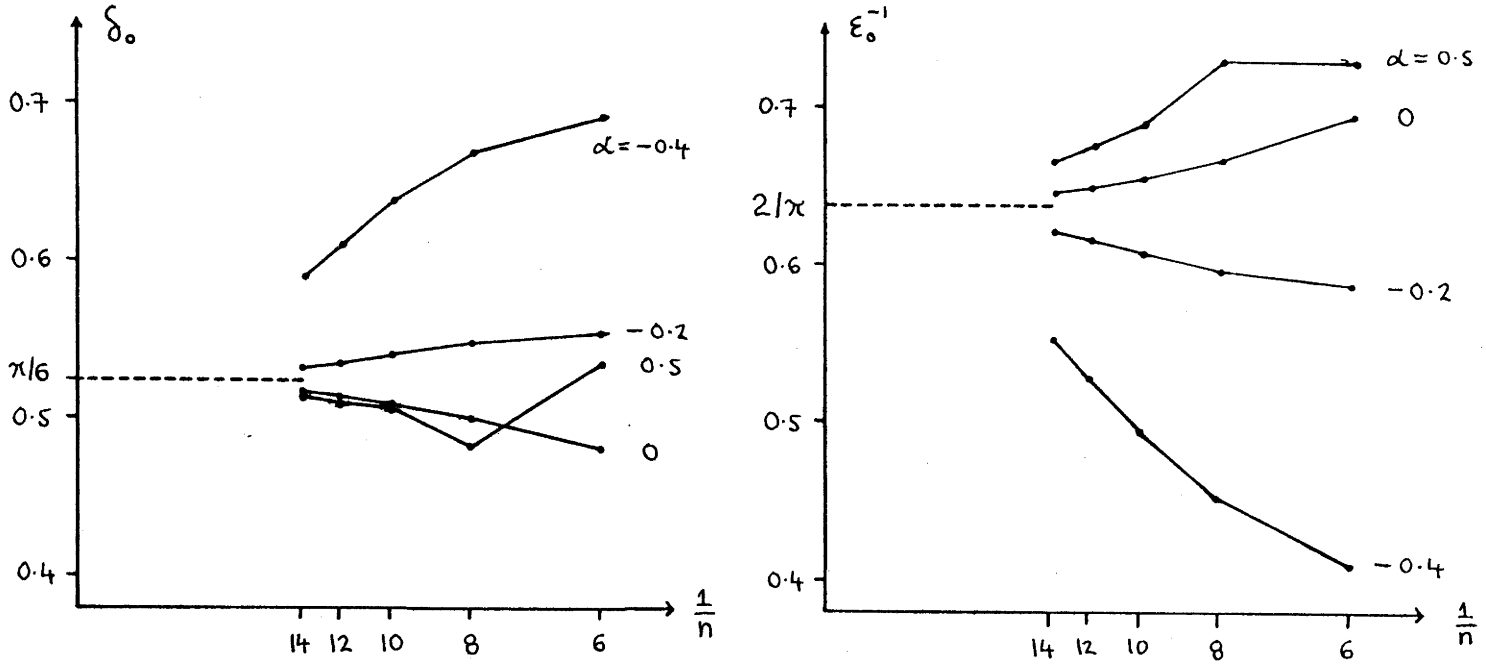

Figure 5.9 Plots of (a) $(\beta f_\infty - \beta f_n)n^2$ and (b) ξ_n/n against 1/n for the indicated values of α. The expected (universal) limits predicted by conformal invariance are shown by the broken line.

5.7 THE ANTIPHASE REGION

The more interesting region of the phase diagram for the BNNNI model is the region $\alpha < -0.5$, in which the ground-state is the chessboard or staircase configuration (Fig. 5.1(b)). We wish to distinguish between the two possible scenarios:

(i) two transitions with an intermediate incommensurately modulated phase (Selke and Fisher 1980)

(ii) a single first order transition (Landau and Binder 1985).

A finite lattice method, using the quantities Y and Z (Eqs. (5.5.3) and (5.5.4)), should in principle be able to locate and distinguish between commensurate, incommensurate, and paramagnetic phases.

For the chiral clock model (Duxbury *et al.* 1984) and the ANNNI model (Beale *et al.* 1985) it is found that Y does not scale at the commensurate to incommensurate phase boundary, but the quantity Z did. However, Y did scale at the higher temperature, incommensurate to paramagnetic phase boundary. Thus the presence of two transitions, separated by an incommensurate phase, is indicated by the scaling of Y and Z at two distinct temperatures.

As indicated in the Introduction to this section, in order to accommodate all of the possible antiphase states for the BNNNI model it is necessary to choose strips whose width is a multiple of four. In Figures 5.10 and 5.11 we show plots of $Y_{n,n-4}$ and $Z_{n,n-4}$ as functions of temperature, for the two cases $\alpha = -0.75$ and $\alpha = -1.0$. We also show in these figures the Monte Carlo (Landau and Binder 1985) and series (Oitmaa and Velgakis 1987) estimates of the transition temperature. In both cases the Y functions show behaviour quite different from the ferromagnetic region (*cf.* Fig. 5.7(a)). There is some indication of scaling at a temperature slightly below the Monte Carlo estimate, followed by a loop and then a rapid decrease in Y. From the $n = 8$ curve it is tempting to conclude that the Y function is developing a flat region of finite extent, indicative of an incommensurate phase with an algebraic decay of correlations. However, the larger n results destroy this viewpoint and, surprisingly, the loop appears

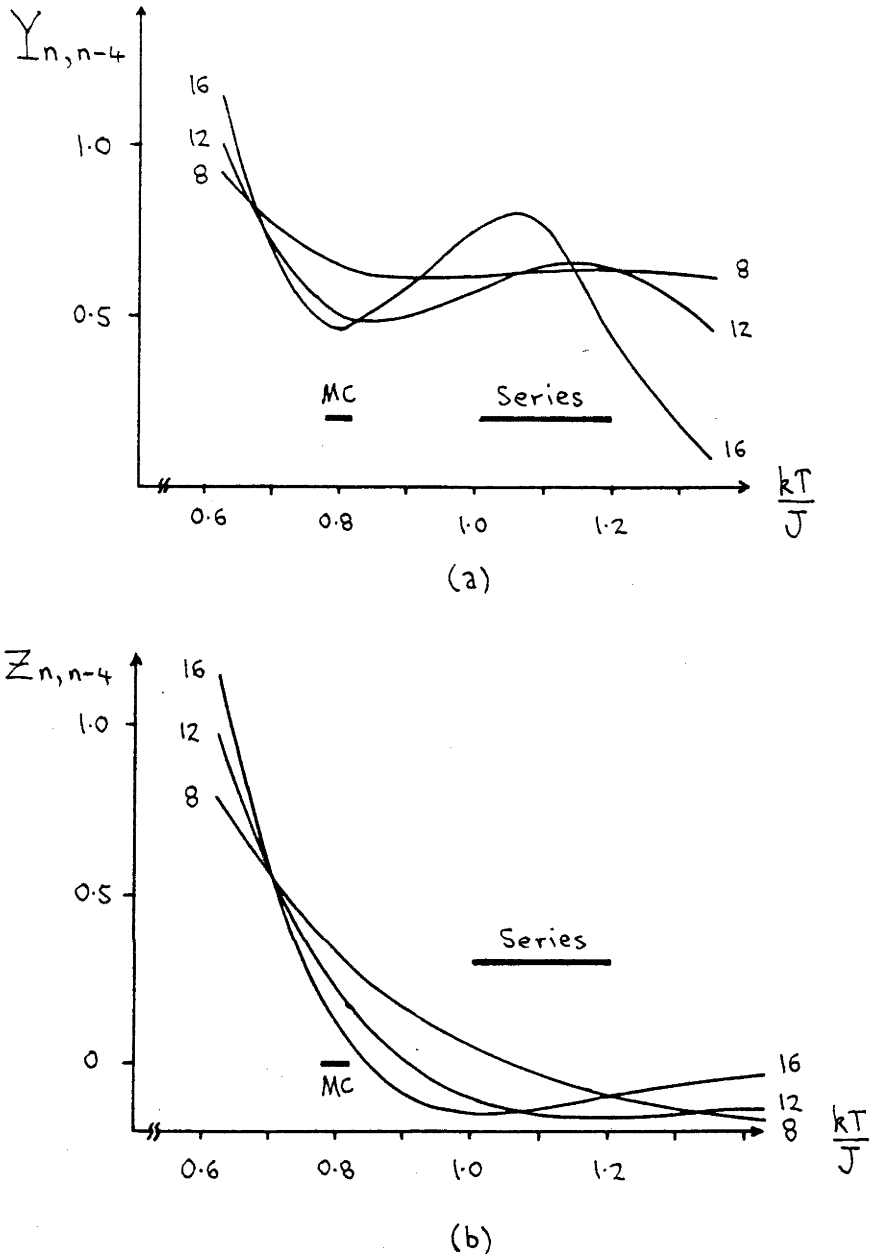

Figure 5.10 The scaling estimators, $Y_{n,n-4}$ and $Z_{n,n-4}$, as functions of temperature for $\alpha = -0.75$. (a) The correlation length estimator $Y_{n,n-4}$. (b) The wavevector estimator $Z_{n,n-4}$. Also shown are the corresponding Monte Carlo and series estimates of the transition temperature.

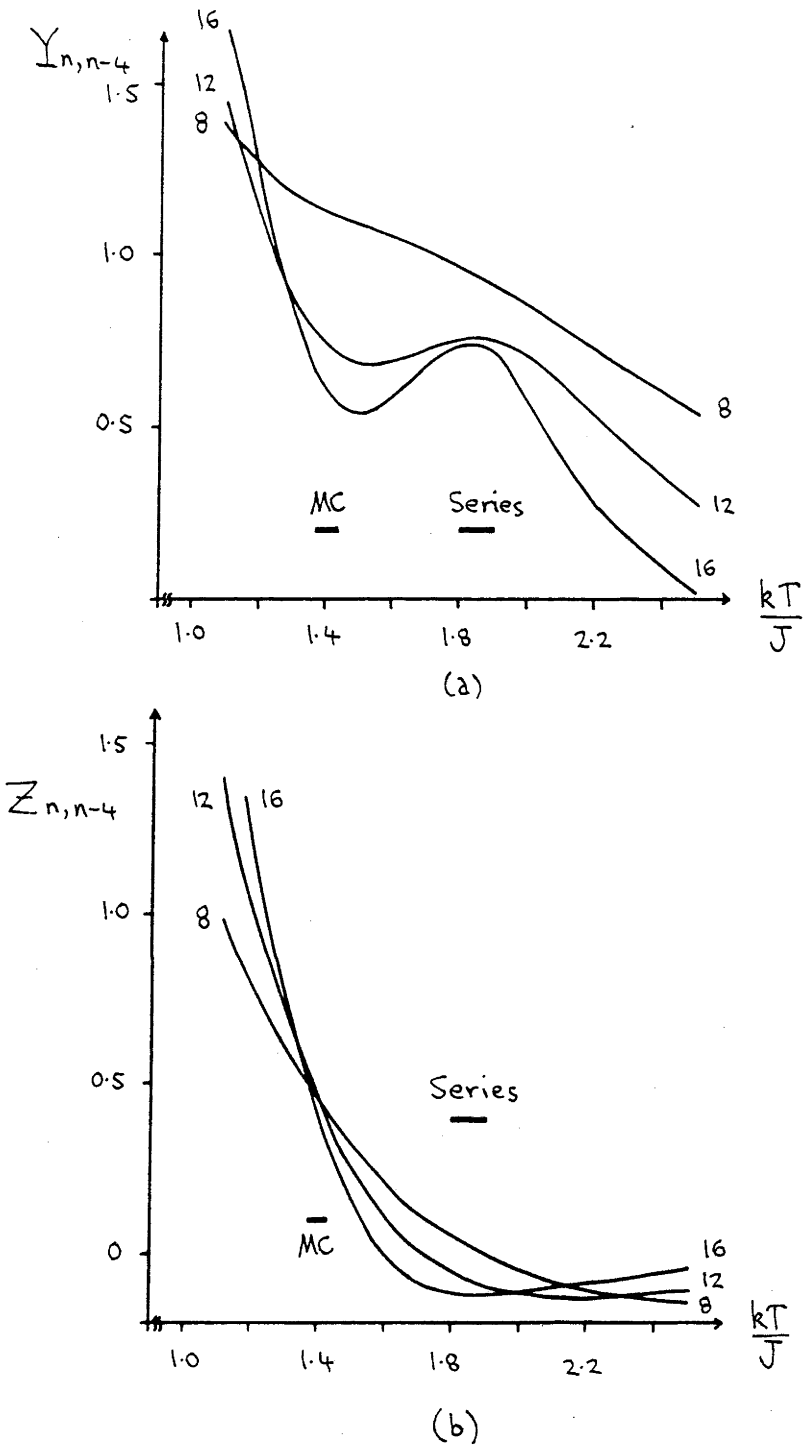

Figure 5.11 Scaling estimators as a function of temperature for $\alpha = -1.0$. (a) The correlation length estimator $Y_{n,n-4}$. (b) The wavevector estimator $Z_{n,n-4}$. Also shown are the corresponding Monte Carlo and series estimates of the transition temperature.

to become more pronounced for larger n. The peak in Y occurs near the series estimate of a transition temperature.

There is some ambiguity in the definition of the Z functions in the antiphase region. The chessboard ground-state and one of the staircase structures clearly have a modulation wavelength of 2 "rows", and hence a wavevector of $q_0 = 1/2$. However, the other staircase structure is fully periodic in the direction of the strip and hence would have $q_0 = 0$. Since the chessboard phase is dominant at finite temperatures, because of higher entropy, we use $q_0 = 1/2$ in defining the Z functions. For $\alpha = -0.75$ the Z show a consistent scaling behaviour at a temperature slightly below the Monte Carlo estimate, as shown in Figure 5.10(b). Figure 5.11(b) shows Z for $\alpha = -1.0$, and again there is an indication of scaling behaviour near the Monte Carlo estimate. In neither case is there any indication of scaling near the series estimate.

As the antiferromagnetic interactions become stronger the behaviour of the Y functions becomes more like the standard Ising case. In Figure 5.12 we show these functions for $\alpha = -2.0$. The curves for $n = 8$ and 12 suggest a single conventional (continuous) transition. However, the curve for $n = 16$ indicates the beginning of possible structures similar to that seen for larger values of α.

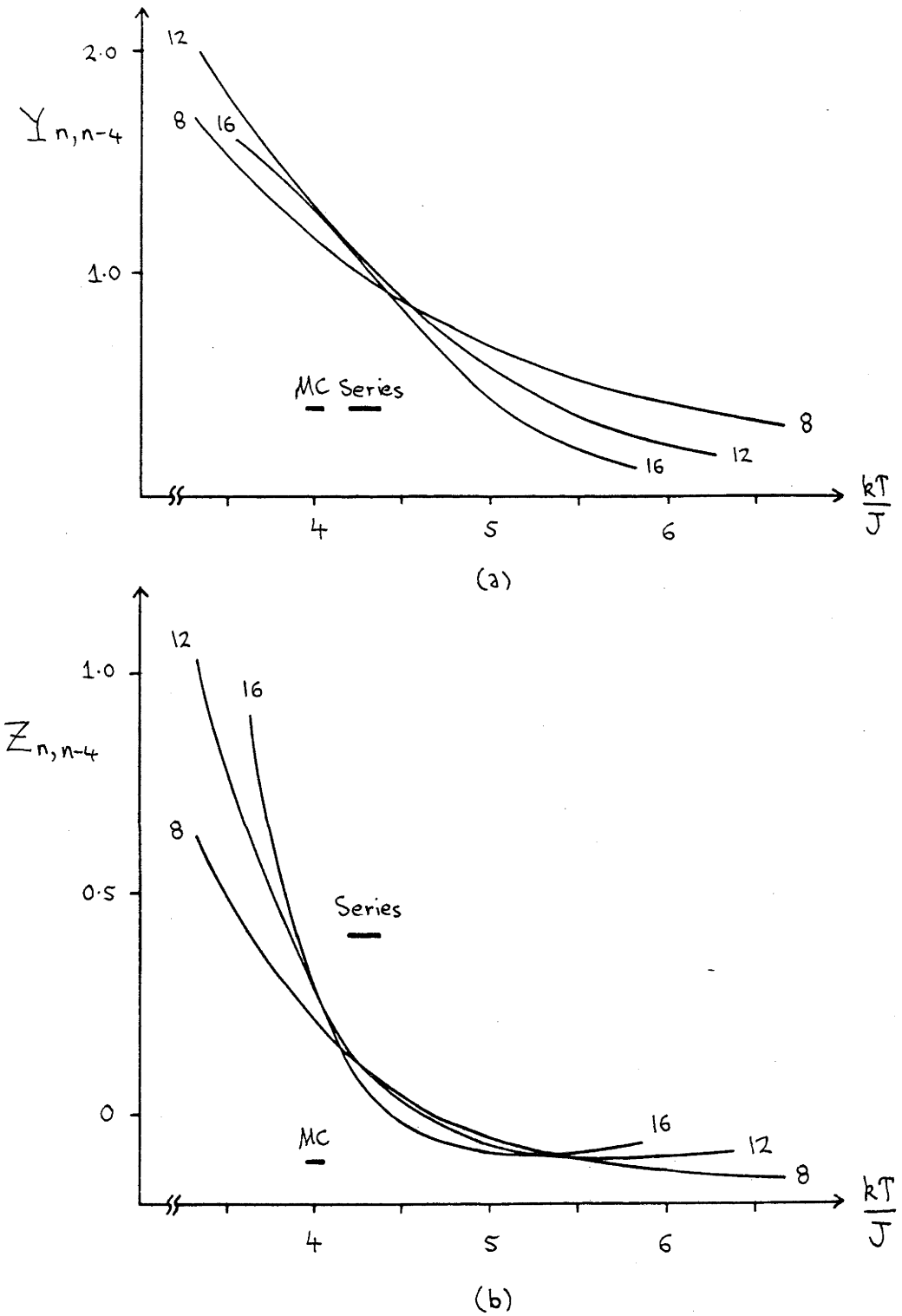

Figure 5.12 Scaling estimators as a function of temperature for $\alpha = -2.0$. (a) The correlation length estimator $Y_{n,n-4}$. (b) The wavevector estimator $Z_{n,n-4}$. Also shown are the corresponding Monte Carlo and series estimates of the transition temperature.

5.8 CONCLUSION

In this chapter, we have carried out extensive numerical studies of the biaxial next-nearest-neighbour Ising model using the well known technique of transfer matrix calculations for finite width strips and scaling arguments. The novel feature of our approach, namely the choice of strips in the diagonal direction with zig-zag rows, allows us to treat quite large strips with widths up to $n = 16$.

Despite the large amount of data, our analysis is inconclusive, at least in the most interesting part of the phase diagram. In the ferromagnetic region, we locate the phase boundary with an accuracy at least equal to the series results of Oitmaa and Velgakis (1987) and obtain clear evidence that the transition is an Ising transition. However, in the antiphase region we are unable to decide in favour of two successive transitions or a single first order transition. Interestingly, we do find distinctive structures in finite lattice estimators at two different temperatures, or rather over an extended temperature range. This would explain why the series and Monte Carlo results find apparent transitions at two distinct temperatures.

Clearly the true behaviour is quite subtle and a final resolution is not likely to be easy.

Appendix 5A *Odering of states and labelling of weights*

To order the states we make use of the one-to-one correspondence between an N-dimensional spin configuration, $\mathbf{s} = \{ s_1, \ldots , s_N \}$, and the integers 0, 1, ... , 2^{N-1}. Define (recall that $s_i = \pm 1$)

$$\begin{aligned} n_1 &= \frac{1}{2}\left(1 - s_N\right) \\ n_2 &= \frac{1}{2}\left(1 - s_{N-1}\right) \\ &\vdots \\ n_N &= \frac{1}{2}\left(1 - s_1\right) \end{aligned} \qquad (5A.1)$$

with

$$p(\mathbf{s}) = \sum_{i=1}^{N} n_i \, 2^{i-1} \quad . \qquad (5A.2)$$

Order the states according to spin reversal:

$$q(\mathbf{s}) = \begin{cases} p(\mathbf{s}) & \text{if } p(\mathbf{s}) \le 2^{N-1} - 1 \\ p(-\mathbf{s}) + 2^{N-1} & \text{otherwise} \end{cases} \qquad (5A.3)$$

For example, for $N = 2$ we order the states as $++, +-, --, -+$:

s	**p(s)**	**q(s)**
$++$	0	0
$+-$	1	1
$--$	3	2
$-+$	2	3

We label the $2^8 = 256$ Boltzmann weights as

$$w_{r,s} = w\left(s_i, s_j, s_k, s_l, s_m, s_n, s_o, s_p \right) \qquad (5A.4)$$

with

$$\begin{aligned} r &= p\left(s_i, s_j, s_k\right) \\ s &= p\left(s_l, s_m, s_n, s_o, s_p\right) . \end{aligned} \tag{5A.5}$$

When spin reversal symmetry is allowed we have for example, $w_{0,0} = w_{7,31}$, though this reduction in notation has not been used explicitly in writing down the structure of the factors **A**, **B**, **C** and **D**.

Appendix 5B *Power method for complex conjugate dominant eigenvalues*

Let **A** be a real non-symmetric $n \times n$ matrix with eigenvalues $\lambda_1, \ldots, \lambda_n$ ordered as

$$|\lambda_1| = |\lambda_2| > |\lambda_3| \geq \ldots \geq |\lambda_n| \tag{5B.1}$$

with $\lambda_1 = \rho \exp(i\theta)$ and $\lambda_2 = \rho \exp(-i\theta)$. Define the kth iterate ($k \geq 1$) of an initial n-dimensional vector $\mathbf{u}^{(0)}$ with $\| \mathbf{u}^{(0)} \| = 1$ (in *e.g.* the ℓ_1 norm) by

$$\mathbf{v}^{(k)} = \mathbf{A}\,\mathbf{u}^{(k-1)} \tag{5B.2}$$

where $\mathbf{u}^{(k)} = \mathbf{v}^{(k)}/\varepsilon_k$ with $\varepsilon_k = \| \mathbf{v}^{(k)} \|$. The modulus ρ and argument θ are determined from any of the real components in the sequence (5B.2) by forming

$$c_i^{(k)} = \left(v_{i.}^{(k)}\right)^2 - \varepsilon_k\, u_i^{(k-1)}\, v_i^{(k+1)} \tag{5B.3}$$

$$p_i^{(k)} = \varepsilon_k \sqrt{c_i^{(k+1)}/c_i^{(k)}} \tag{5B.4}$$

$$\mu_i^{(k)} = \left(p_i^{(k)}\, u_i^{(k-1)} + \varepsilon_k\, v_i^{(k+1)}/p_i^{(k)}\right) / 2v_i^{(k)} \quad ; \tag{5B.5}$$

for then we can show

$$p_i^{(k)} = \rho + O\left(\lambda_3/\rho\right)^k \tag{5B.6}$$

$$\mu_i^{(k)} = \cos\theta + O\left(\lambda_3/\rho\right)^k . \tag{5B.7}$$

In practice we use only the first *m* components of the vectors generated in the sequence (5B.2), leaving *m* sequences of estimates for ρ and $\cos\theta$.

REFERENCES

Affleck I 1986 *Phys. Rev. Lett.* **56**, 746

Alcaraz F C 1986a *J. Phys. A* **19**, L1085

Alcaraz F C 1986b *The critical behaviour of self-dual Z(N) spin systems – finite-size scaling and conformal invariance*, preprint

Alcaraz F C and Barber M N 1987 *J. Phys. A* **20**, 179

Alcaraz F C and Barber M N 1987 *J. Stat. Phys.* **46**, 435

Alcaraz F C and Drugowich de Felício J R 1984 *J. Phys. A* **17**, L651

Alcaraz F C, Barber M N and Batchelor M T 1987a *Phys. Rev. Lett.* **58**, 771

Alcaraz F C, Barber M N and Batchelor M T 1987b *Conformal invariance, the XXZ chain and the operator content of two-dimensional critical systems*, in preparation

Alcaraz F C, Barber M N, Batchelor M T, Baxter R J and G R W Quispel 1987 *Surface exponents of the quantum XXZ, Ashkin-Teller and Potts models*, preprint

Ashkin J and Teller E 1943 *Phys. Rev.* **64**, 178

Avdeev L V and B D Dörfel 1986 *J. Phys. A* **19**, L13

Babelon O, de Vega H J and Viallet C M 1983 *Nucl. Phys. B* **220** [FS8], 13

Balbão D B and Drugowich de Felício J R 1987 *J. Phys. A* **20**, L207

Barber M N 1977 *Phys. Reports* **29C**, 1

Barber M N 1983a in *Phase Transitions and Critical Phenomena* vol 8, eds C Domb and J L Lebowitz (Academic: London) pp 145-266

Barber M N 1983b *Phys. Rev. B* **27**, 5879

Barber M N 1985 *Physica* **130A**, 171

Batchelor M T 1987 *J. Austral. Math. Soc. Ser. B* **28**, 462

Batchelor M T, Barber M N and Pearce P A 1987 *Bethe ansatz calculations for the eight-vertex model on a finite strip*, preprint

Baxter R J 1972 *Ann. Phys. (N.Y.)* **70**, 193

Baxter R J 1973a *Ann. Phys. (N.Y.)* **76**, 1, 25, 48

Baxter R J 1973b *J. Stat. Phys.* **8**, 25

Baxter R J 1980 in Fundamental Problems in Statistical Mechanics V (ed E G D Cohen) (North Holland, Amsterdam) pp 109-141.

Baxter R J 1982 *Exactly Solved Models in Statistical Mechanics* (Academic, NewYork)

Baxter R J, Kelland S B and Wu F Y 1976 *J. Phys. A* **9**, 397

Beale P D, Duxbury P M and Yeomans J 1985 *Phys. Rev. B* **31**, 7166

Belavin A A, Polyakov A M and Zamolodchikov A B 1984 *Nucl. Phys. B* **241**, 333

Berkcan E 1983 *Nucl. Phys. B* **215**[FS7], 68

Bethe H A 1931 *Z. Phys.* **71**, 205

Binder K 1983 in *Phase Transitions and Critical Phenomena* vol 8, ed C Domb and J L Lebowitz (Academic, New York)

Blöte H W J, Cardy J L and Nightingale M P 1985 *Phys. Rev. Lett.* **56**, 742

Borysowicz J, Kaplan T A and Horsch P 1985 *Phys. Rev. B* **31**, 1590

Cappelli A, Itzykson C and Zuber J -B 1987 *Nucl. Phys. B* **280** [FS18], 445

Cardy J L 1984a *J. Phys. A* **17**, L385

Cardy J L 1984b *J. Phys. A* **17**, L961

Cardy J L 1984c *Nucl. Phys. B* **240** [FS12], 514

Cardy J L 1986a *Nucl. Phys. B* **270** [FS16], 186

Cardy J L 1986b *Nucl. Phys. B* **275** [FS17], 200

Cardy J L 1986c *J. Phys. A* **19**, L1093

Cardy J L 1986d *Physica* **140**A, 291

Cardy J L 1987 in *Phase Transitions and Critical Phenomena* , eds C Domb and J L Lebowitz (Academic, London) (to appear)

Cullum J and Willoughby R A 1981 *J. Comp. Phys.* **44**, 329

Davies B 1987 *J. Stat. Phys.* **46**, 535

den Nijs M P M 1979 *J. Phys. A* **12**, 1857

den Nijs M P M 1981 *Phys. Rev. B* **23**, 6111

den Nijs M P M 1983 *Phys. Rev. B* **27**, 1674

des Cloiseaux J and Pearson J J 1962 *Phys. Rev.* **128**, 2131

Destri C and Lowenstein J H 1982 *Nucl. Phys. B* **205** [FS5], 369

de Vega H J and Woynarovich F 1985 *Nucl. Phys. B* **251**, 43

Di Francesco P. Saleur H and Zuber J -B 1987 *Modular invariance in non-minimal two-dimensional conformal theories*, preprint

Domany E and Kinzel W 1981 *Phys. Rev. Lett.* **47**, 5

Dotsenko Vl S 1984 *Nucl. Phys. B* **235**, 54

Duxbury P M, Yeomans J and Beale P D 1984 *J. Phys. A* **17** L179

Elliot R J 1961 *Phys. Rev.* **124**, 346

Faddeev D K and Faddeeva V N 1963 *Computational Methods in Linear Algebra* (Freeman, San Francisco)

Fateev V A and Zamolodchikov A B 1982 *Phys. Lett.* **92**A, 37

Fisher M E 1971 in *Critical Phenomena*, Proc. Int. School of Physics 'Enrico Fermi', Varenna, 1970, Course No 51, ed M S Green (Academic, New York)

Fisher M E 1974 *Rev. Mod. Phys.* **46**, 597

Fisher M E 1985 *J. Appl. Phys.* **57**, 3265

Fisher M E 1986 *J. Magn. Magn. Mater.* **54-57**, 646

Fisher M E and Barber M N 1972 *Phys. Rev. Lett.* **28**, 1516

Fowler M 1982 *J. Appl. Phys.* **53**, 2048

Fradkin E and Kadanoff L P 1980 *Nucl. Phys. B* **170**,1

Friedan D, Qiu Z and Shenker S H 1984 *Phys. Rev. Lett.* **52**, 1575

Friedan D, Qiu Z and Shenker S H 1986 *J. Magn. Magn. Mater.* **54-57**, 655

Gaudin M 1971 *Phys. Rev. A* **4**, 386

Gaudin M 1983 *La Fonction d'Onde de Bethe* (Masson, Paris)

Gaudin M, McCoy B M and Wu T T 1981 *Phys. Rev. B* **23**, 417

Gepner D 1987 *On the spectrum of two-dimensional conformal field theories*, preprint

Gradshteyn I S and Ryzhik I M 1980 *Table of Integrals, Series and Products* (Academic Press, New York)

Grieger W 1984 *Phys. Rev. B* **30**, 344

Hamer C J 1981 *J. Phys. A* **14**, 2981

Hamer C J 1985 *J. Phys. A* **18**, L1133

Hamer C J 1986a *J. Phys. A* **19**, 3335

Hamer C J 1986b *Finite-size scaling corrections for the eight-vertex model*, preprint

Hamer C J, Quispel G R W and Batchelor M T, 1987 *Conformal anomaly and surface energy for Potts and Ashkin-Teller quantum chains*, preprint

Hornreich R M, Liebmann R, Schuster H G and Selke W 1979 *Z. Phys. B* **35**, 91

Hulthén L 1938 *Arkiv. Mat. Astron. Fysik.* **26**A, No.11

Johnson J D, Krinsky S and M^{c} Coy B M 1973 *Phys. Rev. A* **8**, 2526

Kac V G 1979 in *Group Theoretical Methods in Physics* eds W Bieglbock and A Bohm, *Lecture Notes in Physics*, Vol. 94 (Springer-Verlag, New York)

Kadanoff L P and Wegner F J 1971 *Phys. Rev. B* **4**, 3989

Kadanoff L P 1979 *Ann. Phys.* (*N.Y.*) **120**, 39

Kadanoff L P and Brown A C 1979 *Ann. Phys.* (*N.Y.*) **121**, 318

Kaplan T A, Horsch P and Borysowicz 1987 *Phys. Rev. B* **35**, 1877

Katsura S 1962 *Phys. Rev.* **127**, 1508

Kinzel W and Schick M 1981 *Phys. Rev. B* **23**, 3435

Knops H J F 1980 *Ann. Phys.* (*N.Y.*) **128**, 448

Kohmoto M, den Nijs M and Kadanoff L P 1981 *Phys. Rev. B* **24**, 5229

Landau D P and Binder K 1985 *Phys. Rev. B* **31**, 5946

Lieb E H, Schultz T D and Mattis D C 1961 *Ann. Phys.* (*N.Y.*) **16**, 407

Lieb E H and Wu F Y 1972 in *Phase Transitions and Critical Phenomena*, eds C Domb and M S Green, (Academic Press, London) Vol. 1 p331

Martin H O and de Vega H J 1985 *Phys. Rev. B* **32** 5959

Mittag L and Stephen M J 1971 *J. Math. Phys.* **12**, 441

Müller-Hartmann E and Zittarz J 1977 *Z. Phys. B* **27**, 261

Nienhuis B 1982 *J. Phys. A* **15**, 199

Nienhuis B 1984 *J. Stat. Phys.* **34**, 731

Nienhuis B and Knops H J F 1985 *Phys. Rev. B* **32**, 1872

Nightingale M P 1976 *Physica* **83**A, 561

Nightingale M P 1977 *Phys. Lett.* **59**A, 486

Nightingale M P 1979 *Proc. K. Ned. Akad. Wet. Ser. B* **82**, 235

Nightingale M P 1982 *J. Appl. Phys.* **53**, 7927

Nightingale M P and Blöte H W J 1983 *J. Phys. A* **16**, L657

Oitmaa J, Velgakis M J, Batchelor M T and Barber M N 1986 *J. Magn. Magn. Mater.* **54-57**, 665

Oitmaa J and Velgakis M J 1987 *J. Phys. A* **20**,

Onsager L 1944 *Phys. Rev.* **65**, 117

Polyakov A M 1970 Pisma Zh. Eksp. Teor. Fiz. **12**, 538 [1970 JETP Lett. **12**, 381]

Privman V and Fisher M E 1983 *J. Phys. A* **16**, L295

Ree F H and Chestnut D A 1966 *J. Chem. Phys.* **45**, 3983

Reinicke P 1987a *Analytical and non-analytical corrections to finite-size scaling*, preprint

Reinicke P 1987b *Finite-size scaling functions and conformal invariance*, preprint

Runnels L K and Combs L I 1966 *J. Chem. Phys.* **45**, 2482

Selke W and Fisher M E 1980 *Z. Phys. B* **40**, 71

Selke W 1984 in *Modulated Structure Materials*, ed T Tsakalakos (Martin Nigheff) pp 23-42

Sólyom J and Pfeuty P 1981 *Phys. Rev. B* **24**, 218

Stephenson J 1970 *J. Math. Phys.* **11**, 420

Takahashi M and Suzuki M 1972 *Prog. Theor. Phys.* **48**, 2187

Takhtadzhan L A and Faddeev L D 1979 *Russian. Math. Surv.* **34**:5, 11

Temperley H N V and Lieb E H 1971 Proc. Roy. Soc. Lond. A **322**, 251

Thacker H B 1981 *Rev. Mod. Phys.* **53**, 253

Tsvelick A M and Weigmann P B 1983 *Adv. Phys.* **32**, 453

Vanden Broeck J -M and Schwartz L W 1979 *SIAM J. Math. Anal.* **10**, 658

von Gehlen G, Rittenberg V and Ruegg H 1986 *J. Phys. A* **19**, 107

von Gehlen G and Rittenberg V 1986a *J. Phys. A* **19**, L625

von Gehlen G and Rittenberg V 1986b *J. Phys. A* **19**, L631

von Gehlen G and Rittenberg V 1986c *J. Phys. A* **19**, L1039

von Gehlen G and Rittenberg V 1987 *J. Phys. A* **20**, 227

Wegner F J 1972 *Phys. Rev. B* **5**, 4529

Woynarovich F 1982 *J. Phys. A* **15**, 2985

Woynarovich F and Eckle H -P 1987 *J. Phys. A* **20**, L97

Wu F 1971 *Phys. Rev. B* **4**, 2312

Wu F 1982 *Rev. Mod. Phys.* **54**, 235

Yang C N and Yang C P 1966a *Phys. Rev. B* **150**, 321

Yang C N and Yang C P 1966b *Phys. Rev. B* **150**, 327